The further development, application and evaluation of a sediment yield model (WQSED) for catchment management in African catchments.

A thesis submitted in fulfilment of the requirements for the degree of

Doctor of Philosophy

Of

RHODES UNIVERSITY

Grahamstown

South Africa

By

David Gwapedza

ORCID: https://orcid.org/0000-0002-4617-196X

November 2020

DEDICATION

This thesis is dedicated to my brother James Gwapedza

ACKNOWLEDGEMENTS

I express my sincere gratitude to my supervisors Prof. Denis. A. Hughes, Dr. Andrew.R. Slaughter, and Dr. Sukhmani.K.Mantel for all the support they provided throughout my research. It is through their wise counsel; patience and guidance that I have managed to complete this thesis. I am particularly grateful for the exposure and training I received through various consultations and the workshops and conferences that they supported me to attend. I am grateful now and will always be grateful to be a recipient of your excellent supervision.

I extend my gratitude to the Water Research Commission of South Africa for funding support during my masters. I am grateful to the Carnegie Corporation of New York through the Regional Initiative in Science Education (RISE) Programme for funding both my masters and PhD studies. I sincerely thank the Oppenheimer Memorial Trust (OMT) for providing additional financial support for the last year of my PhD. It is because of the financial support provided by the above generous organisations that I managed to begin and complete this thesis.

I cannot forget the SWINDON- EXCEED PhD exchange funded by DAAD, where I was hosted at the Technical University of Braunschweig, Germany. I was warmly welcomed and supervised by Malte Eley and Annika Nolte, and indeed, the entire LEICHTWEIß-Institute for Hydraulic Engineering and Water Resources team. I thank Dr. Jane Tanner for facilitating the exchange and attending an Agent-Based Modelling training workshop in Montpellier, France, during the exchange.

Finally, I am incredibly grateful to the community at the Institute for Water Research, Rhodes University for supporting me during my studies. A special mention to my office mates Sbongiseni Mazibuko and Pierre Kabuya who always shared ideas and advice. I am thankful for my family that has always patiently stood by me throughout this journey. Special recognition goes to my former lecturer and adviser, Dr. Onalenna Gwate; I thank him for seeing potential in me. Finally, I am grateful for my special friends Menelisi Falayi and Noxolo Kheswa; their presence provided a pillar of emotional support and encouragement during an important but challenging phase of my research.

I thank you all and wish that God blesses you abundantly.

It is the Lord my God that has given me the life and health to see this thesis through

ABSTRACT

Erosion and sediment transport are natural catchment processes that play an essential role in ecosystem functioning by providing habitat for aquatic organisms and contributing to the health of wetlands. However, excessive erosion and sedimentation, mostly driven by anthropogenic activity, lead to ecosystem degradation, loss of agricultural land, water quality problems, reduced reservoir storage capacity and damage to physical infrastructure. It is reported that up to 25% of dams in South Africa have lost approximately 30% of their initial storage capacity to sedimentation. Therefore, excessive sedimentation transcends from an ecological problem to a health, livelihood and water security issue.

Erosion and sedimentation occur at variable temporal and spatial scales; therefore, monitoring of these processes can be difficult and expensive. Regardless of all these prohibiting factors, information on erosion and sediment remains an urgent requirement for the sustainable management of catchments. Models have evolved as tools to replicate and simulate complex natural processes to understand and manage these systems. Several models have been developed globally to simulate erosion and sediment transport. However, these models are not always applicable in Africa because 1) the conditions under which they were developed are not as relevant for African catchments 2) they have high data requirements and cannot be applied with ease in our data-scarce African catchments 3) they are sometimes complicated, and there are little training available or potential users simply have no time to dedicate towards learning these models. To respond to the problems of erosion, sedimentation, water quality and unavailability of applicable models, the current research further develops, applies and evaluates an erosion and sediment transport model, the Water Quality and Sediment Model (WQSED), for integration within the existing water resources framework in South Africa and application for practical catchment management. The WQSED was developed to simulate daily suspended sediment loads that are vital for water quality and quantity assessments. The WQSED was developed based on the Modified Universal Soil Loss Equation (MUSLE), and the Pitman model is a primary hydrological model providing forcing data, although flow data from independent sources may be used to drive the WQSED model. The MUSLE was developed in the United States of America, and this research attempts to improve the applicability of the MUSLE by identifying key issues that may impede its performance.

Assessments conducted within the current research can be divided into scale assessment and application and evaluation assessment. The scale assessment involved evaluating spatial and temporal scale issues associated with the MUSLE. Spatial scale assessments were conducted using analytical and mathematical assessments on a hypothetical catchment. Temporal scale issues were assessed in terms of the vegetation cover (*C*) factor within the Tsitsa River catchment in South Africa. Model application and evaluation involved applying and calibrating the model to simulate daily time-series sediment yield. The model was applied to calibrated and validated (split-sample validation) in two catchments in South Africa, two catchments in Zimbabwe and three catchments were selected from the USA and associated territories for further testing as continuous daily time-series observed sediment data could not be readily accessed for catchments in the Southern African region. The catchments where the model was calibrated and validated range in size from 50 km^2 to 20 000 km^2. Additionally, the model was applied to thirteen 'ungauged' catchments selected from across South Africa, where only long-term reservoir sedimentation rates were available to compare with long term model simulations converted to sediment yield rates. The additional thirteen catchments were selected from areas of different climatic, vegetation and soils conditions characterising South Africa and range in size from 30 km^2 to 2 500 km^2.

The current research results are split into a) MUSLE scale dependency and b) WQSED testing and evaluation. Scale dependency testing showed that the MUSLE could be spatially scale-dependent, particularly when a lumped approach is used, resulting in simulations of up to 30% more sediment. Spatial scale dependence in the MUSLE was found to be related to the runoff and topographic factors used and how they are calculated. The current study resorted to adopting a reference grid in applying the MUSLE, followed by scaling up the outputs to the total catchment area. Using a reference grid resulted in a general avoidance of the problem of spatial scale. The adoption of a seasonal vegetation cover factor was shown to significantly account for temporal changes of vegetation cover within a year and reduce over-estimations in sediment output. The temporal scale evaluation demonstrated the uncertainties associated with using a fixed vegetation cover factor in a catchment with variable rainfall and runoff pattern.

The WQSED model evaluation showed that the model could be calibrated and validated to provide consistent results. Satisfactory model evaluation statistics were obtained for most catchments to which the model was applied, based on general model evaluation guidelines (Nash Sutcliffe Efficiency and $R^2 > 0.5$). The model also performed generally well compared to

established models that had been previously applied in some of the study catchments. The highest sediment yields recorded per country were 153 t km^{-2} $year^{-1}$ (Tsitsa River; South Africa), 90 t km^{-2} $year^{-1}$ (Odzi River; Zimbabwe) and 340 t km^{-2} $year^{-1}$ (Rio Tanama; Puerto Rico). The results also displayed consistent underestimations of peak sediment yield events, partly attributed to sediment emanating from gullies that are not explicitly accounted for in the WQSED model structure. Furthermore, the calibration process revealed that the WQSED storage model is generally challenging to calibrate. An alternative simpler version of the storage model was easier to calibrate, but the model may still be challenging to apply to catchments where calibration data are not available. The additional evaluation of the WQSED simulated sediment yield rates against observed reservoir sediment rates showed a broad range of differences between the simulated and observed sediment yield rates. Differences between WQSED simulated sediment and observed reservoir sediment ranges from a low of 30% to a high of > 40 times. The large differences were partly attributed to WQSED being limited to simulating suspended sediment from sheet and rill processes, whereas reservoir sediment is generated from more sources that include bedload, channel and gully processes. Nevertheless, the model simulations replicated some of the regional sediment yield patterns and are assumed to represent sheet and rill contributions to reservoir sediment in selected catchments.

The outcome of this study is an improved WQSED model that has successfully undergone preliminary testing and evaluation. Therefore, the model is sufficiently complete to be used by independent researchers and water resources managers to simulate erosion and sediment transport. However, the model is best applicable to areas where some observed data or regional information are available to calibrate the storage components and constrain model outputs. The report on potential MUSLE scale dependencies is relevant globally to all studies applying the MUSLE model and, therefore, can improve MUSLE application in future studies. The WQSED model offers a relatively simple, effective and applicable tool that is set to provide information to enhance catchment, land and water resources management in catchments of Africa.

TABLE OF CONTENTS

DEDICATION.....i
ACKNOWLEDGEMENTS.....ii
ABSTRACT.....iii
TABLE OF CONTENTS.....vi
LIST OF FIGURES.....x
LIST OF TABLES.....xiii
Chapter 1 Introduction.....1
1.1 Introduction and project overview.....1
1.2 Research aim, objectives and design.....5
1.2.1 Research aim.....5
1.2.2 Research objectives.....5
1.3 Thesis outline.....6
Chapter 2 Erosion and sedimentation.....8
2.1 Introduction.....8
2.2 Water erosion.....9
2.3 Drivers of water erosion.....10
2.3.1 Storm characteristics.....10
2.3.2 Vegetation.....11
2.3.3 Soils.....13
2.3.4 Slope.....14
2.3.5 Connectivity.....15
2.3.6 Human influence.....16
2.4 Impacts of erosion and sedimentation.....17
2.4.1 Land degradation.....17
2.4.2 Effects of sediment on aquatic ecosystems.....18
2.4.3 Water quantity.....18
2.4.4 Water quality.....19
2.5 The impact of climate change on erosion and sedimentation.....20
2.5.1 The impact of climate change on rainfall erosivity.....20
2.5.2 Climate change impact on vegetation.....21
2.6 Erosion, sediment yield and sediment transport models.....22

2.6.1 Empirical, conceptual, and physically-based erosion, sediment yield and sediment transport models 23
2.6.2 Spatial scale: appropriate scales for application of models 24
2.6.3 Spatial scale: lumped and distributed modelling approaches 25
2.7 Application of erosion and sediment transport models in South Africa 26
2.8 Incorporating a sediment model into a South African water resources modelling framework 27
2.8.1 Pitman model 28
2.8.2 Background to WQSED model development 31
2.8.3 The MUSLE 33
2.9 Summary 34
Chapter 3 Study site descriptions 36
3.1 Introduction 36
3.2 Catchments physical characteristics 38
3.3 Available flow and sediment data 45
3.3.1 Flow/runoff data 48
3.3.2 Sediment data 48
3.4 Conclusion 50
Chapter 4 Methodological approaches 51
4.1 Introduction 51
4.1.1 WQSED model structure 51
4.1.2 A slope-based distribution 52
4.2 MUSLE Component 54
4.2.1 Sub-basin flow estimation 54
4.3 Storage component 56
4.3.1 Slope storage and delivery 56
4.4 Simple storage option 59
4.5 Channel component 61
4.5.1 Sediment routing in the main channel 61
4.5.2 Calculation of velocity, depth and river width with different flows 61
4.5.3 Calculation of suspended sediment 63
4.6 Estimating MUSLE parameters 67
4.6.1 Topography (*LS*) factor 67
4.6.2 Vegetation cover (*C*) factor 68

4.6.3 Soil erodibility (*K*) factor 69
4.6.4 Management practice (*P*) factor 71
4.7 Methodological limitations 71
4.8 Concluding remarks 74
Chapter 5 Consideration of spatial scale dependency in the application of the Modified Universal Soil Loss Equation (MUSLE) 75
5.1 Introduction 75
5.1.2 Literature assessments of the spatial scale dependency of the MUSLE 76
5.2 Assessments of erosivity spatial scale dependency 78
5.2.1 Analytical solutions to the Erosivity index (Equation 5.1) 78
5.2.2 A distributed approach with flow routing 79
5.3 Assessments of topography (*LS)* spatial scale dependency 83
5.4. Discussion and conclusions 84
Chapter 6 Evaluating the effect of temporal changes in vegetation cover (*C*) factor on the MUSLE 88
6.1 Introduction 88
6.1.1 *C* factor mapping through remote sensing technologies 89
6.2 Methods 91
6.2.1 Acquiring NDVI data 91
6.2.2 NDVI to *C* factor conversion 92
6.2.3 Sediment yield calculations 93
6.3 Results 94
6.3.1 Fixed *C* factor 94
6.3.3 T35C catchment sediment yield (SY) distribution 98
6.3.4 Validating the *C* factor assessment in the Tsitsa catchment and Inxu sub-catchment 100
6.4 Discussions and conclusions 103
Chapter 7 Regional testing and evaluation of the WQSED model 106
7.1 Introduction 106
7.2 Setting up the models 106
7.2.1 Calibration, validation and assessment of model performance 107
7.3 Results 110
7.3.1 Odzi and Rio Tanama catchments 110

7.3.2 Results of the WQSED (simple storage) simulations for other selected catchments 115
7.4 Sensitivity assessment 118
7.5 Discussion 121
7.5.1 Tsitsa River catchment (South Africa) 121
7.5.2 Odzi and Gwai river catchments (Zimbabwe) 122
7.5.3 Grand Cane, San Patricio and Rio Tanama catchments (USA and associated territories) 124
7.6 Summary and conclusions 126
Chapter 8 Estimating sediment yield in 'ungauged' South African catchments 128
8.1 Introduction 128
8.2 Setting up the WQSED model 128
8.3 Results 131
8.3.1 Mean parameter distributions 131
8.3.2 HML parameter distributions and flow inputs 132
8.3.3 Sediment yield simulated using estimated (mean and HML) MUSLE factors 133
8.4 Discussion 136
8.4.1 Estimated MUSLE factor distributions 136
8.4.2 Regional sediment yield patterns 138
8.5 Conclusion 141
Chapter 9 Conclusions and recommendations 142
9.1 Introduction 142
9.2 Spatial and temporal scale effects associated with MUSLE application (Objectives A and B) 142
9.3 Application and evaluation of the WQSED model (Objectives C and D) 145
9.4 Limitations of the study 148
9.5 Conclusion 148
References 150
Appendix A 172
Appendix B 190
Appendix C 192

LIST OF FIGURES

Figure 1.1 Chapter structure of the thesis. 7

Figure 2.1 An illustration of the three spatial distribution approaches used in sediment yield and transport modelling. 26

Figure 2.2 Conceptual representation of the WQSAM model within the SPATSIM framework The sediment delivery sub-model (WQSED) is circled in red. 28

Figure 2.3 The conceptual framework of the monthly-to-daily flow disaggregation method (Sourced from Slaughter et al. (2015)). 30

Figure 3.1 A map of all the selected study sites in South Africa and Zimbabwe. 36

Figure 3.2 A map of the selected study sites in the United States of America (USA) and overseas territories of the USA. 37

Figure 4.1 Conceptual structure of the erosion and sediment transport (WQSED) model..... 52

Figure 4.2 Calculation of the proportion of the catchment area in each slope zone of high (H), medium (M) and low (L) for the erosion and sediment transport (WQSED) model using a 30m digital elevation model (DEM); the Rio Tanama catchment is used as an example. 53

Figure 4.3 Erosion and sediment transport (WQSED) model conceptual storages. Adapted from Bryson (2015). 54

Figure 4.4 The slope storage and delivery component of the erosion and sediment transport (WQSED) model. Sourced from Bryson (2015)..... 58

Figure 4.5 Conceptual representation of a river channel used to route sediment within the WQSED model. 62

Figure 4.6 Flowchart illustrating the process of determining the Modified Universal Soil Loss Equation (MUSLE) topography (*LS*) factor. Abbreviations: DEM-digital elevation model; SRTM-Shuttle Radar Topographic Mission. 68

Figure 5.1 Relationships between sub-basin area and peak runoff depths required to generate the same erosivity estimate for a total storm depth of 25 mm (based on fixing the 100 ha peak at 6 mm h^{-1}). 79

Figure 5.2 Hypothetical catchment of 20 km^2, subdivided into 20 × 1 km^2 sub-catchment grids. The arrows indicate the assumed directions of flow used in the sub-catchment routing to the final outlet at grid 20. 81

Figure 5.3 Unrouted and routed hydrographs for the 20 km^2 hypothetical catchment (routing based on three different *RK* parameters). 81

Figure 5.4 Illustration of the scale dependency of the topographic factor (*LS*) using a lumped and distributed approach. 84

Figure 6.1 Distribution of monthly NDVI and LAI factor for 2016–2017. 95

Figure 6.2 The relationship between normalised rainfall and temperature with *C* factor; insert linear regression of rainfall, temperature and *C* factor for the years 2016–2017. The climate values were normalised by dividing all values by the first value in the distribution (i.e. Jan). 96

Figure 6.3 Monthly *C* factor distribution of the grass and forest vegetation classes in the T35C catchment for the year 2016 calculated from NDVI. 97

Figure 6.4 Distribution of sediment yield simulated using the fixed and variable (NDVI) *C* factors for catchment T35C in 2016. 98

Figure 6.5 Distribution of sediment yield simulated using the fixed and variable (NDVI) *C* factors for catchment T35C in 2017. 99

Figure 6.6 Sediment yield variation resulting from the fixed and variable (NDVI) *C* factor. 100

Figure 6.7 An illustration of observed SY versus sediment calculated using the fixed and variable (NDVI) *C* factors in the Inxu catchment (Log Y-axis). 101

Figure 6.8 An illustration of observed SY versus sediment calculated using the fixed and variable (NDVI) *C* factors in the Tsitsa catchment (Log Y-axis). 102

Figure 7.1 Observed and simulated sediment output for the Odzi catchment. A. simulations by the Modified Universal Soil Loss Equation (MUSLE), B. MUSLE plus the simple storage model and C. Full version erosion and sediment transport (WQSED) model with complex storage components. The dotted blue line separates the calibration period at the beginning of the time-series and the validation. 112

Figure 7.2 Observed and simulated sediment output for the Rio Tanama catchment. A. simulations by the Modified Universal Soil Loss Equation (MUSLE), B. MUSLE plus the simple storage model and C. Full version erosion and sediment transport (WQSED) model with complex storage components. The dotted blue line separates the calibration period at the beginning of the time-series and the validation. 113

Figure 7.3 Sediment frequency distribution graphs (Log Y-axis) of the erosion and sediment transport model (WQSED) simulations (red lines) versus observations (black lines) for the Odzi (left) and Rio Tanama) catchments and for the calibration and validation periods. 114

Figure 7.4 Linear correlation graphs showing calibration and validation periods of the erosion and sediment transport model (WQSED) sediment yield (SY) simulations for the Odzi and Rio Tanama catchments. 115

Figure 7.5 Observed and simulated WQSED sediment output for the Gwai catchment sub-basins A36 and A38. The dotted blue line separates the calibration period at the beginning of the time-series and the validation. 116

Figure 7.6 Graphs illustrating observed and simulated sediment outputs for the Grand Cane, San Patricio, Inxu and Tsitsa catchments. The dotted blue line separates the calibration period at the beginning of the time-series and the validation. 117

Figure 7.7 The sensitivity of changing storm duration on sediment yield simulations (calculated for the Inxu catchment, South Africa). 118

Figure 7.8 Frequency distributions (Log Y-axis) showing the change in WQSED sediment output relative to the change in storm duration for the Odzi catchment. The ShortD and LongD represent short and long duration types. 119

Figure 7.9 Frequency distributions (Log Y-axis) showing the change in WQSED sediment output relative to the change in storm duration for the Rio Tanama catchment. The ShortD and LongD represent short and long duration types. 120

Figure 8.2 Map showing the distribution of selected study catchments across South Africa. 130

Figure 8.3 Mean High-Medium-Low (HML) catchment erodibility parameters computed for selected South African catchments. 132

Figure 8.4 Linear regression of estimates calculated using mean catchment parameters and mean High-Medium-Low (HML) parameters. 135

Figure 8.5 Map showing the regional sediment yield gradient exhibited through the selected catchments. A. represents the patterns based on reservoir survey, and B. represents modelled patterns. 140

LIST OF TABLES

Table 2.1 A list of human-induced erosion and sedimentation drivers and their impacts. 16

Table 3.1 A summary of catchment physical characteristics. 38

Table 3.2 The geological and climatic characteristics of the selected study areas. 39

Table 3.3 Descriptions of the vegetation coverage and land uses that dominate the selected study areas. 42

Table 3. 4 Summary of available flow and sediment data for selected catchments. 45

Table 4.1 A list of parameters for the Modified Universal Soil Loss Equation of the erosion and sediment transport (WQSED) model. 56

Table 4.2 A list of parameters for the storage component of the erosion and sediment transport (WQSED) model. 59

Table 4.3 A list of parameters for the simple storage option of the erosion and sediment transport (WQSED) model. 60

Table 4.4 A list of parameters for the channel component of the erosion and sediment transport (WQSED) model. 64

Table 4.5 A list of parameters for the erosion and sediment transport (WQSED) model. Parameters with no specific range are indicated with a hyphen (-) and are based on the area of application. 65

Table 4.6 Cover factor (*C*) for South African and Zimbabwean land cover/use categories. 69

Table 4.7 Erodibility factors for soil erodibility classes (Schulze and Lorentz, 1995). 70

Table 5.1 Muskingum routing *RK* values and sediment yield for different routing options applied to the hypothetical catchment and hydrographs shown in Figures 5.2 and 5.3 (total runoff depth = 25 mm). 82

Table 6.1 Dates of images acquired for inter-annual analysis. 92

Table 6.2 Fixed catchment (T35C) *C* factor calculated using maps and values from literature. 94

Table 6.3 Percentage variation between inter-annual and fixed *C* factors for catchment T35C. 96

Table 6.4 Summary of sediment yield (SY) output in the Inxu and Tsitsa catchments compared to observed data. 101

Table 6.5 Summary statistics comparing observed data the SY output attained using a fixed or variable *C* factor at daily and monthly time scales. 102

Table 7.1 Erosion and sediment transport model (WQSED) primary calibration parameters. A hyphen (-) indicates values based on the area of application. 107

Table 7.2 Performance indicators for the Odzi and Rio Tanama catchments. The model simulations were obtained through the application of the model based on a gradient of complexity i.e. from a simple MUSLE to added storage options. 110

Table 7.3 Performance indicators for the application of the erosion and sediment transport model (WQSAM) to additional catchments. 116

Table 7.4 Changes in sediment yield outputs of the WQSED model applied to the Inxu catchment with changes in storm duration in relation to the calibrated duration of 12 hours. 118

Table 7.5 Duration parameters for calculating the minimum and maximum durations for the Odzi (Zimbabwe) and Rio Tanama (Puerto Rico) catchments. 119

Table 7.6 Differences in average WQSED sediment yield estimates between the current study and previous studies for the Gwai catchment. 123

Table 7.7 WQSED model performance after transferring calibrated storage and duration parameters to a neighbouring catchment. 127

Table 8.1 Mean catchment erodibility parameters for selected South African catchments... 131

Table 8.2 Mean total and surface flow for study areas and estimated baseflow fractions. ... 133

Table 8.3 Summary of simulated sediment yield outputs and previous reservoirs estimates. The % difference is calculated based on columns four and five. 134

Table 8.4 Summary of simulated sediment yield outputs and reservoir estimates. The lower and upper bounds represent the ±25% parameter uncertainty range. 136

Chapter 1 Introduction

1.1 Introduction and project overview

Soil erosion and sedimentation are some of South Africa's acute environmental problems with impacts on food (Thompson et al., 2010) and water security (Le Roux and Waal, 2020). Erosion and sedimentation are significant social-ecological problems in South Africa because of the loss of topsoil, biodiversity and reduction in the sustainability of dams and other ecological infrastructure (Le Roux, 2018). The threat of climate change is expected to worsen the problem of water erosion and sedimentation by changing the dynamics of catchment processes related to vegetation cover, soil moisture (Li and Fang, 2016) and runoff. "When climate change issues are superimposed upon the existing vulnerabilities, the effects thereof are exacerbated" (Lötter, 2017). Changes in the patterns of climate, e.g. precipitation and temperature, can significantly and permanently impact catchment erosion and sedimentation processes (Li and Fang, 2016), which in turn may impact rural livelihoods and both the formal and informal agricultural sectors. Nearing et al. (2005) add that there is a significant likelihood of increased global soil erosion induced by climate change, unless preventative measures are taken. Southern Africa is already experiencing an increase in average temperatures and an increase in the variability of precipitation, with a tendency towards more extended drought periods followed by more severe flooding (IPCC, 2012), thus elevating the risk of water erosion and sedimentation.

Although not prioritised as an acute environmental hazard, accelerated soil erosion has affected almost 2 billion hectares of fertile land (Arekhi et al., 2012), more than 50% of pasturelands and 80% of agricultural lands globally (Pimentel et al., 1995). The *South African Yearbook, 2008/9*, reports that South Africa loses 500 million tons of topsoil annually, which is the highest per capita soil loss globally (Lötter, 2017). Of the total land area in South Africa, an estimated 18% has been transformed from natural land to other land-cover types, including cultivation (~11%), degradation (~5%) and settlements (~3%). Cultivation and degradation are both leading drivers of soil loss (Lötter, 2017), posing a risk to South Africa's water resources (Blignaut et al., 2010). With food supply systems already under pressure from climate change and a growing population, ecosystem degradation adds to the looming long-term food security problem in South Africa (Masipa, 2017; Mugambiwa and Tirivangasi, 2017).

The problem of soil erosion is further compounded by the fact that much of the eroded soil is transported through river systems into reservoirs (Vanmaercke et al., 2014). Thus, sedimentation has become a significant threat to reservoir lifespans and functioning (Le Roux, 2018; Msadala and Basson, 2017; Roux and Waal, 2020). Nearly a quarter of reservoirs in South Africa have lost up to 30% of their storage capacity to sedimentation (Msadala et al., 2010; Msadala and Basson, 2017). The loss of reservoir storage capacity results in wide-ranging ecological, social and economic problems, such as a shortage of water for irrigation, domestic and industrial use, as well as a loss in reservoir flood-attenuation capacity. Apart from the consequences of water quantity, excessive sedimentation also affects water quality (Issaka and Ashraf, 2017). In this regard, increased turbidity negatively impacts riverine communities by disrupting the filter-feeding mechanisms of some macro-invertebrates and reducing suitable habitat (Akamagwuna et al., 2019; Bilotta and Brazier, 2008). Other impacts on human society include increasing water treatment costs and other ecosystem services linked to a healthy ecosystem.

Globally, the urgent need to mitigate and adapt to the environmental effects of water erosion/sedimentation is widely recognised (Nearing et al., 2017). In South Africa, the impacts of erosion and sedimentation are recognised from the local to the national levels (e.g. Lötter, 2017). For example, local communities recognise erosion and water pollution as part of the top five ecological challenges in a study conducted in the Eastern Cape Province (Murata et al., 2019). In order to respond to the erosion and sedimentation challenge, information about erosion drivers and processes, and an understanding thereof, is vital. Information on the spatial and temporal distribution of sediment loads is critical and highly sought after for informing catchment management planning. Unfortunately, physical measurements of erosion or sedimentation cannot be meaningfully performed at a large spatial scale because it is expensive and time-consuming (Alewell et al., 2019; Pandey et al., 2016). Therefore, modelling tools are widely used to provide additional information that can be used for catchment management (Pandey et al., 2016). Models also allow for the investigation of different scenarios of future change. However, model results are dependent on our ability to account for the variable natural processes that influence erosion and sediment transport loads, both spatially and temporally (Pandey et al., 2016). Developing reliable models that account for the key processes is dependent on data for input and calibration and validation (de Vente et al., 2013); such data are very scarce in South African catchments, creating

a substantial dilemma in terms of the scientific study and practical application of appropriate models.

The most popularly used erosion and sediment yield models were developed in the United States of America and Europe (Gao, 2008). The Universal Soil Loss Equation (USLE) (Wischmeier and Smith, 1978), as well as later versions of the Modified-USLE (Williams, 1975) and Revised-USLE (Renard et al., 1997) have been applied worldwide (Alewell et al., 2019; Benavidez et al., 2018; Sadeghi et al., 2013). Because they were developed for specific conditions, it often becomes necessary to modify them before application in areas outside of which they were developed (Sadeghi et al., 2013). MUSLE has been included as part of comprehensive hydrology and water quality models such as the Soil and Water Assessment Tool (SWAT) (Arnold et al., 1998; Neitsch et al., 2005) and the Agricultural Catchments Research Unit (ACRU) model (Schulze, 1995). Furthermore, the original USLE was developed for application on a plot scale for estimating long-term soil loss, and application at larger scales introduces spatial scale problems (Chen and Mackay, 2004; Karydas et al., 2014; Pignotti et al., 2017; Vigiak et al., 2015), added to which temporal scale considerations are often ignored (Sadeghi et al., 2013). Notably, as areas of application increase, USLE factors become almost impossible to estimate, and the validation of model outputs becomes a serious challenge unless USLE is linked to a sediment transport model (Alewell et al., 2019).

Some of the more detailed distributed models are data-intensive and challenging to apply to catchments in regions such as sub-Saharan Africa, where data for parameterising complex models are scarce. Simpler lumped empirical models have been applied in southern Africa (Smith, 1999) as they require fewer data to parameterise. Attempts have also previously been made to adapt popular internationally developed models for application in southern Africa (Elwell, 1978; Schulze et al., 1995). However, some of these models have often proved to be either too simplistic, fail to account for important erosion and sediment transport processes, or are too complex and data-intensive to be applicable in data-scarce regions.

Previous experience suggests that the priority for sub-Saharan Africa (SSA) is a model that: 1) maintains a relatively simple structure yet describes important sediment yield process at the catchment scale; 2) can use existing forcing and calibration data; and 3) can be integrated into existing environmental modelling frameworks for integrated assessments. The current study responds to this need by further investigating a sediment model (WQSED: Water Quality and

Sediment Model) that was previously developed by the Institute for Water Research, Rhodes University as part of an MSc project (Bryson, 2015). The focus of the initial development was on semi-arid areas and the spatial and temporal discontinuities expected in the erosion and sediment delivery processes. The key motivation for the study was to add a sediment sub-model to a recently developed water quality model (WQSAM; Slaughter et al., 2017). The Water Quality System Assessment Model was developed within the Institute for Water Research, Rhodes University as part of a Water Research Commission (WRC) project to develop a South African water quality model (Project K5/2448) that would link to a suite of other locally developed and well established hydrology (Pitman, 1973; Hughes, 2013) and water resources yield (Basson et al., 1994) models. The main issue is that WQSAM did not originally include a sediment component, which was always recognised as a structural gap in terms of the impacts of the sediment regime on the dynamics of nutrient and metal cycling. While the further development of WQSED is still directed to this primary purpose, it has other important secondary applications of independently providing catchment-scale simulations of suspended sediment loads that are essential for catchment management and water resources planning. The model responds to issues of water quantity and quality management that are of immense interest to the South African Department of Water and Sanitation (DWS) and the Department of Environmental Affairs (DEA).

The WQSED model was only applied in three semi-arid catchments as part of the Bryson (2015) study, and time-series data of sediment loads were not available for any of them. Therefore, further testing, evaluation and improvement were considered necessary before it could be integrated into the WQSAM model or recommended for use by researchers and water managers in South Africa.

The primary aim of this research is to evaluate and further develop the WQSED model and to determine its usefulness and applicability to data-scarce catchments of sub-Saharan Africa. The model will be primarily applied and tested in South African catchments. However, the application will be extended to other SSA catchments where daily sediment load observations are available. Where possible, the model outputs will be compared to previous estimates based on other methods. However, it is recognised that all of these methods (including WQSED) are extremely difficult to calibrate and validate because of the limitations associated with the lack of observed data (e.g. Le Roux, 2018; Scott-Shaw et al., 2020). While there are previous estimates of long-term sediment yield based on reservoir bathymetric surveys for a number of catchments (e.g. Rooseboom, 1992),

there are very few datasets providing daily time series of sediment load that can be used to assess the outputs of a model such as WQSED (or SWAT, ACRU or any other time series model). Apart from the lack of data available to calibrate and validate this type of model, the other issues that are covered within this study include questions associated with model scale and complexity, as well as the availability of supporting data to establish model parameter values. Simplicity is often seen as a key model characteristic to facilitate catchment management in regions where data are scarce, and modelling expertise is also limited. However, it is also important to recognise that if models are too simple to capture the main dynamics of the system being modelled, the model outputs might be less than reliable when applied, where there are few, or no, calibration data.

1.2 Research aim, objectives and design

1.2.1 Research aim

The overall aim of this study is to further develop an erosion and sediment delivery time series simulation model by ensuring that the model can estimate soil loss and sediment delivery at appropriate spatial and temporal scales with sufficient accuracy for practical applications under different levels of data availability. It is envisaged that the model will apply to catchments in southern Africa characterised by relatively high hydrological variability and for which there is a lack of observed data to validate model inputs and outputs. Providing a relatively simple, practical modelling approach is expected to contribute to catchment management approaches where sediment load represents a critical factor in managing and conserving scarce water resources. This includes issues associated with nutrient and metals cycling as part of broader water quality management, aquatic ecology and the impacts of sediment, as well as the long-term effects of sediment on reservoir management.

1.2.2 Research objectives

To test, apply and evaluate a relatively simple, implementable sediment delivery/transport model (WQSED) and facilitate the further application of the model in data-scarce South African and SSA catchments. The specific objectives of this research are:

A. To assess spatial scale dependency issues associated with the application of the Modified Universal Soil Loss Equation (MUSLE).

- An investigation into the scale dependency of the MUSLE model is performed. The study will isolate key spatial scale issues associated with MUSLE application. MUSLE parameters are investigated for potential scale issues, and recommendations are made as to how these scale dependencies may be minimised.

B. To investigate the effect of temporal variations of the vegetation cover factor on sediment yield simulations using the MUSLE/WQSED.

- An approach for estimating the seasonality of the vegetation cover parameter is investigated, based on a vegetation cover time series using remote sensing data. The model outputs based on both static and dynamic cover parameters are compared.

C. Regional application, testing and evaluation of the WQSED model.

- The model is tested, and comparisons drawn between WQSED outputs and previous estimates from other approaches including the Soil and Water Assessment Tool (SWAT). The sensitivity of model outputs to erosivity parameters will be assessed

D. To apply the model in ungauged catchments under a wide range of different climatic, topographical, vegetative and soil conditions representative of South African catchments.

- This study will apply WQSED to several catchments of varying conditions across South Africa. The influence and sensitivity of model outputs to parameter estimation methods will be assessed. Model outputs will be compared to outputs from previous independent studies and long term observations/calculations of dam sedimentation rates, where available.

1.3 Thesis outline

This thesis is composed of nine chapters and is divided into three parts (Figure 1). Part one is the introduction and context, Part two presents the results and Part three concludes the study. Part one begins with the introduction to the thesis that gives an overview of the research aspects, gap and purpose of the study. This is followed by the literature review Chapter 2 that outlines the aspects of erosion and erosion modelling in SSA, focusing on South Africa. Chapter 3 introduces the selected study sites and their essential attributes. Chapter 4 introduces the model WQSED model structure and discusses data inputs, uncertainties and limitations. Part two starts with Chapters 5 and 6, reporting on the spatial and temporal issues associated with the MUSLE, discussing their impacts and implications on the WQSED model and other models that incorporate the MUSLE for sediment calculation. Chapters 7 and 8 report on the application and evaluation of the WQSED

model. In Chapter 7, the model is calibrated and validated against observed data, and performance is compared to previously applied established models. Chapter 8 reports on the application of the WQSED in ungauged basins and model outputs are compared to previous modelling and reservoir sedimentation studies. Part three (Chapter 9) comprises conclusions and recommendations, discussing the entire study while linking aims to the outcomes, exploring gaps for further research, and limitations and opportunities for future research. Three peer-reviewed journal papers have been published from this thesis: Chapter 5 of the thesis has been published in Gwapedza et al. (2018a), sections of Chapters 7 and 4 have been published in Gwapedza et al. (2018b) and sections of Chapters 8 and 4 have been published in Gwapedza et al. (2020).

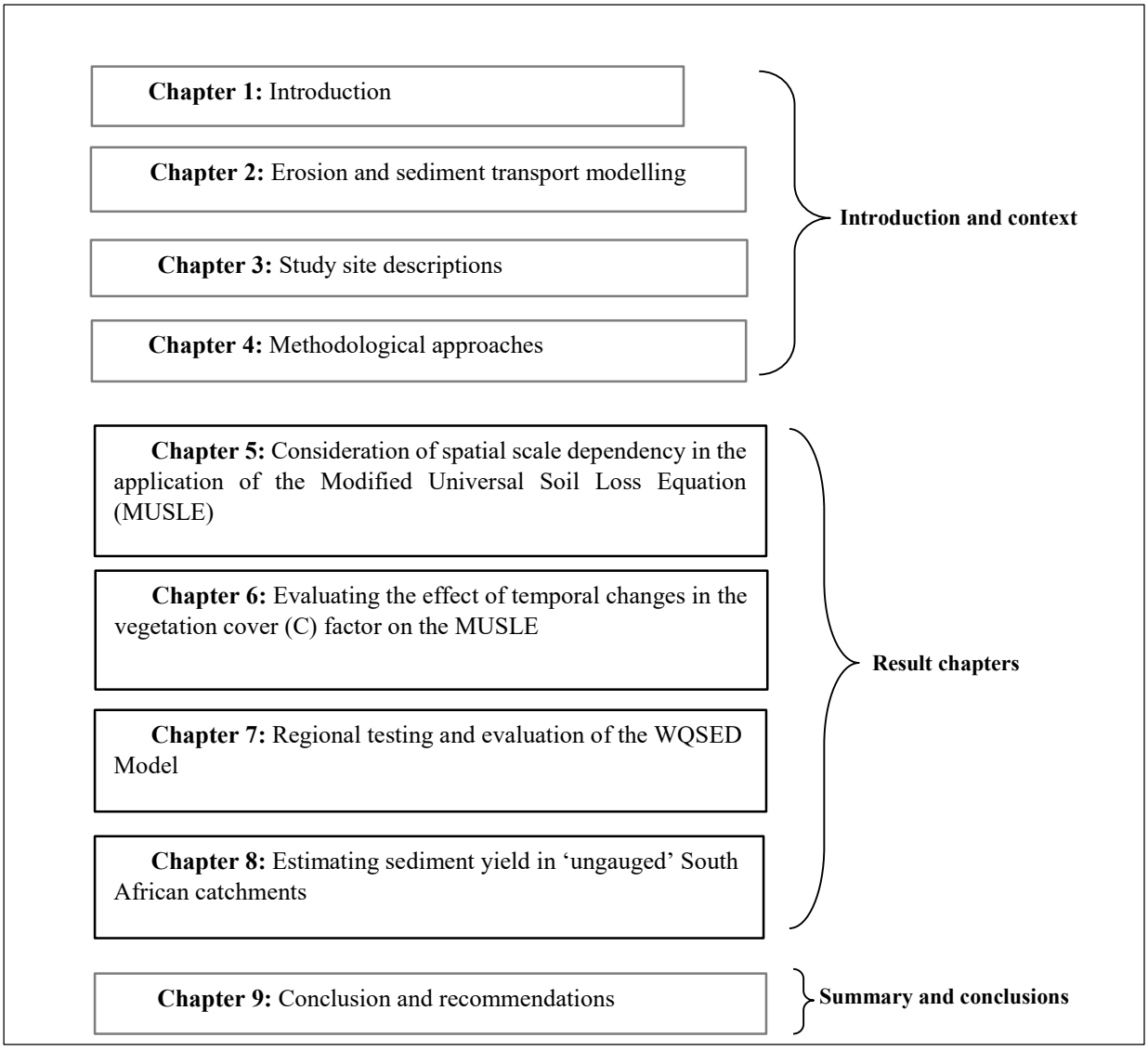

Figure 1.1 Chapter structure of the thesis.

Chapter 2 Erosion and sedimentation

Since this study aims to further develop a new soil erosion and sediment delivery model, this literature review explores relevant literature relating to erosion and sediment transport modelling. This includes literature relating to erosion, sedimentation, and primary sediment drivers such as rainfall/flow, vegetation and slope. This chapter also reviewed established erosion models and how these models vary in their representations of erosion processes and drivers. This is followed by a discussion on the application of sediment transport models in South Africa. Lastly, the review introduces the WQSED model, including a discussion of the motivation for the model, the model type and the processes represented and reasoning for their inclusion.

2.1 Introduction

Soil erosion by water is a natural process that occurs at multiple spatial and temporal scales (Kinnel, 2005). The effects of elevated soil erosion and sedimentation of surface waters through human impacts are regarded as destructive to aquatic ecosystems (Akamagwuna et al., 2019; Chislock et al., 2013); effects extend to economic and social spheres as people require ecosystem services (Pimentel and Burgess, 2013; van Tol et al., 2016). The effective integrated management of catchments requires the quantification of erosion and sedimentation and an understanding of the driving processes (de Vente et al., 2013; Karydas et al., 2014; Pandey et al., 2016). Monitoring of sediment is expensive and labour intensive, resulting in most catchments having limited observational records. Mathematical modelling of erosion and sedimentation can provide data at spatial and temporal scales not possible by monitoring. Mathematical models also help to validate our understanding of the underlying processes of erosion and sedimentation, and these models can additionally be used to investigate 'what-if' scenarios. However, models may need to be tested and evaluated before they can be deemed fit for purpose.

An assessment of a model may include a critique of the model representation of the various erosion processes and drivers. Furthermore, the assessment could focus on the spatial and temporal scales at which the model is applicable or performs more accurately. Models are sometimes developed to work at particular scales, and the rescaling of models and application in different environments raises issues of applicability (Karydas et al., 2014). While perfection in modelling may be hard to

achieve, the testing and evaluation of models can allow us to adapt models for better representation of prominent water erosion processes in diverse local conditions.

2.2 Water erosion

Soil erosion by water mainly involves the detachment, transportation and deposition of soil by surface water processes (Morgan, 2005). Dominant water erosion processes include splash, sheet, rill, gully and instream erosion (Loch and Silburn, 1996; Le Roux et al., 2015). While geologic erosion is regarded as a natural process (Morgan, 2005), accelerated erosion is a more rapid form of erosion resulting from anthropogenic activities (Desta and Adugna, 2012). This form of erosion contributes significantly to land degradation and therefore requires critical consideration.

Splash erosion results from raindrops impacting the soil surface and loosening soil particles (Morgan, 2005). A build-up of a pressure gradient around the edges of the raindrop dislodges soil particles, causing the soil surface to disintegrate (Loch and Silburn, 1996). Sheet erosion occurs when water flows over a soil surface on a gentle and smooth slope (Loch and Silburn, 1996). The 'sheet' of water flows at a relatively uniform depth and results in a relatively uniform removal of the topsoil on the land surface of a similar slope (Desta and Adugna, 2012). Rill erosion occurs when runoff flows over the soil in a defined path, thereby creating a well-defined channel of flow (Desta and Adugna, 2012). Rills are defined as small erosion features and are typically sufficiently shallow to be destroyed by tillage. Rills contribute sediment through inter-rill erosion processes (Morgan, 2005). Gully erosion refers to channels of water flow that are much larger than those operating within rills, which are likely not destroyed by tillage (Rose, 1993). Gullies can act as sediment sources, sinks and conduits. Catchments characterised by well-developed connections between the main rivers and gully networks are likely to record much higher sediment yields (Le Roux et al., 2008).

Instream erosion processes involve the removal of sediment within a river channel. These processes include lateral erosion, which involves the removal of sediment from the bank and the bed of the channel (Desta and Adugna, 2012). Slumping of the banks also occurs when there is massive undercutting of the lower stream bank, which causes the upper bank to collapse into the channel (Merrit et al., 2003). Merrit et al. (2003) state that a large proportion of sediment that is transported during high flows originates from instream storage. Sediment is deposited along the riverbed and

at confluences during periods of low flows in which there is a sudden loss of runoff energy that is typical of flashy arid catchments. Although infrequent, mass sediment movement is another form of water erosion that has the potential to deposit more sediment into the river system compared to other severe types of erosion processes, e.g. rill and gully erosion (Morgan, 2005). Mass sediment movements can take different forms, including soil creep, mudflow rockfalls and landslides, with the various forms being interrelated (Morgan, 2005).

2.3 Drivers of water erosion

2.3.1 Storm characteristics

Storm characteristics such as duration and intensity are essential drivers of water erosion and have been recognised in numerous studies across the world (Mohamadi and Kavian, 2015; Nouwakpo et al., 2016). Assessments of the relationship between rainfall intensity and soil erosion have mostly been conducted on a plot scale or as a controlled simulation experiment. Measurements of rainfall and rainfall intensity on plots have been conducted by Wischmeier and Smith (1962), Zhao et al. (2014), and Martinez et al. (2017). Wischmeier and Smith (1962) measured natural rainfall and the other researchers used rainfall simulators to investigate the effect of rainfall on erosion processes.

A study conducted in Ohio between 1934–1942 showed that the average soil loss per precipitation event increased with the intensity of a storm (Morgan, 2005), which promoted the initial theory that significant erosion is solely a function of peak rainfall intensities. However, 30 years of measurements by Wischmeier (1962) in several states of the United States of America (USA) demonstrated that the rainfall factor used to estimate average annual soil loss must include cumulative effects of the many moderate-sized storms as well as the effects of sporadic severe storms (Renard et al., 1997). However, there remains no consensus on the threshold rainfall intensity for the initiation of erosion processes. Based on studies of catchments in Zimbabwe, Hudson (1981) provides a threshold of rainfall intensity of 25 mm h^{-1}, a value that has since also been found applicable to semi-arid catchments characteristic of sub-Saharan Africa (e.g. Foster and Rowntree, 2012). However, this value is too high for Western Europe where this threshold is rarely exceeded (Morgan, 2005), and arbitrary thresholds of 10 mm h^{-1}, 6 mm h^{-1} and even 1 mm h^{-1} have been used in England, Germany and Belgium, respectively (Renard et al., 1997).

High intensity, high frequency and short duration storms have been shown to transport more sediment (Wei et al., 2007). Similarly, rainstorms with instantaneous peak intensity at the end were shown to generate higher sediment concentrations (e.g. Kaviani and Mohammadi, 2012). Raindrop impact that causes soil detachment is increased during high-intensity storms, and a period of high-intensity rainfall on an already saturated catchment will result in increased runoff. Turner et al. (2018) add that high-intensity storms have a higher erosive power that influences the processes and mechanics of water erosion.

Rainfall quantity, frequency and intensity culminate in high infiltration excess, also known as Hortonian runoff. Hortonian runoff occurs when rainfall exceeds the infiltration rate/capacity of the soil; antecedent conditions are a vital influence for the formation of runoff (Li and Fang, 2016). Furthermore, it plays a part in transporting higher sediment loads. High infiltration excess is typical in sub-humid and semi-arid areas (Li and Fang, 2016) and increases sheet-rill and even gully erosion. This phenomenon is exhibited in arid, semi-arid and sub-humid South African catchments that are characterised by extreme hydrological variability (Rowntree et al., 2016). A study by Grenfell et al. (2014) indicated that extreme rainfall events accounted for a large proportion of mean annual rainfall, with an identified historical storm contributing 22% of annual precipitation. A study by Wang et al. (2016) of a catchment in Beijing found that such high-intensity storms could contribute up to 60% of total soil erosion. High-intensity storms have contributed to extensive sheet-rill erosion and have been the cause of massive gully formation in some South African catchments (Le Roux and Waal, 2020; Mararakanye and Le Roux et al, 2012; Mararakanye and Sumner, 2017). Sediment modelling with explicit representation of gully processes have indicated that these gullies could contribute up to 95% of the total sediment load (e.g. Le Roux, 2018).

2.3.2 Vegetation

Vegetation affects runoff and sediment availability by regulating both erosion and runoff processes (Cadaret et al., 2016; Nouwakpo et al., 2016). Vegetation regulates rainfall/runoff by acting as a protective layer or buffer against the force of raindrops falling from the atmosphere to the soil (Morgan, 2005). The leaves and stems of plants absorb some of the energy of falling raindrops and running water, thereby disrupting the connectivity of runoff (Nouwakpo et al., 2016) and resulting in less force being directed to the soil (Morgan, 2005). Most rainfall is intercepted by vegetation and other ground cover during short-duration storms of low intensity (Owens et al., 2006). In fact,

shrub vegetation can intercept up to 50%–60% and 5%–35% of low-intensity and high-intensity rainfall, respectively (Owens et al., 2006; Taucer et al., 2008), resulting in a considerable delay in runoff generation.

Interception storage is exceeded during high-intensity prolonged rainfall (Dunkerley, 2008). Splash erosion is reduced and sheet-rill and gully processes that are related to flow take over. However, the litter layer below the vegetation can also reduce runoff generation by trapping water for a period of time, thereby encouraging infiltration, even in soils that have reduced infiltration capacity (Pierson et al., 2013; Williams et al., 2014). In fact, Yue et al. (2020) recorded a 68% to 97.4% decrease in runoff due to the effects of vegetation. Pierson and Williams (2016) found that rainfall interception in vegetated areas enhanced infiltration, thereby reducing event runoff by up to 95% compared to bare or sparsely-vegetated areas. Although the observations by Williams et al. (2016) were at the experimental plot scale, the demonstrated effect of vegetation on runoff might be relevant at the hillslope and catchment scale. The presence or absence of vegetation cover regulates runoff generation, thereby controlling the most destructive sheet-rill and gully processes.

Vegetation can regulate sediment availability by protecting the soil from raindrop impact and limiting the erosive energy of flow (Nouwakpo et al., 2016). By providing canopy cover and binding the soil through root systems (Morgan, 2005), vegetation cover minimises the contribution of raindrop splash in mobilising sediment in overland flow (Nouwakpo et al., 2016; Williams et al., 2016). Organic matter in soil originating from plants encourages soil aggregate stability, thus increasing soil shear strength and decreasing the susceptibility of soil to erosion (Pierson et al., 2014). An interdependency therefore exists between vegetation cover and soil erodibility, with vegetation cover increasing the resistance of soil to erosion.

The scientific consensus on the effects of vegetation on erosion has remained largely unchanged. Experimental studies indicate that the presence of vegetation cover can drastically reduce erosion (e.g. Hudson and Jackson 1959; Nouwakpo et al., 2016; Pierson et al., 2013). Hudson and Jackson (1959), in an experiment demonstrating the effect of vegetation cover on erosion, found that the mean annual soil loss over ten years was 126.6 t ha^{-1} for a bare plot and 0.9 t ha^{-1} for a plot containing vegetation (Morgan, 2005). Pierson et al. (2009; 2013) similarly report that water erosion processes are typically negligible when vegetation cover is > 50%. A recent study by Yue et al. (2020) confirmed that vegetation could reduce soil erosion by 98.0% to 99.9% compared to

that of bare land. Overall, it is generally recognised that at least 70% of the ground surface should contain vegetation cover to obtain a meaningful reduction in erosion (Elwell and Stocking, 1976), although a significant reduction in erosion can sometimes be achieved with 30%–40% vegetation cover (Morgan, 2005). The understanding of vegetation effects on erosion has led to a focus within erosion management in South Africa on improving vegetation cover (e.g. Le Roux and Waal, 2020), as recommended by Yue et al. (2020). However, Morgan (2005) warns that the effects of vegetation are far from straightforward, and under certain conditions, plant cover can exacerbate erosion, depending on how vegetation cover interacts with the erosion processes.

2.3.3 Soils

Soil erodibility describes the susceptibility of soil to mobilisation by detachment and transport processes (Renard et al., 1997). Although the resistance of soil to erosion depends in part on topographic position, slope steepness, and the degree of physical disturbance to the soil, such as that occurring during tillage, soil properties are the essential determinants (Tya and Oluwaseye, 2015). Soil erodibility is frequently enhanced by cultivation (Nearing et al., 2017; Turner et al., 2018). The failure to regulate runoff and erosion in catchments is mostly a result of poor soil health (Turner et al., 2018). Once the protective top layer of the soil is eroded away, the underlying soil horizons erode rapidly, resulting in rills and gullies. In an experiment, Ni et al. (2020) observed that soil loss gradually worsened with deeper soil horizons. Once rills and gullies expose deeper soil horizons, even low-intensity rainfall can result in considerable soil loss (Ni et al., 2020).

Soil erodibility varies with aggregate stability, soil texture, shear strength, infiltration capacity, and soil and organic and chemical contents (Renard et al., 1997). Larger soil particles tend to be resistant to sediment transport due to the greater force required for entrainment, whereas fine soil particles are resistant to detachment due to their greater cohesiveness (Renard et al., 1997). Silt tends to be the most susceptible to erosion, and fine sands and soils with silt contents above 40% are highly erodible (Richter and Negendank, 1977). Evans (1980) examined the relationship between soil clay content and erodibility and found that soils with clay content between 9%–30% are the most susceptible to erosion. A study conducted in the Mpumalanga Province, South Africa by Mararakanye and Sumner (2017) found that clay soils are more susceptible to erosion and that duplex and lithic soils are influential in gully erosion. Very shallow oxidic soils with clay and loam exhibited the most significant influence on gully processes. Catchments with duplex soils were also

reported to experience massive erosion in a catchment in the Eastern Cape Province of South Africa (Le Roux and Waal, 2020). Duplex soils are prone to tunnel erosion and dispersion as they tend to have low aggregate stability due to the high adsorption of sodium (Valentin et al., 2005). The combination of duplex soils, poor vegetation and high erosivity has accelerated erosion processes in some parts of South Africa.

2.3.4 Slope

According to Renard et al. (1997), erosion increases as slope increases, with slope length and steepness regarded as the factors driving runoff velocity (Morgan, 2005). Slope length is defined as the horizontal distance from the origin of overland flow to the point where either: 1) the slope gradient declines to a sufficient extent to initiate deposition; or 2) runoff becomes concentrated in a defined channel (Wischmeier and Smith, 1978). Slope steepness reflects the influence of slope gradient on erosion (Renard et al., 1997). Erosion is usually expected to increase with increasing slope steepness and slope length because of respective increases in velocity and volume of surface runoff (Ding et al., 2020; Morgan, 2005). Furthermore, although raindrops splash soil particles randomly on a flat surface, on sloping ground, more soil is splashed downslope than upslope, and the proportion of soil splashed downslope increases as the slope steepens (Morgan, 2005). The impact of soil erosion increases on slopes because there is a positive relationship between the degree of a slope and the amount of topsoil transported as water flows downhill into valleys and streams (Pimentel and Burgess, 2013). Therefore, slope length and steepness contribute to soil erosion by increasing the velocity of runoff, thus enhancing the erosive and transport capacity of surface runoff.

Erosion usually occurs when slope and extended rainfall coincides with poor vegetation cover (Issaka and Ashraf, 2017). Therefore, the influence of slope on erosion can be modified by land cover. Sun et al. (2014) report that under the same slope characteristics, vegetation significantly alters soil erosion. The authors note that soil erosion increased significantly as slope gradient increased. However, there were substantial differences in erosion output under different land uses because of the effect of vegetation on both slope and rainfall/runoff. Previous studies examining the drivers of gully erosion in South Africa have identified the combination of slope and poor vegetation as leading causes (Le Roux and Waal, 2020; Mararakanye and Le Roux et al, 2012; Mararakanye and Sumner, 2017). Mararakanye and Sumner (2017) determined that hillslopes

steeper than 4.5° are at a significantly higher risk of gully formation, particularly at points where overland flow accumulates. This reinforces the effectiveness of vegetation in erosion processes (Ochoa et al., 2016), and therefore vegetation regulates the impact of runoff and slope on erosion.

2.3.5 Connectivity

Within the context of soil erosion and transport, connectivity may be described as the effectiveness of a transfer zone in moving sediment between a sediment source (cut process) and sediment depositional zone (fill process) (Schumm, 1977; Fryirs, 2002). Effective connectivity can result in the deposition of mobilised sediment on lower slopes or onto a river channel as lateral bars, on a floodplain or even further downstream (Harvey, 2001). However, ineffective connectivity can limit the deposition of sediment to short distances. In general, the majority of sediment is deposited along hillslopes and valley bottoms, and only a small proportion of mobilised sediment reaches the bottom of the catchment (Walling, 1983). Three types of connectivity have been identified within the fields of hydrology and geomorphology, namely geomorphological/landscape (linking landscape units), hydrological (water movement) and sedimentological connectivity that focuses on sediment movement through a catchment (Bracken and Croke, 2007).

The effectiveness of sediment transport linkages affects sediment connectivity processes (Fryirs et al., 2007). Linkages can be disconnected, a concept that is known as dis-connectivity (Fryirs et al., 2007). The consideration of dis-connectivity or fill (deposition) processes is important within sediment budgeting as these processes can explain low sediment delivery at the catchment outlet, thus justifying the postulation of Walling (1983) on the matter. Fryirs et al. (2007) add that dis-connectivity plays a vital role in retaining water in the catchment. Depositional features resulting from dis-connectivity can become potential sources of sediment and can be grouped as buffers, barriers and blankets when they limit sediment transfer (Fryirs et al., 2007). These features limit sediment transfer by disrupting longitudinal, lateral, and vertical connectivity (Brierley et al., 2006; Fryirs et al., 2007). In contrast, connectivity can be enhanced by booster features such as gorges, incised channels and sunken lanes that act to concentrate flow and rapidly transport sediment into or through the river system (Brierley et al., 2006; Boardman, 2013).

Overall, the connectivity approach is seen as an improvement to the sediment delivery ratio method (SDR) (Walling, 1983) which is determined by comparing gross catchment erosion and sediment yield but ignores small-scale cut and fill processes and travel distance (Parsons et al., 2006).

2.3.6 Human influence

The contribution of human activities to erosion is well documented globally [e.g. the Global Assessment of Human-induced Soil Degradation (GLASOD)]. Although erosion is a naturally-occurring process, human actions can act to accelerate erosion and sedimentation (Morgan, 2005). Since the effects of humans on erosion are broad, a more concise approach of examining human influence on erosion is to examine the direct and underlying drivers of land degradation as proposed by Mirzabaev et al. (2016). Table 1 presents a list of some prominent human drivers of erosion and sedimentation processes.

Table 2.1 A list of human-induced erosion and sedimentation drivers and their impacts.

Erosion driver	**Type of driver**	**Impact**
Deforestation	Direct	Land clearing for timber and fuelwood leaves the ground surface vulnerable to raindrop and runoff impacts
Cultivation/land tillage	Direct	Cultivation loosens compact topsoil, making it highly erodible. Poor soil management practices such as ploughing on slopes and the use of heavy machinery weakens soil aggregate stability. Pesticides and fertilisers contaminate sediment.
Grazing	Direct	Overgrazing removes the protective cover of vegetation from rangelands, thereby exposing the surface to erosion. Commercial livestock production places pressure on rangelands, and communal grazing is often unplanned.
Construction /mining	Direct	Growing demand for housing, industry, and transport routes has led to the clearing of vast amounts of land using heavy machinery. Large amounts of rock and sand are extracted from river beds, and pits leave the soil structure weakened. Mining activities change the topography of the land and place tons of unconsolidated soil at risk of erosion. Pollutants from mines are absorbed by sediment.

Population density /Poverty	Underlying	A growing population needs more resources. To provide more shelter and food, more land is cleared for farming and settlement. Modification of natural land cover often results in accelerated erosion. Poverty results in opportunistic and unsustainable land use.
Climate change	Underlying	Deforestation, livestock production, burning of fossil fuels and industrial activity are collectively increasing global warming and contributing to climate change. Resultant effects such as desertification and extreme rainfall accelerate erosion processes.

(Adimassu et al., 2020; Compton et al., 2010; Dutton et al., 2018; Lobb, 2008; Nearing, 2013)

2.4 Impacts of erosion and sedimentation

2.4.1 Land degradation

Land degradation has been reported as an environmental concern globally. The Global Assessment of Human-Induced Soil Degradation (GLASOD) estimates that water erosion has degraded up to 8% of the Earth's ice-free surface. Some studies report on localised degradation (e.g. Compton et al., 2010; Gourfi et al., 2018; Mararakanye and Sumner, 2017; Ndomba et al., 2009), various regional intensities of degradation have been reported (e.g. Le Roux et al., 2008; Panagos et al., 2015), and a few studies have reported estimates of global degradation (e.g. Arekhi et al., 2012; Borrelli et al., 2017; Mirzabaev et al., 2016; Pimentel et al., 1995). The main drivers of soil erosion (e.g. land cover change, soil erodibility) are classified as proximate (direct) drivers (Mirzabaev et al., 2016), while soil erosion is categorised as a major element of land degradation. Furthermore, soil erosion is recognised as a significant driver of global land degradation (Azimi Sardari et al., 2019; Devatha et al., 2015; Ding et al., 2020; Le Roux et al., 2008; Xu and Zhang, 2020). Land degradation by erosion has resulted in reduced agricultural productivity, loss of biodiversity and a reduction in ecosystem services (FAO, 2019). As the threat of erosion-enhanced land degradation grows, the risk of desertification has prompted the United Nations Convention to Combat Desertification (UNCCD) to invest more resources and focus on measures aimed at reducing land degradation (Cowie et al., 2018). Two important approaches to combatting erosion and the resultant land degradation are to provide information on erosion and sediment management by performing field studies or mapping and by conducting modelling of erosion/sediment transport.

2.4.2 Effects of sediment on aquatic ecosystems

Eroded soils are transported by runoff into river systems. A balance in sediment supply into river systems is vital for maintaining riverine hydrological, ecological, and morphological functions (Owens et al., 2005). Sediment 'starvation' may cause river bank or channel erosion and the destruction of biological habitats (Kondolf, 1997). On the other hand, anthropogenic activities such as farming and deforestation are primary drivers of erosion (Bilotta and Brazier, 2008; Wang et al., 2020) and provide excessive fine sediments that are detrimental to the river ecosystems (Bilotta and Brazier, 2008). Excessive sediment negatively affects biological habitats and invertebrates living in them through the disruption of feeding mechanisms, abrasion, and burial (Akamagwuna et al., 2019; Bilotta and Brazier, 2008). Sediment supply ultimately alters channel morphology and impacts channel uses such as navigation. The effects of sediments on the hydrological systems can be broadly categorised as water quantity and quality effects.

2.4.3 Water quantity

The loss of reservoir storage through sedimentation by erosion and sediment transport is a phenomenon that has been observed both locally and globally (Bilotta and Brazier, 2008; Ezzaouini et al., 2020; Msadala and Basson, 2017). Numerous studies have estimated sedimentation potential for mitigating reservoir storage loss (Amore et al., 2004; Ezzaouini et al., 2020; Le Roux, 2018; Smetanová et al., 2020; Yang and Lu, 2014). The problem of reservoir storage loss through sedimentation in South Africa was highlighted by an observed rapid loss in the storage of Camperdown Dam (Rooseboom and Lotriet, 1992). Many studies on dam sedimentation in South Africa have since been conducted (e.g. Boardman and Foster, 2008; Compton et al., 2010; Le Roux, 2018; Msadala et al., 2010; Msadala and Basson, 2017). Msadala and Basson (2017) reported storage loss of up to 30% in 25% of the dams in South Africa due to sedimentation. A loss in water storage potential is particularly problematic in a water-stressed country such as South Africa that is dependent on surface water resource, and which faces periods of droughts as well as in which only 8% of the total land area generates about half the runoff (DWAF, 2013).

The problem of sedimentation is also a barrier to planned reservoirs. For example, the planned construction of two large dams in the Eastern Cape, South Africa, is under threat by excessive sedimentation (Le Roux, 2018). In fact, modelling of sediment yield has indicated that both dams

will have a life expectancy of 50 years if no measures to limit erosion in their respective catchments are implemented. Although these estimates appear to point to excessively high sedimentation, they are consistent with other estimates of sedimentation in the region (Msadala et al., 2010). The Xonxa Dam, located in the region, receives sediment loads of up to $1{,}100 \times 10^3$ t year^{-1} (Msadala et al., 2010). Another reservoir near the proposed dam sites (Mount Fletcher Dam, South Africa) has lost 33% of its initial storage capacity in just four years due to sediment deposition. A study conducted in neighbouring Zimbabwe reported that a dam in the Mazowe catchment had lost 26% of its useful lifespan due to sedimentation (Tundu et al., 2018). Therefore, the threat of erosion and sedimentation on water quantity is pertinent and of grave concern to water managers in southern Africa.

2.4.4 Water quality

The transportation of high levels of nutrients and contaminants with fine-grained sediment (<63 µm) has been widely observed (Blake et al., 2003; Ustaoğlu and Tepe, 2019). The loads of nutrients and contaminants in rivers often exceed water quality guidelines, leading to adverse impacts on water quality (Owens et al., 2005). Pollutants introduced to river systems emanate from point and non-point sources (Ustaoğlu and Tepe, 2019), and many nutrients, heavy metals and chemical contaminants adsorb to sediment particles, and are therefore transported along with sediment in river systems (Issaka and Ashraf, 2017). In particular, sediment is capable of carrying abundant heavy metals (Ustaoğlu and Tepe, 2019). High concentrations of chemicals and nutrients in rivers can compromise the health of aquatic ecosystems (Chislock et al., 2013) and result in water becoming unsafe for human consumption and agricultural production.

Sediments transported by rivers often sink in receiving wetlands and reservoirs, carrying adsorbed contaminants to the bottom. In fact, pollution of wetlands has been linked to erosion and deposition processes (Issaka and Ashraf, 2017), and deposition of excessive sediment has been reported to culminate in the deterioration of reservoir water quality (Tundu et al., 2018). While reservoirs, lakes, and wetlands can act as pollutant sinks, with water downstream from a water body significantly better than that of upstream (for example, the Laing Dam on the Buffalo River) (Slaughter, 2011), the storage of contaminants within the sediment at the bottom of reservoirs can

gradually lead to elevated concentrations of contaminants in the sediment. Pollutants stored in sediment can often be mobilised, resulting in re-contamination of the water column (Abrams and Jarrell, 1995). This can happen in particular at the end of summer when stratification of a dam breaks down, leading to turnover of the water column and disturbance of the reservoir bottom (Walker and Luke, 2019). In addition, the process of internal loading (Chislock et al., 2013), releases nutrients such as phosphorous and nitrogen from sediment during anoxic conditions. The resultant water quality problems such as eutrophication (Chislock et al., 2013) and salinisation are recognised as the prominent water quality problems in South Africa (Slaughter et al., 2017). Consequently, water quality modelling is increasingly being used to assess water quality in South Africa (e.g. Banda and Kumarasamy, 2020; Deksissa et al., 2004; Slaughter and Mantel, 2018), given the limitations of physical measurements and biomonitoring. Given the tendency for many contaminants to adsorb to sediment, it is essential that water quality models include erosion and sediment transport estimates.

2.5 The impact of climate change on erosion and sedimentation

The Intergovernmental Panel on Climate Change (IPCC) has stressed the scientific consensus that climate change has been occurring since the Industrial Revolution. Most scientists also agree that the majority of contemporary climate change is due to emissions of greenhouse gasses and rapid economic development (IPCC, 2007). Climate change-driven precipitation and temperature changes have both been reported to have increased globally (IPCC, 2013). Increases in precipitation and temperature affect rainfall erosivity and vegetation cover, which are the prominent drivers of erosion and sediment transport processes.

2.5.1 The impact of climate change on rainfall erosivity

Climate change is expected to increase the frequency and intensity of extreme rainfall events. By using rainfall data generated by downscaled General Circulation Models (GCMs), researchers have been able to apply hydrological and erosion models to evaluate the impacts of climate change on rainfall and erosion (e.g. Eekhout and De Vente, 2020).

Some studies have reported that future changes in precipitation will be accompanied by up to a two-fold increase in runoff and erosion compared to present-day conditions. For example, Zhang

(2007) reported that a maximum increase in precipitation of 18% could result in increases in runoff and soil loss of up to 112% and 167%, respectively. Similar outcomes were reported by O'Neal et al. (2005) and Pruski and Nearing (2002). Based on projected changes to runoff under climate change, Li and Fang (2016) suggest that future increased rainfall in China is likely to result in increased soil loss. However, in a study of the effect of an expected decrease in future precipitation on two agricultural plots in Texas, Pruski and Nearing (2002) found that soil loss increased on one plot and decreased on the other, thereby reflecting a non-linear response of erosion to changes in climate.

Projected increases in precipitation intensity are expected to accelerate rill and gully processes, thus increasing erosion and sediment transport through enhanced topographic connectivity (Li and Fang, 2016). As a result of increased precipitation amount and intensity, gullies are expected to extend and expand headwards by up to 300% for the projected period 2060–2089 across the world (Li and Fang, 2016). Accelerated gully expansion is expected to affect sub-tropical areas such as India and Eastern Africa (Vanmaercke et al., 2016). In comparison, intense rainfall coupled with frozen soil will result in the formation of extensive rill and ephemeral gullies in high-latitude countries (Li and Fang, 2016). In South Africa, more extreme rainfall events are expected under climate change; hence, the potential erosion risk reported in Le Roux et al. (2008) is likely to worsen. Therefore, it is vital to understand climate change effects on various erosion processes so that erosion control measures are targeted at areas that will be impacted the most. Based on the assessment of climate change on rainfall variability and the impact on erosion, it is possible to conclude that climate change will accelerate erosion and sedimentation processes and the effects thereof. Furthermore, climate change acts as a threat multiplier by eroding ecosystems and the livelihoods of people. For management and mitigation purposes, we can apply models to simulate habitat degradation, water quantity and water quality scenarios associated with erosion and sediment transport. Eekhout and De Vente (2020) suggest that the best model for this purpose will be one that accounts for both the impacts of rainfall and runoff as climate impacts may impact both these hydrological processes differently.

2.5.2 Climate change impact on vegetation

Climate change impacts are linked to vegetation because of the effects of vegetation on erosion that have been highlighted in previous sections. Li and Fang (2016) propose that changes in climate can

modify vegetation cover and that regional variations in vegetation will occur as a result of warming temperatures. Climate change is likely to decrease the area of arable land in Kenya by 20% by 2030 (Maeda et al., 2010). Similar results were reported in Southern China in which a 3˚C increase in temperature resulted in a 13% increase in sediment yield (Li and Fang, 2016). However, contrary results were predicted in the El Reno watershed in the USA where climate change was predicted to reduce runoff and erosion because of the increase in evaporation and improved growth of crops induced by higher air temperatures (Zhang and Nearing, 2005). Li and Fang (2016) propose two explanations for the spatio-temporal effects of temperature on soil erosion: (1) temperature rise might selectively contribute to vegetation vitality, stimulating growth in some types of vegetation and inhibiting the growth of others such as winter wheat; (2) high evapotranspiration rates resulting from extreme temperature changes could reduce plant growth, subsequently exacerbating erosion processes.

While increased plant biomass stimulated by temperature increases can counteract the negative effect of increased precipitation on soil erosion processes (Zhang and Nearing, 2005), indications are that soil erosion processes will probably worsen under future climate change. The positive effects of climate change are somewhat limited, and therefore measures to reduce the impact of climate change should be established (Li and Fang, 2016). Some preventative measures to protect the soil from erosion processes include conservation tillage, no-till (Lobb, 2008), afforestation/rangeland rehabilitation (Le Roux and Waal, 2020), and the planting of drought-resistant crops (Li and Fang, 2016).

2.6 Erosion, sediment yield and sediment transport models

Numerical models are useful tools for the estimation of erosion and sediment yield from a catchment, as well as for the analysis of land use impacts on sediment generation (Schmidt et al., 2008). Water erosion processes are complex and variable, and models can be used to simplify, explain, and investigate complex natural processes, and facilitate the investigation of management scenarios. Models are also useful to test our conceptual understanding of erosion and sediment transport processes. They provide vital information for management where it is not feasible or practical to conduct field measurements over a large spatial or temporal extent (Nearing et al., 2005).

2.6.1 Empirical, conceptual, and physically-based erosion, sediment yield and sediment transport models

Water resources models are generally categorised into three groups based on the process they simulate and the algorithms and data they use (Merritt et al., 2003): (1) empirical; (2) conceptual; and (3) physically-based models. In a review of erosion and sediment transport models, Merrit et al. (2003) found that the differences between these three broad categories of models are not always apparent and could be viewed as subjective in some cases. A mix of modules (de Vente and Poesen, 2005) within a single model which encompasses multiple model categories entrenches the subjectivity; empirical components are often embedded within complex rainfall-runoff models, such as the Soil and Water Assessment Tool (SWAT) for example (Arnold et al., 1998; Neitsch et al., 2005), which has been classified as both conceptual (de Vente and Poesen, 2005; Roux et al., 2007) and physically-based (de Vente et al., 2013; Pandey et al., 2016). The current understanding of erosion and sediment transport processes used to develop the different groups of models has been generated mostly using empirical observations from plots and controlled laboratory simulations.

Empirical models are defined as the simplest of the model types (Merrit et al., 2003). Wheater et al. (1993) highlight that they are primarily based on the analysis of observations and aim to characterise system response based on observations with little or no inferences to the processes involved. The most popular empirical models are the USLE and later derivatives MUSLE and RUSLE. Empirical models have fewer computational and data requirements compared to other types of models. Empirical models maintain a high level of temporal and spatial aggregation and are often criticised for unrealistic generalisations of the catchment system (Merritt et al., 2003), ignoring heterogeneity of previously discussed drivers such as rainfall, vegetation, and soils. While the criticism is valid, simple empirical models can be the most suitable option for regions with scarce data as they provide some valuable simulations using minimal data input. Merrit et al. (2003) add that insufficient data often causes some more complicated (conceptual and physical) models to assume that the underlying conditions remain unchanged during the simulated period.

Conceptual models tend to aggregate the spatial and temporal scales of the process but still maintain the conceptual understanding of the essential processes of the system, thereby distinguishing these models from empirical models (Merritt et al., 2003). Conceptual models generate generalised

descriptions of catchment processes but exclude finer details of process interactions that would require detailed catchment data (Sorooshian, 1991). Conceptual models can give qualitative and quantitative feedback on the effects of, for example, vegetation, using limited temporal and spatial data inputs (Merritt et al., 2003).

Physically-based models are characterised by a much more sophisticated model structure than those of either empirical or conceptual models and are based on the solution of physical equations describing the mass and momentum of flow and sediment transport in a catchment (Merritt et al., 2003). According to Le Roux (2008), physically-based models are usually spatially distributed and event-based and therefore have large data requirements compared to empirical and conceptual models. For example, most equations used in physically-based models were developed from small-scale studies with specific conditions, thereby bringing their application to catchments into question (Beven, 1989).

2.6.2 Spatial scale: appropriate scales for application of models

Environmental models are developed for wide-ranging applications, and therefore consider varying temporal and spatial scales (Pandey et al., 2016). Sediment yield models can be classified as field- or watershed-scale models based on the scale at which they can be applied. Field-scale models generally do not consider spatial variability, and therefore maintain spatial uniformity in rainfall and homogeneity in soils, and consider a single land cover. Field-scale models can generally be applied to plot areas <10 km^2, and they usually emphasise onsite impacts of rainfall/runoff sheet-rill processes (Karydas et al., 2014). In contrast, watershed/catchment-scale models are more advanced, emphasising spatial variability of physical catchments' attributes and generally considering catchment areas of >1,000 km^2 (Pandey et al., 2016). Watershed-scale models may divide the watershed area into smaller homogenous units, following which routing functions are employed to move sediment across the entire basin (Pandey et al., 2016).

Karydas et al. (2014) affirm that the ability of geographic information systems (GISs) to manipulate large datasets has enabled the rescaling of models, which is a common phenomenon for USLE-based approaches. This involves the modification of existing components or inheriting modules from existing models. Some models have evolved completely, e.g. the EUROSEM model (Morgan et al., 1998) evolved from a field-scale event-based model to a watershed- and annual-scale model

implemented within a GIS environment. However, negative consequences of rescaling can occur because most erosion parameters are potentially scale-dependent; data collected at plot scale can be inappropriate for use at the watershed scale (de Vente et al., 2013). The scaling up of models through data aggregation leads to Modifiable Areal Unit Problem (MAUP) biases, whereas inverted biases (ecological fallacy) can result from scaling a model down (Karydas et al., 2014). Wong (2009) adds that after spatially aggregating or disaggregating data, tabulated results for different scale levels will not provide a consistent analysis of results. Potential rescaling effects may need to be investigated as part of model development and testing.

2.6.3 Spatial scale: lumped and distributed modelling approaches

Models can be classified as lumped or distributed based on the spatial representation of the catchment they are applied (see Figure 2.1). The classification can be based on the degree to which parameters of a model that influence the modelling of erosion and sediment transport processes are spatially distributed across the modelled catchment (Pandey et al., 2016). Merit et al. (2003) state that while the lumped parameter approach has traditionally been used in models, the exponential increases in computing power have encouraged distributed approaches. Distributed approaches reflect the spatial variability of processes in reality and are more applicable to sediment transport modelling. Typically, distribution involves dividing the catchment into computation grids, where the outputs of each grid are routed through the system and collated to produce catchment scale outputs. Challenges regarding data requirements have arisen in connection to grid size as smaller grids result in increased data requirements if grids require spatially-dependent information. A compromise between lumped and distributed models (semi-distributed) breaks the catchment into a series of sub-catchments (or hydrological response units – HRU) (see Figure 2.1), where the model is applied, and outputs routed to the outlet (Merritt et al., 2003; Pandey et al., 2016). While the lumped approach is less data demanding, it allows for little spatial variability to be accounted for; however, such an approach may be the most appropriate for data-scarce catchments.

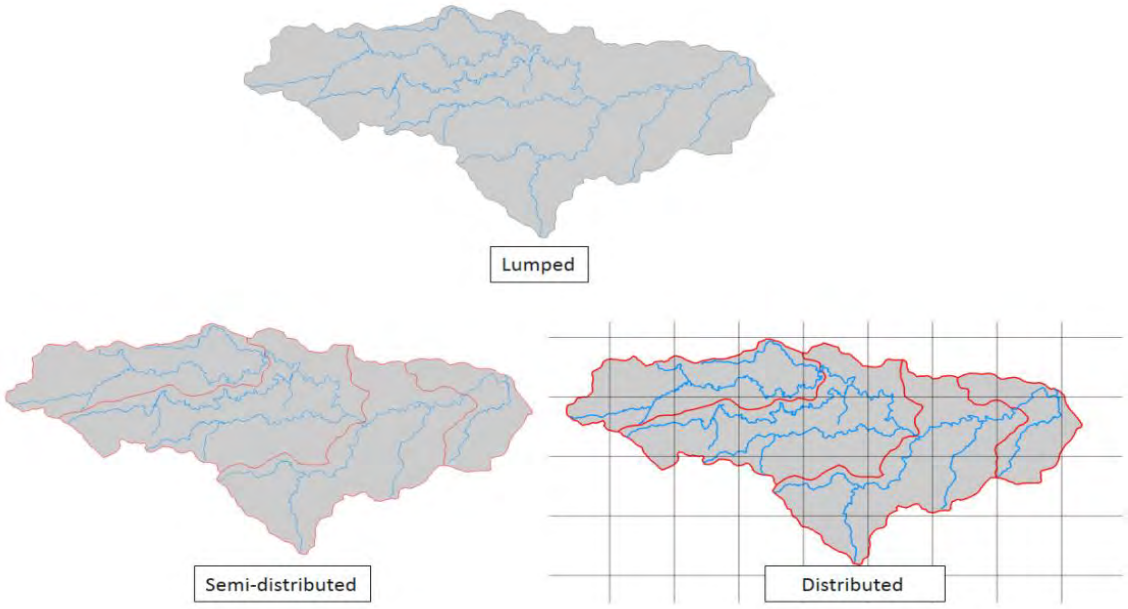

Figure 2.1 An illustration of the three spatial distribution approaches used in sediment yield and transport modelling.

2.7 Application of erosion and sediment transport models in South Africa

Although several international sediment yield and transport models have been developed, only a few of these models have been widely applied in sub-Saharan Africa (SSA). There have been very few cases of application of physically-based models in SSA as the data requirements of these models can rarely be met within the application to SSA catchments without dedicated and costly monitoring programmes (Smith, 1999). Empirically-based models have thus been widely applied to SSA catchments over the years, with the RUSLE found to provide acceptable trends and magnitudes in soil loss estimation (Smith, 1999). Le Roux et al. (2007, 2008) and Le Roux (2012) applied RUSLE to predict water erosion at a national scale in South Africa and produced maps that show the spatial distribution of erosion across the country. The maps were validated successfully (based on the presence and absence of erosion) and are valuable for land rehabilitation planning. However, because the USLE and RUSLE are only capable of calculating long-term sheet and rill erosion (Alewell et al., 2019), they are not appropriate for event-based simulation. This has necessitated the adoption of an event simulation-based model based on the MUSLE (e.g. SWAT) for recent applications in South Africa (see Le Roux, 2018; Scott-Shaw et al., 2020).

Le Roux et al. (2015) applied SWAT for the simulation of sediment yield in the Mzimvubu River catchment in South Africa and reported a mean sediment yield of 1 t ha^{-1} yr^{-1}. The performance of SWAT was not validated in their study because of a lack of observed data. Recently, Scott-Shaw et al. (2020) applied SWAT to a small agricultural catchment in the province of KwaZulu Natal and similarly failed to thoroughly calibrate and validate the sediment output of the SWAT model. The lack of recorded sediment data with which to calibrate and validate sediment transport models remains a significant limitation in South Africa (Van Zyl, 2007). However, in both studies, the output of SWAT enabled the identification of sub-basin contributions to total catchment sediment output, thus highlighting potential source areas.

The Agricultural Catchments Research Unit (ACRU) model (Schulze, 1995) was developed in South Africa. ACRU was recently applied by Otim et al. (2020) to simulate sediment yield from sugarcane fields, with good model performances of > 0.7 Nash Sutcliffe coefficient of efficiency (NSE) (Nash & Sutcliffe, 1970) achieved. Although calibration of the model was not explicitly reported, other studies, e.g. Le Roux and Sumner (2013), report successful application of the ACRU model in South Africa. This model has some similarities to SWAT, including the use of the MUSLE to calculate sediment, a rainfall-runoff model to drive erosivity and a channel module that routes sediment through the catchment. ACRU simulates daily sediment output similar to SWAT. Additionally, ACRU employs a semi-distributed model approach for large catchments and lumps smaller units. Neither the SWAT nor the ACRU models include sediment storage and deposition of sediment expected over larger catchments (de Vente and Poesen, 2005). Another disadvantage is that both models often require the preparation of a large amount of data.

2.8 Incorporating a sediment model into a South African water resources modelling framework

The WQSED model, applied in this study, was developed to provide a model that represents the processes of predominantly semi-arid catchments in South Africa. Maintaining simplicity was considered vital as (1) there are insufficient data available to operate a distributed process-based model; (2) the model should be applicable at the catchment scale where management decisions are usually made; (3) model users in national regulatory agencies are likely to have limited modelling experience; and (4) the model should integrate with the Water Quality Systems Assessment Model (WQSAM) (Figure 2.2). The WQSAM model is the only water quality model that "directly and

seamlessly" links to the Water Resources Yield Model (WRYM) (Basson et al., 1994) and the Water Resources Modelling Platform (WReMP) (Mallory et al., 2011; Slaughter et al., 2017), which are the only system yield models that have become established within water resources management in South Africa. Therefore, WQSAM (and by association WQSED) is directly aligned for practical use within the country's water management framework (Slaughter et al., 2017).

2.8.1 Pitman model

The Pitman rainfall-runoff model was chosen to simulate the flow driver of sediment yield because the model has been developed specifically for and is widely used in SSA (Hughes, 2004, 2013; Kabuya et al., 2020). The model is also part of an interlinked suite of models (including WRYM and WQSAM) that form the Spatial and Time Series Information Modelling (SPATSIM) framework (Hughes and Forsyth, 2006) that are commonly used for water resources management in South Africa.

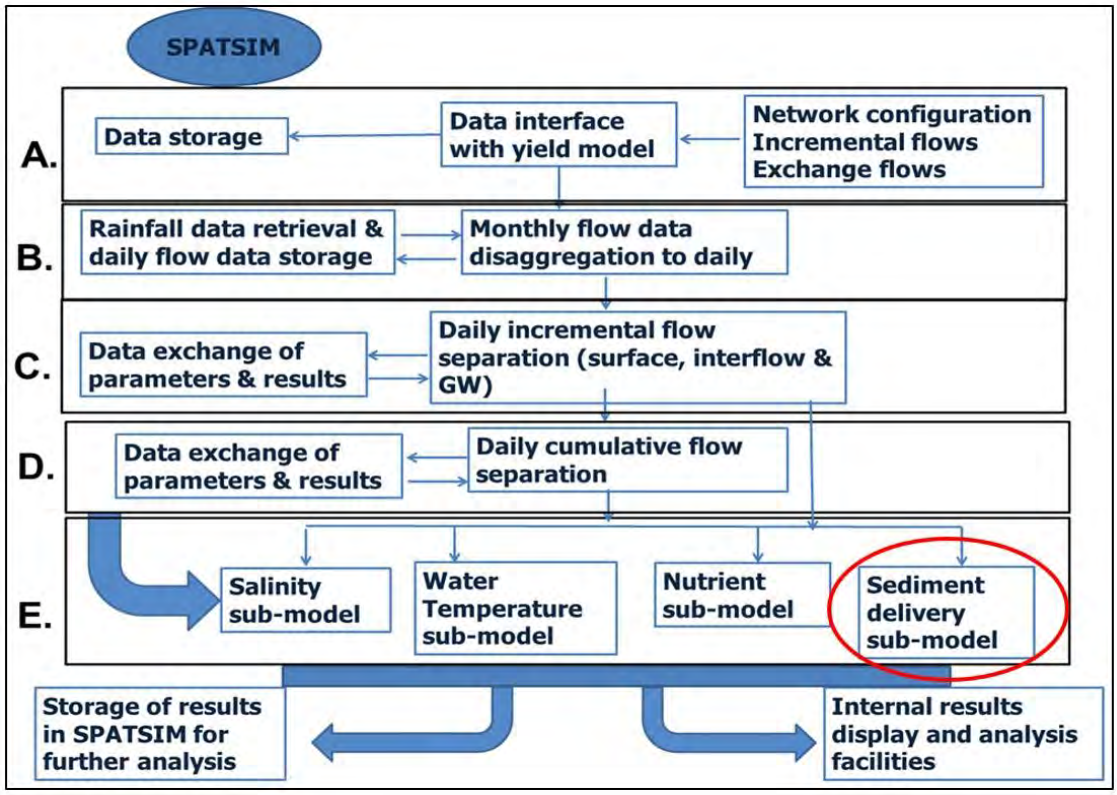

Figure 2.2 Conceptual representation of the WQSAM model within the SPATSIM framework The sediment delivery sub-model (WQSED) is circled in red.

Within the SPATSIM framework, the Pitman model is typically used to generate incremental flows for the WRYM, which feeds into the WQSAM model within which the WQSED will be integrated (see Figure 2.2). The emergent properties that influence erosion and sediment transport that are represented by the hydrological model within the WQSED model are spatial-temporal variability of flow and the relationship between vegetation and flow. The Pitman model provides monthly simulations of surface runoff, and these have to be disaggregated to daily flows before being used with WQSED. The disaggregation model of Hughes and Slaughter (2015) and Slaughter et al. (2015) is commonly used to disaggregate monthly flows within the SPATSIM framework. Recent developments of the Pitman model have been aimed at improving the simulation of different runoff components (see Hughes and Mazibuko, 2018; Hughes, 2019).

2.8.1.1 Disaggregation of monthly incremental flows to daily flows

Since the Pitman model simulates monthly flows and WQSED requires daily flows, the approach taken within WQSED was to disaggregate monthly flows to daily. This disaggregation method was first implemented for use in the Water Quality Systems Assessment Model (WQSAM) (Slaughter et al., 2015), which also requires daily flows. However, the method is applicable within any hydrological application where daily flows are required, such as in WQSED. The detailed approach adopted within the disaggregation model is presented in Slaughter et al. (2015). The conceptual approach taken within the disaggregation model is shown in Figure 2.3.

A summary of the disaggregation process is as follows. First, any observed daily flow data for the catchment are used to derive the flow duration curve (FDC) month to day scaling factors (1 in Figure 2.3). The mean monthly flow and daily flow duration curves are plotted on the same graph. A third FDC is then plotted by scaling the monthly FDC to the same shape as the daily FDC, with particular attention paid towards achieving the highest flows represented in the daily FDC (2 in Figure 2.3). The parameters of the scaling equation are calibrated to achieve a representative scaled FDC. The calibrated scaling equation is then used to scale the simulated monthly FDC to a daily FDC. A minimum of one, but as many as three, time series of daily rainfall data representative of the catchment of interest and time period of the simulation are then collated to derive a single time series of daily antecedent rainfall (3 in Figure 2.3).

The use of antecedent rainfall is designed to generate a continuous time series of an index of catchment 'wetness' (or moisture storage) from a discrete time series of rainfall. The parameters of the approach include a threshold depth (mm), below which rainfall is assumed to be directly evaporated from the surface and does not contribute to moisture storage. The other parameter represents a storage decay parameter that controls the rate of decreases of moisture storage after individual rainfall events have been added to storage.

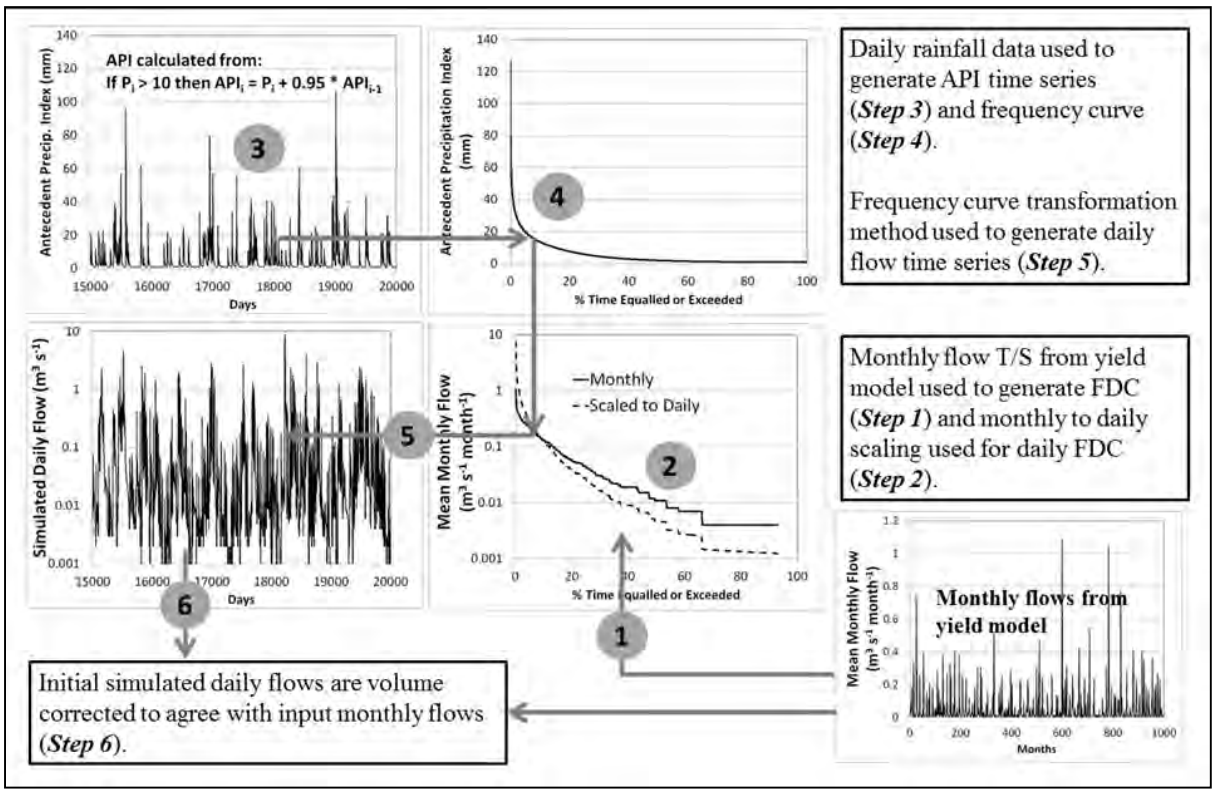

Figure 2.3 The conceptual framework of the monthly-to-daily flow disaggregation method (Sourced from Slaughter et al. (2015)).

Daily rainfall for the disaggregation process is typically derived from ground-based weather stations; however, Hughes and Slaughter (2015) found that the use of global rainfall datasets, such as remote sensing estimates of rainfall, could successfully be used within the disaggregation model. The collated time series of daily antecedent rainfall is then used to generate a daily antecedent rainfall frequency distribution (4 in Figure 2.3). The disaggregation model then steps through the time series of daily antecedent rainfall, and for each day:

a) Determines the frequency of the rainfall from the antecedent rainfall frequency distribution.
b) Identifies the equivalent daily flow for the frequency derived from the scaled FDC in (a), thereby producing a time series of daily flow (5 in Figure 2.3).
c) The time series of daily flows produced in (b) is volume corrected against the original monthly flows (6 in Figure 2.3).

Slaughter et al. (2015) found that the volume correction (c in the list above), which ensures that daily flows summed to monthly volumes are equal to the monthly flows, reduces the sensitivity of the model to some of the parameters, thereby preventing the generation of drastically incorrect disaggregated flows. The disaggregation model has been widely used in African catchments and most recently by Makungu (2020) and (Kabuya et al., 2020).

2.8.1.2 Separation of daily flows into flow fractions

Subsequent to the disaggregation, daily flows are separated into surface flow, interflow, and groundwater, using a simple statistical baseflow separation method (Hughes et al., 2003). This approach requires the setting of two parameter values, whereas the value of a third parameter remains constant as recommended by Hughes et al. (2003), and the approach taken in setting these values is typically to use values determined during previous hydrological modelling studies in similar catchments. This may introduce a source of uncertainty; however, a rigorous determination of appropriate parameter values for the flow separation method is complicated (Kapangaziwiri et al., 2011) due to a number of reasons: the general lack of observed data with which to validate flow separation methods, the range of baseflow separation methods available and the conflicting results they generate, the difficulties in distinguishing between the origins of surface water in regards to flow fractions, and the disparity in temporal scales at which the different flow fractions operate.

2.8.2 Background to WQSED model development

In developing the WQSED model, the issue of scale in sediment delivery modelling was dealt with by focusing on the sediment cascade (Schmitt et al., 2016), incorporating an analysis of connectivity within the catchment which involves features that act as sediment sources, sinks and conduits to transfer sediment (Fryirs et al., 2007). Geomorphologic features that act as sources of sediment include badlands, gully, and the rest of the catchment area from which sediment is derived. Sediment sink features include flood outs and reservoirs (Fryirs et al., 2007). Gully

systems and channels transfer sediment from slope storage to channel storage. Gullies (that are connected) are considered to be a part of drainage features as they are formed by streams eroding head-ward into hill slopes.

An assessment of the emergent properties of semi-arid catchments was performed during the development of the WQSED. The drivers of sediment yield in semi-arid and arid SSA catchments were divided into the categories of climatic, topographic, and connectivity drivers (Bryson, 2015). Distribution function theory was adopted to represent runoff, erosion, and sediment delivery in a simplified way. Sidorchuk et al. (2004) highlight that models based on this approach use mechanistic representations of physical processes and have the benefit of calculating soil detachment and erosion factors from probability distributions and stabilising forces. Similar to the reformulated Basin Sediment Model (BSM) (Moore 1984), the WQSED uses a statistical approach to define sediment accretion and removal by runoff. The approach was considered an advantage because while it attempts to provide a distributed description of the catchment, the approach is less complicated and requires fewer parameters compared to fully-distributed models. Such an approach conforms with Merrit et al. (2003) 's recommendation that models developed for application in data-poor environments be stripped to basic levels, retaining only those processes that impact generation and export processes.

Consequently, three distribution functions, namely sediment availability (soil loss), sediment transfer (storage), and sediment removal (delivery) were considered within the WQSED model. These functions are associated with an erosion model and a hydrological model. Based on the distribution functions, three model components were conceived:

1. Sediment storage and delivery estimation
2. Surface flow estimation based on the Pitman model (Pitman, 1973; Hughes, 2013)
3. Erosion estimation (based on the MUSLE)

Linking existing approaches increases the likelihood of use by water resources managers and ensures that established routines do not require redevelopment while making creative use of existing approaches (Gao, 2008).

2.8.3 The MUSLE

The MUSLE is an improvement of the USLE developed by Wischmeier and Smith (1978). The USLE and the revised versions (RUSLE and MUSLE) are among the most widely used erosion and sediment yield models to compute potential erosion and sediment yield in the fields of hydrology and environmental engineering (Mishra et al., 2006). The USLE was initially conceived to estimate the rate of soil loss from small plots. Subsequently, when applied to larger spatial scales, the USLE gave significant errors (Kinnell, 2005). The USLE was developed to estimate long-term annual erosion, and it is generally considered inappropriate for estimating erosion or sediment yield for individual storm events over large areas (Kinnell, 2005). This was attributed to the fact that the USLE does not directly consider runoff. Instead, the USLE is used together with delivery ratios to determine sediment yield; however, the ratios may not always be predicted accurately because they vary considerably due to temporal changes in rainfall (Arekhi et al., 2012). Because of uncertainty surrounding the delivery ratio, Williams and Berndt (1977) proposed the MUSLE, which replaces the rainfall factor with a runoff factor. The MUSLE increases the accuracy of sediment yield prediction by incorporating flows and eliminates the requirement for delivery ratios (Arekhi et al., 2012).

According to Sadeghi et al. (2013), combining the sediment delivery ratio (SDR) with gross erosion to determine sediment yield is tedious if one is interested in particular rainfall events. The rainfall factor of the USLE does not adequately account for the effective rainfall that generates sufficient runoff to mobilise sediment, which is an important factor in erosion and sediment delivery (Sadeghi et al., 2013). Williams (1975) used 778 storm-runoff events collected from 18 small watersheds (in the USA), with areas varying from 15 ha to 1 500 ha, slopes from 0.9% to 5.9% and slope lengths of 78.64 m to 173.74 m (Williams and Berndt, 1977) to generate the Modified USLE (MUSLE) in the following general form:

$$Sy = \alpha \times (Q \times qp)^b \times K \times L \times S \times C \times P \qquad \text{(Equation 2.1)}$$

where *Sy* is sediment yield (in tonnes) on a storm basis for the entire catchment, *Q* is the volume of runoff (in m^3), *qp* is the peak flow rate (in $m^3\ s^{-1}$) and *K*, *L*, *S, C* and *P* are the soil erodibility (in $t\ ha\ h\ MJ^{-1}\ mm^{-1}$), slope length, slope steepness, crop management and soil erosion control practice factors, respectively, similar to the USLE, and *a* and *b* are location coefficients. For the

area (Oklahoma and Texas) where the equation was developed, the *a* and *b* coefficients were 11.8 and 0.56, respectively (Williams and Berndt, 1977).

A review of the international application of the MUSLE by Sadeghi et al. (2013) evaluated the applicable conditions and methods used to determine the MUSLE parameters. The trends in the methodology to determine the factors in the MUSLE indicated that for the erodibility factor, most values were obtained from the Wischmeier and Smith (1978) diagrams, with the erodibility estimation methodology not affecting the accuracy of the results. The topography factor was estimated by the direct use of a topographic map at a scale of 1:50 000 in most studies, with the use of GIS providing greater efficiency in parameter estimation and improved performance of model estimates. Crop management and control practice factors were mainly estimated by using existing data, with the incorporation of temporal variation of these factors resulting in significant improvements in performance. MUSLE was shown to yield different results (overestimation and underestimation) in different areas but showed better performance in conditions similar to where it was initially developed. In other applications, MUSLE was embedded within other models making it difficult to attribute model performance solely to the MUSLE. Sadeghi et al. (2013) concluded that application of the MUSLE might provide consistent results when applied under appropriate conditions similar to those of the original model, or when the model factors are calibrated accordingly. Arekhi et al. (2012) departs from the notion of calibrating the original, citing improper application of the model, and advising the collection of more continuous, reliable observed data (corroborated by Sadeghi and Mizuyama, (2007)) for testing the MUSLE before any modification.

2.9 Summary

Water erosion and sedimentation processes have been shown to vary spatially and temporally. Erosion gradually worsens from sheet to rill and gully processes as rainfall intensity and duration and amount increase. Apart from rainfall, physical factors that include slope soils and vegetation can aggravate erosion processes. Vegetation could be a vital erosion controlling factor as it increases soil resistance to erosion and depletes the slope effect on runoff energy. Erosivity and vegetation are the essential factors in erosion and sediment processes, and should therefore be prioritised in erosion studies.

Through human activities, land cover undergoes transformation exposing the soil to other erosive forces. Without the protective cover, the effects of erosion will lead to increased land degradation. Degradation affects water resources, depleting the storage capacity of dams and silting up river systems, resulting in disruption of the aquatic ecosystem. Water quality problems such as nutrient and heavy metal contamination can make water unsafe for human and agricultural use. All the adverse effects of erosion and sedimentation are likely to be exacerbated by climate change. However, the majority of problems emanating from erosion and sedimentation are of a human construct; positive human behaviour to minimise the erosion effects can moderate the degradation of the environment. The reviewed erosion processes and influencing factors are essential for the study because they point to some of the main concepts and critical processes that should be considered within a model that estimates erosion and sediment transport.

Models are presented as tools to generate information that can be used to understand erosion processes and their spatial distribution. Although many models have been developed worldwide, only a few sediment transport models have been applied in parts of South Africa, sometimes without calibration or validation because of lack of appropriate observed data. Therefore, previous studies have focused on long-term erosion for reservoir sedimentation and land rehabilitation, overlooking sediment as a water quality problem. The large data requirements of physical and complex conceptual models have restricted their application. Although simpler empirical models such as RUSLE have been applied extensively in South Africa, their failure to simulate event sediment yield has constrained their adoption for application at finer temporal scales. Additionally, problems associated with rescaling models developed at the plot scale for catchment-scale applications in South Africa require more investigation. As noted above, a recently developed sediment transport model (WQSED) links an event-based lumped empirical model (MUSLE) to a semi-distributed hydrological model (Pitman) and incorporates storages and delivery components. In this study, the WQSED model will be applied, tested and evaluated in catchments in South Africa and southern Africa where continuous daily observed sediment loads can be accessed. Scale issues associated with (rescaling) the MUSLE sub-model will be assessed. The testing will be the first comprehensive testing of the model since it was developed and is expected to yield an appraisal of model performance and inform improvements and further developments before integration with the WQSAM and broader use by the water resources community for practical assessments and research.

Chapter 3 Study site descriptions

3.1 Introduction

This chapter describes the study areas in South Africa and Zimbabwe (Figure 3.1) in which the erosion and sediment transport model (WQSED) was tested. The selected South African catchments are widely spread across the country to represent the variability in climatic, topographical, vegetative and soil conditions of South African catchments. Overall, catchment selection was constrained by the availability of observed daily sediment output or long-term reservoir sediment.

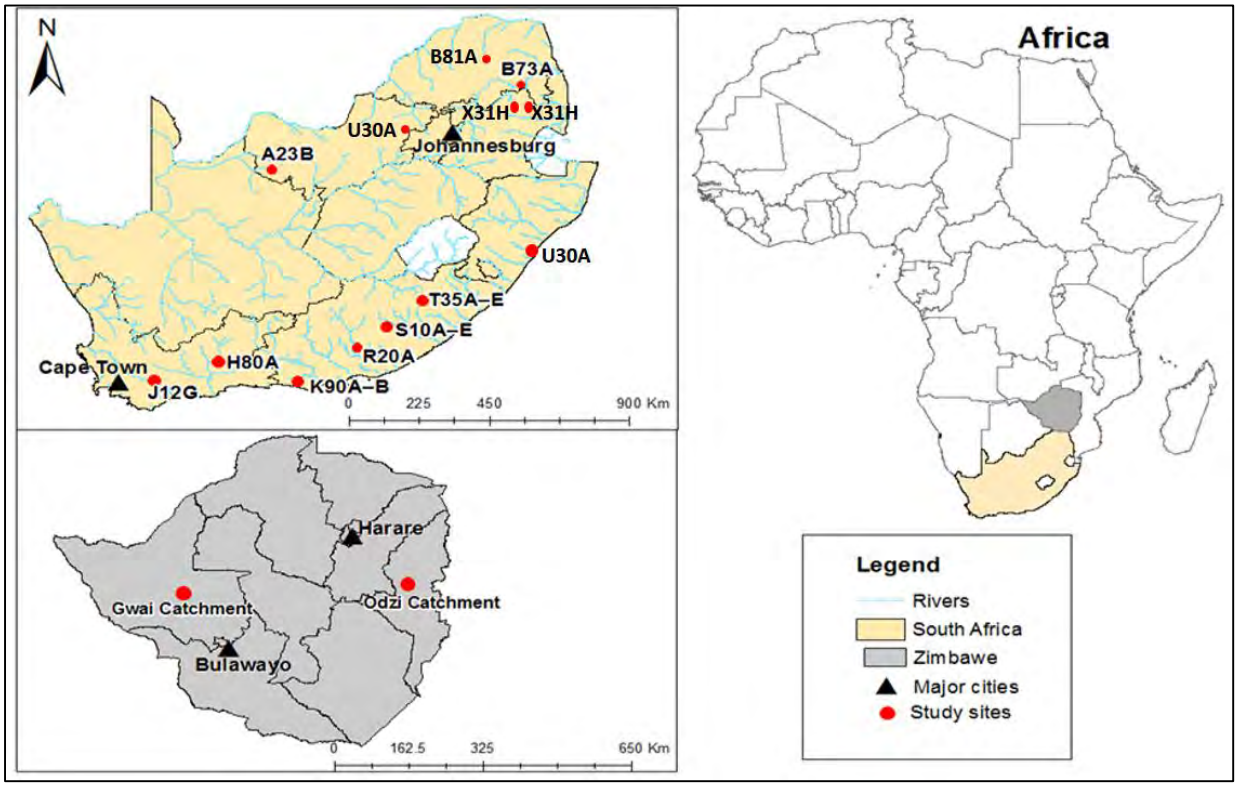

Figure 3.1 A map of all the selected study sites in South Africa and Zimbabwe.

Most of the selected catchments contain major dams with observed dam sedimentation data. These sedimentation data were compared with long-term sediment yield rates estimated by the WQSED model. Note that continuous daily sediment discharge data are not widely available/accessible in South Africa. The Zimbabwean study sites were selected to allow a regional calibration, validation

and evaluation of the WQSED model using observed daily sediment records. Observed instream sediment records were accessed only for the Tsitsa (South Africa), Gwai (Zimbabwe) and Odzi (Zimbabwe) river catchments as part of regional testing and evaluation of the WQSED model in Southern Africa (Chapter 8).

An additional three catchments within the United States of America (USA)and territories of the USA (Figure 3.2) were selected due to the availability of continuous daily observations of sediment yield. Catchments in the USA which do not experience significant snowfall were selected to avoid cold-region processes that would not be representative of typical southern African catchments for which the model has been developed.

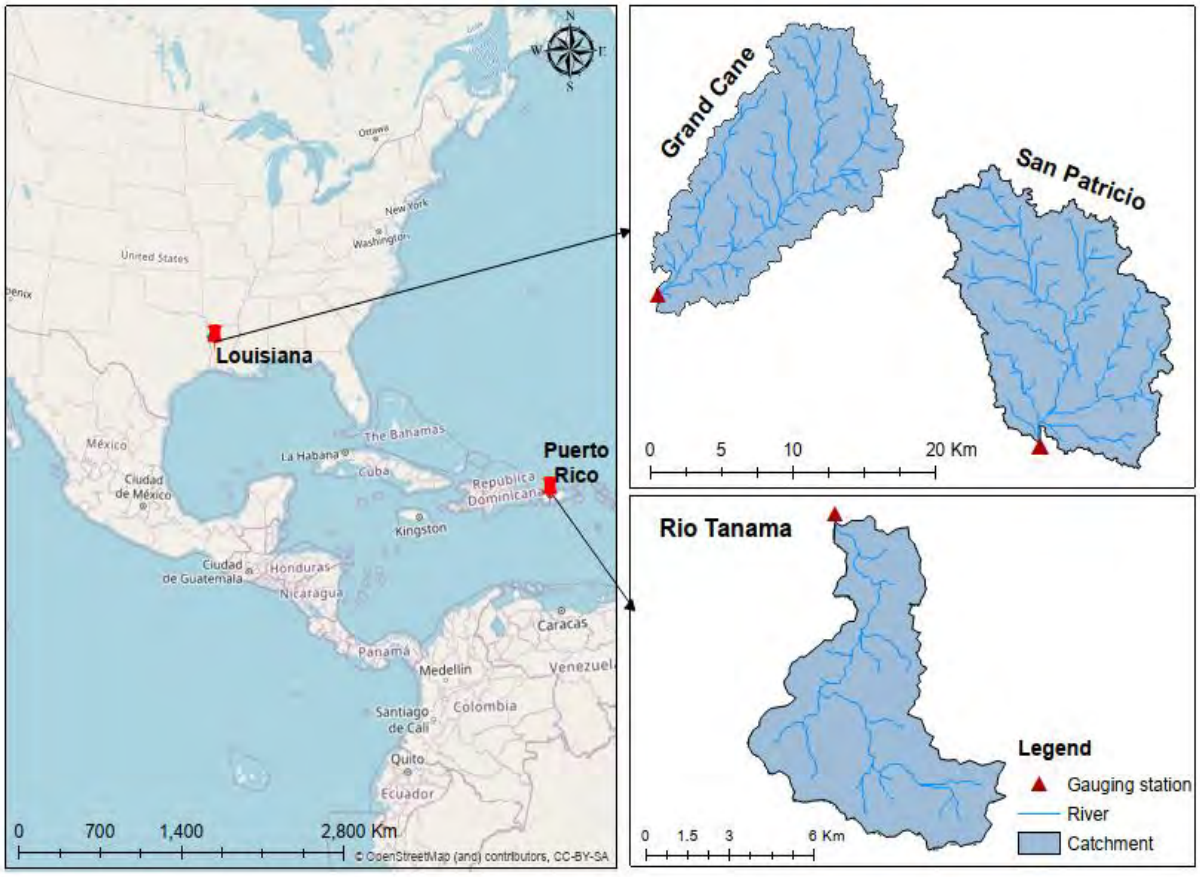

Figure 3.2 A map of the selected study sites in the United States of America (USA) and overseas territories of the USA.

3.2 Catchments physical characteristics

Table 3.1 A summary of catchment physical characteristics.

Name	Location	Size (km^2)	Climate zone	Altitude (m)	MAP (mm)	Average monthly temperature (°C)
T35A–E	Eastern Cape, SA	2 016	Sub-humid	900–2 500	914	15
S10A–E	Eastern Cape, SA	1 282	Sub-humid	900–2 000	567	18
R20A	Eastern Cape, SA	31	Temperate	600–1 400	1 500	17
K90A–B	Eastern Cape, SA	362	Temperate	200–600	700	17
H80A	Western Cape, SA	150	Temperate	600–1 200	500	15
J12G	Western Cape, SA	768	Semi-arid	300–1 900	700	17
A22B	North West, SA	187	Semi-arid	700–1 500	600	19
B73A	Limpopo, SA	136	Subtropical	500–1 500	600	22
U30A	KwaZulu-Natal, SA	382	Subtropical	100–1 068	900	18
X22E	Mpumalanga,SA	60	Semi-arid	1 000–1645	600	17
X31H	Mpumalanga,SA	44	Semi-arid	889–1 658	600	17
A21K	North West, SA	116	Semi-arid	1 200–1 845	600	19
B81A	Limpopo,SA	126	Subtropical	1 489–1 886	600	20
Odzi	Manicaland, Zim	2 436	Subtropical	700–2 200	1 200	22
Gwai	Matabeleland North, Zim	44 300	Semi-arid	600–1 500	700	25
Grand Cane	Louisiana, USA	183	Humid-subtropical	13–120	1250	20
San Patricio	Louisiana, USA	202	Humid-subtropical	13–120	1250	20
Rio Tanama	Puerto Rico, USA	49	Rainforest	200–800	2 000	25

Abbreviations: MAP: mean annual precipitation; SA: South Africa; Zim: Zimbabwe; USA: United States of America

Table 3.1 shows the variations in the climate of selected catchments; the climate information is closely related to the MAP. Notably, the catchments selected from the USA exhibit the highest rainfall. Significant variations in topography are exhibited; the low altitude catchments from the USA and KwaZulu-Natal are all located near the coast. Descriptions of climate, vegetation, geology and soils for each catchment are presented in the following tables. Appendix A provides additional information, maps and images.

Table 3.2 The geological and climatic characteristics of the selected study areas.

Catchment	Geology/soils	Climate/rainfall	References
T35A–E	• Dominant geological formation is the fine sandstones from the Clarens formation, followed by mudstones from the Elliot formation and sandstones of the Molteno formation. • Soil depth is limited on the steep slopes and gradually deepens towards the foot slopes and floodplain areas due to colluvium and alluvial deposits.	• Sub-humid climate. • A distinct seasonality in rainfall and temperatures. • 80% rainfall occurs during the summer (October to March) whereas winters are generally dry.	(Le Roux et al., 2015; Schulze, 2007)
S10A–E	• Geology consists of the Peninsula Formation that dominates the northern escarpment and the Ceres Formation that dominates the southern areas. • Formations consist of sandstones, shales and tillites of the Cape Supergroup that are highly erodible.	• Sub-humid climate. • Winter and summer rainfall.	(Schulze, 2007)
R20A	• Geology consists of the Karoo dolerite subgroup, and a small proportion of the Adelaide. • Soils in the mountainous areas (Karoo dolerite group) are thin, shallow and poorly drained compared to the deep well-drained soils of the foothills (Adelaide group), which are prone to erosion because of reduced vegetation cover.	• Warm to temperate climate. • Summer rainfall (October–March) and some slight winter rain.	(Middleton and Bailey, 2008)
K90A–B	• Geology consists of sandstone and quartzite, resulting in grey sandy soils and Table Mountain Sandstone. • Podzolic and litholic soils are dominant in the catchment. • Valley bottoms consist of permanent and seasonally saturated hydric soils.	• Temperate oceanic climate. • Winter and summer rainfall.	(Czeglédi, 2013; Mucina and Rutherford, 2010)
Gwai	• Dominated by highly erodible regosols. • Another dominant soil group is the very fertile reddish-brown fessiallitic soils. • Other soils groups include Lithosols, Lithormophic/heavy clays and reddish-brown arid soils.	• Warm semi-arid climate. • Rainfall period begins in October/November and ends in March/April.	(MINADER, 2015;ZINWA, 2019)

Table 3.2 (Cont.) The geological and climatic characteristics of the selected study areas.

Catchment	• Geology/soils	• Climate/rainfall	References
H80A	• Dominant geology is the Nardouw and Peninsula formations. • Bands of the Nardouw border the north and south of the catchment.	• Cold semi-arid climate. • Higher rainfall on the escarpment.	(Climatology Staff, 2012; Schulze, 2007).
Louisiana (Grand Cane & San Patricio)	• Strata of Tertiary materials. • Soils are dominated by brackish organic and mineral coastal deposits. • Geologic faults are found throughout the basin	• Tropical sub-humid climate. • Rainfall occurs during winter and spring months.	(Sabine River Basin (SRB) report, 2009; Zhu et al., 2011)
Rio Tanama	• Geology is dominated by volcanic rocks. • Coastal alluvium plains. • Sandy clays dominate the catchment.	• Warm rainforest type of climate • Although rainfall is scattered throughout the year, most occurs from May through to October.	(Monroe,1980)
J12G	• Dominant geology is the Waltevrede formation. • Other geological formations include the Nardouw, Ceres and Bidouw. • Sandstone and shale soils dominate the area.	• Dry and cold semi-arid climate. • Summer and winter rainfall regime.	(Mucina and Rutherford, 2006; Schulze, 2007)
A22B	• Geology comprises of the Silverton, Daspoort and Strubenkop formations. • Soil with low erodibility.	• Hot semi-arid climate. • Rainfall seasons starts late October and ends in March.	(Schulze, 2007)
B73A	• Geology is composed of granite rock, covering > 75% of the area. The rest of the catchment is covered in quartzite and shales.	• Dry climate. • Rainfall is higher on the escarpment. • Lower lying areas are warmer and drier.	(DWAF, 2004)
Odzi	• Geology is dominated by granite bedrock and weathered sandy soils. • Highly erodible coarse-grained sands and sandy loam soils dominant.	• Humid subtropical climate. • Seasonality in rainfall, season usually commences in November and ends in March.	(Lidén et al., 2001)

Table 3.2 (Cont.) The geological and climatic characteristics of the selected study areas.

Catchment	• Geology/soils	• Climate/rainfall	References
U30A	• Geology is dominated by the Natal and Mapumulo formations • Soils consist of shales and weathered sandy granitic soils.	• Humid subtropical climate. • Seasonality in rainfall, the season usually commences in November and ends in March.	(DWAF, 2004; Schulze, 2007)
X22E	• .Geology is dominated by the Nelspruit formation consisting of granite rock and weathered sandy soils.	• Dry climate. • Rainfall is higher on the escarpment. • Lower lying areas are warmer and drier	(DWAF, 2004; Schulze, 2007)
X31H	• .Geology is dominated by the Nelspruit formation consisting of granite rock and weathered sandy soils.	• Dry climate. • Rainfall is higher on the escarpment. • Lower lying areas are warmer and drier	(DWAF, 2004; Schulze, 2007)
A21K	• Geology comprises Rashoop, Rayton and Magaliesberg formations. Soils consist of weathered shale and sandy granite soils.	• Hot semi-arid climate. • Rainfall seasons starts late October and ends in March	(DWAF, 2004; Schulze, 2007)
B81A	• Geology is dominated by the Pietersburg, Turfloop and Goudplaats formations. • Soils consist of weathered sandy granitic soils.	• Dry climate. • Rainfall is higher on the escarpment. • Lower lying areas are warmer and drier.	(DWAF, 2004; Schulze, 2007)

Table 3.3 Descriptions of the vegetation coverage and land uses that dominate the selected study areas.

Catchment	Vegetation	Land use	References
T35A–E	• Dominated (60%) by the grassland biome whereas Eastern Valley Bushveld thrives along river channels. • Vegetation is largely influenced by altitude and burning. • Afromontane forest occurs along drainage lines and ravines where fire has minimal effect. • Small natural forest also occurs alongside forest plantations.	• Small urban centres and a large sparse rural settlement. • Extensive commercial agriculture, cultivation and livestock farming. • Small scale subsistence farming and livestock rearing	(Le Roux et al., 2015)
S10A–E	• Dominated by grasslands covering > 70% of the total area. • Patches of Acacia Karoo thornveld as well as Afromontane forest and sub-arid thorn bushveld. • Lower reaches are comprised of valley thicket. Alien invasive species dominated by black wattle have a significant presence in the catchment, particularly along the riparian zone.	• Human urban and rural settlements comprise a major land use in the catchment. • Livestock, subsistence, and commercial farming, as well as forest plantations. • Game farming and small-scale mining activities.	(NLC, 2014; DWAF, 2009)
R20A	• Dominated by thicket and bushland covering > 50% of the area. • Indigenous forest and forest plantations cover the rest of the catchment.	• The catchment does not have any significant land use besides forest plantations.	(NLC, 2014)
K90A–B	• Dominated by fynbos shrubland. • Other cover types including grassland, thicket and forest, Palmiet, ferns, grasses and reeds dominate the valley bottom peatland. • A portion of the catchment consists of degraded vegetation comprising invasive alien species.	• Nature reserves, orchards, livestock farms and vegetable farming. • Agriculture consists of large-scale commercial farming. • Urban and rural settlements.	(Mucina and Rutherford, 2010)

Table 3.3 (Cont.) Descriptions of the vegetation coverage and land use that dominate the selected study areas.

Catchment	Vegetation	Land use	References
H80A	Fynbos dominates, covering ~60% of the catchment. Mixture of temperate forest, transitional forest and scrub.	Dominant land use is commercial cultivation (dryland and irrigated), comprising approximately 15% of the entire catchment. Mining, sheep and ostrich farming in the more arid areas.	(NLC, 2014)
Louisiana (Grand Cane & San Patricio)	Dominant vegetation is forest. Mixture of grassland and scrub. Wetlands. Small patches of barren land.	Dominant land use is pasture farming. Other crops account for a small proportion of total land use. Limited urban development.	(Sabine River Basin (SRB) report, 2009)
Rio Tanama	Dominant vegetation is evergreen rainforest (>70%).The remaining vegetation is a mixture of shrub and grassland.	Dominant land use is urban development in the form of settlements and transport networks.	Landcover map
J12G	85% low shrub land comprising mostly fynbos. Bare ground constitutes 12% of the total area.	Dominated by wildlife and nature reserves A small patch of cultivation in the north of the catchment.	(NLC, 2014)
A22B	Dominated by grassland, indigenous forest and thicket bush. Significant portion of degraded land.	Cultivation dominates land use, comprising both subsistence and commercial agriculture. Mining activities are prominent. Mixture of small urban and rural settlements.	(NLC, 2014)
B73A	Dense indigenous forest and timber plantations at high altitudes. Lower catchment is sparsely vegetated by open scrub.	Timber plantations. Human settlements occupying the south-eastern side. North-east dominated by commercial farming activities.	(NLC, 2014)
Odzi	Natural forest, savannah grassland and bushveld. Large-scale plantations of pines and gumtrees are common.	Dominated by commercial and communal farming. Rural areas dominate the settlement pattern; some small urban centres are dotted around the area.	(Kemerink-Seyoum et al., 2017)

Table 3.3 (Cont.) Descriptions of the vegetation coverage and land use that dominate the selected study areas.

U30A	• The catchment is dominated by thicket/dense bush and grasslands. • Forest plantations also occur in the catchment	• The land use is dominated by settlements followed by commercial and subsistence cultivation.	(NLC, 2014)
X22E	• Plantations and woodlots dominate the catchment. • Wetlands and grasslands are the other significant vegetation types.	• Plantations are the dominant land use. • Settlements are limited.	(NLC, 2014)
X31H	• Plantations and woodlots dominate the catchment. • Wetlands and grasslands are other significant vegetation types that occur in the area.	• Dominant land use is forest plantations and orchards. • Human settlements are limited.	(NLC, 2014)
A21K	• Woodlands and grasslands make up >65% of the catchment. • Low shrubland and dense bush make up the rest of the vegetation cover.	• Land use is dominated by irrigated cultivation and orchards. • Mining and forest plantations are some of the other land-use types.	(NLC, 2014)
B81A	• Dominant vegetation is forest plantations. A significant portion of the catchment is covered in thicket and open bush. • Grasslands are limited.	• Dominant land use is cultivation. • A large portion of land is occupied by plantations and human settlements are sparse	(NLC, 2014)

3.3 Available flow and sediment data

Table 3. 4 Summary of available flow and sediment data for selected catchments.

Catchment	Sediment yield data			Flow/runoff data		
Name	**Description**	**Period**	**Source**	**Description**	**Period**	**Source**
Tsitsa	Measured daily	09/12/2015–31/01/2017	Geography Department, Rhodes University	Measured daily	09/12/2015–31/01/2017	Department of Water and Sanitation, South Africa
Inxu	Measured daily	01/10/2016–30/04/2017	Geography Department, Rhodes University	Measured daily	01/10/2016–30/04/2017	Geography Department, Rhodes University
Odzi	Measured daily	12/11/1978–31/05/1988	Department of Water Development (DWD), Zimbabwe (now ZINWA)	Measured daily	12/11/1978–31/05/1988	Department of Water Development (DWD), Zimbabwe (now ZINWA)
Gwai (A36)	Measured Monthly	01/10/1992–31/03/2011	Zimbabwe National Water Authority (ZINWA)	Measured daily	01/10/1992–31/03/2011	Zimbabwe National Water Authority (ZINWA)
Gwai (A38)	Measured Monthly	01/02/1995–31/03/2011	Zimbabwe National Water Authority (ZINWA)	Measured daily	01/02/1995–31/03/2011	Zimbabwe National Water Authority (ZINWA)
Grand Cane	Measured daily	01/10/1980–30/09/1984	United States Geological Survey (USGS)	Measured daily	01/10/1980–30/09/1984	United States Geological Survey (USGS)
San Patricio	Measured daily	02/02/1981–28/06/1985	United States Geological Survey (USGS)	Measured daily	02/02/1981–28/06/1985	United States Geological Survey (USGS)
Rio Tanama	Measured daily	01/01/1968–31/12/2005	United States Geological Survey (USGS)	Measured daily	01/01/1968–31/12/2005	United States Geological Survey (USGS)

Table 3.4 (Cont.) Summary of available flow and sediment data for selected catchments.

Ntabelanga	Erosion and Sediment yield rates	Long-term rates	Msadala et al. (2010)	Simulated Monthly	01/10/1920–31/10/1990	Water Resources of South Africa 1990 (WR90)
Xonxa	Erosion and Sediment yield rates	Long-term rates	Msadala et al. (2010)	Simulated Monthly	01/10/1920–31/10/1991	Water Resources of South Africa 1990 (WR90)
Maden	Erosion and Sediment yield rates	Long-term rates	Msadala et al. (2010)	Measured daily	01/01/1980–31/07/2000	Department of Water and Sanitation, South Africa
Churchill	Erosion and Sediment yield rates	Long-term rates	Msadala et al. (2010)	Simulated Monthly	01/10/1920–31/10/1991	Water Resources of South Africa 1990 (WR90)
Duiwenhoks	Erosion and Sediment yield rates	Long-term rates	Msadala et al. (2010)	Simulated Monthly	01/10/1920–31/10/1992	Water Resources of South Africa 1990 (WR90)
Prinsriver	Erosion and Sediment yield rates	Long-term rates	Msadala et al. (2010)	Simulated Monthly	01/10/1920–31/10/1993	Water Resources of South Africa 1990 (WR90)
Koster	Erosion and Sediment yield rates	Long-term rates	Msadala et al. (2010)	Measured daily	01/02/1966–31/07/2000	Department of Water and Sanitation, South Africa
Klaserie	Erosion and Sediment yield rates	Long-term rates	Msadala et al. (2010)	Measured daily	01/10/1961–03/31/1973	Department o f Water and Sanitation, South Africa

Table 3.4 (Cont.) Summary of available flow and sediment data for selected catchments.

Witklip	Erosion and Sediment yield rates	Long-term rates	Msadala et al. (2010)	Measured daily	01/02/1982–28/02/2002	Department of Water and Sanitation, South Africa
Hazelmere	Erosion and Sediment yield rates	Long-term rates	Msadala et al. (2010)	Measured daily	01/11/1975–31/08/2020	Department of Water and Sanitation, South Africa
Da Gama	Erosion and Sediment yield rates	Long-term rates	Msadala et al. (2010)	Measured daily	01/12/1963–30/09/1961	Department of Water and Sanitation, South Africa
Buffelspoort	Erosion and Sediment yield rates	Long-term rates	Msadala et al. (2010)	Measured daily	01/08/1973–30/01/2020	Department of Water and Sanitation, South Africa
Ebenezer	Erosion and Sediment yield rates	Long-term rates	Msadala et al. (2010)	Measured daily	01/10/1948–30/09/1954	Department of Water and Sanitation, South Africa

3.3.1 Flow/runoff data

Most of the flow data used within this study (summarised in Table 3.6) comprises data recorded by gauging stations within the selected catchments. Most of these flow data for catchments in the USA and South Africa were freely downloaded from the United States Geological Survey (USGS; https://waterdata.usgs.gov/nwis/rt, last accessed 27 October 2020) and the Department of Water and Sanitation (DWS; http://www.dwa.gov.za/Hydrology/Verified/hymain.aspx, last accessed 20 August 2020), respectively. Data for most of the Zimbabwean catchments were obtained from the Zimbabwe National Water Authority (ZINWA). Flow data for ungauged South African catchments were obtained through monthly hydrological model simulations generated through the 1990 Surface Water Resources of South Africa study (WR90; Midgley et al., 1994) and updated to 2012 (WR2012; http://waterresourceswr2012.co.za/). WR2012 provides simulated runoff and other hydrological information for all South African catchments and is a valuable resource for water resources managers, planners and researchers, who routinely use these data. Runoff simulations in WR2012 were derived using the Pitman model calibrated against streamflow gauges for gauged catchments and through parameter regionalisation for ungauged catchments.

3.3.2 Sediment data

Calibration of the WQSED model is ideally against continuous daily sediment observations. These data are generally not available in South Africa and most developing countries due to the expenses associated with sediment sampling, with most countries reducing sediment and flow monitoring activities, as highlighted in Milliman and Farnsworth (2011). Much of the data that have been collected are either not easily accessible or require a high payment to gain access (Syvitski, 2003). The limited observed data that are available usually comprise a few event-specific and discontinuous samples collected through manual sampling techniques (Bannatyne et al., 2017; Kundu et al., 2015; Lidén et al., 2001). Thus, these data are generally not reliable indicators of sediment transport during high flow periods when most sediment is transported since high flow events are generally not sampled due to safety concerns (Bannatyne et al., 2017).

The daily sediment data accessed for the USA catchments were freely downloaded from the USGS website. The sediment data for the South African catchments were available from the

Geography Department at Rhodes University and consisted of limited records since much of the data remains embargoed until the ongoing government-funded sampling program is concluded. The data for the USA catchments were collected using an automated sampler, whereas the sediment data for the South African catchments were manually collected by citizen technicians (Bannatyne et al., 2017) under the Tsitsa project. The project is funded by the Department of Environment, Forestry and Fisheries (DEFF), Chief Directorate: Natural Resource Management Programmes (NRM), Directorate: Operational Support and Planning. Although numerous sediment observations for South Africa are reported in publications such as Vanmaercke et al. (2014), much of these data comprise reservoir sedimentation calculations by Rooseboom (1992) and discontinuous samples collected in studies, such as by Scott et al. (1998). These data are not appropriate for calibrating continuous daily simulations of sediment transport by the WQSED model. However, reservoir sedimentation calculations (Rooseboom, 1992) and long-term sediment simulations (Le Roux et al., 2008) have been compared with simulations in catchments where continuous daily data are not available (Chapter 8).

The sediment data for Zimbabwean catchments were obtained from ZINWA. The flow and sediment data for the Odzi were measured under the Streamflow and Sediment Gauging and Modelling project in Zimbabwe (GAMZ); Lidén et al. (2001) gives details on the GAMZ sampling program. The project was undertaken by the Department of Water Development (DWD) in Zimbabwe together with the Swedish Meteorological and Hydrological Institute (SMHI). It was funded by the Swedish International Development Co-operation Agency (SIDA) through the Working Group for Tropical Ecology, Uppsala University (Karlsson and Rahmberg, 1999). The Gwai catchment data obtained from ZINWA were unfortunately at a monthly timescale and showed substantial data gaps (e.g. ten monthly observations spread over 15 years). In addition, the metadata for the dataset was not immediately available. Therefore, the Gwai data have been treated as highly uncertain, and were used in this study to demonstrate the actual state of some of the data records that are reported in global and continental reports. The conspicuous absence of reports/publications on validated daily time step sediment models applied to southern African catchments is a reflection of the scarcity of observed data.

3.4 Conclusion

The catchments used in this study were selected based on the availability of daily observed sediment yield data. There was a need to test the model more widely in South Africa because this is the primary focus of the model application. Since observed data were not abundant or readily accessible in South Africa or other African countries, USA catchments were selected to test the model performance using long continuous observed data records. There remains a pertinent need for funding to be directed towards sediment monitoring in South Africa. Most importantly, it is recommended that sediment and other relevant data that may be useful to researchers must be made freely available and accessible.

Chapter 4 Methodological approaches

4.1 Introduction

The erosion and sediment transport model (WQSED) is a daily-time-step model that operates in a semi-distributed manner, mirroring the spatial distribution system of the Pitman model (Pitman, 1973; Hughes, 2013). A description of the model structure, function and parameters of WQSED is given in this chapter, and Bryson (2015) provides a more detailed description of the conceptual development of the model. The different components of the model, including the basic MUSLE and the additional storage and channel functions, are described in this chapter. Two storage options are presented, a complex storage consisting of several units that is reported in Bryson (2015) and a simpler storage option with a single storage unit as presented in Gwapedza et al. (2020). The simple storage option was added because the original multiple storages are rather difficult to calibrate. Therefore, it was necessary to add a simple option and evaluate how it performs relative to the original complex storage. Parameter inputs needed for each of the model components are presented at the end of each section and a table with overall parameters, their ranges and methods of derivation is placed at the end of the model description sections. The discussion explores the potential issues that are likely to affect model application and performance.

4.1.1 WQSED model structure

The structure of the WQSED model incorporates three main components, namely flow, erosion, and storage and transport functions. Flow acts as the primary driver of the simulations of sediment yield and transport by the model, as flow generates the erosive force that transports sediment through the catchment. Erosion is calculated using the MUSLE, which is then routed through the slope and gully storages. The conceptual sediment storages allow for a simplified representation of catchment sediment movement processes. Sediment is moved out of these storages based on non-linear functions between sediment output and relative storage and runoff. A channel transport function based on computations of suspended sediment transport by van Rijn (1984) is used to transport the sediment within the channel, out of headwater sub-basins and through downstream sub-basins. A detailed description of each of the components is given in this chapter. A simplified conceptual structure of the WQSED model is presented in Figure 4.1.

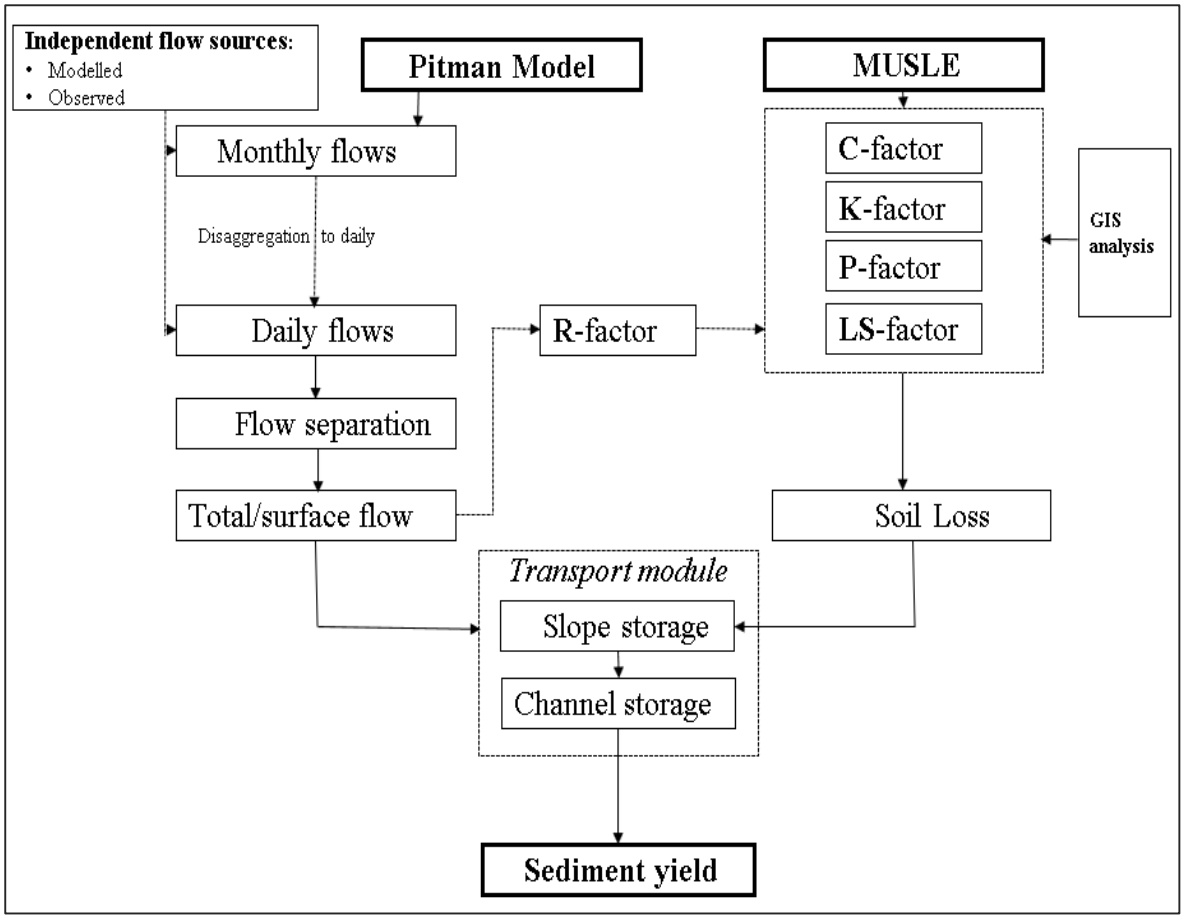

Figure 4.1 Conceptual structure of the erosion and sediment transport (WQSED) model.

4.1.2 A slope-based distribution

WQSED operates in a semi-distributed manner in which outputs from individual sub-basins are routed to the catchment outlet; however, an intra-basin distribution is also employed to represent sub-grid effects within each sub-basin. The distribution system used is based on the assumption that the catchment can be divided into areas of high, moderate and low runoff (Bryson, 2015). This spatial discretisation into three runoff zones is based on the topography of the basin, and the three runoff zones may also be referred to as slope zones. The slope categories are high, medium, and low (HML), representing high, moderate and low runoff zones, respectively. The zones are defined using guidelines from FAO (2006), with the high and low slope zones defined as greater than 20 degrees and less than 6 degrees, respectively (Figure 4.2). The proportion of the catchment area in each zone is used as input into the WQSED and to calculate slope zone inputs.

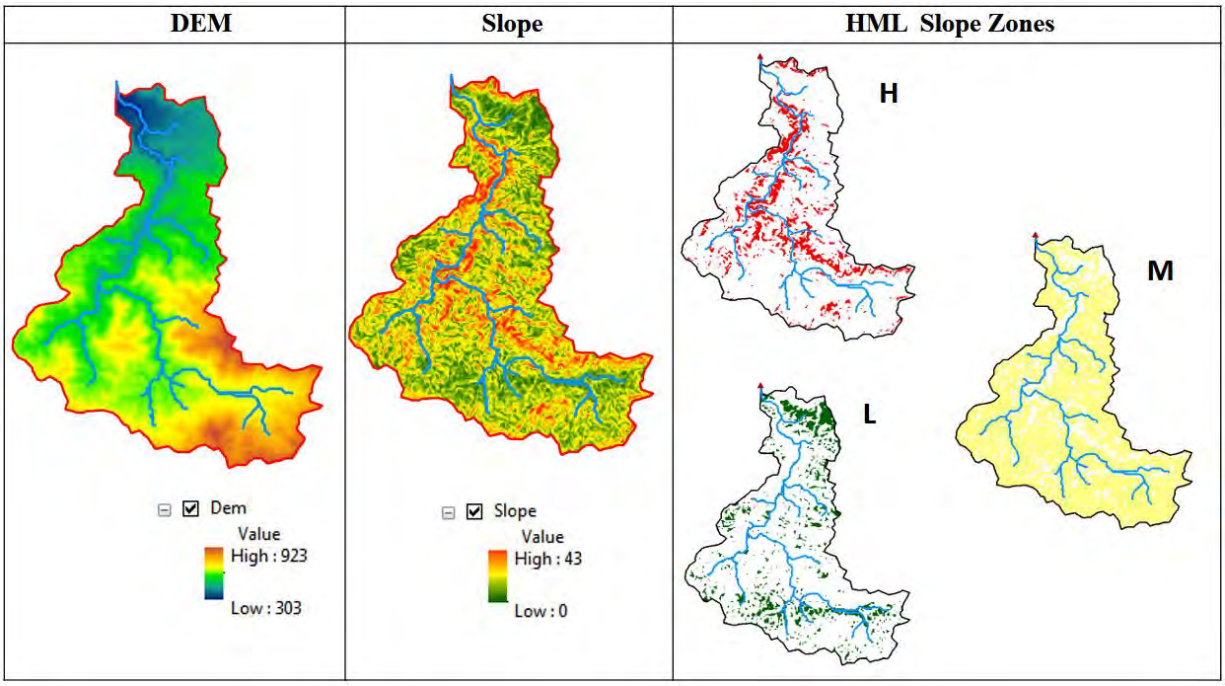

Figure 4.2 Calculation of the proportion of the catchment area in each slope zone of high (H), medium (M) and low (L) for the erosion and sediment transport (WQSED) model using a 30m digital elevation model (DEM); the Rio Tanama catchment is used as an example.

The MUSLE is applied to each of the HML slope zones, and the resulting eroded sediment is routed through slope and gulley storages (Figure 4.3). The MUSLE is applied to estimate erosion in WQSED because of its ability to estimate soil loss on a single-storm basis. A daily flow time series can therefore be used as input into the model, as discussed in Section 4.2. The MUSLE is applied to a single 150 ha area for each zone in an attempt to avoid excessive spatial scale issues, and sediment output is scaled to represent the entire area of the slope zone. Chapter 5 and Gwapedza et al. (2018b) discuss the spatial-scale dependencies that influenced how the MUSLE is currently applied in the WQSED. The input parameters for the MUSLE module within WQSED include independent values for *K*, *LS*, *C* and *P* for each of the slope zones, while the approach for distributing the flow data and the estimation of the erosivity component of MUSLE is discussed in Section 4.2.1 below.

The total erosion outputs of individual HML zones are routed through a series of conceptual storages (Figure 4.3) to simulate total sediment output from the sub-basin. Conceptual sediment storages are used to relatively simply represent typical sediment sinks and sources that occur in a real environment (Bryson, 2015). Each HML zone is assumed to have a hillslope and gully/channel storage component. Sediment calculated using the MUSLE (***SA***, Figure 4.3) is

first added to the hillslope storage of that slope zone (***S***, Figure 4.3). Outputs from the hillslope storages are released to the channel/gully storage of the same slope zone (***C_{prop}***, Figure 4.3), and the hillslope storage of the next slope zone. As shown in Figure 4.3, the gulley storages are also linked to each other and to the slope storage from zone H, through zone M, to zone L.

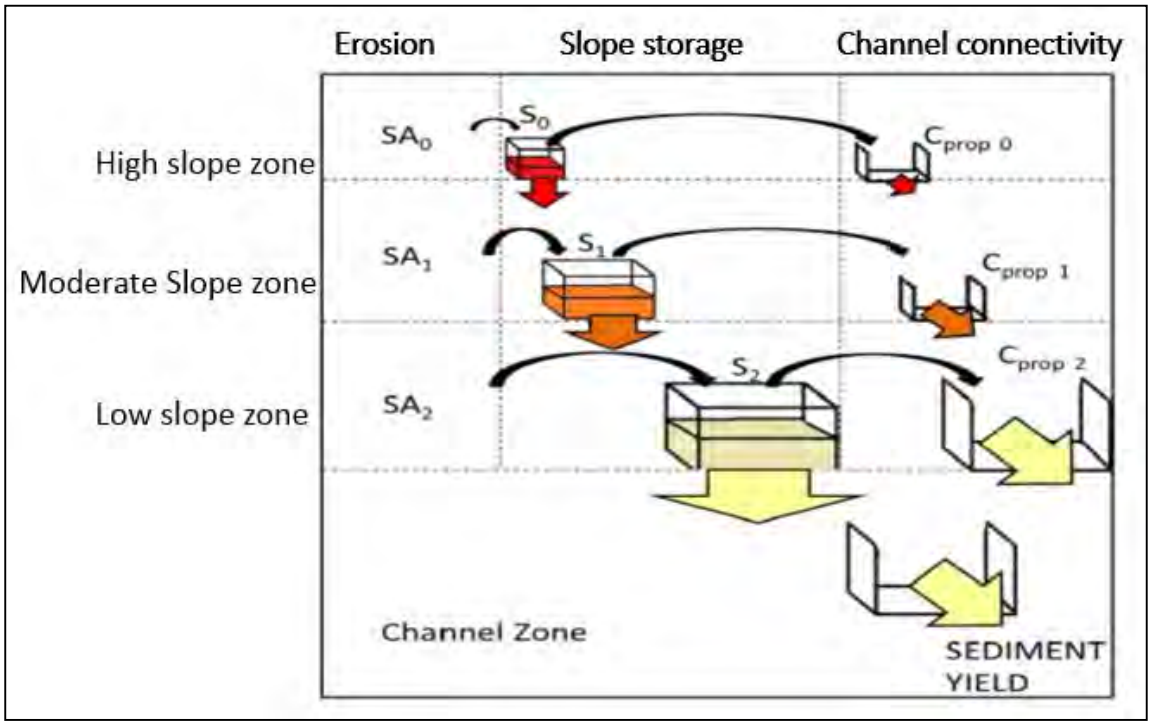

Figure 4.3 Erosion and sediment transport (WQSED) model conceptual storages. Adapted from Bryson (2015).

4.2 MUSLE Component

4.2.1 Sub-basin flow estimation

The WQSED model assumes that runoff is related to slope gradient, with higher slopes producing higher flow and more significant erosion. Consequently, zones with higher slopes/flow are assumed to produce more erosion and sediment delivery relative to zones of lower slope and flow (Pimentel and Burgess, 2013); however, this also depends on the amount of sediment held in storage within a slope zone and other MUSLE inputs. Equations 4.1–4.9 govern the flow estimation within the model.

The catchment surface runoff depth (*Depth*) is calculated from the input surface flow data ($Flow_s$) in $m^3\ s^{-1}$:

$$Depth = Flow_s \times 3.6 \times 24/Area \quad \text{(Equation 4.1)}$$

where *Area* is the sub-basin area (km^2).

The storm duration associated with the surface flow on each day is calculated using:

$$D = Vsf^{Dpow} + D_{con}, \quad \text{(Equation 4.2)}$$

where D is the duration (hours) and D_{pow} and D_{con} are power and constant parameters, respectively. *Vsf* is the surface flow depth in mm d^{-1}. All three runoff zones are assumed to have the same duration of runoff. The duration is used to calculate peak runoff, which is an input for the calculation of the MUSLE *R*-factor.

The runoff depths for each slope zone are calculated with the assumption that the high runoff zone generates 75% more runoff than the moderate runoff zone, which in turn is assumed to generate 75% more than the low runoff zone (Bryson 2015):

$$Depth_H = \frac{Depth}{H+\left(\frac{M}{1.75}\right)+\left(\frac{L}{3.0625}\right)}, \quad \text{(Equation 4.3)}$$

$$Depth_M = Depth_H/1.75, \quad \text{(Equation 4.4)}$$

$$Depth_L = Depth_H/3.0625, \quad \text{(Equation 4.5)}$$

where *Depth* is the runoff depth for the entire catchment (mm d^{-1}), H, M and L are the proportions of the catchment area that fall within the high, medium and low runoff zones, respectively, and $Depth_H$, $Depth_M$, and $Depth_L$ are the runoff depths (mm d^{-1}) for the high, medium and low runoff zones, respectively.

The peak runoff depth for each runoff zone is calculated assuming a simple symmetrical triangle:

$$QP_H = \frac{Depth_H}{0.5 \times D}, \quad \text{(Equation 4.6)}$$

$$QP_M = \frac{Depth_M}{0.5 \times D}, \quad \text{(Equation 4.7)}$$

$$QP_L = \frac{Depth_L}{0.5 \times D}, \quad \text{(Equation 4.8)}$$

where QP_H, QP_M, and QP_L are the peak runoff depths for the high, medium and low runoff zones, respectively (in mm d^{-1}).

The MUSLE equation used within the model is an alternative form of Equation 2.1 (Chapter 2) and estimates sediment yield (*Sy*) in t ha^{-1} (Williams and Berndt, 1977), using values of total runoff depth (*QD*) in mm and peak runoff (*qdp*) in mm h^{-1} in Equation 4.9. The equation can be derived by substituting $\alpha \times (Q \times qp)^{b}$ for *Q* and $qdp \times Area \times 10/3{,}600$ for *qp* in Equation 2.1, with the result dividing by *Area* to obtain a result in t ha^{-1} instead of in tonnes:

$$R = 1.586 \times (QD.qdp)^{0.56} \times (Area)^{0.12} \qquad \text{(Equation 4.9)}$$

where *Area* is the total catchment area in ha.

Equation 4.9 is therefore applied to each slope zone using the $Depth_{H, M, L}$ values for QD and $QP_{H, M, L}$ for qdp. The parameters in Table 4.1 are required as input for the MUSLE component of the model.

Table 4.1 A list of parameters for the Modified Universal Soil Loss Equation of the erosion and sediment transport (WQSED) model.

Number	Parameter/information
1	Topographic (*LS*) factor
2	Vegetation (*C*) factor
3	Soil erodibility (*K*) factor
4	Management practice (*P*) factor
5	Surface runoff (*Q*)
6	Catchment area and proportion of HML zones
7	Duration parameters (D_{pow} and D_{con})

4.3 Storage component

4.3.1 Slope storage and delivery

As illustrated in the conceptual representation of the model in Figure 4.3, the erosion model (MUSLE) makes sediment available for routing through the various storages within the catchment. Sediment movement from the storages, and to the outlet, occurs when the flow energy is sufficient and when there is enough sediment in the storage. Each runoff zone has

two storages, hillslope storage and channel (or gully) storage, which include all drainage features and gullies. The maximum storage capacity for each runoff zone as well as for the main channel is estimated from:

$$S_{max} = A \times p \times d, \quad \text{(Equation 4.10)}$$

where S_{max} is the maximum sediment storage capacity (kg) of the runoff zones or main channel, A is the area (m^2) of the runoff zone of the channel, p is the bulk density (kg m^{-3}), and d is the assumed maximum depth (m) of the stored sediment. The proportion of gully or channel storage in each runoff zone is then calculated:

$$C_{prop} = LnDD, \quad \text{(Equation 4.11)}$$

where C_{prop} is the proportion of the total storage in a runoff zone that is assumed to be represented by gully or channel storage, Ln is the natural logarithm, and DD is the drainage density (km /km^2) of the channel features in that zone.

Sediment moves from the high runoff zone to the low runoff zone, into the channel and out of the catchment (Figure 4.4). The model attempts to represent the stochastic nature of erosion by accounting for the dynamic movement of sediment between and within the conceptual storages.

Sediment is added to the three slope storage zones during each time interval of the model using Equation 4.12:

$$SS(t) = SS(t-1) + S_{input}, \quad \text{(Equation 4.12)}$$

where $SS(t-1)$ is the sediment storage at the end of the previous time interval, $SS(t)$ is the new storage (before transport of other storages), and S_{input} is the sediment generated using the MUSLE.

The output from each storage component is calculated using the peak surface runoff (q_{sed} mm h^{-1}) for that runoff zone relative to the maximum mean daily total flow depth (q_{max} mm h^{-1}) for the whole catchment (over the whole time series) and a threshold flow depth (q_t, mm h^{-1}), as well as a power function for the amount of sediment currently in storage relative to the maximum possible storage.

If $q_{sed} > q_t$ then:

$$S_{out} = \frac{q_{sed} - q_t}{q_{max} - q_t} \times SS \times (SS / S_{max})^{pow} \quad \text{(Equation 4.13)}$$

where *pow* represents power.

For the main channel storage, the peak runoff value is based on the total flow depth of the entire basin for a given day. The maximum mean daily total flow depth is pre-calculated from the full time series of flow data input.

As depicted, the C_{prop} value (i.e. the proportion of total sediment storage for the runoff zone considered to be contained in channel features) is used to determine the destination of the sediment. $S_{out} \times C_{prop}$ is added to the channel storage within the same runoff zone, whereas $S_{out} \times (1 - C_{prop})$ is added to the slope storage of the next runoff zone in the cascade (see Figure 4.4). The outputs from the channel storages are directed to the next channel storage in the cascade, whereas all outputs from the lower runoff zone are directed to the main channel. The outputs from the main channel become the final sediment delivery for the sub-basin. Sediment can therefore accumulate within the storages until a runoff event flushes stored sediment to the catchment outlet. Figure 4.4 summarises the sediment storage and delivery process from high to moderate to low runoff zones before exiting the catchment. Parameters and information required for the storage component of WQSED are shown in Table 4.2.

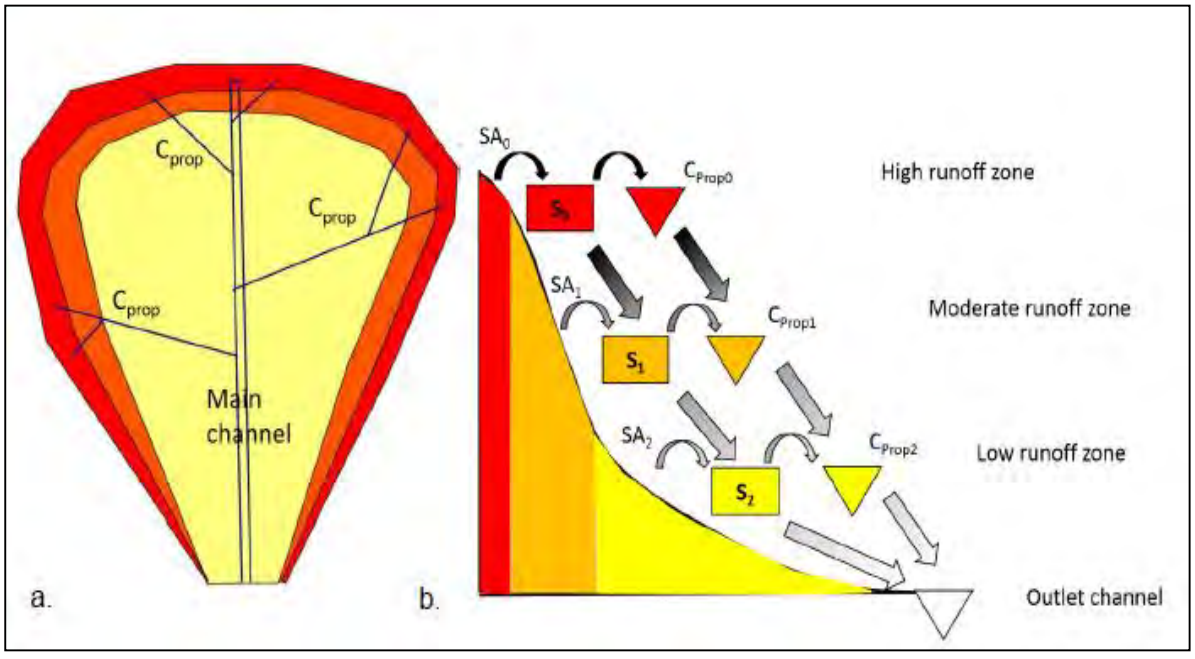

Figure 4.4 The slope storage and delivery component of the erosion and sediment transport (WQSED) model. Sourced from Bryson (2015).

Table 4.2 A list of parameters for the storage component of the erosion and sediment transport (WQSED) model.

Number	Parameter/information
1	Maximum storage for high, medium, low (HML) zones
2	The proportion of storage in gullies (C_{prop})
3	Drainage density (DD)
4	Initial storage fraction
5	Sediment storage ratio power (pow)
6	Threshold flow for sediment delivery
7	Peak flow scaling
8	Maximum mean total flow (q_{max})

4.4 Simple storage option

The simple storage option operates according to principles similar to the storage component reported in Section 4.3, with the exception that the multiple storage components are eliminated; instead, a single storage is used. When applying the storage, the first step is to estimate the proportion of the daily MUSLE sediment output (MS_i) that contributes directly to sediment delivery at the catchment outlet (SD_i) on the same day (i). This is based on a power function (parameter SPOW1) of the average of the available sediment at the start and end of the day relative to a maximum possible storage parameter (SS_{Max}). The initial estimate of the available sediment at the end of the day (TS_i) is given by:

$$TS_i = MS_i + SS_i \quad \text{(Equation 4.14)}$$

The direct estimate of sediment delivery is given by:

$$SDD_i = MS_i \times ((TS_i + SS_i)/2 \times SS_{max})^{SPOW1} \quad \text{(Equation 4.15)}$$

The updated total sediment in storage after direct delivery is then given by:

$$TS_i = MS_i + SS_i - SDD_i \quad \text{(Equation 4.16)}$$

A second component of the storage model assumes that sediment can be removed from storage during higher stream flows. These estimates are based on power functions of relative streamflow discharge and relative sediment storage. The discharge power function is:

$$Qfact_i = \left(Qi/(Q_{max} \times 1.2)\right)^{QPOW} \quad \text{(Equation 4.17)}$$

where $Qfact_i$ is the streamflow factor, Qi is the current day streamflow ($m^3\ s^{-1}$), $Q_{max}$is the maximum daily streamflow in the input data, and *QPOW* is a power parameter. The total flow is used to drive the movement of sediment through the storages of the storage model, whereas only surface runoff is used to drive the MUSLE as the sub-surface flow is unlikely to impact on slope erosion.

The sediment storage factor ($SSfact_i$) is given by a relationship similar to that defined in Equation 4.15 using an additional power parameter (SPOW2):

$$SSfact_i = \left((SS_i + TS_i)/(2 \times SS_{max})\right)^{SPOW2} \quad \text{(Equation 4.18)}$$

The final downstream output from storage (SSD_i) is given by Equation 4.19 after which the storage is updated (Equation 4.20) for the following day, and the total sediment delivery becomes the sum of SSD_i and SD_i

$$SSD_i = TS_i \times Qfact_i \times SSfact_i \quad \text{(Equation 4.19)}$$

$$SS_{i+1} = SS_i + MS_i - SD_i - SDD_i \quad \text{(Equation 4.20)}$$

The main objective of using average sediment storage values in Equations 4.15 and 4.19 is to smooth the effect of very large sediment inputs from the MUSLE during any one day. Parameters for the simple storage option are presented in Table 4.3. The storage version is implemented in a spreadsheet and has not yet been added to the SPATSIM framework.

Table 4.3 A list of parameters for the simple storage option of the erosion and sediment transport (WQSED) model.

Number	Parameter/information
1	Maximum catchment storage (SS_{max})
2	Initial storage (TS_i)
3	Sediment storage power (*QPOW*)
4	Threshold flow for sediment delivery
5	Peak flow scaling
6	Maximum daily total flow (Q_{max})

4.5 Channel component

4.5.1 Sediment routing in the main channel

The sediment routing module is an extension to the model developed by Bryson (2015). The sediment calculated for each slope zone using the MUSLE and the slope delivery routine is accumulated in the main channel outlet of a sub-basin. This approach was sufficient in the initial stages of model development to simulate sediment yield from single or lumped sub-basins. A sediment routing module was developed to extend model functionality to enable the movement of sediment generated at sub-basin level across multiple sub-basins to the outlet of the entire catchment.

4.5.2 Calculation of velocity, depth and river width with different flows

Estimates of velocity (m s^{-1}), depth (m) and width (m) with different daily flows (m^3 s^{-1}) are required to calculate the transport of suspended sediment. Calculating these estimates requires certain assumptions in regard to the channel shape and additional user input, namely river channel maximum width (m) and slope. Figure 4.5 illustrates the assumptions made in regard to the channel shape.

The model first steps through all the sub-catchments (nodes) in the modelled system during the sediment routing procedure, and calculates width ($Width_{bed}$), depth (*Depth*), flow (*Q*) and velocity (*Vel*) in one cm increments of depth using the set parameters of $Width_{max}$ and *Slope*, until the maximum depth for the channel is reached. These values are stored in a lookup table that is accessed during sediment routing.

$Width_{bed}$ is assumed to be 60% of $Width_{max}$. Equation 4.21 calculates *Depth* at bank full to determine the range of depths for the lookup table:

$$Depth_{max} = 0.6 \times \left(\left(\frac{Depth}{0.45}\right) 2.08\right) 0.35 \qquad \text{(Equation 4.21)}$$

$Depth_{max}$ is the depth at bank full and determines the range of depths for which *Q*, *Vel* and *Width* are calculated in one cm increments of *Depth*.

The angle α (Figure 4.5) is presented in the subsequent calculations:

$$Opp = \frac{(Width_{max} - (Width_{max} \times 0.6))}{2} \quad \text{(Equation 4.22)}$$

$$Hyp = (Opp^2 + Depth_{max^2})^{0.5} \quad \text{(Pythagoras Theorem)} \quad \text{(Equation 4.23)}$$

$$\alpha = arcsin\left(\frac{Opp}{Hyp}\right) \quad \text{(Equation 4.24)}$$

For each 1 cm increment of *Depth* from 1 to $Depth_{max}$:

$$N = 0.1 - \left(\frac{\text{Depth}}{Depth_{max}} \times 0.06\right) \quad \text{(Equation 4.25)}$$

where *n* is Manning's roughness over an assumed range of 0.04 to 0.1, with 0.1 the value at the lowest depth and 0.04 the value at $Depth_{max}$.

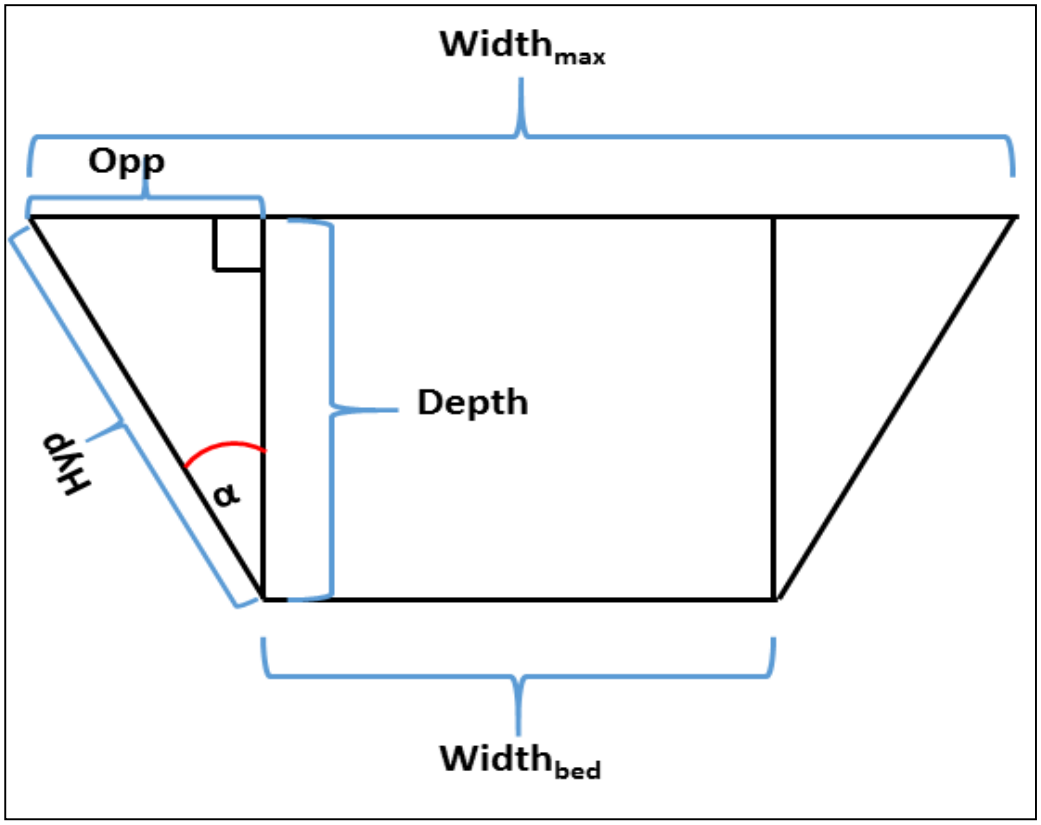

Figure 4.5 Conceptual representation of a river channel used to route sediment within the WQSED model.

To calculate the wetted perimeter and area with change in depth:

$$Hyp = \left(\frac{Depth}{\mathrm{Cos}\,(a)}\right) \quad \text{(Equation 4.26)}$$

$$Opp = (Hyp^2 - Depth^2)^{0.5} \quad \text{(Equation 4.27)}$$

$$Wetted\ Perimeter = Hyp \times 2 + Width_{max} \times 0.6 \quad \text{(Equation 4.28)}$$

$$Area = (Width_{max} \times 0.6 \times Depth) + (Depth \times Opp) \quad \text{(Equation 4.29)}$$

$$Vel = \frac{((\mathrm{Area/Wetted\_Perimeter})^{0.67} \times Slope^{0.5})}{n} \quad \text{(Equation 4.30)}$$

$$Width_{bed} = (Width_{max} \times 0.6) + (Opp \times 2) \quad \text{(Equation 4.31)}$$

$$Q = (Area \times Vel) \quad \text{(Equation 4.32)}$$

For each 1 cm increment of *Depth* from 1 cm to $Depth_{max}$, *Depth*, $Width_{bed}$, *Vel* and *Q* are stored in a lookup table.

4.5.3 Calculation of suspended sediment

The approach adopted follows the method for suspended load transport for steady flow proposed by Van Rijn (1984):

$$q_b = a_s \times p_s \times Vel \times d_{50} \times {M_e}^{2.4} \times (D^*)^{-6} \quad \text{(Equation 4.33)}$$

$$M_e = \frac{(Vel - Vel_{critical})}{[(\mathrm{s}-1)g d_{50}]^{0.5}} \quad \text{(Equation 4.34)}$$

$$\mathrm{D^*} = \mathrm{d_{50}} \left[\frac{(S-1)g}{V^2}\right]^{0.33} \quad \text{(Equation 4.35)}$$

$$Vel_{critical} = a \times (\mathrm{d_{50}} \times 10{,}000)^b \quad \text{(Equation 4.36)}$$

$$s = \frac{P_s}{P_w} \quad \text{(Equation 4.37)}$$

where q_b is suspended load transport (kg m^{-1}), a_s is assumed to be 0.012 (Van Rijn, 1984), ρ_s is the density of the sediment (kg m^{-3}) and is assumed to be 1 200, d_{50} is the median particle size (mm), M_e is the mobility parameter, $Vel_{critical}$ is the critical depth-averaged velocity for

initiation of motion (m s^{-1}), g is the acceleration of gravity (m s^{-2}), which is known to be 9.81, v is the kinematic viscosity coefficient (m^2 s^{-1}), which for water at 20°C is known to be 1 x10^{-6}, s is relative density, and ρ_w is the density of water (kg m^{-3}) and is assumed to be 1 000.

The values of a and b are calculated through linear regressions of the relationship between $Vel_{critical}$ and d_{50} given by Van Rijn (2012):

$$a = 0.225 \times Depth^{0.15} \quad \text{(Equation 4.38)}$$

$$b = 0.49 \times Depth^{-0.02} \quad \text{(Equation 4.39)}$$

For each day, WQSED uses the cumulative total flow (m^3 s^{-1}) for the sub-basin to obtain *Depth*, *Width,* and *Vel* from the aforementioned lookup table in memory. Using the equations given above, the load of sediment that can be carried in suspension (kg m^{-3}) is calculated by multiplying q_b by *Width*. The loads of sediment entering the sub-basin from upstream are summed, and the final load (kg m^{-3}) is compared to the load that can be carried in suspension. If the load entering the sub-catchment is greater than the load that can be carried in suspension by the cumulative flow, the difference is added to the channel storage. However, if the load entering the sub-catchment is smaller than that which can be carried in suspension by the cumulative load, the difference is taken from any available channel storage on the assumption that the available energy can erode the sediment stored in the channel. The load in suspension is passed to the sub-catchment downstream on a daily time step. Parameters for the channel routing are shown in Table 4.4. Table 4.5 gives a list of all WQSED model parameter inputs, their ranges and some options for how parameter values can be determined.

Table 4.4 A list of parameters for the channel component of the erosion and sediment transport (WQSED) model.

Number	Parameter/information
1	Channel width
2	Channel slope
3	Channel length

Table 4.5 A list of parameters for the erosion and sediment transport (WQSED) model. Parameters with no specific range are indicated with a hyphen (-) and are based on the area of application.

Parameter		Description	Parameter Estimation	Parameter range	
1	*Q* depth power (D_{pow})	The runoff depth power parameter for calculating storm duration from daily surface flow volume.	Calculations are based on flow data and estimated storm duration. Calibration parameter.	Min.	Max.
				0	-
2	*Q* depth constant (D_{con})	The runoff depth constant parameter for calculating storm duration from daily surface flow volume.	Calculations are based on flow data and estimated storm duration. Calibration parameter.		
				1	24
3	Drainage density (*DD*)	The drainage density parameter accounts for the river network coverage within the basin.	Calculated by dividing length of channel by catchment area.		
				-	-
4	Initial storage fraction	A parameter that gives the fraction of total sediment storage that is available for transport.	Calibration parameter.		
				0	1
5	Sediment storage ratio power	A sediment storage power function.	Calibration parameter.	0	-
6	Threshold flow for delivery (mm/hr)	A parameter that gives a threshold flow that is necessary for sediment delivery to commence.	Estimates are based on hydrological data. Calibration parameter.		
				-	-
7	Peak scaling	A parameter for scaling peak time series flows.	Is fixed at a default value of 1.	0	1
8	Channel width (m)	A parameter that defines the average width (m) of the main channel within the basin.	Estimated from channel measurements in Google Earth.		
				-	-
9	Channel slope (degrees)	A parameter that defines the average slope of the main channel within the basin.	Calculated from measurements from Google Earth or calculated from DEM.		
				-	-

Table 4.5 (cont.) A list of erosion and sediment transport (WQSED) model parameters. Parameters with no specific range are indicated with a hyphen (-) and are based on the area of application.

Parameter		Description	Parameter Estimation	Parameter range	
10	Channel length (Km)	A parameter that defines the length (km) of the main channel within the basin.	Calculated from existing river coverages or digitised lengths from Google Earth.		
				-	-
11	Soil erodibility (*K*)	The soil erodibility parameter defines the mean resistance of the soils within the basin to erosion.	Estimated from existing soil database.		
				0	1
12	Catchment slope (*LS*)	A parameter that represents the mean slope of the basin in degrees.	Calculated by analysing DEM in GIS.	0	-
13	Cover (*C*)	A parameter that represents the mean vegetation coverage within the catchment.	Calculated from existing land cover coverages or direct conversion of NDVI.		
				0	1
14	Practice (*P*)	A parameter that represents the management interventions to reduce erosion.	Estimated through GIS analysis of slope and land cover.		
				0	1
15	Maximum storage	Defines the amount of total soil storage within the catchment in tons.	Calculated based on soil depth, bulk density and catchment area.		
				-	-
16	Gully store proportion (C_{prop})	Defines the proportion of sediment storage that is in gully features.	Calculated as the natural logarithm of *DD* in a slope zone.		
				0	1
17	Catchment area (km^2)	The total basin area in km^2.	GIS analysis of existing coverages.	-	-

Abbreviations: DEM-digital elevation model; GIS- geographic information system; NDVI- normalized difference vegetation index

4.6 Estimating MUSLE parameters

4.6.1 Topography (*LS*) factor

Several *LS* estimation methods exist, including ground-based, flow path and cumulative cell length (FCL), and the LS-TOOL method (Zhang et al., 2013). The current study uses the unit contributing area (UCA) (Moore and Wilson, 1992) approach because of its ease of use within GIS and because it has been shown to calculate *LS* with good accuracy compared to field data (Oliveira et al., 2015), similar to the LS-TOOL method (Zhang et al., 2013).

The precision with which the *LS* factor can be estimated depends on the resolution of the DEM used. Comprehensive GIS-based methods for calculating the *LS* factor are presented in Zhang et al. (2013). The LS factor map was generated in ArcGIS using the Raster Calculator (Jain et al., 2010) by using the *LS* equation given by Moore and Wilson (1992):

$$LS = \left(\frac{\text{FA} * \text{cell size}}{22.13}\right)^{0.4} \times \left(\frac{\sin(\text{slope}) 0.01745}{0.0896}\right)^{1.3}, \qquad \text{(Equation 4.40)}$$

where FA is flow accumulation and cell size is the DEM grid resolution. Figure 4.6 illustrates the calculation procedure.

The Shuttle Radar Topographic Mission (SRTM) DEMs used in the present study are known to contain topographic errors caused by the height of dense tree canopies (Yamazaki et al., 2017). Unfortunately, the current analysis had already been completed by the time the new 90m error-corrected product (Yamazaki et al., 2017) was made available. Although the evaluation of changes in *LS* associated with the use of the error-corrected DEM may be valuable, the area of the selected catchments in Southern Africa comprises up to 60% grassland. Thus, it is unlikely that significant areas of dense tree canopy cover exist that could potentially induce large errors. Moreover, the selected catchments are steep headwater areas located in mountainous regions, where the accuracies of the corrected DEM are low (Yamazaki et al., 2017). A finer 30m SRTM DEM was used for calculating the *LS* factor in this study.

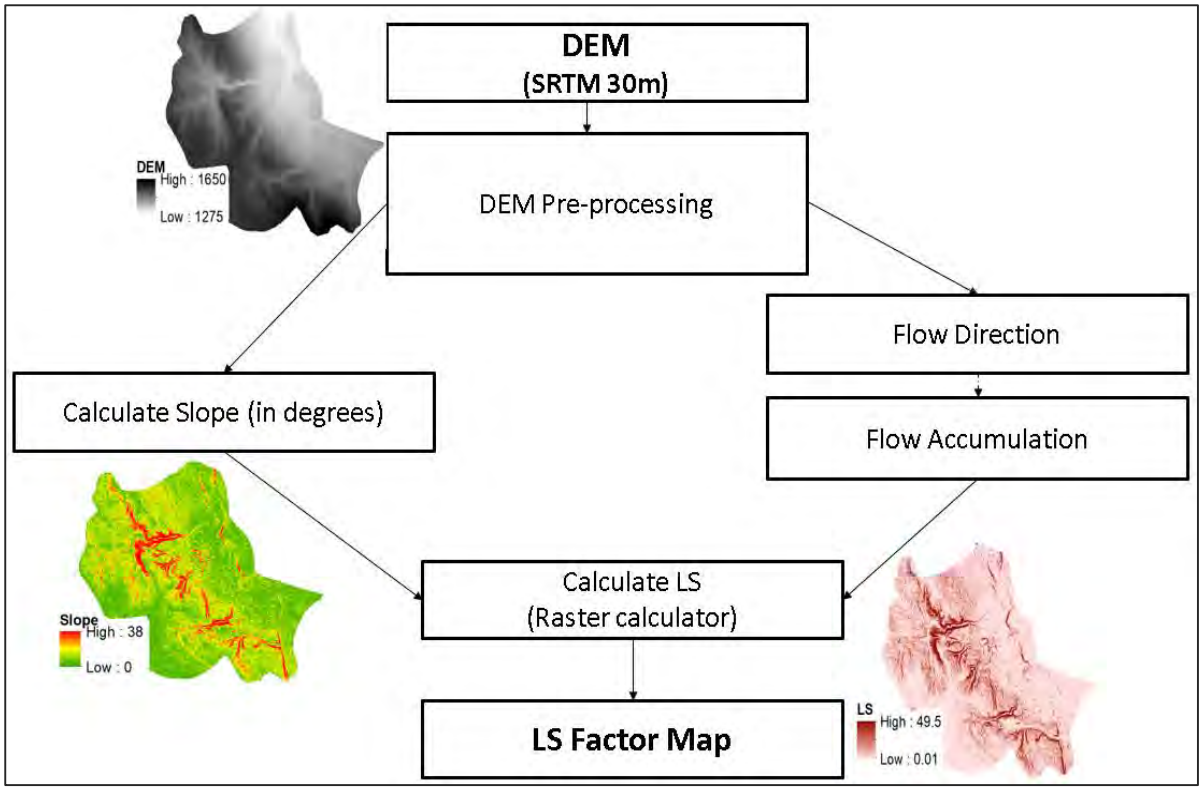

Figure 4.6 Flowchart illustrating the process of determining the Modified Universal Soil Loss Equation (MUSLE) topography (*LS*) factor. Abbreviations: DEM-digital elevation model; SRTM-Shuttle Radar Topographic Mission.

4.6.2 Vegetation cover (*C*) factor

The cover factor was determined for each land cover type using guidelines published by Wischmeier and Smith (1978); the guidelines consist of lookup tables showing the *C* factor values that can be used for different land cover classes. *C* values assigned in previous studies e.g. Ayalew et al. (2015), Jang et al. (2015), Ranzi et al. (2012), and Shinde et al. (2011), were used to verify the derived *C* factor classes. Table 4.6 shows the *C* factor values assigned for South African and Zimbabwean land cover types. The *C* values for the USA (and associated territories) were accessed from the SWAT crop database (Neitsch et al., 2005.

The vegetation cover factor was determined using the South African National Land Cover Database (NLC, 2014) created for the Department of Environmental Affairs (DEA) by GEOTERRAIMAGE; the dataset can be accessed from the South African National Biodiversity Institute (SANBI) website (https://www.sanbi.org/, last accessed 09 February 2020). Land cover data for the USA was accessed from ArcGIS Online

(https://www.arcgis.com/index.html, last accessed 20 August 2020), and the data for Zimbabwe was physically accessed from Dabane Water Workshops. HML zone cover properties were extracted using the Clip tool in ArcMap to extract data from the maps using HML zone proportions.

The attribute table containing land cover categories was exported to Microsoft Excel 2016, where *C* values were assigned to respective land cover classes. Land cover categories with the same *C* value were lumped together. Assigned *C* values were weighted according to the proportion of the HML zone covered by particular land cover classes.

Table 4.6 Cover factor (*C*) for South African and Zimbabwean land cover/use categories.

Land cover type	**C**
Forest, bush, thicket	0.009
Grasslands	0.12
Cultivated lands	0.37
Low shrub	0.013
Open bush	0.012
Bare/degraded land	1
Plantations / Woodlots	0.012
Waterbodies	0.01
Wetlands	0.038
Settlements	0.1

4.6.3 Soil erodibility (*K*) factor

Generally, *K* factor computations are based on the USLE method (Wischmeier & Smith, 1978). Since empirical observations are generally not possible for catchment-scale studies, soil erodibility calculations are typically based on readily available soil data. Example calculation approaches can be found in the literature for the USLE (Wischmeier & Smith, 1978) and RUSLE (Renard et al., 1997).

In South Africa, the erodibility of various soil forms and series has been rated by the Agricultural Research Council - Institute for Soil, Climate and Water (ARC-ISCW, 2005)

based on the Binomial Classification System. The current study derived *K*-values for South African soils from the Schulze and Horan (2007) database, which forms part of the South African Atlas of Climatology and Agro Hydrology (Schulze, 2007), based on the soil form and series information for each land type. *K* values were calculated for the application of the MUSLE model within the ACRU model and were taken directly from RUSLE *K* (Renard et al., 1997) calculations for global soils with limited available soils information. $K = 7.594(0.0034 + 0.0405\exp(-1/2(log(Dg) + 1.659/0.7101)^2))$, (Equation 4.41)

where

$$Dg(mm) = \exp(0.01 \sum f_i \ln m_i) \quad \text{(Equation 4.42)}$$

Dg is the mean particle size diameter, f_i is the primary particle size fraction in percent, and m_i is the arithmetic mean of the particle size limits of that size. The updated version of the AUTOSOILS model of Pike and Schulze (1995) was used to compute the *K* factor for South Africa (Schulze and Horan, 2007). The ARC-ISCW soil erodibility rating was used together with the erodibility classes given by Schulze and Lorentz (1995) (Table 4.7) in areas where soils information was not available.

For the USA catchments, the soil erodibility factor was accessed from ArcGIS Online (https://www.arcgis.com/index.html, last accessed 20 August 2020). The method used to calculate soil erodibility is contained in the USA National Soil Survey Handbook (https://www.nrcs.usda.gov/wps/portal/nrcs/detail/soils/ref/?cid=nrcs142p2_054242) and is generally similar to the method of Renard et al. (1997). The Zimbabwean catchments data was calculated using Equation 4.41 from soils data physically accessed from the Dabane Water Workshops GIS database.

Table 4.7 Erodibility factors for soil erodibility classes (Schulze and Lorentz, 1995).

K-Factor	**Soil erodibility class**
> 0.70	Very High
0.50–0.70	High
0.25–0.50	Moderate
0.13–0.25	Low
< 0.13	Very Low

4.6.4 Management practice (*P*) factor

The *P* factor relates to soil conservation methods, implemented mostly in agriculture, to reduce the rate of soil loss (Ayalew, 2015). These practices include contour and strip farming. The *P* factor has a value between 0 and 1, where 1 (indicating no practice) is assigned as the *P* factor for non-agricultural lands (Ayalew, 2015; Jang et al., 2015; Luo et al., 2016). Most studies using the USLE, Revised Universal Soil Loss Equation (RUSLE) and MUSLE usually set the *P* factor to the default of 1, indicating that no conservation practice is implemented (Sadeghi et al., 2013). This may be partly attributed to the *P* factor being too complex to quantify or due to study areas not having significant agricultural activity.

The catchment *P* factor is derived by using an STRM 30m DEM to calculate catchment slope categories (Section 4.1.2) overlaid with a map of cultivation (Jang et al., 2015) extracted from land use/land cover maps. A layer specifying the percentage of cultivated land in each slope category is derived, following which the Wischmeier and Smith (1978) tables for estimating *P* factor for various slope classes are used to assign the *P* factor values for cultivated land in each slope category. The resulting *P* factor (for each HML zone) is weighted against the total area of that zone to derive the mean *P* factor that is input into the MUSLE.

4.7 Methodological limitations

The WQSED model was designed to maintain a relatively simple structure while incorporating important erosion and sediment transfer mechanisms. The distribution of a catchment into slope zones enables the model to account for the variations in erosion processes within a catchment. The simplification of complex erosion processes results in some aspects of the entire system not being represented in the model. The MUSLE model that is used to calculate erosion/soil loss was designed to consider sheet and rill erosion (William, 1975) and may not be able to efficiently simulate sediment from non-sheet or -rill sources. The MUSLE was developed based on data observed at the plot scale and for catchments of less than 1 500 hectares (William, 1975). Applying MUSLE to larger catchments introduces uncertainties associated with spatial scale. Therefore, although the WQSED model inherits the advantages and limitations associated with the MUSLE, the present scale issues associated with the MUSLE are assessed with a view to limiting some of the limitations.

Although GIS has proved to be a valuable resource in environmental modelling (Karydas et al., 2014), the estimations of MUSLE erodibility factors remain uncertain (Alewell et al., 2019) at the catchment scale. The uncertainty is tied to the spatial and temporal resolution of input data (Gwapedza et al., 2018). Large pixels cluster information in a grid, often resulting in the loss of spatial variability (Tian et al., 2020) and loss of accuracy of grid values where there is large finer-scale variability. Additionally, pixel clustering for land cover classification lumps similar pixels of dominant vegetation over large areas (Wang et al., 2002), leading to erroneous assumptions of constant vegetation. Furthermore, some MUSLE factors cannot be accurately estimated over large areas (see Alewell et al., 2019), leading certain authors to extrapolate plot-scale observations to the catchment scale (e.g. Almagro et al., 2019), which can lead to unreliable results (Beven, 1989). Lack of representative soil data has led to researchers using soil colour (Hellden, 1987) or simple versions of *K* equations proposed by Renard (1997) to estimate the *K* factor. Soil stoniness is generally not accounted for in many catchment-scale studies due to ambivalent effects at the catchment scale (Alewell et al., 2019). Since there are uncertainties associated with the estimation of some erodibility factors (Chandramohan et al., 2015) and since the MUSLE only takes an average or weighted value for the entire catchment, some researchers have resorted to estimating maximum and minimum ranges of the factors, following which the factors are calibrated using the ranges to constrain the calibration values (e.g. Briak et al., 2016; Chen and Mackay, 2004; Luo et al., 2016; Yesuf et al., 2015).

Flow inputs into the WQSED also introduce some uncertainties. Since the flow input into the MUSLE is the major driver of erosion simulations, the quality of flow inputs largely determines the accuracy of MUSLE simulations (Sadeghi et al., 2013). The flow drivers into WQSED are derived from either simulations or observations, and therefore the model inherits the uncertainties associated with these data sources. The use of monthly flow data simulated by hydrological models such as the Pitman model in WQSED requires these flows to be disaggregated from monthly to daily using a process that is dependent on rainfall data. Although the disaggregated daily flows are volume corrected to match the simulated monthly flow volumes (Slaughter et al., 2015), the daily flows inherit the uncertainties of the simulated monthly flows.

The temporal distribution of the rainfall used to disaggregate monthly flows to daily should be representative, as this will affect the accuracy of the WQSED model in simulating sediment yield. Additional uncertainty is introduced by the flow separation procedure as there is generally no data to validate the baseflow separations due to field measurements of the various

flow fractions being currently unavailable. Therefore, although the WQSED model is versatile enough to accept both observed and simulated forcing flow data, the model runs the risk of inheriting the uncertainties associated with external flow sources.

The WQSED model was created based on geomorphological principles, where assumptions on the representation of processes are simplified. These simplifications are not only based on the current available understanding of geomorphological principles but were implemented to ensure that the resultant model is workable and not data-intensive, incorporating only those processes that explain the majority of variation in sediment generation and transport. This follows the principle of de Vente and Poesen (2005), who advises that models should be designed around the available data. Therefore, the WQSED model was developed to meet the needs of data-scarce Southern African catchments. However, some model simplifications fail to account for important sediment generation and transport processes. The C_{prop} gulley connectivity function considers gullies to be conduits of sediment and the lack of an explicit gully function may affect model performance in catchments dominated by gully processes (de Vente et al., 2013). The channel transport module considers sediment suspension, movement and deposition as the only channel processes, whereas channel erosion processes are also important sources of sediment (Fryirs et al., 2007). Model outputs are likely to be affected by such structural deficiencies. Additionally, most of the storage parameters are optimised through calibration (e.g. Picouet et al., 2001), requiring observed daily sediment data which are usually unavailable. However, the current WQSED version is best suited to the available data, and there is an opportunity to improve the model by adding further gully and channel processes as part of future developments.

Besides input data, the general lack of calibration and validation data also represented a significant limitation during the development of the model. To calibrate the model, continuous observed daily sediment data are required. Observed sediment data at other temporal resolutions, such as monthly and yearly data (where individual daily samples are not accessible), can also be used to calibrate the model by aggregating model outputs to match the requisite resolution. Unfortunately, observed sediment data are generally not available for most southern African catchments. In the absence of observed sediment data, sedimentation rates estimated from dam sedimentation and erosion risk maps represent the only viable option to validate model outputs. Remote sensing applications are also being developed to monitor suspended sediment concentration (Volpe et al., 2011). Although dam sedimentation rates and erosion rates may not be entirely accurate or at an appropriate temporal scale, they are valuable

in indicating if the model is simulating representative long-term sediment yields. It is important to highlight that the WQSED model outputs that are not appropriately validated should be used with caution, as would be the case with any other model simulations that have not undergone rigorous validation.

4.8 Concluding remarks

The methodological approach taken within the present study is a synthesis of modelling approaches to further develop an existing sediment model applicable to data-scarce catchments in southern Africa. Linking popular and appropriate models enables increased user adoption and reduce the burden of learning a new model. WQSED is a multi-purpose model that can be used for both management and research scenarios. By linking with the Pitman model, WQSED is more versatile in data-scarce environments as it can access flow data from hydrological models. WQSED was linked to a water quality model, WQSAM, as a sub-model providing sediment concentration data. The advent of global datasets allows data demands of the WQSED to be met more thoroughly, although many parameters are dependent on calibration. The WQSED maintains a relatively simple structure but manages to capture important sediment generation and transport processes. The distribution of a catchment into sub-basins and sub-basins into slope zones allows for spatial variability (sub-grid effects) within a single sub-basin. While long-term averages of sediment yield are generally used for management purposes, daily outputs of sediment yield provided by WQSED are valuable for water quality assessments.

Chapter 5 Consideration of spatial scale dependency in the application of the Modified Universal Soil Loss Equation (MUSLE)

5.1 Introduction

The problems of scale in model applications arise when a model is applied at a scale that is beyond that used to develop the underlying assumptions and processes governing the model. The MUSLE was developed based on research conducted on small catchments (<20km^2). Furthermore, it was developed to be applied using a lumped modelling approach. Over the years' researchers have adapted the MUSLE for use in large catchment areas and within semi-distributed models (Gwapedza et al., 2018b). It is important to highlight the problems associated with adapting the MUSLE to estimate sediment yield over large areas and to propose approaches to minimise the effects. Although some papers have addressed approaches to be used in the application of the MUSLE (Jha et al., 2004; Sadeghi et al., 2013), there remains little clarity regarding the spatial scale dependencies associated with applying the MUSLE approach to a wide variety of different catchment situations. The present chapter provides an evaluation of the spatial scale dependencies of the MUSLE and represents part of the further development of the WQSED model that is presented in Chapter 4.

While reviewing the original version of the WQSED model (Bryson, 2015), it became evident that the outputs of the MUSLE can be highly dependent on the spatial scale at which the model is applied. The rainfall-runoff and water resources yield models that form part of the SPATSIM modelling framework used in this study are based on a semi-distributed spatial distribution system, where the spatial scale can vary quite substantially between different applications. The same is true for models that are based on gridded distribution systems as the grid size used may vary with the total basin area being modelled. The spatial scale dependencies of the MUSLE are therefore an important consideration in the application of existing models or the development of any new model.

In an attempt to isolate the spatial scale-dependent properties of the MUSLE, previously published studies (Amore et al., 2004; Chen and Mackay, 2004; Sadeghi and Mizuyama, 2007; Arekhi et al., 2012; Sadeghi et al., 2013; Chaplot, 2014; Jang et al., 2015; Lou et al., 2016) that applied the MUSLE were scrutinised to identify any spatial scale limitations and to assess how previous users had solved the problem of scale dependency. In the current chapter, further

assessments of the likely effects of scale are also investigated using analytical methods and some hypothetical examples.

5.1.2 Literature assessments of the spatial scale dependency of the MUSLE

The first observation from the literature is that the terms 'soil erosion' and 'sediment yield' are used interchangeably to refer to the outputs from the MUSLE, compared to the original USLE method that distinguished between small scale 'soil erosion' and larger scale 'sediment yield'; the two being linked by sediment delivery processes (Wischmeier and Smith, 1978). Secondly, many studies do not specify the units of some or all of the parameters, or the units specified (notably for erosivity *(R)* and soil erodibility (*K))* are inconsistent across the studies. There are different definitions of the unit for the *K* factor, whereas some sources do not provide any information on the unit of *K* (Lim et al., 2005; Luo et al., 2016). Sadeghi et al. (2014) refer to the units as $t\,h\,MJ^{-1}\,mm^{-1}$, whereas others have used $Mg\,MJ^{-1}\,mm^{-1}$. A conference proceedings paper by Cârdei (2010) focused on the dimensionality of both the USLE and MUSLE and concluded that the equations are incorrect in terms of dimensional analysis. However, the original USLE was never meant to be a physical equation that is dimensionally correct but rather a statistical equation designed to fit empirical observations. The same must therefore be true of the MUSLE. This lack of dimensionality in the equation precludes any possibility of theoretically assessing the scale dependency of the equation.

K was originally defined (Wischmeier and Smith, 1978) as a soil erodibility 'factor' applicable to a unit plot (22.1 m long on a 9% slope). This suggests that *K* may assume different values when applied to large heterogeneous areas compared to small homogeneous areas. However, *K* appears to have been considered independent of scale in all reported studies. The definition of *K* in the MUSLE is the soil loss per unit erosion index, suggesting that *K* is not scale-dependent, and the same is true of the non-dimensional cover and practice factors. The issue of spatial scale dependency referred to so far is different from issues of spatial averaging over heterogeneous catchment areas. However, it is inevitable that the values for *K,* cover *(C)* and practice *(P)* will be different for basins of different sizes; such differences would be related to spatial averaging rather than spatial scale dependencies in the approach used to estimate their values. These parameters are also linear scaling factors in the MUSLE and therefore the effects of changes in their values are far more transparent than the effects of the non-linear erosivity

factor (*R*: Equation 5.1). The key issue is that *K* changes with scale, but these changes are associated with spatial averaging.

While the topographic factor (*LS*) is also a linear scaling factor, there is a possibility that it could be scale-dependent. This depends upon the calculation methods used, many of which will be based on processing digital elevation model (DEM) data (Alewell et al., 2019). With respect to the erosivity factor, runoff depth could be scale dependent, given typical spatial variations in both rainfall inputs and runoff response, whereas the specific peak runoff values (expressed in mm h^{-1}) will almost always reduce for larger catchments, due to the effects of runoff routing and the associated attenuation. The key issue addressed in the present chapter is therefore whether the ways in which the *LS* and *R* factors are estimated will account for spatial scale effects in catchments of highly variable size. A recent article focussing on the SWAT model by Pignotti et al. (2017) suggested that decreasing the grid (or hydrological response unit: HRU) resolution from a reference 30 m HRU model to 60 m and 1 000 m (i.e. 1 km^2), decreased the sediment yield by 20% and 60%, respectively. Unfortunately, there is insufficient detail in the paper regarding the sediment parameters and simulations to allow these reductions in sediment yield to be attributed to any specific cause, or to isolate the spatial scale effect differences in the hydrological data from other effects on the MUSLE simulations. A literature review examination (e.g. Amore et al., 2004; Chen and Mackay, 2004; Jha et al., 2004; Chaplot, 2014; Vigiak et al., 2015) of spatial scale effects in the use of either the USLE or the MUSLE reached, did not provide detailed insights into the reported spatial scale dependencies. Although these contributions demonstrate the recognition of some spatial scale effects, there remains insufficient detail on the scale effects of all the inputs to the MUSLE for different spatial scales. Therefore, it is not possible to fully understand the reasons for the differences in simulated sediment yields that are reported.

Chen and Mackay (2004), Chaplot (2014) and Vigiak et al. (2015) concluded that the SWAT model estimates of sediment yield are non-linearly related to the sub-basin area used. Chen and Mackay (2004) provide a detailed analysis of some scale effects, specifically in the erosivity equation. However, they do not include any explicit analyses of the spatial scale effects on the links between the hydrological modelling approaches used to estimate runoff volume (or depth) and peak flow, and the estimates of erosion. Thus, there are indications in the literature for the existence of spatial scale effects in sediment yield models that make use of the MUSLE, but there are no clear guidelines regarding how these effects should be taken into account. The

following sections make use of some analytical assessments as well as explorations of the spatial scale effects using hypothetical (but realistic) examples of inputs to the MUSLE.

5.2 Assessments of erosivity spatial scale dependency

The methodological approach taken within the current study makes use of analytical approaches together with well-controlled hypothetical data (Gwapedza et al., 2018). The use of analytical methods was adopted because it is much easier to isolate the spatial effects of MUSLE when it is not embedded within a complex integrated model. In the current study, an alternative MUSLE equation (Equation 5.1) that estimates the sediment yield (*Sy*) in t ha^{-1} was used:

$$R = 1.586.\ (QD.qdp)^{0.56}.\ (Area)^{0.12} \qquad \text{(Equation 5.1)}$$

where *QD* is total runoff depth in mm, *qdp* is peak runoff in mm h^{-1} and *Area* is total catchment area in ha.

5.2.1 Analytical solutions to the Erosivity index (Equation 5.1)

The assessment of the erosivity factor was based on a reference runoff depth of 25 mm and a peak discharge of 6 mm h^{-1} for a 100 ha sized sub-basin. Various sub-basin areas ranging from 10–100 000 ha were used to analyse the change in the peak discharge that is necessary to maintain the same erosivity over the various sub-basin areas. In comparing a distributed model approach to a lumped approach, the average runoff depth (*QD*) over the total area will be the same regardless of the number of sub-basins (this is necessary to ensure that the hydrological mass balance is independent of the distribution approach). However, the peak runoff (*qdp*) would be expected to decrease as the sizes of the sub-basins increase. This is based on the fact that higher peak to volume ratios would be expected in smaller sub-basins (all other factors being the same) and *vice versa*, due to the attenuation effects of flow routing.

To obtain the same erosivity value per unit area from Equation 5.1, it is clear that the product of runoff depth and peak (*QD.qdp*) must decrease in proportion to the increase in area to the power of ~0.214 (0.12/0.56). Figure 5.1 illustrates the results of an analysis for an example runoff event of 25 mm occurring over a 100 000 ha basin with different sub-basin areas

(ranging from 10 ha to a lumped approach, i.e. using between 1 and 10 000 sub-basins). The vertical axis shows how the average *qdp* value must change for the different distribution systems used (based on first fixing the specific peak discharge at 6 mm h^{-1} for 100 ha sized sub-basins) to achieve the same erosivity estimate. The peak (*qdp*) value varies from ~1.4 mm h^{-1} for the lumped approach, to ~9.8 mm h^{-1} for the approach using the smallest sub-basins (10 ha). The *qdp/QD* ratio similarly varies from 0.05 (lumped) to 0.39 (10 ha sub-basins).

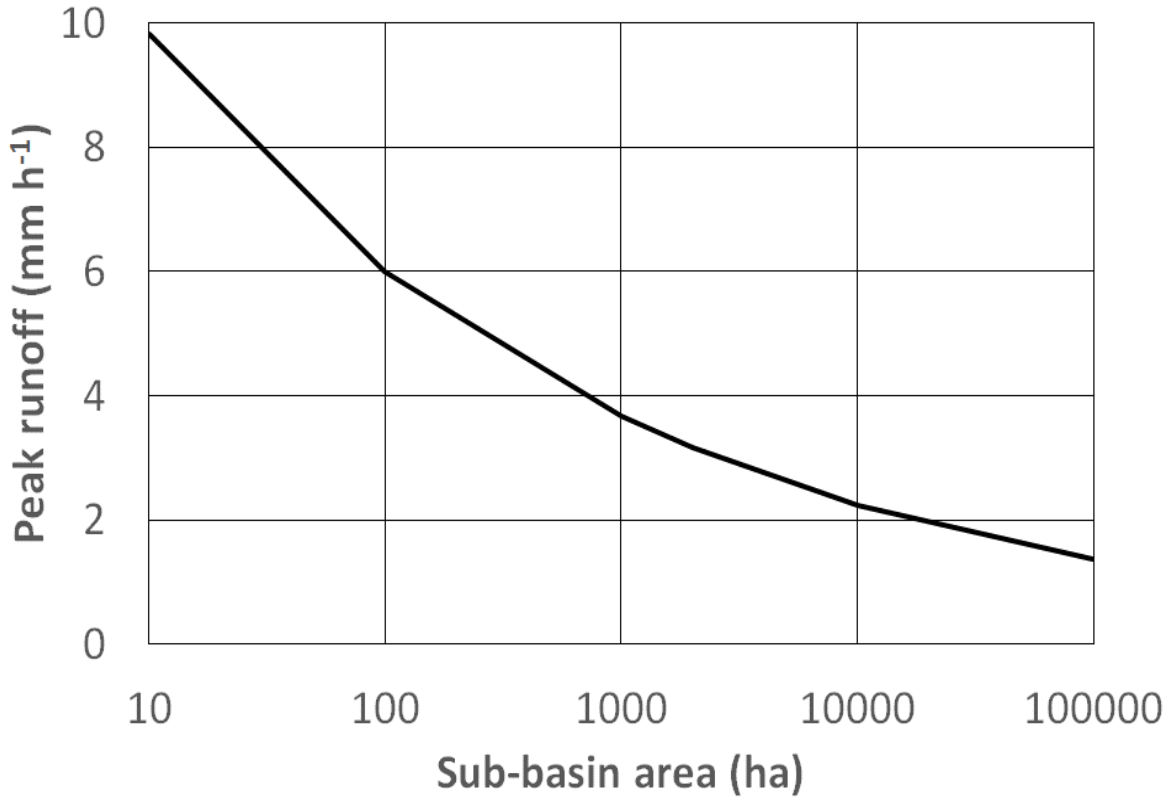

Figure 5.1 Relationships between sub-basin area and peak runoff depths required to generate the same erosivity estimate for a total storm depth of 25 mm (based on fixing the 100 ha peak at 6 mm h^{-1}).

5.2.2 A distributed approach with flow routing

A hypothetical basin and flow routing were used in order to represent and analyse the effects of flow attenuation. Figure 5.2 illustrates a hypothetical catchment of 20 km^2, which has been divided up into 20 grids. The arrows in the figure indicate the assumed flow paths that link all of the grids to the outlet at grid 20. While different routing approaches are available, the Muskingum equation (Balaz et al., 2010) was used in the present study to route flow through the 20 grids (sub-catchments). The main motivation for using this approach was based on the

availability of parameter estimation guidelines for South Africa (Bauer and Midgley, 1974). A hypothetical hydrograph based on reference total runoff depth of 25 mm with a peak of 6 mm h^{-1} was applied to the total area (20 km^2) of the hypothetical catchment shown in Figure 5.2.

Regional storage (*RK*) parameters (Bauer and Midgley, 1974) were used to achieve the various plausible hydrograph attenuation levels for a catchment in South Africa. The hydrograph routing was based on assuming that the eight headwater grids have a higher runoff response than the mean for the catchment (35 mm depth and 8.4 mm h^{-1} peak), and that six mid-reach grids (20 mm and 4.8 mm h^{-1}) and six downstream grids (17 mm and 4.0 mm h^{-1}) have a below-average response. Different assumptions about the spatial distribution of runoff depth and peak would give different results but the example used is considered sufficient to illustrate the spatial scale dependencies of the MUSLE.

The MUSLE was applied using various peak attenuation outcomes to analyse how much peak attenuation would be required to achieve the same erosion output between a lumped and a distributed modelling approach. This example assumes spatial uniformity (across all of the grids) in the other parameters of the MUSLE (erodibility factor $K = 0.3$, *LS* factor = 7, *C* factor = 0.05 and *P* factor = 0.9).

The solid black line in Figure 5.3 shows an unrouted hypothetical hydrograph based on a total runoff depth of 25 mm with a peak discharge of 6 mm h^{-1} that has been applied to the total area (20 km^2) of the hypothetical catchment shown in Figure 5.2. The remaining three hydrographs represent the results of applying the Muskingum routing equation to the grid system to obtain the cumulative hydrograph at the outlet using the regional estimation equations for parameter *RK* provided by Bauer and Midgley (1974).

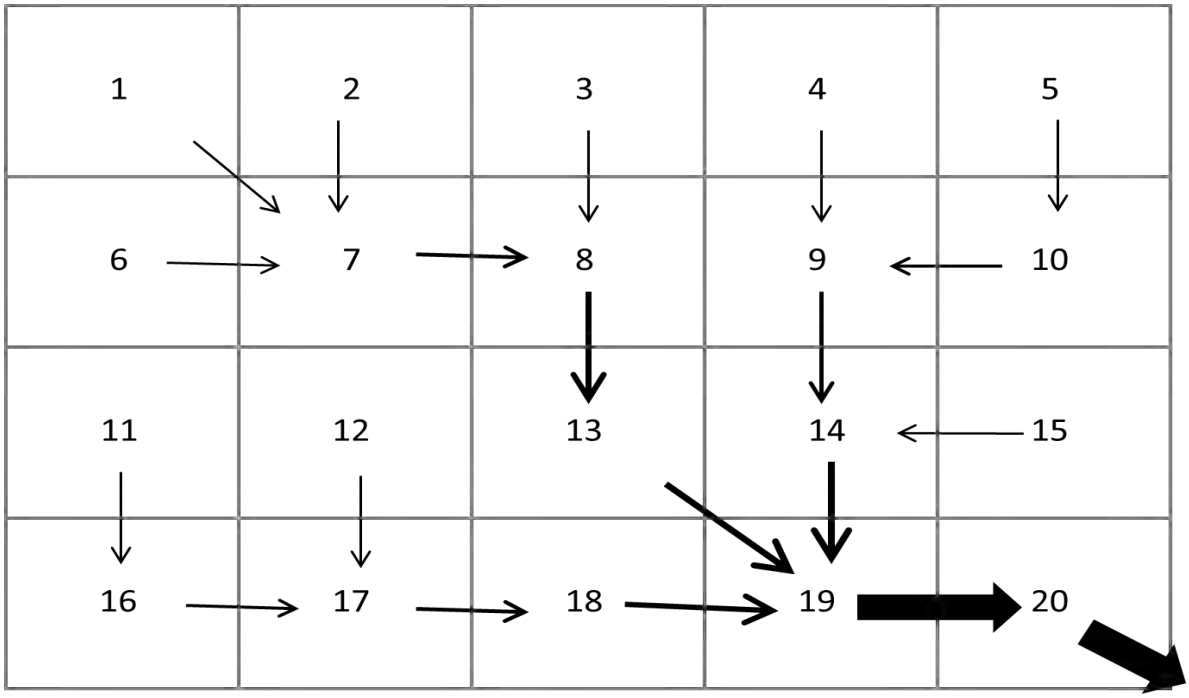

Figure 5.2 Hypothetical catchment of 20 km^2, subdivided into 20 × 1 km^2 sub-catchment grids. The arrows indicate the assumed directions of flow used in the sub-catchment routing to the final outlet at grid 20.

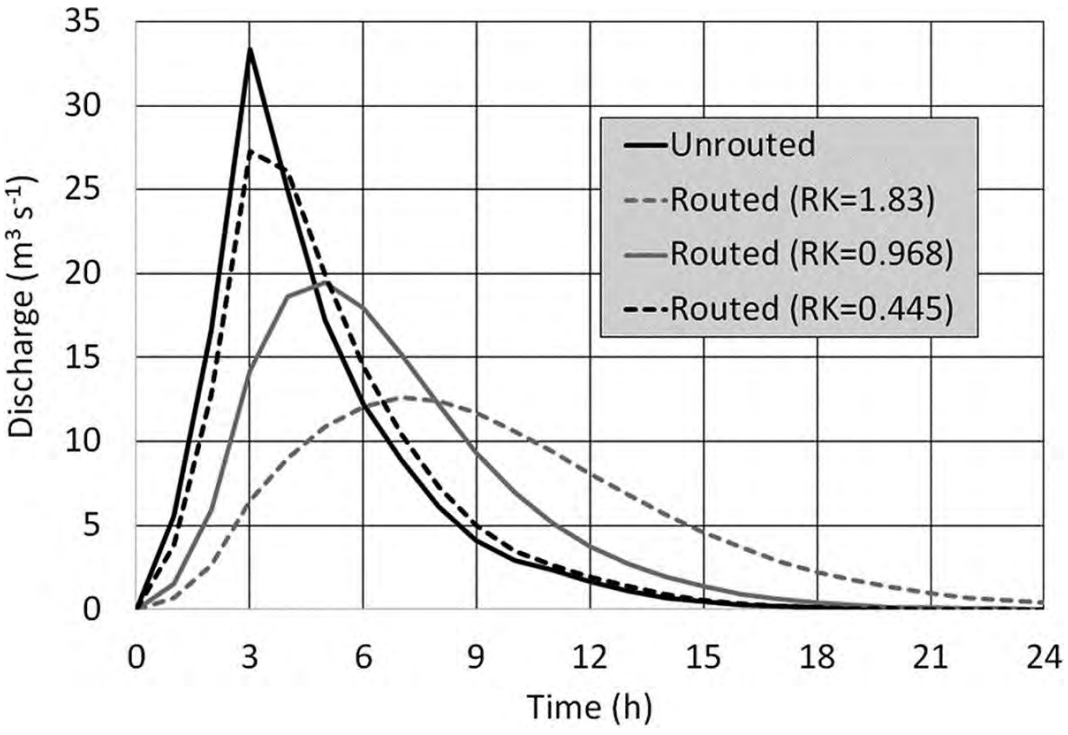

Figure 5.3 Unrouted and routed hydrographs for the 20 km^2 hypothetical catchment (routing based on three different *RK* parameters).

Table 5.1 lists all the *RK* values used, the runoff depth and peak values and the final calculated erosion (or sediment yield). Inevitably, the lumped approach, but with the same hydrograph and no routing (row 2), provides a much higher sediment yield than all the other estimates. However, this is a very unrealistic situation as it would be highly unlikely for a 20-km^2 catchment to have the same shape hydrograph as a 1-km^2 catchment. Row 3 lists the erosion estimate based on a mean (or representative) hydrograph for all grids, calculated for a single grid and then scaled to the total catchment, assuming no loss of sediment in the catchment. The results in row 4 are based on the three different hydrograph shapes referred to above and the total erosion mass is very similar to row 3. Varying the shapes of these three hydrographs within hydrologically realistic ranges, while retaining the weighted mean response of 25 mm and 6 mm h^{-1}, did not make much difference to the overall result.

Table 5.1 Muskingum routing *RK* values and sediment yield for different routing options applied to the hypothetical catchment and hydrographs shown in Figures 5.2 and 5.3 (total runoff depth = 25 mm).

K values (h)	**Depth (mm) & Peak (mm h^{-1})**	**Total catchment sediment yield (t)**	**Sediment yield relative to the unrouted grid value (row 3, distributed grid)**
No flow routing (lumped)	25 & 6.00	12 345	1.43
No flow routing (mean grid)	25 & 6.00	8 617	1
No flow routing	8 grids: 35.0 & 8.4	8 680	1.01
(distributed grid)	8 grids: 20.0 & 4.8		
	6 grids: 16.7 & 4.0		
1.83	25 & 2.22	7 079	0.82
1.303	25 & 2.84	8 126	0.94
1.162	25 & 3.06	8 461	0.98
0.968	25 & 3.44	9 040	1.05
0.863	25 & 3.65	9 348	1.08
0.794	25 & 3.77	9 516	1.1
0.545	25 & 4.55	10 579	1.23
0.482	25 & 4.67	10 725	1.24
0.445	25 & 4.80	10 898	1.26

Notes: The second row applies the erosivity equation (Equation 5.4) using the unrouted hydrograph for the total catchment. The third row computes the total sediment yield by applying the erosivity equation to individual grids (1 km^2) for a mean hydrograph shape and summing the sediment yield for all grids. The third row assumes three different hydrograph shapes for the grids. The other rows apply the erosivity equation using the routed hydrographs for the total catchment.

As illustrated in Figure 5.3 and Table 5.1, the regional *RK* values suggest a very wide range of attenuation effects over a 20km^2 catchment, from quite low to very high degrees of attenuation. The range of lumped (after hydrograph routing) erosion estimates range between 18% lower and 26% higher than that of the mean gridded estimate in row 3. As noted in the analytical analysis of the erosivity equation (Equation 5.1) illustrated in Figure 5.12, the MUSLE is very sensitive to the assumptions made about the shape of a lumped hydrograph response (rows 5 to 13), whereas it is much less sensitive to the assumptions made about how the hydrological response is distributed in a gridded approach (rows 3 and 4).

5.3 Assessments of topography (*LS)* spatial scale dependency

A single headwater catchment (48 km^2) of the Tsitsa River (outlet at 31.041°S 28.488°E) in the Eastern Cape of South Africa was used to investigate the potential spatial scale dependencies of *LS*. The *LS* factor was determined using the Shuttle Radar Topography Mission (SRTM) DEM data with a 30 m spatial resolution. The DEM data were analysed using ArcGIS 10.3 (ESRI Inc.). Detailed *LS* calculation methods are presented in Chapter 7 and in Gwapedza et al. (2018). The *LS* factor was determined for the entire catchment (lumped value) and for each of 55 × 1 km^2 grids (distributed values) covering the total catchment area (with some small overlaps into adjacent catchments).

The frequency histogram (Figure 5.4) shows the gridded *LS* values which have a mean of 5.7 and a median of 4.95. The lumped value for the entire catchment was calculated as 7.3, which lies at approximately the 70th percentile on the gridded cumulative distribution. These *LS* values suggest that a lumped approach would generate higher erosion values than the summation of the values for the distributed grids.

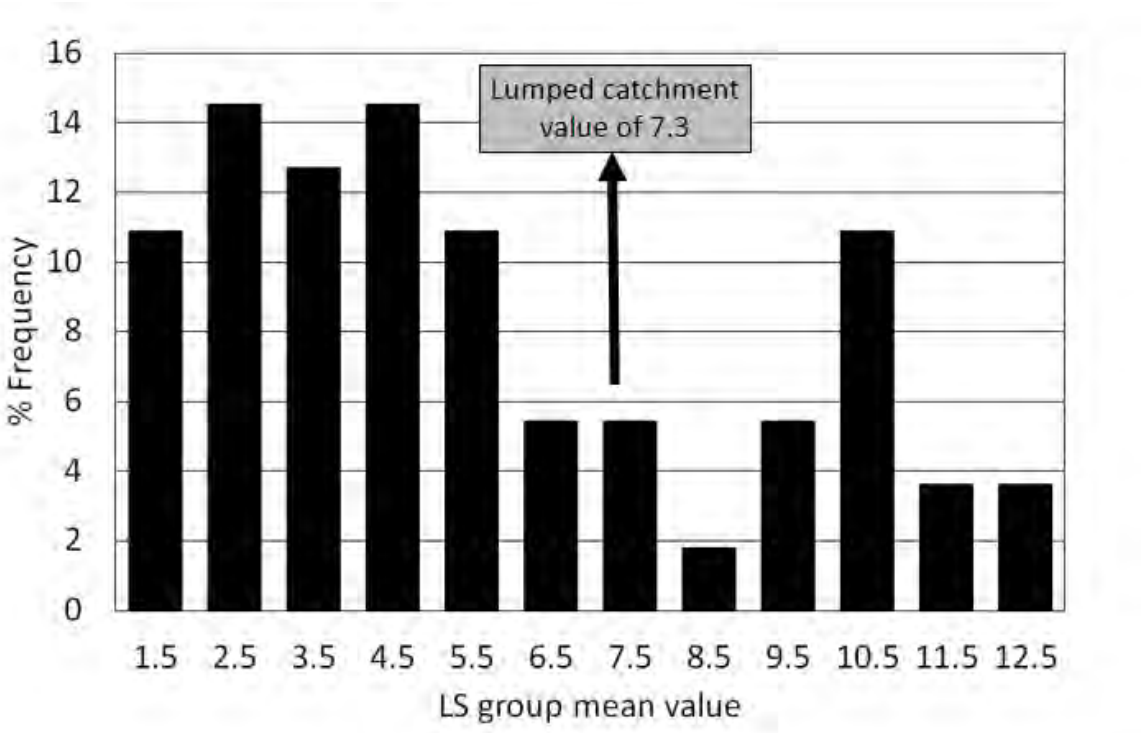

Figure 5.4 Illustration of the scale dependency of the topographic factor (*LS*) using a lumped and distributed approach.

However, the erosivity factor will also change between the lumped and distributed approaches. Therefore, the MUSLE has been applied with similar values as those used in the previous hypothetical example, assuming that the higher runoff estimates are applicable to the higher *LS* values and *vice versa*. For the lumped estimate, a total runoff depth of 25 mm and a *qdp* value of 3.06 mm h^{-1} were used, as these were found to provide the closest value for total erosion compared to the distributed model in Table 5.1. The gridded total erosion (corrected by 48/55 to account for the extra area occupied by the grids) was 20 226 t, whereas the lumped result was 23 475 t, some 16% higher than the gridded value. This relatively simplified example therefore suggests that the spatial scale uncertainties associated with the *LS* factor are quantitatively quite similar to that of the erosivity factor (Table 5.1).

5.4. Discussion and conclusions

The main scientific questions related to spatial scale and sediment yield are rooted in the hydro-geomorphological processes involved and it could be argued that they should really be resolved through detailed field studies (Sadeghi et al., 2013). However, such studies are not always

possible and Sadeghi et al. (2013) also noted that the results from small plot studies may not improve the accuracy of basin-scale estimates. It should also be acknowledged that basin-scale estimates are important from a practical water resources management perspective and that these are frequently required in data-scarce and large basin environments. The detailed guidelines offered by Renard et al. (1997) for predicting soil erosion using the Revised Universal Soil Loss Equation (RUSLE) are designed for field-scale studies and refer to the type of data that are available for the USA. These types of guidelines are therefore not appropriate for either large basins, or for data-scarce regions. It is therefore not unreasonable to suggest that there are important scientific questions about the way in which soil erosion and sediment yield estimation methods are included within basin-scale hydrological and water quality simulation models, as well as about the uncertainties associated with applying such models in different environmental situations.

The present study demonstrates that the MUSLE has the potential to generate different estimates of erosion depending on the spatial scale of the area under consideration and whether a lumped or distributed modelling approach is adopted. The erosion estimates are also sensitive to the size of sub-areas (or grids) used in a distributed, or semi-distributed, approach. This serves to illustrate that the MUSLE is spatially scale-dependent, and estimates of sediment yield across a large basin area (lumped approach) tend to result in larger values compared to the sum of estimates over smaller sub-basin areas (distributed approach), unless some of the other parameters of the model are re-calculated to compensate for the spatial scale effects. It is acknowledged that the largely hypothetical examples used are simplified and that the scale dependencies in real basin simulations might be far more complex. However, from a mathematical perspective, the general conclusions regarding spatial scale dependencies reached using the hypothetical analyses will be equally applicable in real-world examples.

The specific dependencies will always depend on the specific model and, for example, how the hydrology parameters and algorithms interact with the MUSLE at different spatial scales. The examples used suggest that the spatial scale dependencies are not very large as long as realistic approaches are used to quantify the parameters. For example, it would not be considered realistic to use a lumped approach without flow routing with a peak discharge that is applicable to a smaller scale (Table 5.1, row 2). This inevitably results in a much higher sediment yield estimate (12 345 t for the example given) than achieved when using a distributed approach (~8 600 t), while different methods of dealing with the effects of spatial variability in peak values

(Table 5.1, rows 5–12) suggest a lower range of sediment yield estimates (7 000 to 11 000 t). The effects of estimating the *LS* factor using different spatial scales was found to be in the same range. It is acknowledged that these spatial scale effects might be quite small compared to other uncertainties associated with the application of the MUSLE in real-world situations. However, users of the MUSLE should still make every effort to minimise the spatial scale effects as far as possible.

It has been noted that several publications (Chen and Mackay, 2004; Jha et al., 2004; Chaplot, 2014; Vigiak et al., 2015) have recognised the effects of spatial scale on simulated sediment yields. This contribution is designed to add to the growing body of evidence that supports the need for careful sensitivity testing in the application of any model that makes use of the MUSLE. The results of the present study suggest that the focus should be on the erosivity equation (Equation 5.1) and the *LS* factor, but clearly the methods used for spatial averaging of the other factors will also play a role. The scale dependency of the *LS* factor has only been briefly addressed in the present study, but the results suggest that it has the potential to be important. However, this issue certainly requires further investigation as any spatial scale dependencies are likely to vary a great deal with the topographic variations of a specific catchment, as well as with the methods used to estimate *LS*.

If the runoff depth and peak components of the erosivity equation are modelled explicitly for each grid of a fully distributed model, it seems likely that the scale dependency issues will be minimised. However, many models of this type allow for different grid sizes depending on the total catchment area (to limit model run times in large catchments), in which case some spatial scale problems may persist. Vigiak et al. (2015) suggested that the impacts of varying grid size in the SWAT model can be reduced by using a threshold area, and if the grid size is greater than this threshold, the sediment yield estimates are computed for the threshold area and then scaled to the total grid area [or 'linearised proportionally' in the words of Vigiak et al., 2015)]. The greatest potential problems with scale dependency are likely to occur in lumped (or semi-distributed, sub-basin) models where the modelled spatial domain can vary hugely. A similar approach to that used by Vigiak et al. (2015) could be the application of the erosivity equation to a fixed (small) representative area, and the scaling-up of the estimated erosion value to obtain an estimate for the entire sub-basin. With such an approach, it is assumed that the input MUSLE factors represent mean (or median) values for the whole sub-basin but are appropriate to the

representative spatial scale used. The results of the hypothetical example (Figure 5.3) listed in Table 5.1 suggest that the model is not very sensitive to likely uncertainties in the variability of the depth and peak runoff terms of Equation 5.1 across small sub-basins (or grids). This sensitivity is far less than the potential differences between the use of a lumped or gridded approach, depending upon any assumptions about flow routing and attenuation. In many lumped (or semi-distributed) approaches, the likely hydrological inputs to the model will be daily simulations of runoff volume at the outlet of the sub-basin (Hughes and Slaughter, 2015). If a 'representative grid' approach were to be used, the important issue would therefore be to estimate the peak value for the representative area. This is perhaps a better defined and more tractable modelling question than dealing with the other issues of scale dependency. However, the analytical approaches used in the present study (Sections 5.3.1 and 5.3.3) also indicate that it is possible to pre-calculate the likely impacts of varying spatial scale and to compensate for them using appropriate methods to quantify the scale dependencies in the relationship between runoff depth and peak in Equation 5.1. The present study also identified some spatial scale dependencies in the topographic factor (*LS*) and these would be more difficult to resolve with a representative area type of approach.

Chapter 6 Evaluating the effect of temporal changes in vegetation cover (*C*) factor on the MUSLE

6.1 Introduction

The relationship between precipitation, vegetation and erosion is well known, having been documented in the early work of inter alia Langbein and Schumm (1958) and the recent work of Martinez et al. (2017). The understanding of the effect of vegetation on erosion ensured that it was listed as one of the parameters within the USLE (Wischmeier and Smith, 1978). However, representing vegetation spatial and temporal change within models remains a challenge and recent work refers to attempts to find an appropriate temporal scale for parameterising the vegetation cover (*C*) parameter, typically using remote sensing techniques (Alexandridis et al., 2015; Schmidt et al., 2018). Wischmeier and Smith (1978) provide look-up tables for the USLE to guide the derivation of *C* values for specific vegetation coverage categories. However, the same authors warn that these may not be directly applicable to conditions outside the areas in which the estimation methods were developed. Renard et al. (1997) further developed guidelines for *C* factor estimation, with a focus on conditions in the USA where detailed vegetation cover data are available. Despite the restricted applicability of these results, their insights remain a crucial starting point for developing region-specific guidelines, particularly for countries such as South Africa where field measurements are scarce and the use of less detailed, low-resolution satellite data is a more accessible option. It therefore remains important to explore different methodologies for deriving the value of *C* (Sadeghi et al., 2013; Vrieling et al., 2008a) while also paying attention to temporal variations as a way of reducing some of the many uncertainties associated with modelling erosion and sediment yield.

The *C* factor as defined in the MUSLE is generally similar to that defined in the Universal Soil Loss Equation (USLE) (Wischmeier and Smith, 1978) and the Revised USLE (RUSLE) (Renard et al., 1997). Both studies suggest that because the USLE was developed to estimate long-term average soil loss, the factors in the equation (including the C factor) represent an integrated average annual condition. Renard et al. (1997) suggest the effects of vegetation cover fluctuations associated with rainfall and temperature tend to average out over time. Williams (1975) proposed the runoff factor for representing specific events, and suggested that the new equation (MUSLE) could be coupled with a hydrological model (Smith et al., 1984) to simulate time series of sediment yield. However, the original USLE factors were maintained (Karydas

et al., 2014; Smith et al., 1984) without an indication of how variations in the *C* factor should be accounted for. The *C* value is a simple linear scaling factor in MUSLE and understanding the effects of changes to the value for a single storm event (or day) is trivial. However, if the C value varies systematically with the value of the erosivity factor (*R* – based on runoff estimates), the effects on both long-term sediment yield, as well as the frequency distribution of daily sediment yield, are not readily predictable. Similarly, the implementation of the MUSLE in this study (WQSED model) includes sub-grid effects in an attempt to account for some of the spatial variations in the MUSLE parameters across a single sub-basin modelling spatial unit. The relationships between the sub-grid estimates of *C* and the other MUSLE factors (including the time varying relationships with *R*) suggest that predicting the effects of spatial variability in the *C* value may also be non-trivial.

As the spatial scale of applications of USLE-based models has extended from the plot to the watershed scale with the help of GIS (Karydas et al., 2014), some of the USLE factors have become difficult to estimate as prescribed in the original USLE and RUSLE handbooks (Alewell et al., 2019). However, GIS and remote sensing data have enabled erosion factors to be mapped over large areas, although limitations associated with accuracy still exist (Colman et al., 2019; Karydas et al., 2014; Schmidt et al., 2018; Sepuru and Dube, 2018).

The aim of this chapter is to explore the impact of different approaches to estimating the *C* factor on simulated sediment yield using the T35C sub-catchment of the Tsitsa River catchment as an example. The approaches include comparisons between a fixed value and a time-varying value, as well as the use of NDVI remote sensing data to quantify the time-series variation in *C*. The current version of the model is based on fixed *C* values and this part of the study is designed to assess whether adopting a more detailed approach to the *C* value estimation methods can be justified in terms of improved results.

6.1.1 *C* factor mapping through remote sensing technologies

Traditionally, the *C* factor has been determined by field measurements and interpolation (Wischmeier and Smith, 1978) using look-up tables for different land cover classes. This approach is only feasible at plot or field scales and becomes increasingly prohibitive as the area of the study increases because accurate measurements are expensive and time-consuming, and standard equipment is often not available (Vrieling et al., 2008). Recent applications of USLE and MUSLE type models are frequently at the basin scale (Noor et al., 2010; Arekhi et al., 2012; Sadeghi et al., 2013; Pan and Wen, 2014) and therefore *C* factor mapping using remote

sensing data has been adopted (Vrieling et al., 2008). A common approach is the use of classification of satellite imagery to derive land cover/use from which the *C* factor is then calculated (e.g. Almagro et al., 2019).

During the classification of multi-spectral satellite imagery, thematic information relating to land cover is extracted using semi-automated routines (Sepuru and Dube, 2018). Various methods of classifying satellite imagery have been developed. These can be merged into two distinct categories, namely supervised and unsupervised classification methods (Sepuru and Dube, 2018). Classification methods cluster pixels within the satellite image based on their similarity, in order to create land cover maps. The traditional method of assigning *C* factor values from the literature to classified land cover maps gives results that are constant over large areas (de Asis and Omasa, 2007) and fails to represent the spatial variability of vegetation cover (Wang et al., 2002). Errors in classification (Sepuru and Dube, 2018) are also introduced to the resultant *C* factor map (de Asis and Omasa, 2007). Therefore, direct regression of NDVI to the *C* factor is now used as an easier and cost-effective method of determining a spatially variable *C* factor (de Asis and Omasa, 2007; Phinzi et al., 2020; Vrieling et al., 2008).

Different land cover types have different spectral signatures, and it is possible to isolate land cover types in a satellite image based on spectral properties. Vegetation indices such as the NDVI are continuous variables that allow for a detailed spatial and temporal comparison (Vrieling et al., 2008), whereas land cover/use databases do not offer such flexibility. Vegetation indices are influenced by pigmentation, moisture content and the physiological structure of a vegetation type. Chlorophyll absorbs more red and blue bands in the visible spectrum and reflects green bands. In the near-infrared spectrum, the reflectance is high and proportional to the leaf development and cell structure, whereas in the mid-infrared spectrum, the reflectance is based on the content of water in the leaves. Leaves of low water content reflect highly whereas those of high water content absorb light of the mid-infrared spectrum and reflect less.

The Normalised Difference Vegetation Index (NDVI) is a measure of plant ‘greenness’ used to assess vegetation health. It is calculated as a ratio of the different reflectance signals between the infrared and red bands (Gandhi et al., 2015; Sepuru and Dube, 2018). The NDVI is one of the most widely-used vegetation indexes to investigate vegetation health (Vrieling et al., 2008b), and an important index used in vegetation and climate change research (Gandhi et al., 2015). NDVI values range from +1.0 to −1.0. Areas of bare soil, rock and snow have low NDVI

values of <= 0.1. Sparse vegetation such as grass and shrubs may have NDVI values ranging from 0.2 to 0.5, whereas dense forest vegetation may exhibit NDVI ranges of 0.6 to 0.9 (Weier and Herring, 2000). Green vegetation, therefore, yields high NDVI values, bare soil the lowest and water yields negative values.

Several studies (De Jong, 1994; van der Knijff et al., 1999; Cai et al., 2000) have attempted to develop NDVI to *C* factor conversion methods. However, limitations include the fact that NDVI is sensitive to vegetation vitality which is not consistently correlated to its soil protective function (De Jong, 1994). In spite of the limitations, NDVI continues to be a commonly used method to determine the *C* factor for large spatial scales (e.g. Alexandridis et al., 2015; Bhat et al., 2017; de Asis and Omasa, 2007; Islam et al., 2020; Le Roux et al., 2008; Phinzi et al., 2020; Sulistyo, 2016; Sun et al., 2014). The close relationship between NDVI and Leaf Area Index (LAI) (Fan et al., 2009; Palmer et al., 2017) has also led to LAI being used to estimate the *C* factor (e.g. Panagos et al., 2014). However, satellite LAI data has been criticised for poor representation of short stature vegetation (Fan et al., 2009), and for at times being inaccurate by a factor of 2 (Glenn et al., 2008). The two vegetation indices represent some of the more widely used methods to estimate the spatial and temporal variability of the *C* factor (Oliveira et al., 2015; Panagos et al., 2014; Sepuru and Dube, 2018) and this is important for catchment-scale modelling.

6.2 Methods

6.2.1 Acquiring NDVI data

Mean monthly values of catchment NDVI were accessed from Google Earth Engine (GEE) based on a script made available by the GEE developers (https://code.earthengine.google.com/,accessed July 2020). LAI was also accessed from GEE in order to assess the relationship between LAI and NDVI in the catchment. For spatially distributed NDVI data it was necessary to download and process images within GIS. Therefore, 'Landsat 8 OLI/TIRS C-1 Level-2' images were acquired. The data are atmospherically corrected surface reflectance values. The satellite imagery used within the present study is freely downloadable from the United States Geological Survey (USGS) Earth Explorer (https://earthexplorer.usgs.gov/,accessed January 2018), a service that provides satellite imagery.

The imagery acquired was generally of good quality because images with >10 % cloud cover were filtered in the search criteria. Two approaches were used to assess the impacts of a variable *C* factor. The first represents an inter-annual analysis over six years starting in 2013 (the launch year of the satellite) and based on data for a single month. Satellite images from March were chosen at the suggestion of Vrieling et al.(2008) that a single image selected over the main erosive season can suffice to describe the variability in the *C* factor. The second represents an intra-annual analysis using data for all months over two years, 2016–2017.

For the downloaded satellite images, the red (band 4) and near-infrared (band 5) data of Landsat 8 images were used in the analysis. NDVI was computed from these band images using the 'Raster calculator' tool in ArcGIS 10.3. The expression for calculating the NDVI is:

$$NDVI = \frac{NIR-Red}{NIR+Red} \quad \text{(Equation 6.1)}$$

Table 6.1 Dates of images acquired for inter-annual analysis.

Year	**Date image was taken**
2013	28 March
2014	14 March
2015	08 March
2016	19 March
2017	18 March
2018	09 March

6.2.2 NDVI to *C* factor conversion

Several methods of scaling NDVI to the *C* factor were assesed in order to find a method that could be applicable to the present study area. The assement revealed that some methods failed to calculate *C* from NDVI above certain thresholds (De Jong, 1994; Suriyaprasit and Shrestha, 2008; Durigon et al., 2014) (see Appendix B.1B). Other methods calculated *C* factors that were high (Sulistyo, 2016). Only the method proposed by Van der Knijff et al. (1999) gave reasonable *C* factor values without the need for modification (Equation 6.2); hence it was adopted for use in the current study:

$$C = exp\left[-\alpha.\frac{NDVI}{(\beta-NDVI)}\right] \quad \text{(Equation 6.2)}$$

In Equation 6.2, α and β are parameters that determine the shape of the NDVI - *C* factor curve, with values of 2 and 1, respectively, suggested. A low NDVI suggests little or no vegetation and results in a high *C* factor, while a high NDVI results in a lower *C* factor.

The method proposed by Van der Knijff et al. (1999) has been criticised for underestimating the *C* factor in areas with intense rainfall (Durigon et al., 2014), with specific reference to a catchment in Brazil. However, a recent study by Almagro et al. (2019) in a tropical Brazilian catchment reported that the same method over-estimates the *C* factor. Such disparities indicate the uncertainties associated with the method so that it is vital to validate predicted *C* factor values with field-collected data (Suriyaprasit and Shrestha, 2008). In the current study, validation of the predicted *C* factor yielded linear regression R^2=0.75 when compared to field validation data (See Appendix B.1A).

Differences in the intra-annual variations in the *C* factor were also analysed for the two most prominent natural vegetation cover classes: grass (74%) and thicket/forest (5%). This analysis was designed to assess which class was more variable and thus might have a significant influence on the mean catchment *C*. Unnatural vegetation classes (e.g. cultivation and plantations) were not included because their temporal variation may depend on human influence and the management information with regards to planting and cropping is not easily accessible.

6.2.3 Sediment yield calculations

Three catchments that include the Tsitsa river and its tributaries Inxu and Mooi (T35C) rivers were considered for the analysis. T35C was used for the long term inter-annual analysis and two-year intra-annual. The other two catchments subsequently served to validate the outcome of the T35C analysis based on observed sediment data. The sediment yield calculations were conducted using the MUSLE as applied within the WQSED model (Chapter 4). The storage model was not included as the assessment sought to analyse direct MUSLE simulations. The focus of the application was to assess whether the potential temporal variability in *C* factor would lead to large differences in cumulative sediment yield. To achieve this, the model was first run with fixed *C* factor inputs calculated using the widely used land cover/use maps and secondly run with variable *C* factor inputs calculated using the NDVI method (section 6.2.1). Although the model was applied at a daily timescale, computed monthly *C* factors were held constant over the entire month and over the entire year for the intra-annual and inter-annual

analysis, respectively. The fixed *C* factor was held constant across all the time scales. The flow data input to the model was based on records of observed daily discharge. Sediment outputs were evaluated using the R^2, PBIAS and Nash Sutcliffe Efficiency (NSE) (Nash and Sutcliffe, 1970). Tables with the calculated MUSLE factors are presented in Appendix C.2.

6.3 Results

6.3.1 Fixed *C* factor

The *C* factor for catchment T35C was calculated as **0.098.** Table 6.2 summarises the *C* factor calculation for the T35C catchment using landcover/use maps and *C* values from the literature. The total weighted *C* factor (column 5, last row) was used as the *C* factor value within the MUSLE.

Table 6.2 Fixed catchment (T35C) *C* factor calculated using maps and values from the literature.

Class Name	Pixel count	% of total	*C* factor	Weighted *C* factor
Thicket /Forest	13 441	5.1	0.009	0.000461
Woodland/Open bush	4 234	1.6	0.012	0.000194
Low shrub land	1 306	0.5	0.013	0.000065
Plantations	38 838	14.8	0.012	0.001776
Cultivated	3 553	1.4	0.37	0.005008
Settlements	728	0.3	0.1	0.000277
Wetlands	5 897	2.2	0.038	0.000854
Grasslands	194 031	73.9	0.12	0.088708
Waterbodies	31	0	0.01	0.000001
Bare Ground/Degraded	417	0.2	1	0.000715
Total	**262 476**	**100**		**0.098**

6.3.2 NDVI and variable *C* factors

Figure 6.1 illustrates that the NDVI values are higher for the summer rainfall months and lower during the generally drier and cold winter months. They generally start to increase with the onset of the rainfall season after September. Figure 6.2 indicates that there was a weak positive

linear relationship (R^2=0.49) between NDVI/*C* factor and rainfall and a somewhat stronger linear relationship (R^2=0.55) with temperature. A similar trend in the monthly NDVI was noted for 2017 (Figure 6.1). The lowest *C* values occurred in February during both years (0.02 in 2016 and 0.016 in 2017), while the highest values of 0.30 and 0.32 were obtained in September for 2016 and 2017, respectively. The LAI displays a similar seasonal trend compared to the NDVI; a strong linear regression (R^2=0.88) is exhibited between the LAI and NDVI (Figure 6.1).

The inter-annual *C* factor distribution presented in Table 6.3 shows the differences between the variable *C* factor (based on March NDVI data) and the fixed value. It is immediately clear that *C* factors calculated for March are much lower than the fixed values calculated from the literature values of vegetation cover types. Figure 6.2 illustrates that late autumn to early spring *C* values are much higher compared to either the fixed *C* value or the single month NDVI estimate. However, as already noted, the important issue with respect to impacts on sediment yield depends on the seasonal variations in the erosivity factor that is driven by the runoff data.

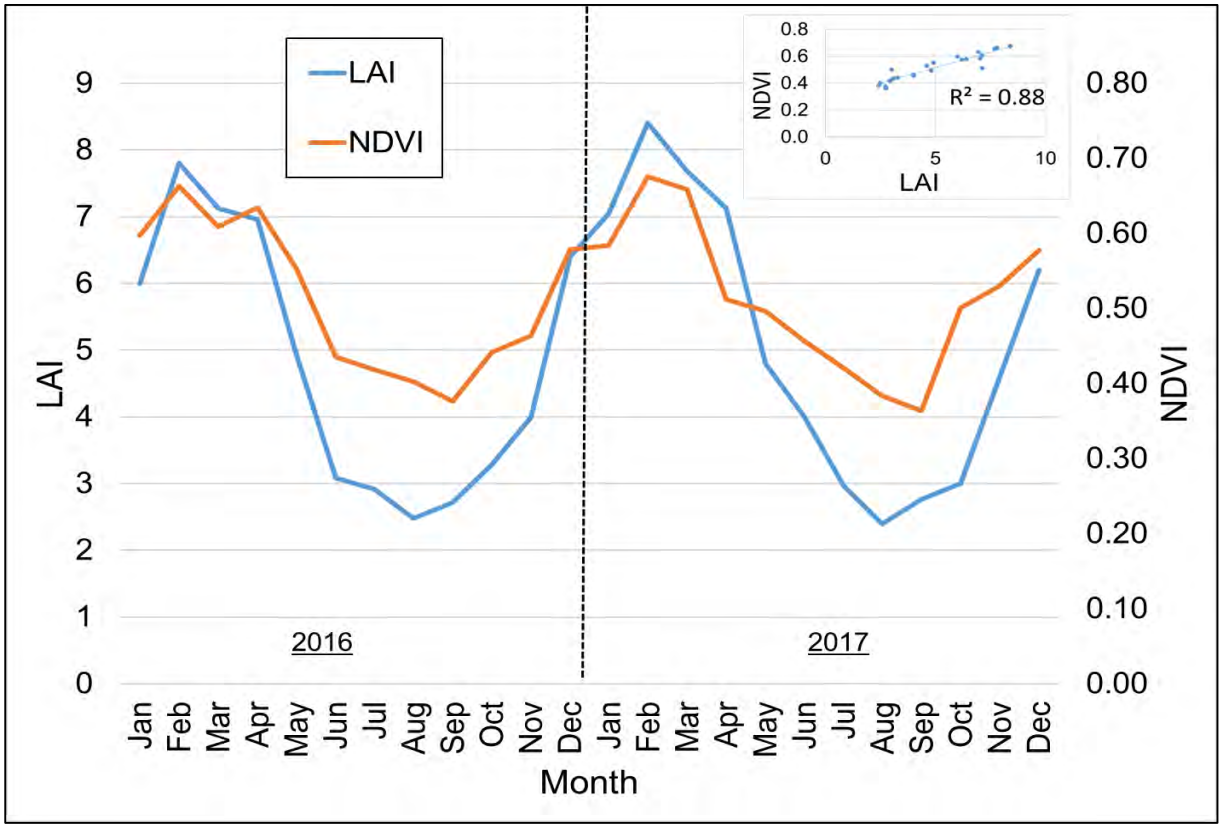

Figure 6.1 Distribution of monthly NDVI and LAI factor for 2016–2017.

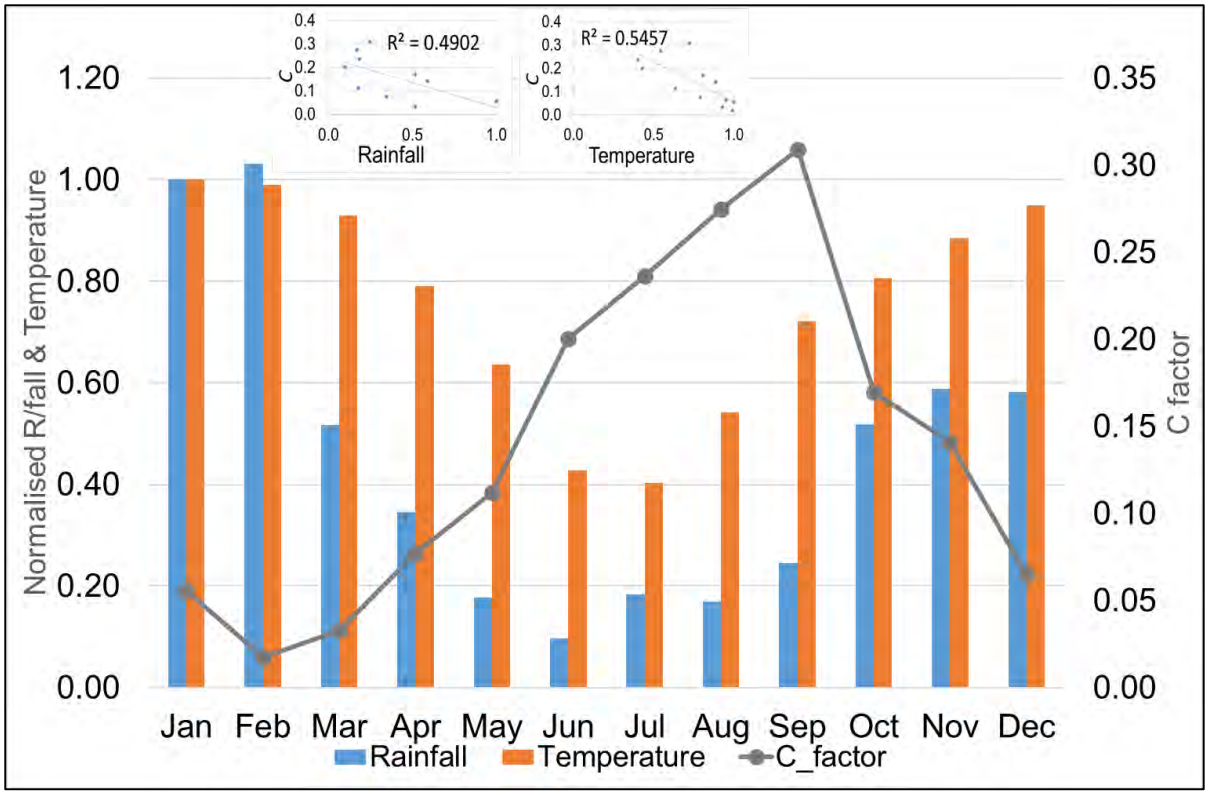

Figure 6.2 The relationship between normalised rainfall and temperature with *C* factor; insert linear regression of rainfall, temperature and *C* factor for the years 2016–2017. The climate values were normalised by dividing all values by the first value in the distribution (i.e. Jan).

Table 6.3 Percentage variation between inter-annual and fixed *C* factors for catchment T35C.

Year	NDVI	*C* factor	% of fixed *C* (0.098)
2013	0.67	0.017	17
2014	0.70	0.009	9
2015	0.68	0.014	14
2016	0.65	0.024	24
2017	0.67	0.017	17
2018	0.69	0.012	12

Figure 6.3 illustrates the variation in the *C* factor values derived from NDVI data for the two main vegetation types within the T35C catchment. The maximum and minimum values represent the range of calculated NDVI *C* values across all the pixels that were classified into

the two vegetation types. The grassland type has the largest seasonal range, particularly in the maximum values, as well as the largest difference between maximum and minimum values. This could reflect the fact that grasslands in this area include both natural grassland, as well as heavily grazed and therefore degraded grassland. The minimum values for the thicket/dense bush vegetation type are always 0, while the maximum values vary from 0.04 in the wet season to 0.21 in the dry season. This may reflect the variations in the location of the bush areas within the landscape, the consistently low values lying in well-watered valley bottom locations, while the more variable *C* values reflecting locations on slopes and ridges that are more prone to seasonal variations in moisture availability.

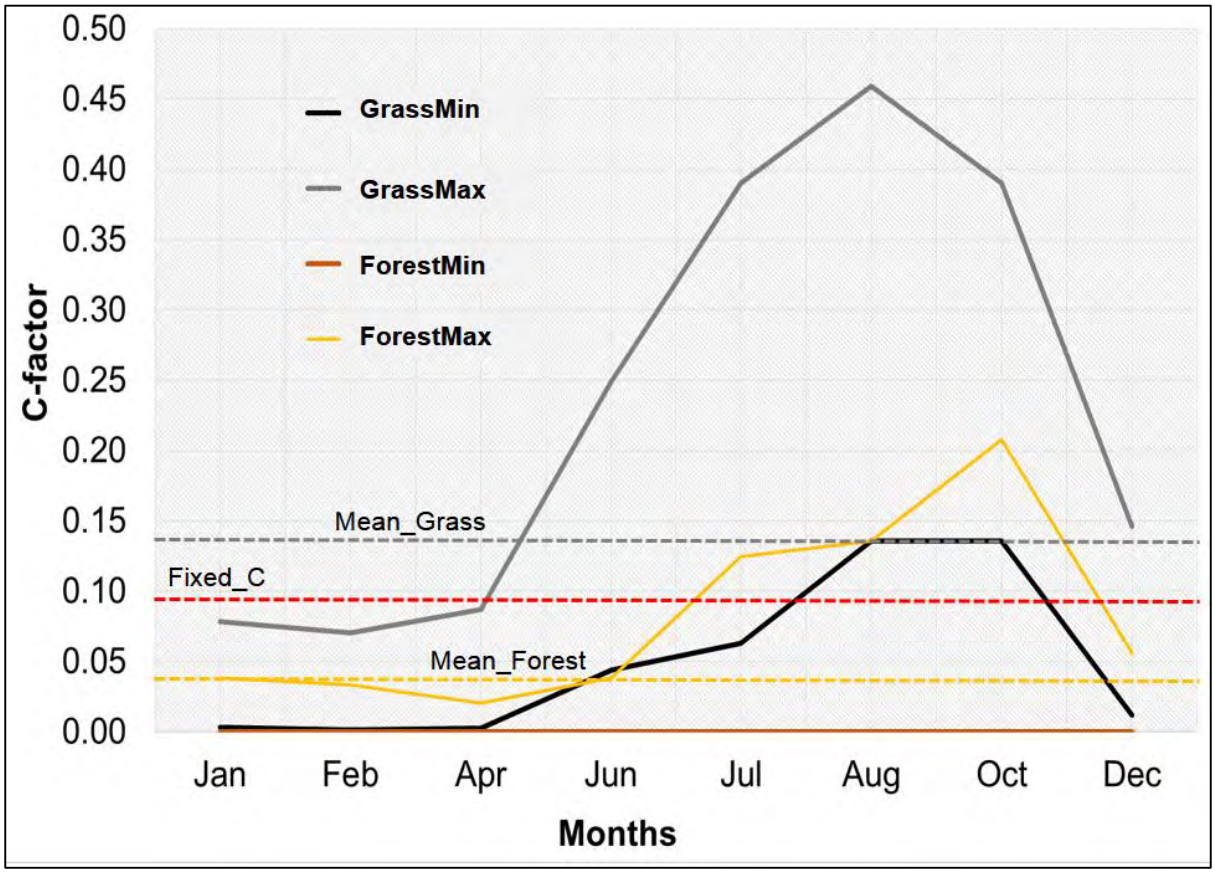

Figure 6.3 Monthly *C* factor distribution of the grass and forest vegetation classes in the T35C catchment for the year 2016 calculated from NDVI.

6.3.3 T35C catchment sediment yield (SY) distribution

The results for 2016 (Figure 6.4) show that the fixed *C* factor yielded much higher sediment output compared to the variable *C* factor, with total annual sediment yields calculated as 5 464×10^3 and 4 625×10^3 tons, respectively. The major differences occur in the three main summer runoff months. These impacts are somewhat offset by higher sediment yields using the variable *C* factor in the winter and spring months, when the *C* values are quite substantially higher than the fixed value. The results for 2017 (Figure 6.5) also display the typical seasonal variability exhibited in 2016. However, there is a larger difference between the total sediment yields simulated using the fixed (5 203×10^3 tons) and dynamic (2 871×10^3 tons) *C* factors. In this year the sediment generated during the two main summer months (January and February) is substantially reduced, there is little sediment generated during the winter and during the months of November and December the fixed and variable *C* values are similar. The analyses of the two years clearly indicate that the differences between the use of fixed and variable *C* factor values are dependent upon the rainfall and streamflow regime during the year and whether the dominant erosion and transport events occur during the year when the variable values are close to, or very different from, the fixed estimates.

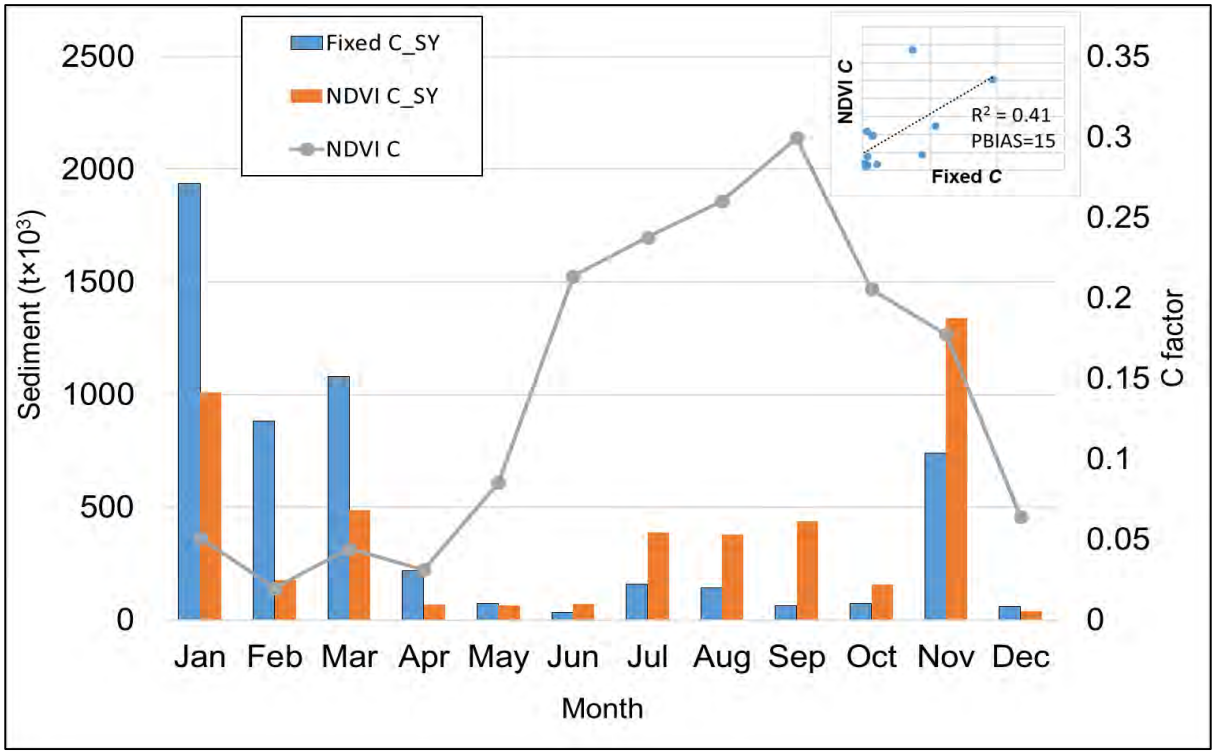

Figure 6.4 Distribution of sediment yield simulated using the fixed and variable (NDVI) *C* factors for catchment T35C in 2016.

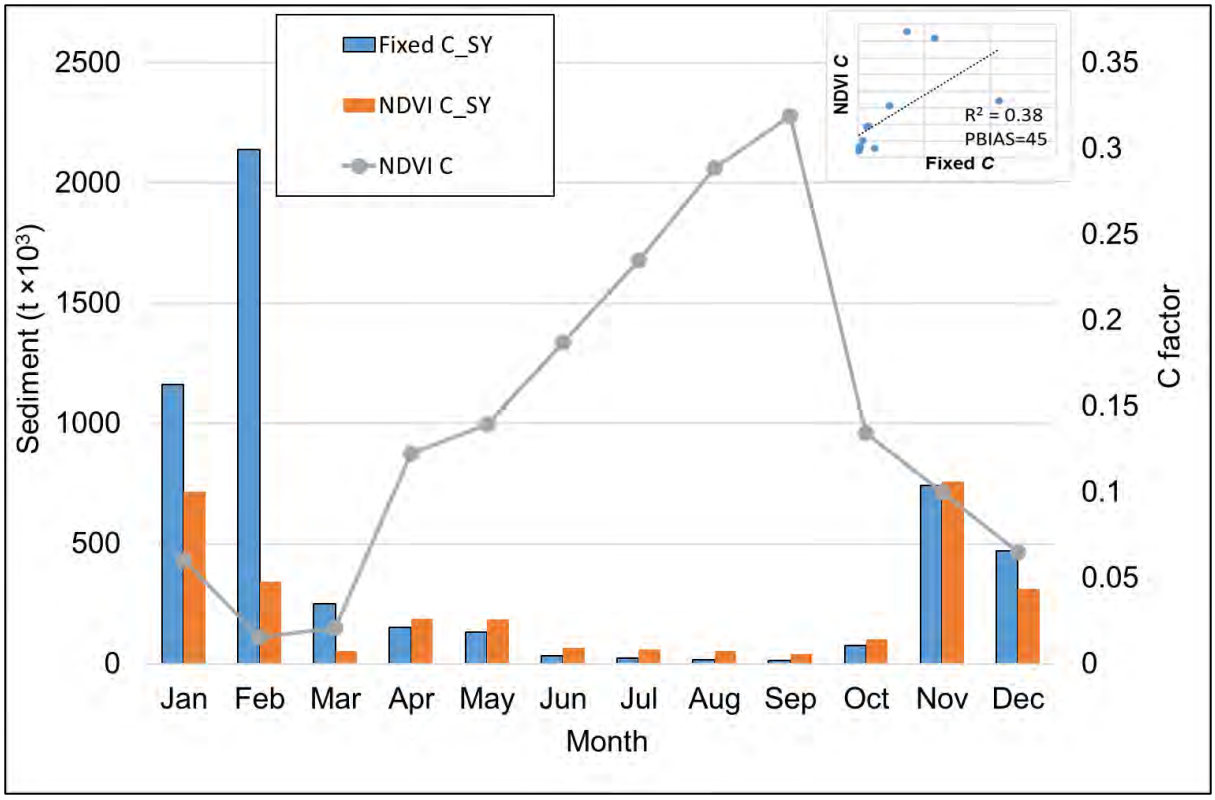

Figure 6.5 Distribution of sediment yield simulated using the fixed and variable (NDVI) *C* factors for catchment T35C in 2017.

Figure 6.6 shows the results of the inter-annual analysis using annual variations in the *C* factor based on March NDVI data, compared with a fixed *C* value. The differences are substantially greater than those revealed by the intra-annual analysis based on 2016 and 2017. The variable C value results in approximately 85% less sediment compared to 16% and 45% less based on the intra-annual analysis for 2016 and 2017. This is, of course, a result that could have been predicted from the data provided in Table 6.3 which indicates that the March-based *C* values are only ~15% of the fixed value. The clear conclusion is that using a single month to determine the annual variability in *C* values is likely to be a very uncertain exercise.

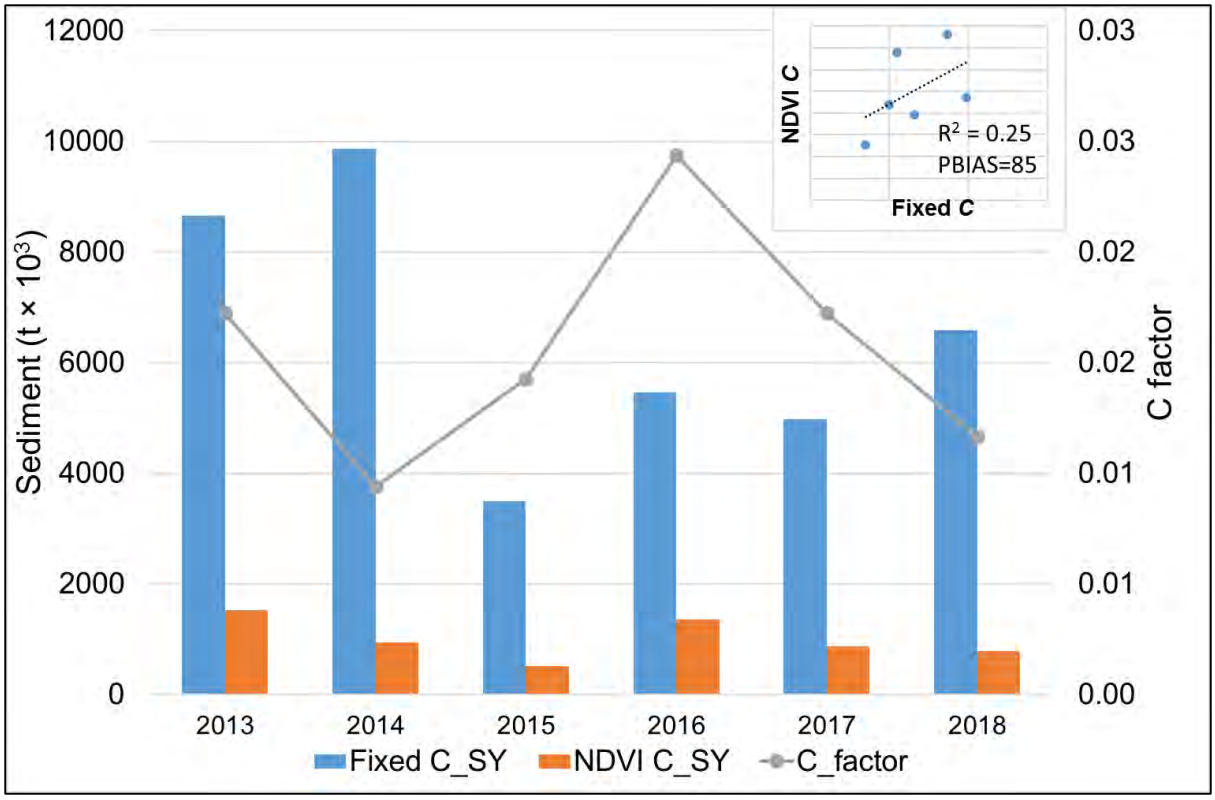

Figure 6.6 Sediment yield variation resulting from the fixed and variable (NDVI) *C* factor.

6.3.4 Validating the *C* factor assessment in the Tsitsa catchment and Inxu sub-catchment

The results summarised in Table 6.4 and in Figures 6.7 and 6.8 corroborate the findings reported in Section 6.3.3, showing that the use of a fixed *C* factor results in the over-estimation of sediment yield when compared to observed data in both sample catchments. However, the R^2 values for both daily and monthly time scales suggest that the poor results are a consequence of systematic bias. Given that the *C* factor is a linear multiplier in the MUSLE, it could be calibrated (together with the other linear factors in the equation) to generate a much more acceptable result on the basis of the NSE and PBIAS statistics. This would involve reducing the fixed *C* value. For the Inxu, the use of a variable *C* factor leads to an under-estimation of about 78%, and while the NSE and PBIAS statistics are much improved, the R^2 values for daily and monthly are much lower compared with the fixed *C* factor result. The conclusion is that the un-calibrated model result is better, but also that a simple scaling calibration would be less effective. For the Tsitsa, the variable factor model results in over-estimation (but less than with a fixed factor), and the conclusions about further calibration are the same as for the Inxu catchment.

Table 6.4 Summary of sediment yield (SY) output in the Inxu and Tsitsa catchments compared to observed data.

Catchment	Fixed *C* value	Sediment yield (ton ×10^3)			SY relative to observed	
		Fixed *C*	Variable *C*	Observed	Fixed *C*	Variable *C*
Inxu	0.13	11 312	840	1 072	10.60	0.80
Tsitsa	0.12	785	455	362	2.20	1.30

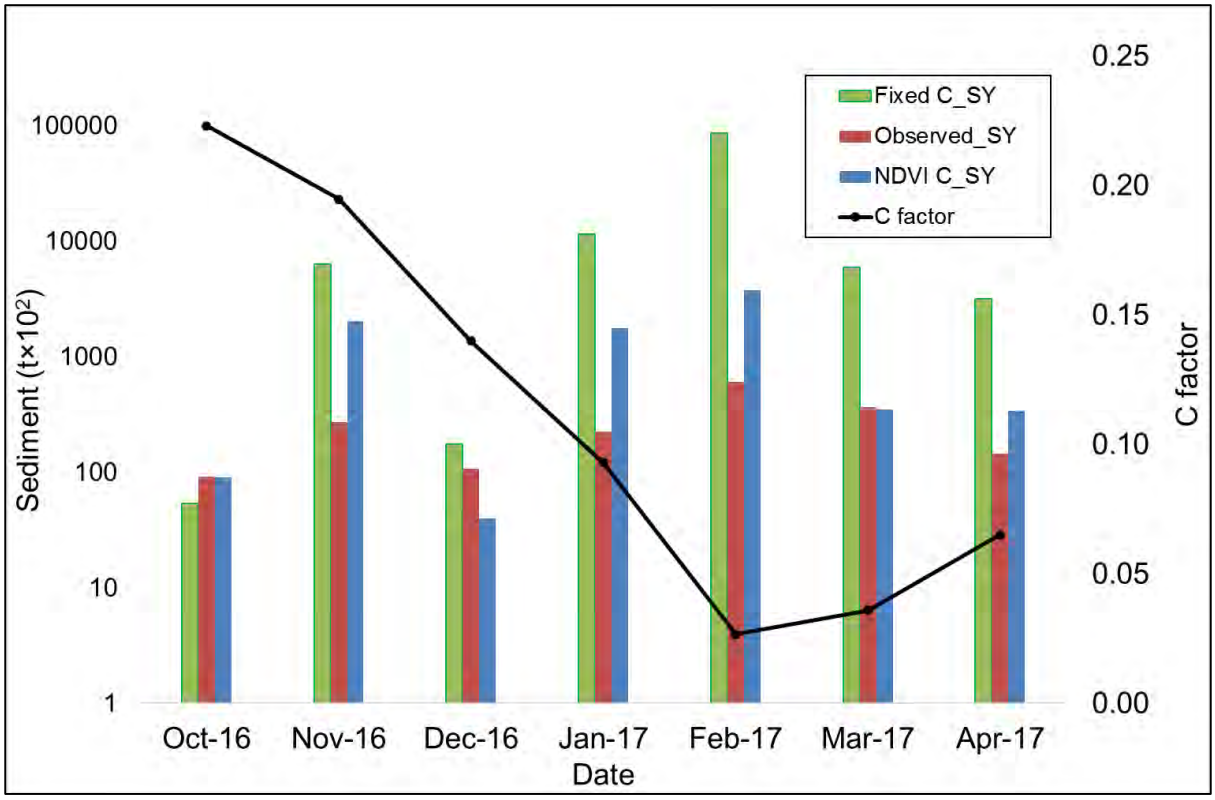

Figure 6.7 An illustration of observed SY versus sediment calculated using the fixed and variable (NDVI) *C* factors in the Inxu catchment (Log Y-axis).

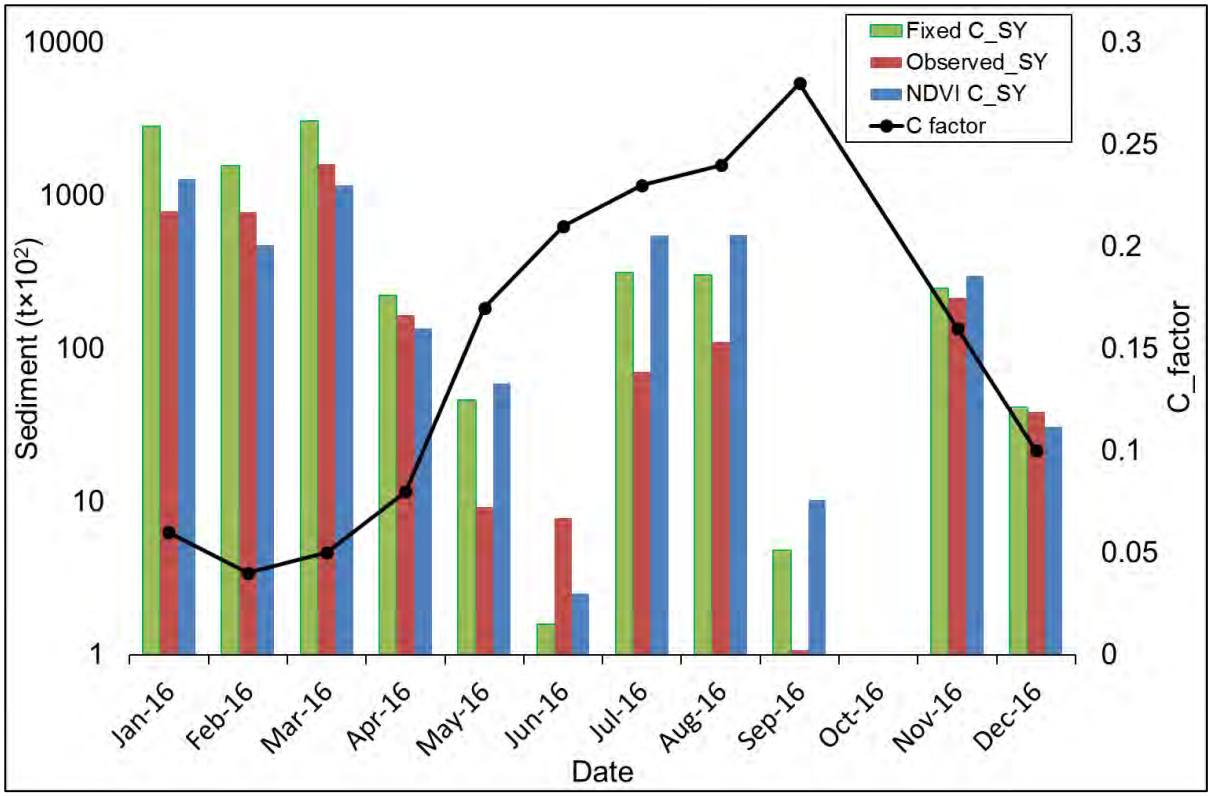

Figure 6.8 An illustration of observed SY versus sediment calculated using the fixed and variable (NDVI) *C* factors in the Tsitsa catchment (Log Y-axis).

Table 6.5 Summary statistics comparing observed data the SY output attained using a fixed or variable *C* factor at daily and monthly time scales.

		Daily			Monthly		
Catchment	***C* factor type**	**R^2**	**NSE**	**PBIAS**	**R^2**	**NSE**	**PBIAS**
Inxu	Fixed *C*	0.76	-32	954	0.99	-0.81	954
	Variable *C*	0.52	0.37	-21	0.67	0.49	-21
Tsitsa	Fixed *C*	0.75	-0.22	115	0.89	-0.92	117
	Variable *C*	0.45	0.40	22	0.65	0.62	26

The observed records that are available for the Inxu catchment preclude an analysis of the seasonal variations in sediment output. However, the relatively short record for the Tsitsa suggests that winter runoff and sediment yield can play a quite important role, at least in some years. It is therefore interesting to note that the largest over-simulations occur in the late autumn to early summer months, when the estimated *C* values are quite high. This could reflect the

uncertainties in the use of the NDVI data to estimate the *C* values, particularly when the NDVI values are low in winter, when the organic matter cover on the soil surface still provides some protection from erosion.

6.4 Discussions and conclusions

In general, the analysis showed greater intra-annual variability in the *C* factor as compared to inter-annual variability. The findings of Vrieling et al. (2008) support the above result as they found that vegetation cover, and hence the *C* factor, can show high intra-year variability, depending on seasonal effects and land management. A correlation of *C* factor values between the months of years 2016 and 2017 yielded 0.9, indicating that there was little variability in the distribution of *C* factor values on a month-to-month basis for the two years. The results also indicate that the grass vegetation class has the highest seasonal variation, and this has the greatest impact on sediment yield as it has the highest spatial coverage in the T35C catchment.

The linear regressions between the *C* factor, temperature and rainfall (Figure 6.2), show that there are no strong individual linear relationships between rainfall or temperature and the *C* factor derived from NDVI, although the relationship with temperature is slightly higher. This can be partly attributed to the fact that both temperature and moisture availability are likely to affect increased NDVI values (Lin and Fang, 2016), and that vegetation cover response to rainfall and temperature is likely to be lagged. The strong linear relationship between LAI and NDVI (Figure 6.1) in the catchment is important (Fan et al., 2008) as both have been criticised (Schmidt et al., 2018) for different reasons: NDVI for failure to represent the erosion resistance of poor vitality vegetation as it is bound to chlorophyll reflectance, and LAI for failure to represent short stature vegetation (e.g. grasses).

Additional criticism concerning the failure of both LAI and NDVI to represent poor vitality and above-ground biomass of short stature vegetation (during winter), reveals a major shortcoming of the two spectral indices. This limitation is apparent in Tsitsa catchment results, where over-estimates in winter dominated the simulations, while many of the over-estimates for the short Inxu data record is in spring and early summer before the NDVI values reach their highest peaks. Accordingly, the popular methods of calculating the integrated *C* factor at plot scale then extrapolating/scaling the information to larger areas using land use/land cover areas (e.g. Colman et al., 2019) have already been identified as flawed by Beven (1989). Both the Inxu and Tsitsa examples highlight the likely over-simulations that might occur by using an

uncalibrated fixed *C* factor based on land cover and look-up tables. While the use of the NDVI-derived variable *C* values improved the simulations, there remain substantial uncertainties in the applicability of the NDVI-based estimation methods for the *C* factor. The developers of the NDVI to *C* factor conversion methods did not seem unaware of the limitations of the index but sought to conduct a direct conversion based on the similarity of the range of NDVI values to the original *C* factor range.

The results of the present study suggest that failure to account for temporal changes in vegetation cover may add to some of the many uncertainties associated with modelling sediment yield. The sediment yield simulations using the fixed *C* factor were generally higher mainly because the wet summer season *C* values are typically lower than the fixed value. The fact that a high *C* factor might not translate into high sediment yield if there is a limited runoff during the winter season is a somewhat obvious conclusion. However, the admittedly short period of data for the Tsitsa catchment suggests that winter rainfall and runoff is possible in at least some years and locations in this general region. This implies that the over-estimation of the *C* factor in winter could be important and represents a major limitation of the NDVI estimation approach. It is also evident from both catchments that the transition months from low to high *C* values (autumn), and from high to low values (spring) can represent periods when sediment load over-estimations occur. The overall conclusion is that while the NDVI approach is useful in terms of identifying spatial variations in the *C* value, the actual estimation equation (Equation 6.1) requires some revisions. It is likely that these revisions may be site-specific. For example, the effects of using the approach in the winter rainfall regions of the Western Cape Province may be quite different to the effects illustrated in the T35 region of the Eastern Cape (mainly summer rainfall, but with some winter rainfall), and may be different again in other parts of South Africa where winter rainfall is very rare. The inter-annual analysis, based on annual variations using a fixed month, illustrated that this somewhat simpler approach to allowing for *C* variations will be very uncertain. This is particularly true for a region with a variable rainfall (and therefore runoff) regime in which high rainfall events can occur during most months of the year, even if they are more frequent during the summer months.

The analysis of *C* variability across the two vegetation types (Figure 6.3) suggests that any revisions to the NDVI-based estimation approach may also need to be vegetation-type specific. The seasonal and spatial variations in the derived *C* values are much greater for the dominant grassland type than for the less frequent bush/forest type. A further, potentially related, issue is that over-grazing has often been cited as one of the reasons for high sediment loads in the

T35 region (Le Roux, 2018; van Tol et al., 2016). However, it is also suggested that a great deal of the sediment load may be derived from gully erosion (Le Roux, 2018) which is not explicitly simulated by the MUSLE and therefore is a potentially different issue, unrelated to how the seasonal *C* values are estimated.

The availability of satellite data and GIS processing tools allows an alternative approach to the use of a lumped *C* factor estimation using land cover maps, by employing spatially distributed approaches based on spectral indices such as NDVI. Nevertheless, access to high-quality satellite data is often expensive and some available data may not be useful for analysis because of problems such as poor resolution and cloud cover. Although cloud cover removal techniques are available, this only adds uncertainty to the quality of the pre-processed image. Consequently, some of the 30m Landsat data used were carefully selected and manually processed to ensure the quality of the NDVI output. However, as the analysis was conducted in a single region over a small number of years, assessments that are more robust are needed to investigate the NDVI to *C* factor conversion used in this initial assessment. Nevertheless, the study highlights the variations in outputs associated with different approaches to estimating the *C* factor. Increasing spatial and temporal resolution is vital for describing catchment processes in greater detail. Maintaining simplicity in model parameterisation is also central to the current research and the results should assist potential users to anticipate the likely effects of scale (temporal and spatial) in MUSLE applications. Overall, the current study shows the importance of adopting a monthly/seasonal distribution of *C* factor values when applying the WQSED model and other models that use the MUSLE to calculate sediment, but also highlights a number of uncertainties in the current methods used to calculate the variability of the *C* factor.

Chapter 7 Regional testing and evaluation of the WQSED model

7.1 Introduction

Sediment yield models that provide reliable simulations are needed if they are to be integrated into catchment management and planning. Although the reliability of model estimates can only be tested and validated against observations, daily observations of sediment data are generally not accessible in most African catchments, and this lack of data constrains the usefulness of model estimates. Although several sediment modelling studies have been conducted in South Africa since 2005 (e.g. Grenfell and Ellery, 2009; Le Roux, 2018; Le Roux et al., 2008; Phinzi et al., 2020; Scott-Shaw et al., 2020), some of these studies were not validated because of a scarcity of observed data. Although previous model estimates are often used to 'validate' simulated outputs in the absence of observed data, this approach cannot be considered a reliable method of validation; independent sources of sediment yield data are therefore required.

This chapter aimed to calibrate and validate the application of WQSED to various catchments in South Africa using observed data. However, since this project could only gain access to data for two South African catchments (Tsitsa and Inxu sub-catchments) with short (one season) observed sediment records, the application of the model was extended to catchments in Zimbabwe (Gwai and Odzi) for which there are some limited observed sediment data. Additional catchments were selected from the United States of America (USA) (Grand Cane and San Patricio catchments) and the USA territory of Puerto Rico (Rio Tanama catchment) to supplement the model testing exercise. Model parameterisation was based on the parameter estimation approach outlined in Chapter 4. Lists of parameters for all the catchments are presented in Appendix C.2.

7.2 Setting up the models

The data inputs for the WQSED model can be broadly categorised as flow inputs and input data that describe the physical catchment conditions. The flow inputs include time series of daily basin total flow and separated surface runoff through which the model simulates sediment yield at a continuous daily time scale. As the WQSED does not directly simulate flow, flow inputs into the model can either be based on simulations by a hydrological model or on observed data; the accuracy of simulated sediment yield is therefore largely dependent on the accuracy of the flow inputs. Observed flow should be used if a complete dataset is available,

while simulated flow used if observed flow data are absent, incomplete or deemed unreliable. Appendix C.1 shows the graphs of observed flow discharge and sediment loads from the selected catchments.

Three components of the WQSED model, namely MUSLE and the simple and complex storage options (See Chapter 4), are a main focus in this chapter. Sediment yield from the three components are separately compared with observed data to evaluate the performance of the model as complexity increases. The WQSED model outputs are time series of total daily erosion and sediment yield (both in metric tonnes) at the outlet of each sub-catchment. Secondary outputs (from the complex storage version) include a time series of sediment concentrations, sediment outputs per slope zone and sediment storage based on the slope distribution approach described in Chapter 4 (section 4.3).

7.2.1 Calibration, validation and assessment of model performance

The WQSED model requires calibration of the input parameters shown in Table 7.1. Calibration is considered successful when simulated outputs reflect the temporal and spatial variation of the observed data. The model is typically run with an initial set of estimated parameters, after which manual parameter adjustment is performed to ensure the best fit between the observed and simulated data.

Table 7.1 Erosion and sediment transport model (WQSED) primary calibration parameters. A hyphen (-) indicates values based on the area of application.

	Parameter	**Parameter range**	
		Min.	Max.
1	*Q* depth power (D_{pow})	0.0	-
2	*Q* depth constant (D_{con})	1.0	24.00
3	Initial storage fraction	0.0	1.00
4	Sediment storage ratio power	0.0	-
5	Threshold flow for sediment delivery	0.0	-
6	Proportion of sediment in gully storage (C_{prop})	0.0	1

D*pow* and D*con* in Table 7.1 are duration parameters that are considered to be of a priority since although optimum catchment storm durations are not known, storm duration affects both the MUSLE and storage models. The duration parameters are optimised to reduce or increase sediment output from the MUSLE. This chapter includes a sensitivity assessment of the storm duration effects on simulated sediment output. The storage fraction and ratio parameters (3 and

4 in Table 7.1) are either increased or decreased to maintain high or low sediment delivery from the storage module, respectively. The parameters are optimised to ensure that the storage achieves a dynamic equilibrium in which stored sediment is not consistently accumulated or lost. The sediment delivery threshold is optimised to constrain the discharge events that lead to sediment delivery; decreasing the threshold limits sediment delivery during low flow periods. Increasing C_{prop} enhances catchment connectivity and increases sediment delivery. For most catchments, optimising the durations to constrain MUSLE sediment export into storages, and threshold flow to control the timing of sediment delivery to match the observed data are vital for successful calibrations.

The calibration effort involved splitting the available observed data into two independent datasets. The point at which the observed dataset is split aims to capture the range of variation in the flow of the entire observed dataset, in each of the calibration and validation datasets. However, since some of the observed datasets are relatively short, some validation periods are generally much shorter compared to calibration periods. Two catchments with more than ten years of observations (Odzi and Rio Tanama) are regarded as the benchmarks of the model evaluation. Odzi and Rio Tanama are presented first and are used to demonstrate the performance of the model as complexity increases with the addition of storage components. The results of the other catchments with shorter records of observed data are subsequently reported; these results are based on the application of the simpler storage option of the model.

In this study, the coefficient of determination (R^2), the Nash-Sutcliffe coefficient of efficiency (NSE) (Nash and Sutcliffe, 1970) and the percentage bias (PBIAS) are applied to assess the goodness of fit between observed and simulated data.

The coefficient of determination R^2 is widely used for model evaluation and is given as:

$$R^2 = \frac{[\sum(\boldsymbol{Y}_{obs}-\bar{Y}_{obs})\times(\boldsymbol{Y}_{sim}-\bar{Y}_{sim})]^2}{[\sum(\boldsymbol{Y}_{obs}-\bar{Y}_{obs})^2\times(\boldsymbol{Y}_{sim}-\bar{Y}_{sim})^2]} \qquad \text{(Equation 7.1)}$$

In Equation 7.1, $\mathbf{Y}_{obs}$ and $\mathbf{Y}_{sim}$ represent observed and simulated sediment yield, respectively, whereas $\bar{Y}_{obs}$ and $\bar{Y}_{sim}$ represent the mean of observed and simulated sediment yield, respectively. R^2 ranges from 0 to 1, with higher values indicating a better fit between simulated and observed values, and values above 0.5 generally considered acceptable (Moriasi et al., 2007). Although the R^2 indicator has been widely used for model evaluation, it is over-sensitive to extreme values (outliers) and is insensitive to additive and proportional differences between

model predictions and measured data (type II errors) (Legates and McCabe, 1999; Moriasi et al., 2007).

The NSE is a normalised function that determines the relative residual variance compared to the observed data variance (Moriasi et al., 2007), and indicates how well the observed and simulated data compare on the 1:1 line. The NSE is given as:

$$\mathrm{NSE} = 1 - \left[\sum \frac{(\mathbf{Y}_{obs} - \mathbf{Y}_{sim})^2}{(\mathbf{Y}_{\mathrm{obs}} - \bar{Y}_{\mathrm{obs}})^2}\right] \qquad \text{(Equation 7.2)}$$

The NSE ranges between $-\infty$ and 1.0. While models generating NSE values between 0.5 and 1.0 are considered generally acceptable, an NSE of 1 is the optimal value. The NSE is commonly used in hydrological modelling and is well reported in the literature. The percentage bias (PBIAS) is also used to show the differences between observed and simulated values and is given as:

$$\mathrm{PBIAS} = 100 * \left[\frac{(\bar{Y}_{sim} - \bar{Y}_{obs})}{\bar{Y}_{obs}}\right] \qquad \text{(Equation 7.3)}$$

A $-5\% <$ PBIAS $< 5\%$ is considered to be the target for successful calibration and model performance.

Moriasi et al. (2007) highlight that the levels of acceptability based on the objective functions vary with the type of the variable being simulated. An NSE value of > 0.50 and a $-25\% <$ PBIAS $< 25\%$ can be considered acceptable for streamflow, whereas a $-55\% <$ PBIAS $< 55\%$ can be considered acceptable for sediment (Moriasi et al., 2007).

The results obtained in this study are assessed based on the model evaluation guidelines given by Moriasi et al. (2007), consistent with the model evaluation guidelines of Borah and Bera (2004). These are general guidelines based on statistics reported from past studies that have modelled sediment yield. The guidelines are also based on results obtained using various models in various parts of the world.

7.3 Results

7.3.1 Odzi and Rio Tanama catchments

As shown in Figure 7.1, the simulations of sediment for the Odzi catchment capture the timing of the observed sediment data time series; the dotted blue lines in Figure 7.1 split the calibration and validation periods. Table 7.2 shows that sediment was relatively well estimated by the MUSLE component when compared to observed data. Nevertheless, the model simulations for both the calibration and validation periods obtained high PBIAS values. Table 7.2 shows that the addition of a simple storage model generally improved the statistical performance of the model. The more complicated (full version) storage component exhibited improved performance in terms of the PBIAS. Figure 7.1 shows that the introduction of the storage models reduces some of the small sediment peaks exhibited by the MUSLE during low flow periods.

Table 7.2 Performance indicators for the Odzi and Rio Tanama catchments. The model simulations were obtained through the application of the model based on a gradient of complexity, i.e. from a simple MUSLE to added storage options.

Catchment	WQSED components	Calibration			Validation		
		R^2	NSE	PBIAS	R^2	NSE	PBIAS
Odzi	MUSLE	0.84	0.67	80	0.68	0.60	68
	MUSLE+ simple storage	0.85	0.81	34	0.67	0.67	36
	MUSLE+ complex storage	0.81	0.71	−2	0.67	0.66	−1.5
Rio Tanama	MUSLE	0.42	0.32	31	0.4	0.34	40
	MUSLE+ simple storage	0.71	0.70	5	0.61	0.60	44
	MUSLE+ complex storage	0.62	0.58	−41	0.57	0.56	−27

The MUSLE exhibited a poor performance for the Rio Tanama catchment (Figure 7.2; Table 7.2). Figure 7.2A shows that the MUSLE could not represent most of the peak events, including the intermediate peaks. The MUSLE generally overestimated low sediment events and under-simulated peak sediment events. The introduction of the simple storage model (Figure 7.2B) significantly improved the simulation by representing many of the intermediate sediment peaks. Table 7.2 exhibits a significant statistical improvement in the model simulations, particularly during the calibration period. Although the introduction of the more complex storage component (Figure 7.2C) attained improvements in model simulations compared to

MUSLE (Table 7.2), these improvements were much lower compared to those gained by the simple storage. However, both the simple and complex storage components obtained similar performances for the validation period since the use of the complex storage component yielded an improved PBIAS.

Additional graphical assessments of the WQSED model (based on complex storage option outputs) using X-Y scatter plots and frequency curves are presented in Figure 7.3 and Figure 7.4, respectively. The higher degree of scatter in peak observed sediment outputs resulted in the model failing to simulate some of the peaks in the observed data (Figure 7.4). The scatter plots exhibited the effect of the five large peaks in the Rio Tanama catchment. Furthermore, the sediment cumulative frequency curves (Figure 7.3) indicated that high peaks were generally under-stimulated, whereas very low sediment yield events were generally over-simulated in the Rio Tanama. However, the frequency curve for validation of the model results for the Odzi catchment showed that the model performed well.

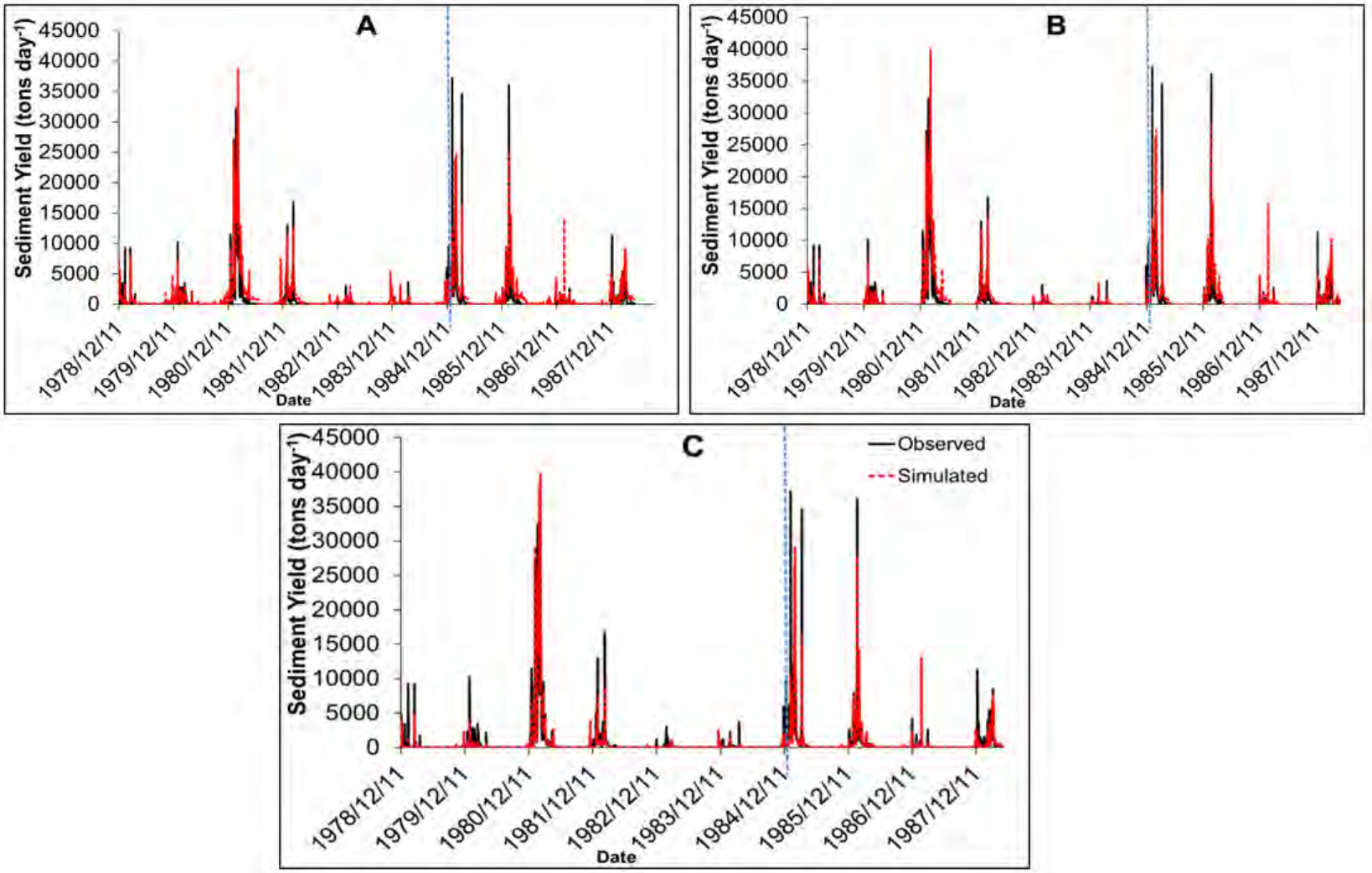

Figure 7.1 Observed and simulated sediment output for the Odzi catchment. A. simulations by the Modified Universal Soil Loss Equation (MUSLE), B. MUSLE plus the simple storage model and C. Full version erosion and sediment transport (WQSED) model with complex storage components. The dotted blue line separates the calibration period at the beginning of the time-series and the validation.

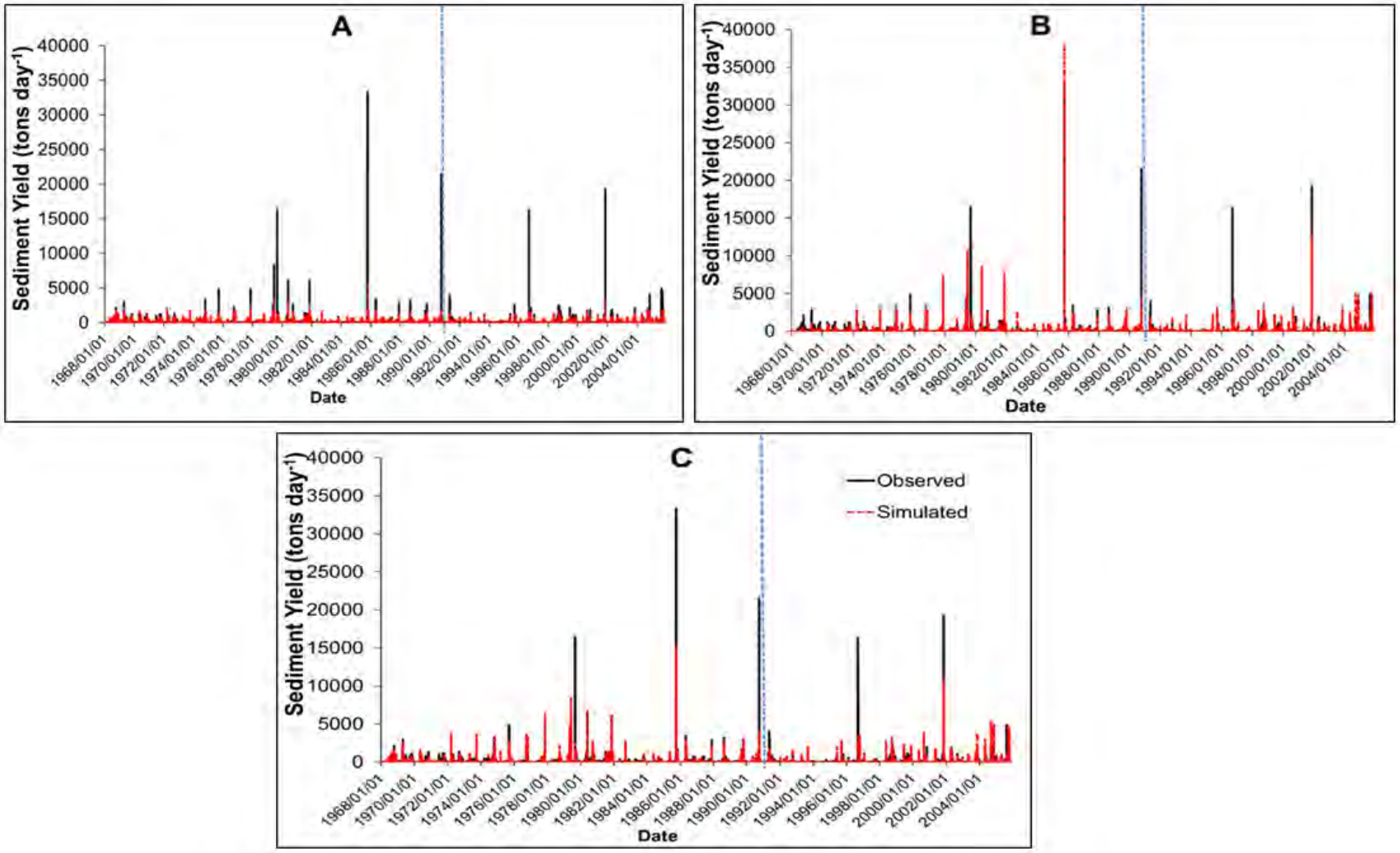

Figure 7.2 Observed and simulated sediment output for the Rio Tanama catchment. A. simulations by the Modified Universal Soil Loss Equation (MUSLE), B. MUSLE plus the simple storage model and C. Full version erosion and sediment transport (WQSED) model with complex storage components. The dotted blue line separates the calibration period at the beginning of the time-series and the validation.

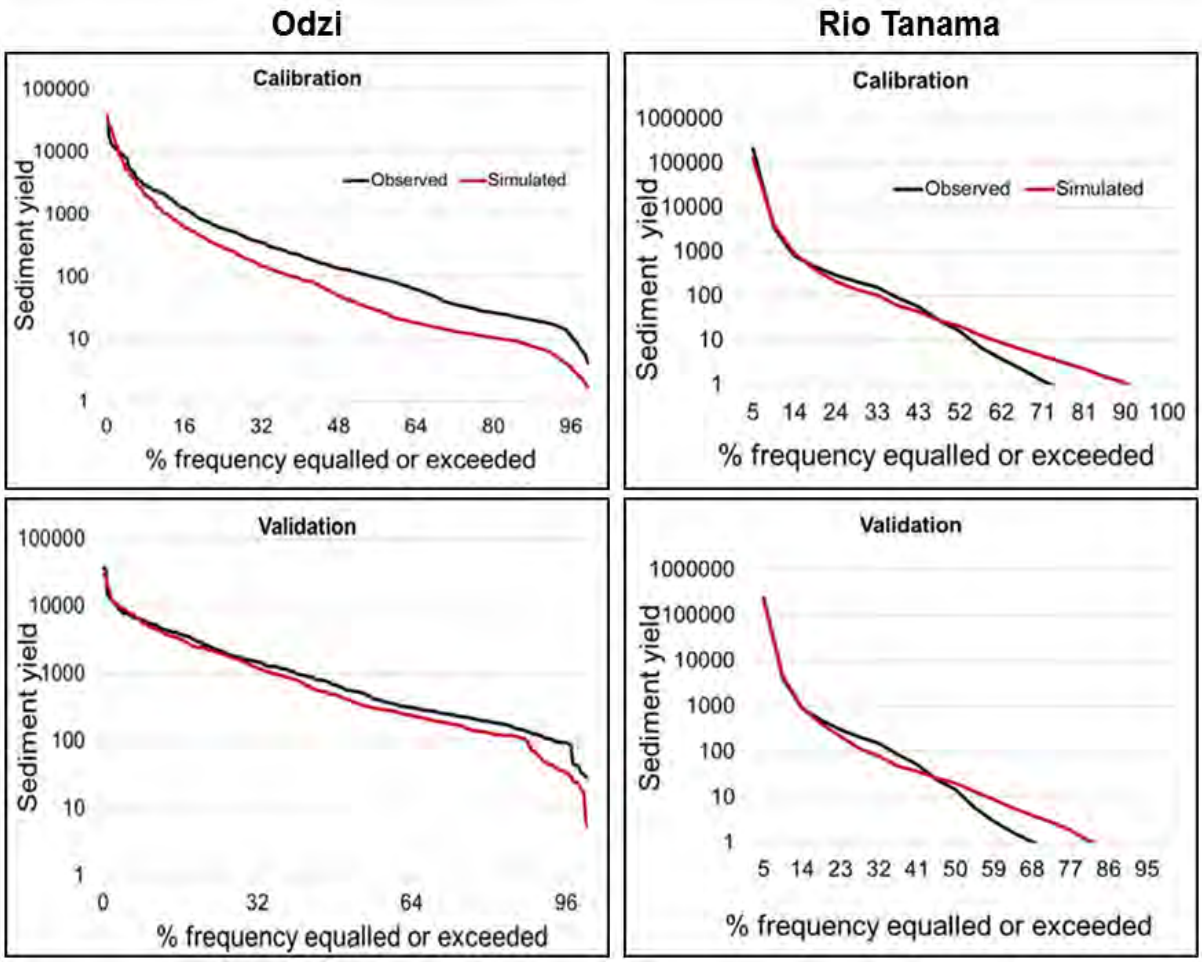

Figure 7.3 Sediment frequency distribution graphs (Log Y-axis) of the erosion and sediment transport model (WQSED) simulations (red lines) versus observations (black lines) for the Odzi (left) and Rio Tanama) catchments and for the calibration and validation periods.

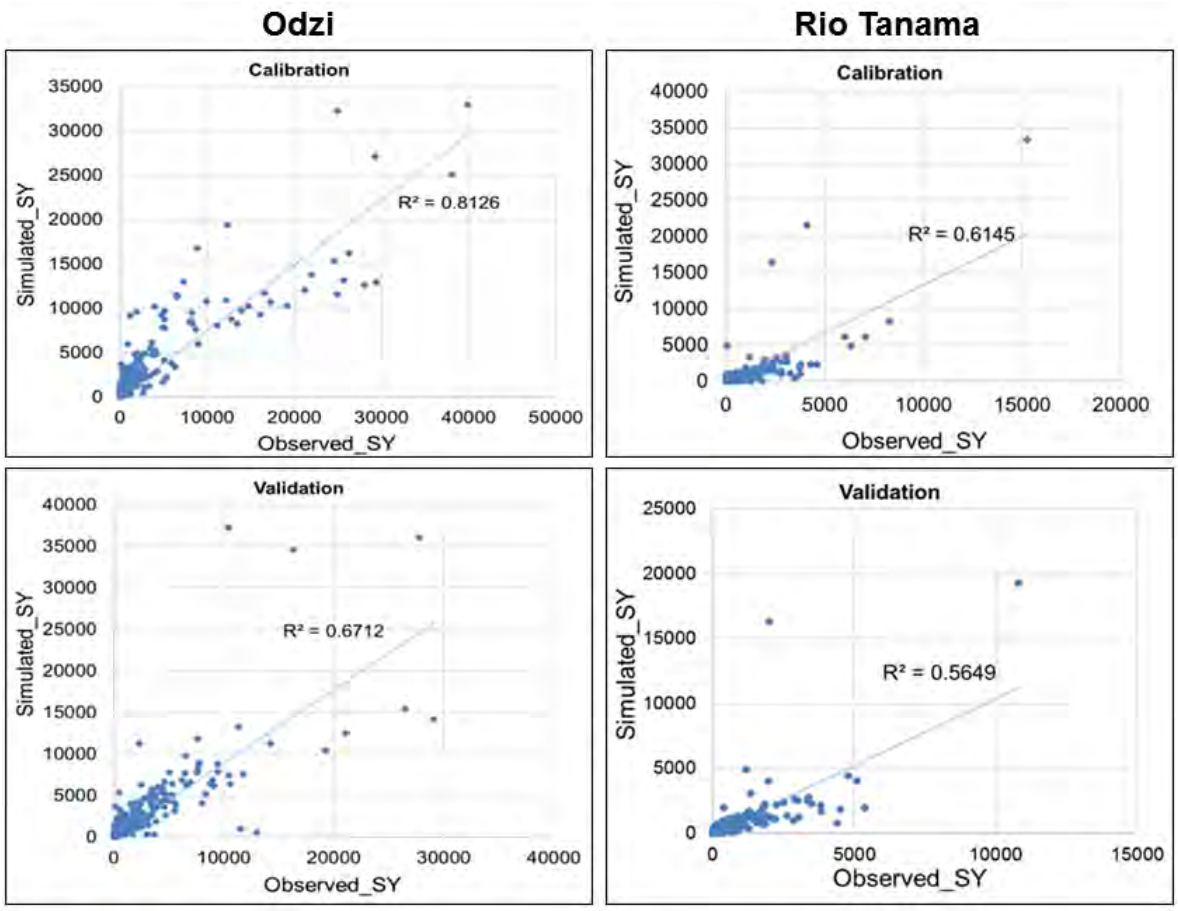

Figure 7.4 Linear correlation graphs showing calibration and validation periods of the erosion and sediment transport model (WQSED) sediment yield (SY) simulations for the Odzi and Rio Tanama catchments.

7.3.2 Results of the WQSED (simple storage) simulations for other selected catchments

The results of applying the WQSED model to the additional catchments are visually illustrated in Figures 7.5 and 7.6, whereas Table 7.3 provides a summary of the statistical evaluation of the model results. Table 7.3 shows that although the model performed relatively well for both the calibration and validation stages, the model performed poorly during the validation period of the Gwai catchment where observed data are very sparse. As shown in Figures 7.5 and 7.6, there was a lack of observed data for most of the catchments.

Similar to the results shown in the previous section (Figures 7.1 and 7.2), the results of applying the WQSED model to the additional catchments (Figure 7.6) indicate a general agreement in the timing of sediment between the observed and simulated data. However, some large peaks in sediment output were generally under-simulated.

Table 7.3 Performance indicators for the application of the erosion and sediment transport model (WQSED) to additional catchments.

Catchment	Country	Calibration			Validation		
		R^2	NSE	PBIAS	R^2	NSE	PBIAS
Grand Cane	USA	0.58	0.56	−11	0.61	0.58	−31
San Patricio	USA	0.60	0.59	−38	0.69	0.66	−34
Inxu	SA	0.97	0.89	4	0.72	0.76	36
Tsitsa	SA	0.64	0.62	−12	0.60	0.55	−35
Gwai (A38)	ZW	0.91	0.90	−5	0.81	0.53	55
Gwai (A36)	ZW	0.89	0.84	−22	0.02	−0.91	6.5

Abbreviations: USA-United States of America; SA-South Africa; ZW-Zimbabwe

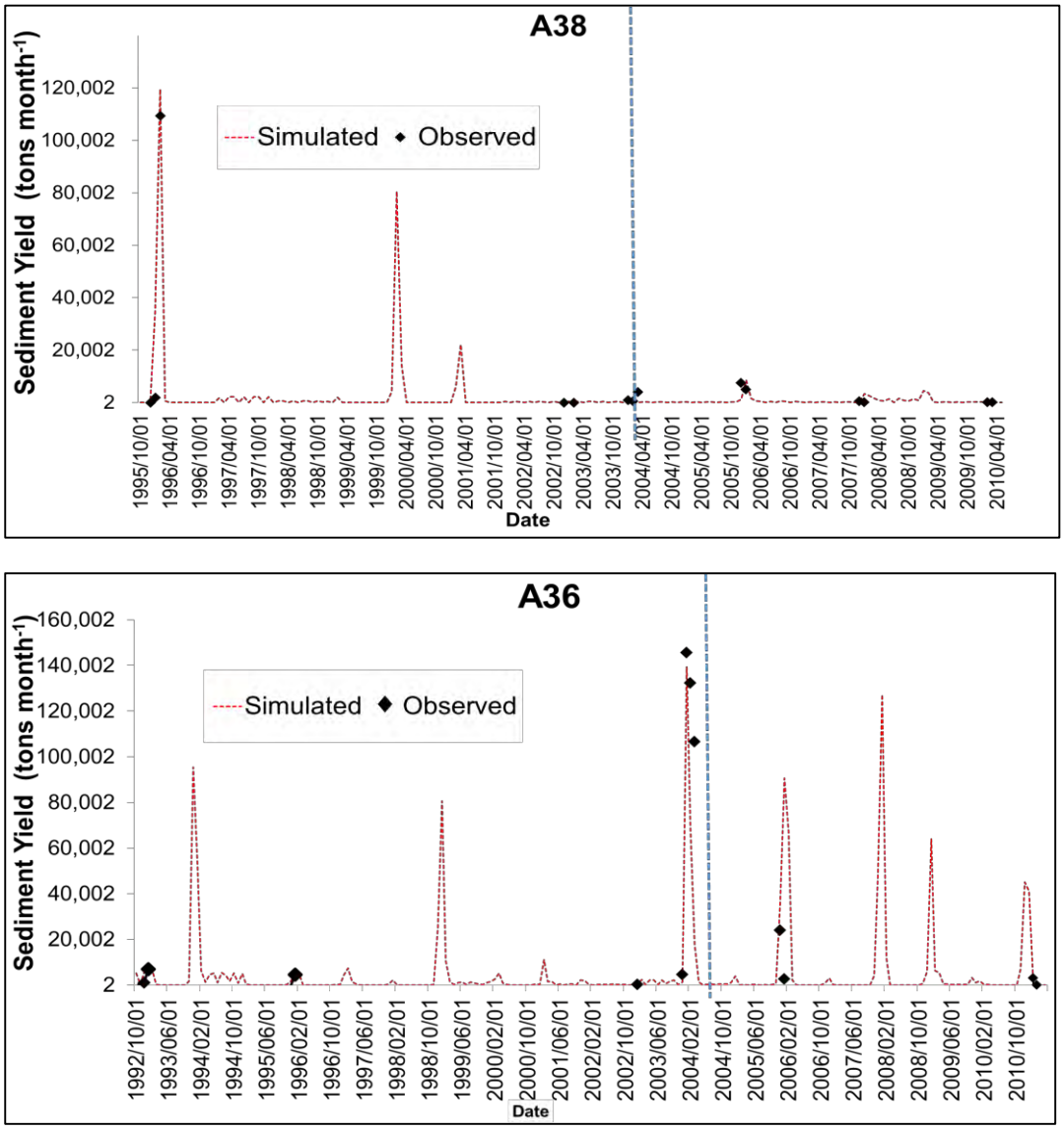

Figure 7.5 Observed and simulated WQSED sediment output for the Gwai catchment sub-basins A36 and A38. The dotted blue line separates the calibration period at the beginning of the time-series and the validation.

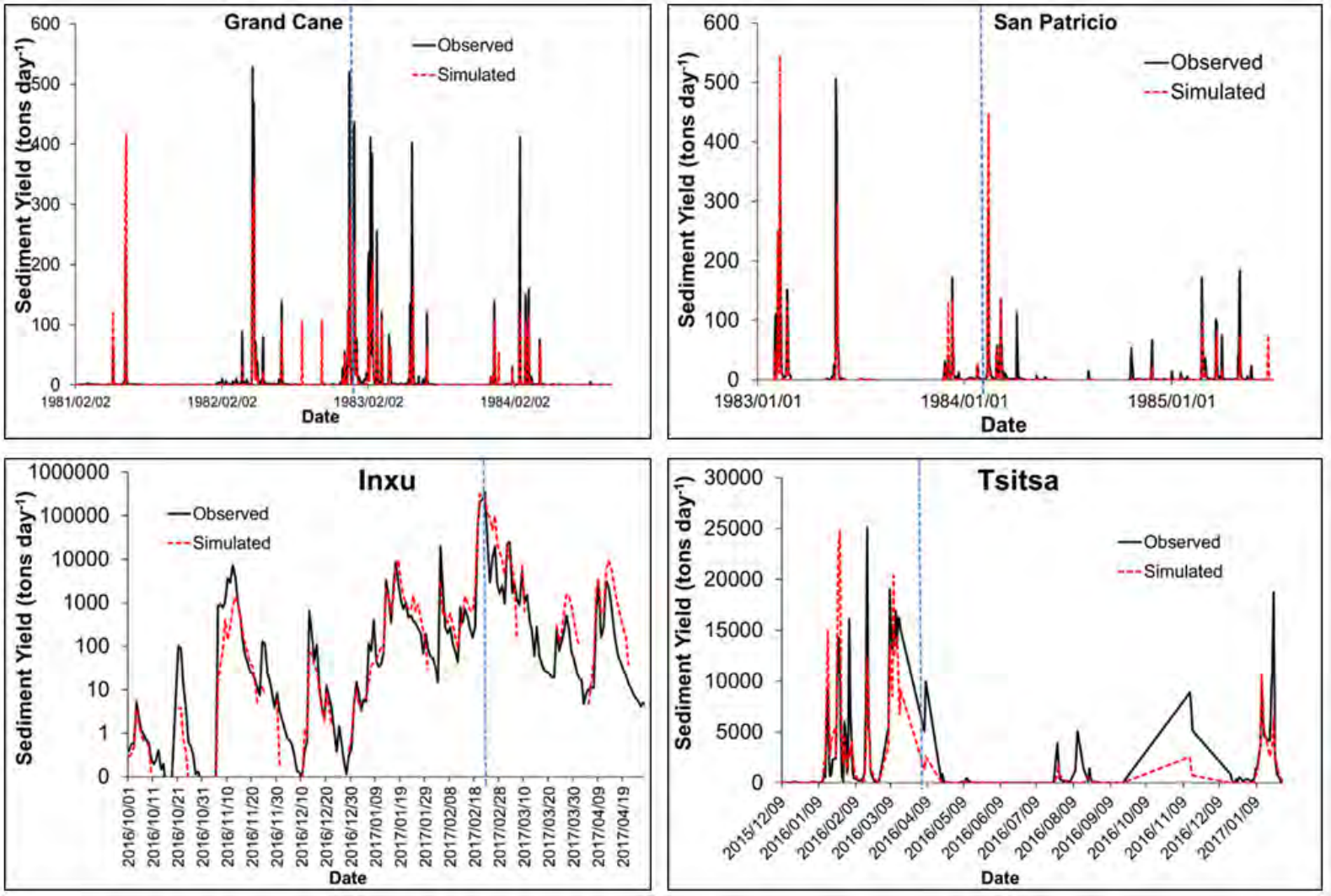

Figure 7.6 Graphs illustrating observed and simulated sediment outputs for the Grand Cane, San Patricio, Inxu (Log Y-Axis) and Tsitsa catchments. The dotted blue line separates the calibration period at the beginning of the time-series and the validation.

7.4 Sensitivity assessment

The results of the sensitivity analysis (Table 7.4 and Figure 7.7) indicate that the model simulates considerably higher sediment output for storms of short duration. Table 7.4 shows that a 6-hour reduction in duration results in a 23% higher sediment output when compared to a similar increase in duration. Storms of short duration are typically more intense and have higher erosivity.

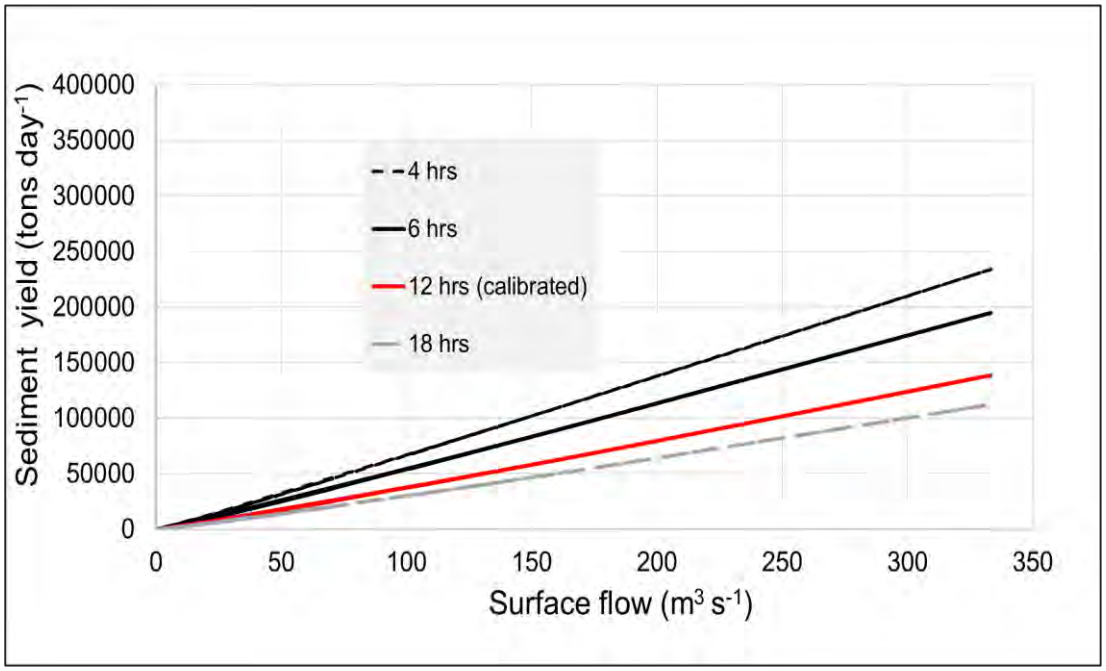

Figure 7.7 The sensitivity of changing storm duration on sediment yield simulations (calculated for the Inxu catchment, South Africa).

Table 7.4 Changes in sediment yield outputs of the WQSED model applied to the Inxu catchment with changes in storm duration in relation to the calibrated duration of 12 hours.

Storm duration (hr)	Sediment yield (t $\times 10^3$)	Sediment yield relative to the calibrated duration
18	1 298	0.80
12	1 622	1.00
6	2 319	1.43
4	2 839	1.75

Additional sensitivity assessments were conducted for the benchmark Odzi and Rio Tanama catchments. The storm duration parameters in Table 7.5 show the variation in D_{pow} and D_{con}

parameters that are necessary to calculate the duration of different catchments, and these vary based on runoff depths calculated for that catchment.

Table 7.5 Duration parameters for calculating the minimum and maximum durations for the Odzi (Zimbabwe) and Rio Tanama (Puerto Rico) catchments.

Catchment	Duration type	D_{pow}	D_{con}	Max Duration (h)
Odzi	Short	0.80	2.00	2.00
	Long	0.80	22.00	23.00
	Calibrated	0.80	12.00	13.00
Rio Tanama	Short	0.20	1.00	2.00
	Long	0.20	22.00	24.00
	Calibrated	0.80	10.00	14.00

The results for the Odzi catchment (Figure 7.8) show that a short storm duration yields higher sediment output than the observed data. Average sediment outputs are almost two times higher than observed data for the short duration but 34% lower for the long duration. For the peak sediment yield outputs, results range 10% below and above the observed data when the long and short durations are applied.

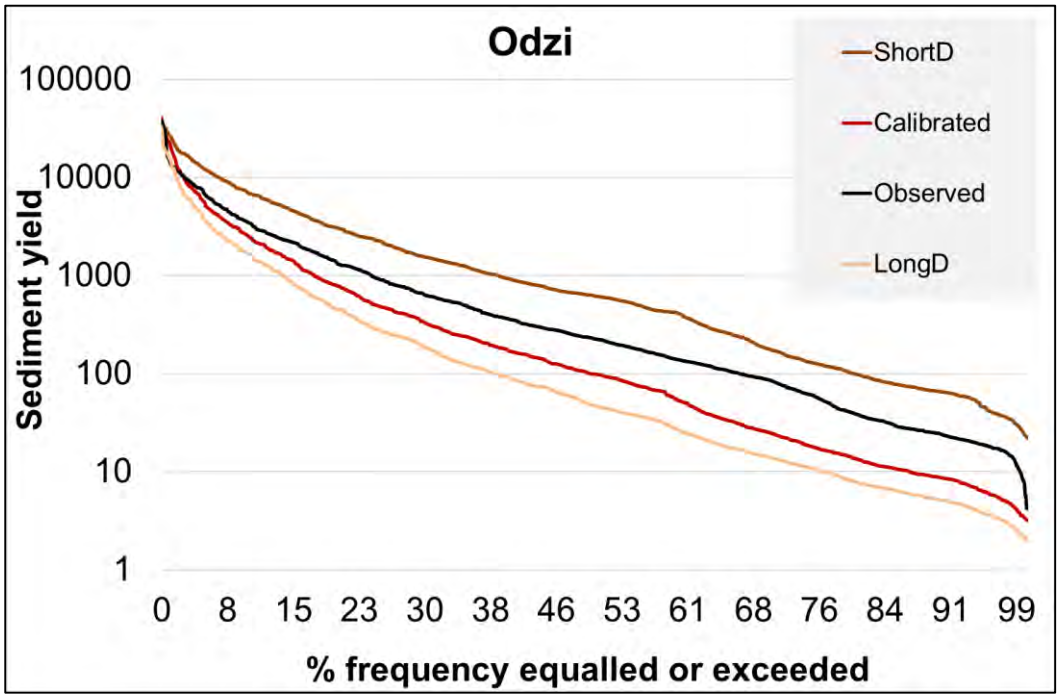

Figure 7.8 Frequency distributions (Log Y-axis) showing the change in WQSED sediment output relative to the change in storm duration for the Odzi catchment. The ShortD and LongD represent short and long duration types.

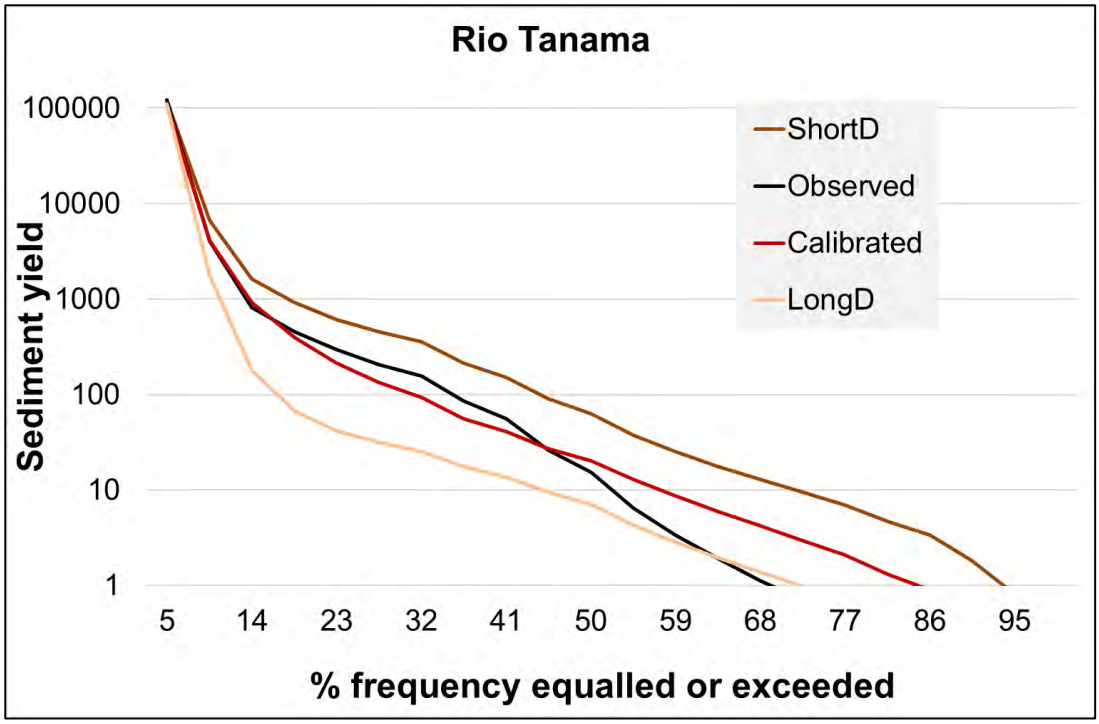

Figure 7.9 Frequency distributions (Log Y-axis) showing the change in WQSED sediment output relative to the change in storm duration for the Rio Tanama catchment. The ShortD and LongD represent short and long duration types.

In the Rio Tanama catchment (Figure 7.9), the frequency curves indicate that the short duration yields higher sediment output compared to observed data, whereas the long duration results in much lower sediment output compared to the observed frequency curve. The average sediment outputs for the long duration are 53% lower than the observed, whereas the short duration sediment outputs are 65% higher than the observed sediment output. The results from the Odzi and Rio Tanama exhibit a similar trend to the Inxu catchment storm duration assessment (Table 7.4).

The sensitivity analysis results indicate that model outputs are very sensitive to estimates of storm duration and how these affect the calculations of peak discharge and, therefore, the *R* factor in the MUSLE. Shorter durations associated with thunderstorms have higher peak intensity compared to longer duration frontal rainfall and will inevitably generate more sediment yield. Gwapedza et al. (2020) highlight that the erosivity factor maintains a considerable influence on sediment output as the model is driven by runoff. However, the effect of erosivity is dependent on other interacting factors such as vegetation cover.

7.5 Discussion

7.5.1 Tsitsa River catchment (South Africa)

The evaluation of the goodness-of-fit statistics for the simulations of the WQSED model indicates that the model performed moderately well according to the standards for evaluation of sediment yield models by Moriasi et al. (2007). A significant amount of missing data for the Tsitsa catchment negatively impacted the model evaluation. The results of the present study were also consistent with those of a study by Le Roux et al. (2015) in which the application of ArcSWAT to the catchment reported sediment yield output of between 0.003 t km^{-2} day^{-1}–0.55 t km^{-2} day^{-1}. The simulated sediment yield of the present study of 0.42 t km^{-2} day^{-1} was close to the 0.48 t km^{-2} day^{-1} of the observed data. The consistency between the WQSAM and Arc SWAT models' results within the application to the Tsitsa catchment may be partly attributed to both models using the MUSLE to estimate sediment yield.

The study by Le Roux et al. (2015), based on additional modelling of gully expansion in the Tsitsa catchment, suggests that gully erosion, which is not accounted for by the MUSLE, increases sediment yield by a factor of 20, thereby raising the sediment yield rate to approximately 11 t km^{-2} day^{-1}. Although the observed data do not appear to support the assertion of gullies contributing excessive amounts of sediment, they do indicate the possibility of gullies pushing significant amounts of sediment to the catchment outlet, which may partly explain the failure of the WQSED model to predict some of the sharp sediment peaks (Figure 7.5). The calibration of the storage parameters significantly improved the simulation by changing the timing of outputs from storage to match peak flow events. The threshold flow for delivery parameter exhibited greater sensitivity in controlling sediment output from storage. However, the sediment simulation for the Tsitsa catchment by the WQSED model remained poor compared to that of the Odzi catchment, due to apparent mismatches in the flow and observed sediment data. These mismatches are likely associated with hysteresis effects (Martin et al., 2014; Picouet et al., 2001; Soler et al., 2008). Grenfell and Ellery (2009) similarly reported seasonal hysteresis effects in the Umfolozi catchment in South Africa, which they attributed to the depletion of sediment supply at the onset of the rainy season. Sediment depletion is not prevalent in the Inxu sub-catchment as most flow peaks are associated with significant sediment output (see Appendix C.1). Since high rates of erosion occur near the outlet of the Inxu catchment (Le Roux et al., 2015), the travel time/distance of sediment (Seeger

et al., 2004) is less compared to that of the Tsitsa catchment, which incorporates the Inxu sub-catchment.

The sediment yield of the Tsitsa catchment can be attributed to the relatively high levels of erodibility of the catchment. Field studies revealed that degradation of the grasslands by overgrazing is further worsening the erosion risk. Past erosion risk studies classified the Tsitsa catchment as a high erosion risk area in South Africa (Borrelli et al., 2017; Le Roux et al., 2008, 2015). Van Tol et al. (2016) suggested that land degradation resulting from erosion threatens the viability of agricultural systems in the catchment and that farming could be contributing to high erosion rates because of high erosion rates of abandoned farmland. Akamagwuna et al. (2019) identified degradation of the water quality of riverine ecosystems associated with high sediment discharge. In addition, estimated high sediment loads are expected to result in loss of reservoir storage and a negative impact on the storage capacities of planned reservoirs (Le Roux, 2018).

7.5.2 Odzi and Gwai river catchments (Zimbabwe)

The WQSAM simulations for the Odzi River catchment indicated that while the model managed to sufficiently represent the timing of observed sediment yield, the model could not represent the peaks and tended to over-estimate sediment at average and low flows. The observed data for the selected period (1978–1988) indicates that the average daily sediment yield for the catchment is 505 t day^{-1}, which was similar to the simulated average sediment yield of 495 t day^{-1}. The goodness-of-fit statistics for the simulations were satisfactory according to model evaluation guidelines for sediment yield estimation by Moriasi et al. (2007). However, the model's failure to simulate some of the peaks in sediment yield in this catchment was a shortcoming as this catchment is particularly flashy, with most sediment yield occurring during peak flow events.

A study by Lidén et al. (2001) in which the HBV-SED model was applied to the Odzi River catchment, similarly reported a failure to simulate individual peaks. This failure was attributed to errors in the modelled runoff data (Lidén et al., 2001). Although observed flow data were used as the forcing data within the WQSED model in the current study, a similar problem was experienced. Therefore, the under-estimation of sediment peaks may be linked to sediment emanating from sources that are not explicitly considered within the WQSED model structure, such as gullies and channel/bank sources. It is also possible that the peaks in the observed data

represent systematic sediment measurement errors associated with manual sampling tools and methods (Bannatyne et al., 2017; Karlsson and Rahmberg, 1999). If this is the case, the accuracies of both the HBV-SED and WQSED models in simulating sediment for this catchment cannot be rigorously assessed until accurate observed measures of sediment become available. The WQSED simulations were an improvement on those of the HBV-SED in which the differences between average annual observed and simulated sediment yield were up to 25%. This validates the WQSED model's performance to be similar to that of a well-established model such as HBV-SED.

The lack of observed data for calibration of the model to the Gwai catchments resulted in model simulations not being adequately evaluated and validated. The same problem would likely occur within the application of the WQSED model to the majority of catchments in southern Africa. The model simulations for the Gwai catchment shown in the present study are therefore initial outcomes that will require further validation as further observed data become available. However, the WQSED model simulations were also evaluated against independent measurements and estimations performed in previous studies within the catchment.

The difference in sediment yield between the two basins (Table 7.6) is likely due to the varying land use/land cover distributions between the two sub-basins. Sub-basin A36 mostly comprises cultivated land whereas bush is the dominant land cover in sub-basin A38. The WQSED simulation of greater sediment yield from sub-basin A36 may be due to high agricultural activity (Turner et al., 2018) in that basin. Firth (1991) concluded that sub-basin A36 falls into an area of the Gwai River catchment affected by extensive erosion.

Table 7.6 Differences in average WQSED sediment yield estimates between the current study and previous studies for the Gwai catchment.

Study	**Average sediment yield rate (t km^{-2} year^{-1})**	**% difference**
Ward (1980)	34	0.0
A38	20	41
A36	25	26

Ward (1980) measured sediment yield in a part of the Gwai River catchment from 1975–1978 and reported yields of 8 t km^{-2}, 23 t km^{-2} and 70 t km^{-2} over the three hydrological years, respectively. Although the average sediment yield of the Ward (1980) study is up to 40% higher

than the yields reported in the current study, the Ward (1980) study reveals the high interannual variability in sediment yield that can be produced by a catchment. The results of the current study similarly exhibited temporal variability in sediment yield (Figure 7.5).

The calibration and validation processes of the WQSED model in the Gwai study were hindered by both insufficient observed data and differences in temporal scale between observed data and model simulations. Since observed data were aggregated to monthly means and the WQSED model simulates sediment yield at a continuous daily time step, aggregating daily-simulated data to monthly means was necessary for calibration and validation. Consequently, only 15 individual observations were available for the calibration and validation of 252 months of aggregated daily sediment yield simulations, with direct comparisons between only 6% of the simulated data possible. Sadeghi and Mizuyama (2007) show that the MUSLE will perform well if sufficient observed data are available for calibration. The lack of observed data for this catchment precluded any rigorous assessment of the model performance; therefore, more observed data is needed against which the model simulations can be assessed before any concrete conclusions can be made. However, the WQSED model's application to the Gwai catchment is vital for highlighting the quality of observed data that is typically available in southern African catchments and illustrating the scarcity of sediment observations.

7.5.3 Grand Cane, San Patricio and Rio Tanama catchments (USA and associated territories)

The results of the model evaluation within the catchments of the USA and associated territories exhibit a considerable variation in sediment output between catchments selected in the State of Louisiana and Puerto Rico. In Louisiana, the Grand Cane (GC) and San Patricio (SP) catchments exhibited a sediment yield rate of 0.2 t ha^{-1} $year^{-1}$ and 0.1 t ha^{-1} $year^{-1}$, respectively. In Puerto Rico, the Rio Tanama (RT) catchment had a sediment yield rate of 3.4 t ha^{-1} $year^{-1}$. Although all catchments investigated have similar ranges of discharge and soil erodibility, the Rio Tanama catchment exhibits a much higher sediment output. Notably, since forest is a dominant land cover in all catchments investigated, the *C* factors applied to the catchments were low; a study conducted by Gellis et al. (2006) on the Loiza Basin (Puerto Rico) indicated that forest land cover contributed the least to total sediment. Puerto Rico and Louisiana catchments have considerably different topographies, with the *LS* of the Rio Tanama higher than those in Louisiana by a factor of three. In addition, the Rio Tanama receives on average 700 mm more rainfall per year, thereby generating a discharge volume comparable to those of

the other catchments, but from a catchment area that is three times smaller. Therefore, a combination of high *LS* and erosivity could be contributing to the greater sediment yield rate in the Rio Tanama catchment.

A recent global erosion assessment by Borrelli et al. (2017) indicates that Grand Cane and San Patricio catchments fall within low erosion zones. Previous studies conducted in the Louisiana catchments have focused on analysing the existing observation data, e.g. Rosen and Xu (2011). Since the United States Geological Survey (USGS) manages a relatively comprehensive flow monitoring network in the region (Xu and Rosen, 2012), there are limited flow modelling studies for the area. A study by Rosen and Xu (2011) found that rivers in the GC and SP region generally have lower sediment yields than rivers outside the region, with all rives in the region experiencing a decline in sediment load from 1990 to 2008. Interestingly, more sediment yield is required to offset the sinking of coastal areas (Xu and Rosen, 2012). A dichotomy is thus presented between the North American and Southern African catchments that grapple with having to limit sediment yield.

Previous studies conducted in catchments neighbouring the Rio Tanama in Puerto Rico reported sediment yield rates ranging between 0.2 t ha^{-1} $year^{-1}$–12 t ha^{-1} $year^{-1}$ (see Korman et al., 2020; Larsen and Webb, 2009; Yuan et al., 2016). The sediment yield for the Rio Tanama reported in the present study falls within the range reported by previous studies, and is significantly higher than those for the Grand Cane and San Patricio catchments. An investigation into sediment loss in the Rio Tanama and influencing factors by Yuan et al. (2015) identified anthropogenic developments, slope and precipitation as the major factors driving sediment output. Gellis et al. (2006) cite land-use developments as an additional driver of sediment output and emphasized that sediment originating from construction sites was higher than that originating from forests in the Loiza catchment by a factor of 30. As in Southern Africa, Puerto Rico struggles with high river sediment yields (Gellis et al., 2006). Poor coastal water quality associated with river sediment yield in Puerto Rico has been linked to the loss of coral reefs (Korman et al., 2020; Larsen and Webb, 2009), which poses an urgent problem given that tourism comprises a significant component of that country's economy (Gellis et al., 2006). Some proposed mitigation strategies to reduce sediment yield include vegetation restoration and paving roads that connect to coffee farms (Korman et al., 2020).

7.6 Summary and conclusions

The WQSED model was applied to catchments in two sub-Saharan countries in the current study. The aim was to evaluate the model performance at a regional scale and against models previously applied in these regions, where applicable. The choice of catchments for the study was limited by the scarcity of continuous observed sediment data. For example, sediment data available for some catchments comprised of as little as one (grab sample) observation per year. Obviously, this level of observed data is insufficient for evaluating a daily-time-step sediment yield model. However, limited monthly observed sediment data were available for the Gwai River catchment against which the WQSED model simulations could be assessed. Additional assessments were conducted for catchments in the USA and associated territories where observed sediment data are more abundant.

The calibration procedure yielded reasonable performance statistics comparable to established models for most of the catchments under study. The performances of WQSED within the applications to the Odzi and Tsitsa river catchments were similar to those of the HBV-SED and SWAT models which were previously applied to the same catchments. However, the WQSED has an advantage over other established models in that it is relatively simple. The approach adopted in WQSED is supported by Griensven et al. (2013) who concluded that complicated models do not necessarily provide better results than simpler models, although complicated models may describe the process in greater detail. It is essential to highlight that observed flow inputs were used within the current evaluation of WQSED, as the model does not simulate flow independently, whereas models such as SWAT and HBV-SED do. As sediment yield simulations are dependent on the quality of the flow input data, the success of the WQSED application may also be attributed to the use of observed flow data.

A comparison of the model performances between the incorporating of a simple or detailed (full version) storage (Table 7.2) shows that the inclusion of a storage model improves the performance of the MUSLE. However, the more complex storage model did not outperform the simpler storage, and in fact, the WQSED model with the simple storage performed better during calibration. This result can be attributed to either the simple storage model being relatively easier to calibrate and/or the WQSED model with the more complicated storage performing relatively poorly. A similar outcome was reported in Tan et al. (2018) in an assessment of various sediment models. A notable outcome of the current study was that both storage options performed relatively well; hence, there may be no need to maintain a

complicated storage module in WQSED. An additional critical issue is that storage modules require some calibration with observed data. Therefore, the application of the model in ungauged catchments of South Africa may be problematic.

Table 7.7 WQSED model performance after transferring calibrated storage and duration parameters to a neighbouring catchment.

Catchment parameter transfer		**Model performance**		
From	To	R^2	NSE	PBIAS
Tsitsa	Inxu sub-catchment	0.88	0.51	47
Grand Cane	San Patricio	0.76	0.22	28

Nevertheless, an assessment of the transferability of calibrated parameters to neighbouring catchments with similar physical attributes (see Table 7.7), exhibited that there is potential for regionalisation of WQSED parameters for application to ungauged basins. As this was only performed for two catchments, more parameter transfer assessments are needed to corroborate the current outcome and validate the model's ability to provide reliable simulations in ungauged basins.

The WQSED was shown to consistently under-estimate most peak sediment yield events. The failure to estimate peaks was displayed across most of the catchments under study. A possible explanation is that the WQSED simulates rill and sheet erosion based on the MUSLE, whereas gully erosion that has the potential to contribute large amounts of sediment is not explicitly considered. Although the WQSED model does have a gully connectivity parameter, increasing gully connectivity in the current study failed to sufficiently raise the simulated peaks to match the observed. This is because the gully connectivity parameters change the organisation of storages by increasing or decreasing the proportion of sediment storage in gully stores and have a negligible impact on sediment supply from the MUSLE. Changing the duration parameters to achieve shorter storm durations had a linear effect; increasing the erosivity of lower flows (by raising MUSLE *qdp*) and raising the low simulations thus further exacerbated the error. The storage module absorbed sediment during low flow events and delivered sediment during high flow events, a phenomenon that is consistent with the highly variable hydrology (in time and space) of most South African catchments (Rowntree et al., 2016). The inclusion of a storage module resulted in a significant improvement in the model representation of peak and recession sediment loads and enhanced the model performance.

Chapter 8 Estimating sediment yield in 'ungauged' South African catchments

8.1 Introduction

In the previous chapter, the WQSED model was calibrated and validated against observed daily sediment yield. However, because of the scarcity associated with daily sediment discharge measurements in South Africa, only two catchments (Tsitsa and Inxu) in the same region were evaluated. Because the WQSED model was primarily developed for application to South African catchments, it was necessary to extend the application to 'ungauged' catchments for further testing. The catchments are termed 'ungauged' because no daily observed sediment discharge data are available. However, discharge data are available for some of the catchments, while estimated long-term reservoir sedimentation rates are available for all catchments. Therefore, in this chapter, simulated sediment outputs are evaluated against existing long-term reservoir sedimentation data reported in previous studies. However, it should be recognised that these estimates are subject to uncertainties associated with estimating the trap efficiencies of the reservoirs, as well as the level of compaction in the reservoir basin. A similar assessment was conducted recently in Morocco by Ezzaouini et al. (2020) using the MUSLE. The estimates were much lower than observations, and it was concluded that much of the sediment deposited in the reservoir emanated from channel erosion, which is not simulated by the model (Ezzaouini et al., 2020). Despite the under-simulation, the use of the MUSLE proved vital for estimating hillslope contributions to reservoir sediment. Apart from comparing WQSED sediment estimates to previously reported reservoir rates, regional sediment yield patterns and associated influencing factors are appraised in this chapter. The outcomes of this assessment are potentially useful for catchment management.

8.2 Setting up the WQSED model

The parameter values derived for the study catchments were used to set up the WQSED model. The WQSED model is accessed through the SPATSIM modelling framework (Hughes and Forsyth, 2006), an interface that enables a user to input data, run models and visualise model outputs. The requirements for the WQSED include general information that relates to catchment size and name. Inputs of daily time series of runoff data are required, and observed flows were used where available, whereas simulated flows from the water resources database

(WR90; Midgley et al., 1994) were used in some of the poorly-gauged catchments that were selected for the study. The monthly flows were disaggregated to daily following the method of Hughes and Slaughter (2015) and Slaughter et al. (2015). Daily total flow separation to obtain surface flow was conducted following the baseflow separation method of Hughes et al. (2003); existing regional baseflow parameters were used, and expert advice was sought to confirm realistic baseflow ranges in the absence of validation data. The flow data used in this chapter range in length from 10 to 70 years and it is acknowledged that the shorter records may not be adequately representative to determine long-term yields. However, the study was constrained by the data that are available.

Parameters describing catchment physical properties (Chapter 4) are inputs into the model. Two sets of parameters are required, a set of 'catchment parameters' and another of 'sub-basin parameters'. The sub-basin parameters are specified per slope zone (H, M and L). A general distinction between the two parameter sets is that the catchment parameters describe the basin hydrological properties, whereas the sub-basin parameters are essentially the parameter values of the HML MUSLE factors. Additionally, mean catchment (and not HML) parameter values for the MUSLE were also applied to assess the sensitivity of the model sub-basin structure versus applying simpler mean catchment MUSLE inputs. It is essential to highlight that the sub-basin parameters were derived using the parameter estimation approach (see Chapter 4) whereas the catchment properties such as drainage density, channel length and slope were derived using measurements from existing shapefiles and the DEM. The calibration parameters associated with storage were not calibrated because there were no appropriate observed data. The focus of this part of the study is on the total transported sediment volumes, while the storage parameters largely affect shorter-term variations in sediment yield. The estimated storage parameters were therefore checked to ensure that there were no systematic increases (eroded sediment getting lost in storage) or decreases (sediment yield increased through releases from storage) in the storages over the full simulation period. Effectively, this approach means that short-term sediment storage and delivery dynamics do not affect the total estimated sediment volumes. Some observed data were available for the T35A-E catchments, which form part of the Tsitsa catchment, the calibration of which is reported in the previous chapter. The calibration parameters derived in the previous chapter were used for the T35A-E. Notably, the calibrated Tsitsa storm duration average of 12 hours was applied to all the catchments, representing a balance between short duration and long duration rainfall (Gwapedza et al., 2020).

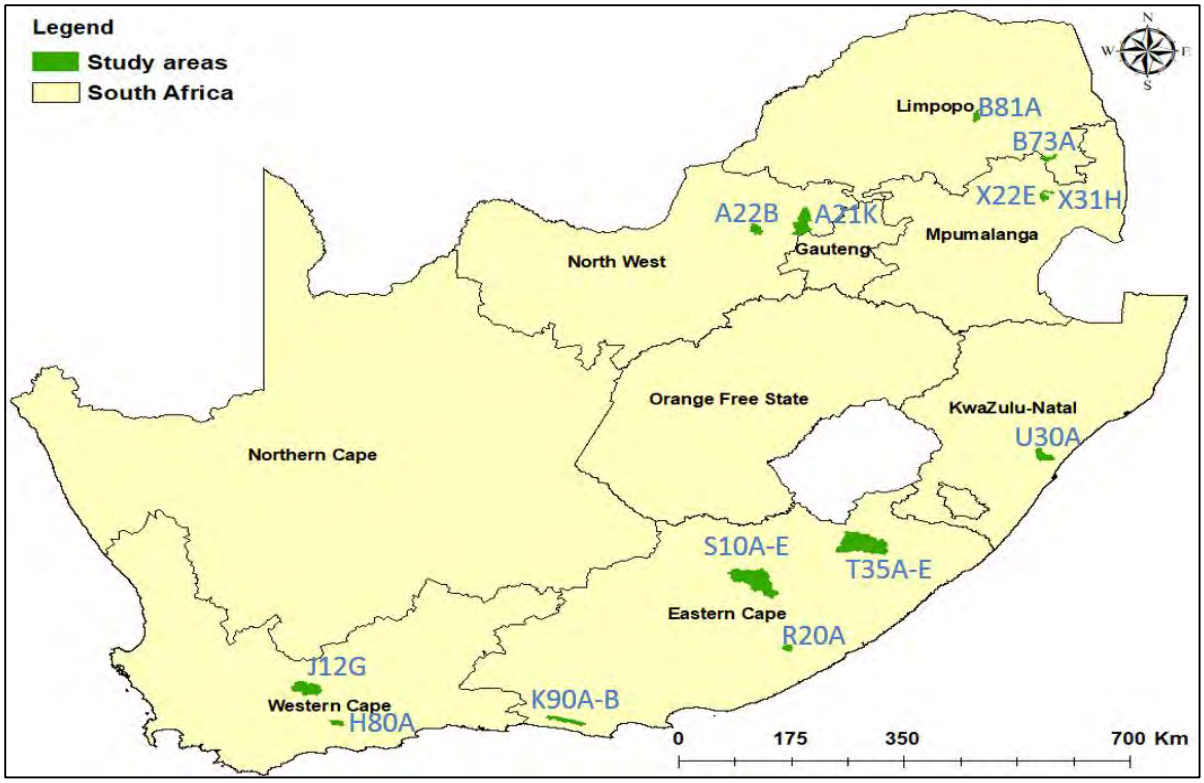

Figure 8.1 Map showing the distribution of selected study catchments across South Africa.

The model was set up for 13 catchments (covering 22 quaternary catchments) across South Africa, varying in size from 30 km^2 to over 1 000 km^2. Catchments were selected to capture the various physiographic and climate conditions represented in the country and to assess the sediment yield patterns across varying regions. Figure 8.1 shows the distribution of the selected study sites across the country. More catchments were selected from the Eastern Cape Province of South Africa as the province is considered an erosion 'hotspot' when compared to other regions. More importantly, the T35A–E catchments are a proposed site for the construction of two large dams, making this an area of immense practical interest. All other study sites had existing dams, and rates of sedimentation for the dams were initially provided by Rooseboom (1992) and were later updated by Msadala et al. (2010). The observed data were compared to simulated data by aggregating total simulated volumes and converting them to sediment yield rates (t ha^{-1} year $^{-1}$). Additionally, a simple uncertainty assessment was conducted by establishing 25% upper and lower bounds on either side of the estimated MUSLE and storm duration parameters to evaluate if the previous yield estimates fall within the likely uncertainty range of the model simulations.

8.3 Results

8.3.1 Mean parameter distributions

The mean parameter distributions (Table 8.1) estimated using available GIS data show that the topographic factor varies between 1 and 9.7. The average *LS* factor amongst the study sites is 6.3, and more than 75% of the selected sites had an *LS* factor greater than five. The lowest *LS* factor value was estimated for the A22B catchment located in the North West Province, and the highest *LS* factor was estimated for the H80A catchment located in the Western Cape Province. The *C* factor ranges between a low of 0.01 and a high of 0.17. The Maden Dam (R20A) catchment exhibits the lowest *C* factor of 0.01 (largely indigenous forest), and the highest *C* factor (0.17) is found in the Koster Dam (A22B) catchment (degraded land, sparse bush and cultivation). The soil erodibility does not exhibit the sharp variability shown by the *LS* and *C* factors. The highest values (0.6) of soil erodibility are calculated for the K90A–B catchments located in the south-western area, while the lowest (0.2) are calculated for the B73A catchment located in the northeast. The management practice factor displays the least variability compared to all the other estimated MUSLE factors. The highest *P* factor (1) is estimated for the Witklip and Ebenezer catchments located in the north-eastern region, and the lowest *P* factor (0.8) is estimated for the B73A catchment in the north-western region. Table 8.1 summarises the estimated MUSLE erodibility values.

Table 8.1 Mean catchment erodibility parameters for selected South African catchments.

Catchment	**Dam**	**Area (km^2)**	***K***	***LS***	***C***	***P***
R20A	Maden	30	0.24	7.70	0.010	0.92
B73A	Klaserie	136	0.20	9.00	0.040	0.80
A22B	Koster	187	0.28	1.00	0.170	0.88
J12G	Prinsriver	768	0.40	6.90	0.060	0.99
H80A	Duiwenhoks	150	0.30	9.70	0.050	0.96
K90A–B	Churchill	362	0.60	6.15	0.030	0.97
S10A–E	Xonxa	1 282	0.41	3.90	0.150	0.94
T35A–E	Ntabelanga	2 016	0.33	5.88	0.122	0.94
U30A	Hazelmere	382	0.30	7.18	0.097	0.87
X22E	Witklip	60	0.30	7.96	0.017	1.00
X31H	Da Gama	44	0.30	6.73	0.017	0.93
A21K	Buffelspoort	116	0.21	6.20	0.077	0.93
B81A	Ebenezer	126	0.21	7.13	0.014	1.00

8.3.2 HML parameter distributions and flow inputs

The distributed parameter distributions based on calculating MUSLE factors per slope zone (Figure 8.2) exhibit various patterns that indicate variability across the HML factors and the various catchments under investigation. The variability of the topography factor is as expected, given the definition of the zones using the slope. The *K* factor varies very little (Figure 8.2B), while the *C* factor exhibits a pattern that is opposite to the *LS* factor with low slope zones having generally higher *C* factors (Figure 8.2C). The *P* factor (Figure 8.2 D) indicates variation from the mean catchment *P* factor but no variation in high zone *P* across all catchments and little variation in moderate zone *P* factor.

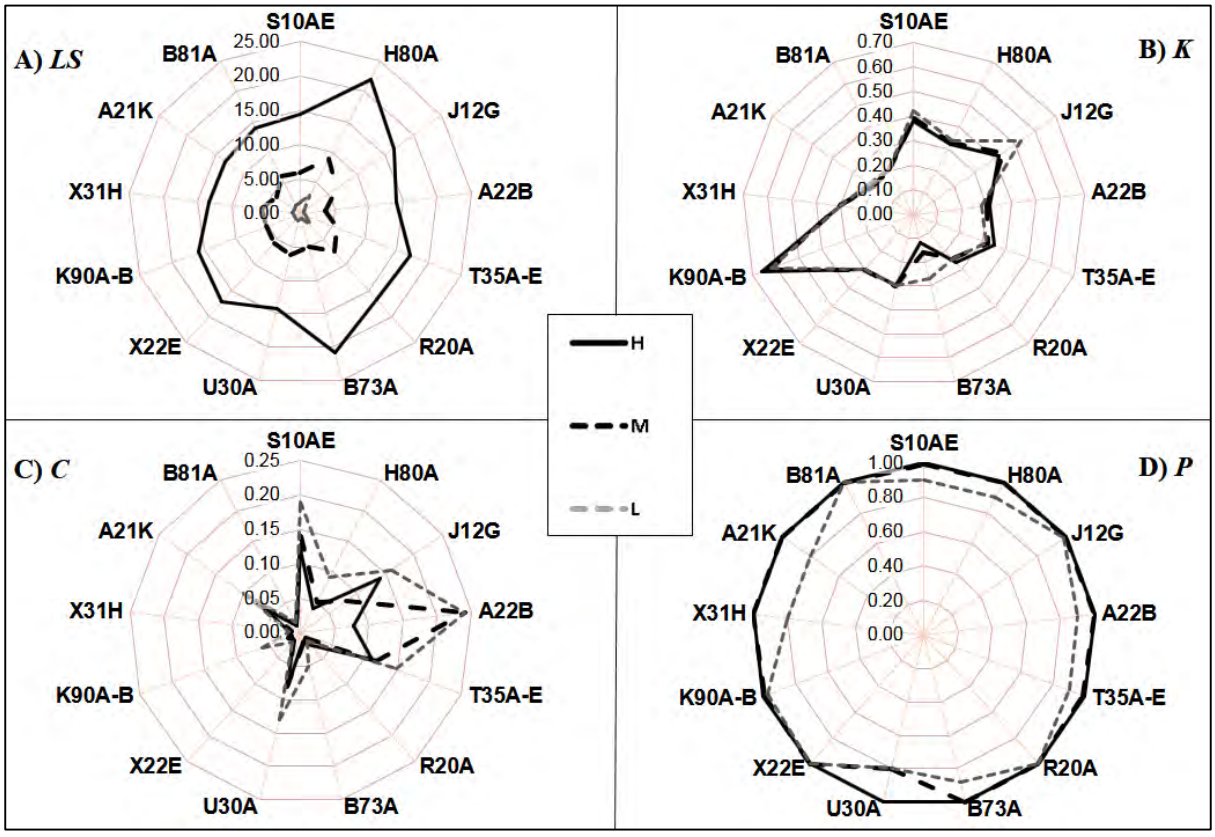

Figure 8.2 Mean High-Medium-Low (HML) catchment erodibility parameters computed for selected South African catchments.

The flow inputs (Table 8.2) vary across the catchments; catchments in the sub-humid and sub-tropical climate zones generally exhibit higher flows. Some larger catchments e.g. Ntabelanga (Table 8.1) have larger catchment areas, and thus have much higher flow compared to smaller catchments, because of the larger contributing areas. Catchments in the semi-arid areas generally exhibit comparatively lower flows than catchments in other climate zones. Baseflow

percentages are higher for catchments with higher slopes and sparse vegetation e.g. Xonxa, and higher for catchments with dense vegetation e.g. Maden, where higher infiltration rates were anticipated.

Table 8.2 Mean total and surface flow for study areas and estimated baseflow fractions.

Catchment	Climate	Mean totalflow ($m^3 s^{-1}$)	Mean surfaceflow ($m^3 s^{-1}$)	% baseflow
Ntabelanga	Sub-humid	3.80	2.70	29
Xonxa	Sub-humid	1.24	0.90	27
Klaserie	Sub-tropical	0.73	0.39	46
Churchill	Temperate	0.81	0.35	57
Duiwenhoks	Temperate	0.98	0.39	60
Prinsriver	Semi-arid	0.14	0.08	42
Koster	Semi-arid	0.18	0.07	61
Maden	Temperate	0.29	0.09	69
Hazelmere	Sub-tropical	1.53	0.69	55
Witklip	Semi-arid	0.08	0.03	56
Da Gama	Semi-arid	0.31	0.09	70
Ebenezer	Sub-tropical	0.74	0.23	69
Buffelspoort	Semi-arid	0.32	0.15	53

8.3.3 Sediment yield simulated using estimated (mean and HML) MUSLE factors

Table 8.3 presents the results of the model simulations using both mean catchment parameters and HML zone parameters. The simulations are compared with the previous catchment sediment yield rates calculated from reservoir survey data from Msadala et al. (2010). However, the sediment yield estimates for the Ntabelanga Dam (yet to be constructed) are based on the Le Roux (2018) case study.

The results of the sediment yield simulations (Table 8.3, column 4) show that the Witklip catchment had the lowest long-term sediment yield rate of 1.5 t ha^{-1} $year^{-1}$. The highest long-term sediment yield rate of 21.4 t ha^{-1} $year^{-1}$ is simulated for the Ntabelanga catchment. The simulated average sediment yield rate of the study regions is 5.3 t ha^{-1} $year^{-1,}$ and only 23% of the study sites exceed the calculated catchment average. The results summarised in Table 8.3 indicate that the lowest sediment yield rates are generally found within the arid and temperate

catchments, whereas the highest sediment yield rates are in the sub-humid and sub-tropical catchments. The catchments located in the Eastern Cape Province (Xonxa and Ntabelanga) exhibit high rates of sediment yield. Considerable variations exist between simulated sediment yield rates and the previous rates based on reservoir infilling. The variation ranges from just 31% difference to more than forty times of differences in sediment yield rates.

Table 8.3 Summary of simulated sediment yield outputs and previous reservoirs estimates. The % difference is calculated based on columns four and five.

Catchment	**Climate**	**Model estimates**		**Previous estimates**	**% Difference**
		(t ha^{-1} year^{-1})		(t ha^{-1} year^{-1})	
		Mean parameters	HML parameters	Msadala et al. (2010)	
Ntabelanga	Sub-humid	21.6	21.4	86.0	-75
Xonxa	Sub-humid	3.8	3.7	8.9	-58
Klaserie	Sub-tropical	4.6	2.3	1.2	91.6
Churchill	Temperate	6.9	4.5	0.1	4400
Duiwenhoks	Temperate	2.5	3.9	0.4	875
Prinsriver	Semi-arid	2.4	3.1	1.3	138
Koster	Semi-arid	4.7	2.5	0.3	733
Maden	Temperate	3.3	4.3	0.5	1700
Hazelmere	Sub-tropical	10.2	9.9	7.1	39
Witklip	Semi-arid	1.4	1.5	4.0	-63
Da Gama	Semi-arid	3.6	5.4	3.4	59
Ebenezer	Sub-tropical	2.0	2.1	1.6	31
Buffelspoort	Semi-arid	6.3	4.9	1.3	277

Column 4 in Table 8.3 presents the results simulated using HML zone parameters, and they neither show a consistent increase nor decrease in sediment output relative to column 3. Notably, sediment output is shown to increase significantly in catchments such as the Da Gama and Duiwenhoks. However, using HML parameters led to prominent decreases in the Koster, Klaserie, Churchill and Buffelspoort catchments. Of the HML parameters *K*, *C* and *LS*, *LS* is shown to contribute the most to the increased sediment output (Figure 8.3) when HML zone parameters are used. The combination of *K* and *C* factors do not result in outputs that are much different from using the *K* factor alone, though *C* is shown to influence the decreases in sediment output. However, when *LS* is added to the *C* and *K* factors, the average sediment output for all the sites increases by up to 30%.

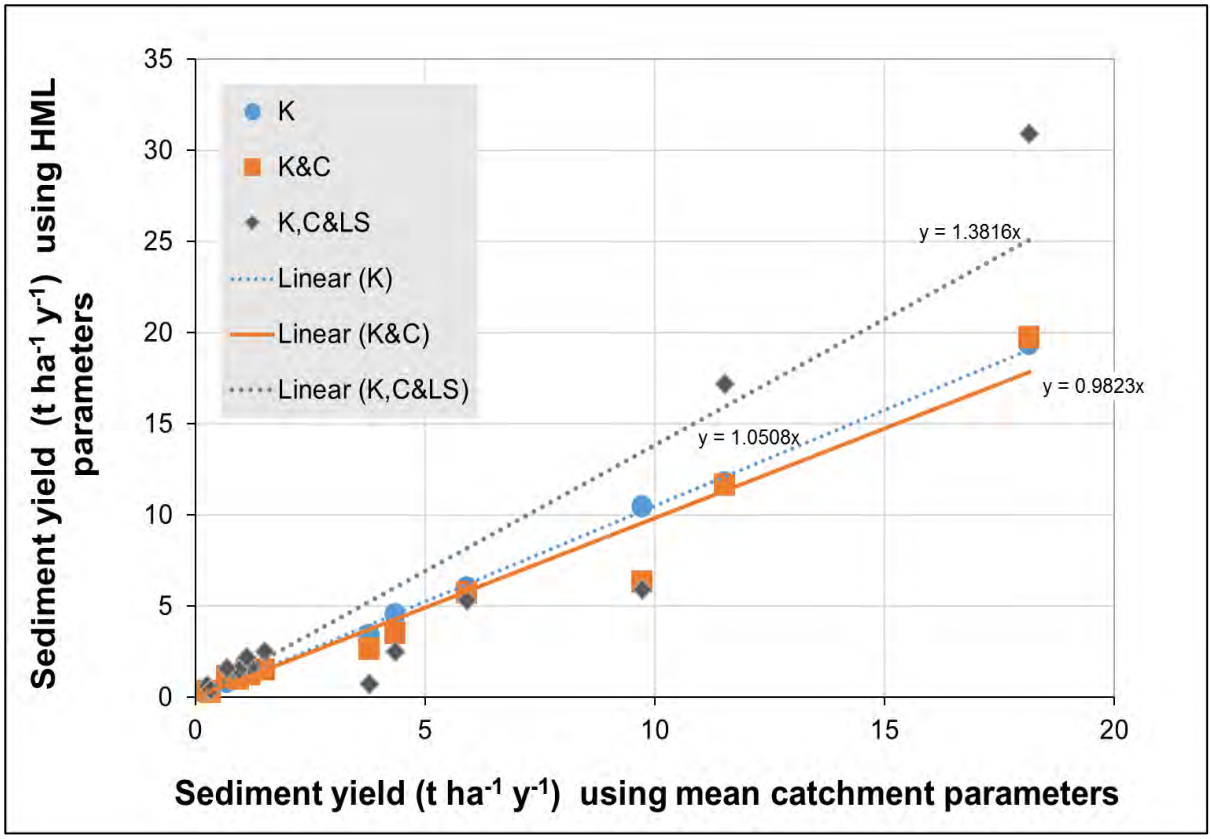

Figure 8.3 Linear regression of estimates calculated using mean catchment parameters and mean High-Medium-Low (HML) parameters.

The comparison of the Msadala et al. (2010) reservoir estimates with model estimates based on the ±25% (upper and lower) uncertainty bounds for parameters is shown in Table 8.4. Reservoir yield rates of 5 catchments (constituting 38% of the total) are captured within the uncertainty bounds. Although most catchments are outside the ±25% uncertainty bounds, several catchments e.g. Xonxa, Buffelspoort and Witklip, are close to the bounds. The rest of the catchments, including Churchill, Duiwenhoks, Koster and Maden, are poorly represented. According to the reservoir surveys, most of the poorly represented catchments have very low sediment yield rates.

Table 8.4 Summary of simulated sediment yield outputs and reservoir estimates. The lower and upper bounds represent the ±25% parameter uncertainty range.

Catchment	Lower bound	Dam estimate	Upper bound
Ntabelanga	5.99	86.00	49.30
Xonxa	1.04	8.88	8.57
Klaserie*	***0.66***	***1.22***	***5.46***
Churchill	1.28	0.10	10.44
Duiwenhoks	1.08	0.43	8.90
Prinsriver*	***0.85***	***1.29***	***6.95***
Koster	0.75	0.27	6.17
Maden	1.20	0.49	9.73
Hazelmere*	***2.82***	***7.14***	***25.30***
Witklip	0.42	4.02	3.46
Da Gama*	***1.49***	***3.39***	***12.24***
Ebenezer*	***0.57***	***1.56***	***4.66***
Buffelspoort	1.38	1.26	11.36

****Catchments where dam estimates fall within the upper and lower bounds***

8.4 Discussion

8.4.1 Estimated MUSLE factor distributions

The use of lumped (mean) catchment values for the MUSLE factors requires less effort for processing spatial datasets but is inconsistent with the distribution approach adopted for the WQSED model. The adoption of the lumped catchment means *LS* parameterisation will generally underestimate the *LS* factor in the H zone and overestimate the *LS* factor in the L zone. The lumped approach also fails to account for the spatial variability of slope within the selected catchments, as well as the relationships between slopes and other MUSLE factors. The use of the mean lumped *LS* (without considering variations of other MUSLE factors) is likely to result in large under- or over-estimations of sediment yield depending on the particular break down of the catchment into HML zones. Although the adopted HML approach has advantages, including being consistent with the model structure, the model could still fail to account for quite large variations within each HML zone. The HML parameterisation approach is, therefore, still prone to the potential spatial scale effects reported in e.g. Gwapedza et al. (2018) and Karydas et al. (2014). Spatial scale effects influenced by parameter aggregation (Chen and Mackay, 2004) can be resolved by adopting a fully distributed approach which would require a more complex model and significant input data if daily sediment transport is required.

However, it must be acknowledged that the HML approach is also subject to all the uncertainties associated with the assumptions made about the distribution of the runoff factor (depth and peaks) across the three zones, in the absence of any real data.

The parameter assessment showed that the vegetation cover (*C*) is the most variable parameter across the three slope zones (Figure 8.2). Additionally, no specific pattern was exhibited by the variation as patterns varied from one catchment to the next. The *C* factor is primarily influenced by the climatic zonation of respective catchments, as climate correlates with vegetation cover. The patterns exhibited by *C* (Figure 8.2C) suggest that the *C* factor (vegetation) gradually increased (worsened) with a decrease in slope. This pattern means that vegetation cover increases on higher slopes; hence, high erosion rates resulting from high slopes are to an extent mitigated by better vegetation cover, and *vice versa,* highlighting the importance of restoring vegetation cover as a method of reducing erosion and sediment yield (see Le Roux and Waal, 2020; Nearing et al., 2017). The degree of mitigation is, of course, affected by the actual values of the various parameters and, for example, a low *C* factor of 0.11 in the H zone in T35A-E will be less important than the *LS* factor value of 16.5. The pattern of decreasing vegetation in the L zone is likely attributed to human disturbance since human settlements and economic activities such as agriculture are more widespread in the ML zones of most catchments (NLC 2014).

The soil erodibility factor distribution (Table 8.1, Figure 8.2) shows that the majority of selected study sites have moderately erodible soils. The Churchill Dam Catchment (K90A–B) has a high erodibility factor that is associated with the Podzolic (sandy) soils dominating that region. An empirical study conducted in the T35 catchments discovered that part of the catchment is covered by dispersive soils (Le Roux et al., 2015) that have high infiltration rates and crumble and dissolve when exposed to water. Le Roux et al. (2015) study shows that our previous understanding of the soils of the area (Schulze et al., 2007) requires revision as the *K* factor of the area may be higher. However, it is also important to note that the dispersive soils' spatial coverage in the T35 catchments has not yet been sufficiently mapped. Depending on spatial coverage, a small area coverage of dispersive soils may have little effect on a weighted mean catchment *K* factor. This may be a limitation in the application of models that lump large areas when the resolutions of most available datasets are coarse.

The management practice (*P*) factor distribution (Table 8.1, Figure 8.2) shows that most of the study areas have high *P* factor values of > 0.8, suggesting that there are poor agricultural

management practices within the study areas. However, this high value is also mainly a result of agriculture constituting a small percentage of the total area in most of the catchments, since non-agricultural land is assigned a *P* factor of 1 (indicating no management practice). Estimating the *P* parameter according to the HML zones leads to a slight improvement by capturing some of the spatial variability within the catchments. Figure 8.2D shows that all the study catchments have a *P* of 1 in the H zone and minimal variation in the M zone. Significant *P* variation is exhibited in the L zone. This pattern is linked to the pattern exhibited by the *C* factor, since low slopes are ideal for agricultural activity, while there is less agriculture in the M zone and mostly none in the steep H zone. Two of the MUSLE factors (*LS* and *P*) are shown to be consistently high in the H zone, leaving the *K* and *C* factors as the primary regulators of erosion rates within the H zone.

8.4.2 Regional sediment yield patterns

The simulated sediment yield results (Table 8.3 and Figure 8.4) showed that the catchments located in the Eastern Cape (T35A-E and S10A-E) have the highest sediment yields. Le Roux et al. (2015) conducted an erosion modelling study in the Umzimvubu catchment in the Eastern Cape and reported high sediment yields ranging up to 150 t ha^{-1} $year^{-1}$. The higher soil loss rates in the Eastern Cape (reported in Le Roux et al., 2008) can also be attributed to human influence, as poor land management and overgrazing continue to destroy the vegetation cover (Le Roux and Waal, 2020; van Tol et al., 2016). The result of the current study also points to higher sediment yields in the Eastern Cape region. Global studies (e.g. Borrelli et al., 2017) and continental studies (e.g. Vanmaercke et al., 2014) highlight that the areas north of the Eastern Cape followed by the primarily semi-arid northern parts of the country are generally high erosion zones. The temperate southern and semi-arid northern parts of the country have much lower erosion rates compared to the sub-humid Ntabelanga catchment. The lower soil loss rates are attributed to the vegetation cover and less intensive rainfall regime in the region. Low *C* values tend to mitigate against higher values in the other factors for the H and M zones. For example, when the addition of the HML *LS* parameter increased sediment output dramatically in steep catchments such as H80A (H *LS* = 22), the high *LS* coincided with a low *C* factor of 0.05, ensuring that while the *LS* is >100% higher than the mean *LS* value, the sediment output only increased by 32%.

Comparison of the model estimates and reservoir survey estimates (Table 8.3) showed that the WQSED manages to capture some of the regional patterns of sediment yield (see Figure 8.4).

However, actual sediment yield rates (Table 8.3) did not compare very well. The poor performance of the WQSED model can be attributed to a variety of factors. Firstly, the WQSED only simulates soil loss from the sheet, rill and inter-rill processes because it is based on the MUSLE. Therefore, sediment yields from areas with extensive active gully processes in the Eastern Cape and the north of the country (see Mararakanye and Le Roux, 2012) are likely to be under-simulated. In a recent study, Ezzaouini et al. (2020) compared MUSLE simulations to bathymetric survey data, reported underestimations and concluded that most sediments entering the dam were from non-sheet or rill processes. Secondly, uncertainties in the parameter estimation could be contributing to model failure to simulate low sediment yields. The extent of vegetation protection of soils in catchments such as Maden (mostly indigenous forest with a well-developed litter layer) was likely underestimated by using vegetation maps and assigning *C* values *a priori*. Despite using a 250m soil erodibility database, the data is still largely coarse, especially when applied to small catchments such as Maden. Some of the very low observed sediment yields occur in mountain catchments (e.g. H80A and K90A-B), where at least some of the steep parts (the H zone) have bare rock. These are often not reflected as areas with low erodibility in the databases and are not well captured by classified land cover/land use maps; this could also contribute to over-estimation, particularly given the assumptions in WQSED that these are the zones with the highest erosivity factors. Where possible, field campaigns could bridge input data uncertainty by providing additional information to supplement data derived from existing databases.

Additional uncertainties associated with flow separation have already been reported in previous chapters. An assessment conducted to ascertain how much baseflow separation would be necessary to attain a result in the reservoir estimates range indicated that unrealistic baseflow fractions of >90% are necessary to bring model estimates within the range of reservoir estimates. Baseflow fractions that high would be unrealistic even for densely vegetated catchments like the Maden, where infiltration rates are assumed to be high. Notably, calibrating the scale and power parameters (Equation 2.1; Chapter 2) in the MUSLE erosivity equation (e.g. Ezzaouini et al., 2020) would generally have a similar effect on the erosivity. Therefore, a calibration range (for the coefficients) may be necessary to constrain MUSLE erosivity and ensure that calibrations are based on realistic erosivity assumptions.

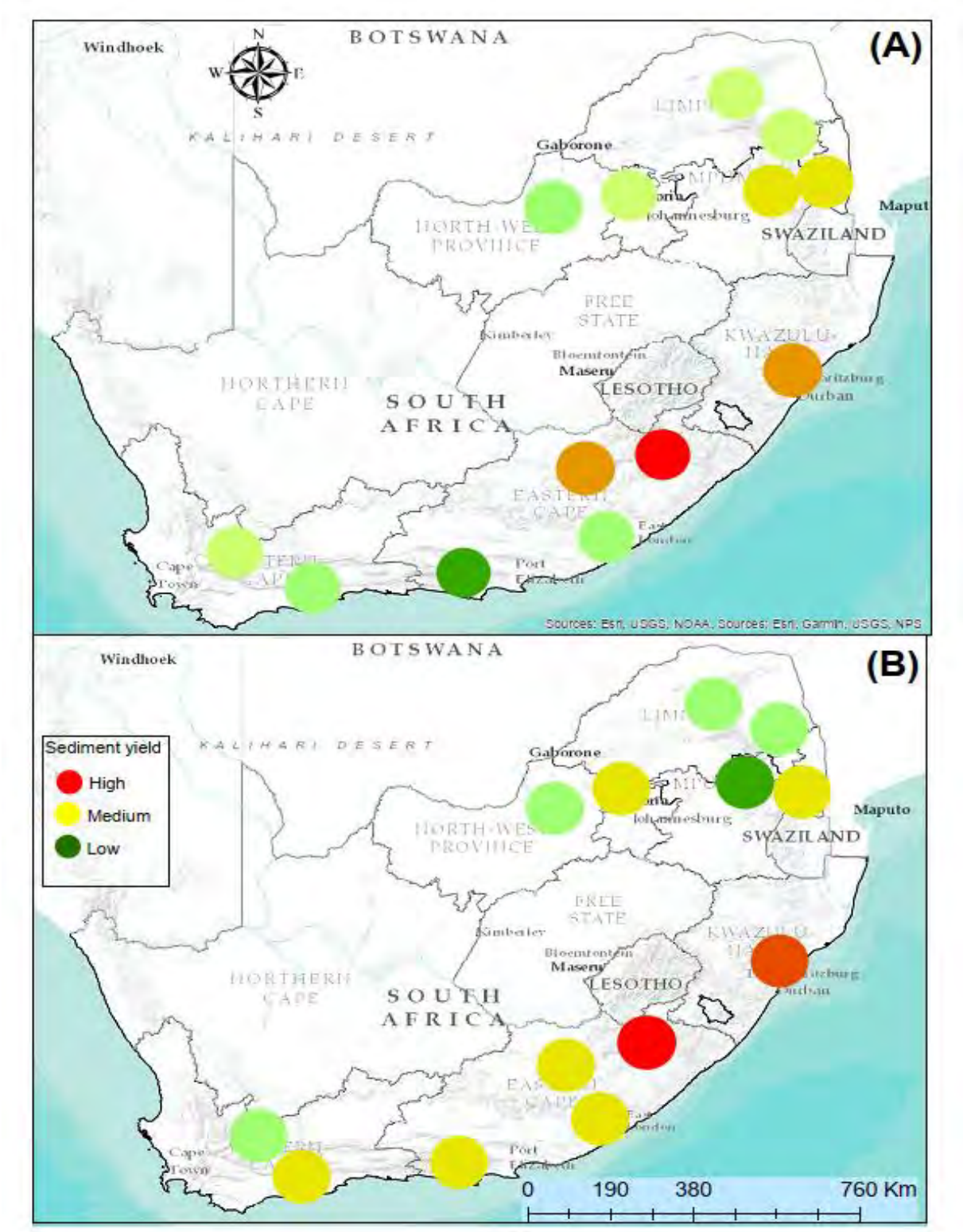

Figure 8.4 Map showing the regional sediment yield gradient exhibited through the selected catchments. A. represents the patterns based on reservoir survey, and B. represents modelled patterns.

Overestimations emanating from the current WQSED application could also be related to uncertainties associated with what happens to sediment when it reaches the dam. Modelled sediment is assumed to enter the dam and settle over time. However, some dams are equipped with sediment traps that can reduce the amount of sediment entering the dam (Rooseboom, 1992), and some of the sediment may be lost during reservoir water releases and spills. A further potential problem is that some of the catchments have quite extensive networks of small farm dams, many of which are located on the main tributary river channels, acting as sediment traps.

8.5 Conclusion

The application of the WQSED model with HML factors for study areas indicated the sensitivity of the model outputs to parameter aggregation, and highlighted the importance of parameterising the model following the model distribution approach. However, the resultant sediment yield outputs were generally poor compared to the observed reservoir sedimentation rates, although some catchments were relatively close to the observed data. Notably, the reservoir rates for several catchments (38%) fell within the ±25% parameter uncertainty range. Although the WQSED model simulates sheet-rill processes and is generally unsuitable for estimating actual reservoir sediment volumes in catchments where gully or channel processes are dominant, model outputs were generally shown to replicate the spatial erosion patterns of the previous estimates. The results are essential for highlighting hillslope sediment contribution to reservoir sediment. The knowledge of spatial patterns of sediment yield and influencing factors is vital for catchment management initiatives that aim to reduce hillslope erosion contributions to reservoir sedimentation. Additionally, scenarios associated with changes in rainfall, vegetation and related human impacts can be assessed. Beyond water quality applications, the WQSED model could be a useful resource for regional sediment yield assessments. Further resolving the reasons for some of the very large discrepancies in MUSLE estimates compared to the observed reservoir sedimentation rates was beyond this study's limited resources. However, this is obviously a very important issue if the MUSLE-based WQSED model is to be used with any confidence in the future.

Chapter 9 Conclusions and recommendations

9.1 Introduction

This study focused on the further improvement, testing and evaluation of a recently developed erosion and sediment transport model (WQSED). While the model has mostly been applied and validated in southern Africa and parts of the USA (and associated territories), its suitability for application in South Africa requires further investigation. The development of the WQSED model was achieved by adding conceptual sediment storages and a channel routing module to the modified universal soil loss equation (MUSLE) (Williams, 1975). The approach used to simulate the daily flow data needed to force the WQSED model, is the application of a mechanistic hydrological model (the Pitman model) (Pitman, 1973; Hughes, 2013), which was developed in South Africa, coupled with a month-to-day disaggregation method (Hughes and Slaughter, 2015). However, flow data from other independent sources (including observed streamflow) may also be used. The model is part of and in addition to an existing suite of commonly used water resources management models in South Africa (SPATSIM; Hughes and Forsyth, 2006). Primarily, the model was developed to provide sediment simulations to the Water Quality Systems Assessment Model (WQSAM) (Slaughter et al., 2017). The initial testing of the WQSED model was followed by identifying scale issues associated with the application of the model. Subsequently, the calibrated model performance was assessed against established sediment yield models.

9.2 Spatial and temporal scale effects associated with MUSLE application (Objectives A and B)

Universal Soil Loss Equation (USLE) (Wischmeier and Smith, 1978) and other USLE based models e.g. MUSLE, are largely derived from plot scale assessments. Upscaling these models to catchment scale is usually necessary because that is the scale at which information for managing catchments is usually required. However, upscaling leads to errors associated with spatial and temporal scale (Karydas et al., 2014). Spatial scale issues affecting the MUSLE have been reported as part of the SWAT model applications (Neitsch et al., 2005), e.g. Chen and Mackay (2004), Pignotti et al. (2017), and Vigiak et al. (2015). Although the previous studies focused on SWAT Hydrological Response Units' (HRUs') size and grid resolution, the

potential spatial scale effects were evident. It was important that these scale effects were investigated as part of the WQSED development.

Furthermore, a review of the worldwide application of MUSLE by Sadeghi et al. (2013) indicated that accounting for temporal variation in the MUSLE could improve performance, although this was rarely taken into account by existing studies. Therefore, it was imperative that temporal variation be assessed to provide more insights into the sensitivity of the MUSLE to temporal variations. The issues of scale reported in previous studies arose during initial testing of the WQSED model and these were investigated as part of model development. When investigating the effects of scale on the MUSLE, a distinction was made between spatial and temporal scale effects. The primary research question was to investigate whether the outputs and performances of the MUSLE were different when applied at different spatial and temporal scales.

Hypothetical study catchments were used to investigate spatial scale effects. While hypothetical catchments could be viewed as abstract, their use is justified, as the scientific and mathematical principles remain the same for a real-world situation. Notably, attempts to isolate the scale effects in a complex real-world situation would be confounded by the myriad of interrelated processes present, and it could therefore be argued that the use of a hypothetical catchment allows the spatial scale effects of the MUSLE to be more easily isolated, by excluding the effects of confounding processes from the analysis. After applying the MUSLE to hypothetical catchments of varying sizes, it was discovered that: 1) the MUSLE simulates different amounts of sediment depending on whether a lumped or distributed discretization of the catchment is used in the modelling approach, and 2) these differences are primarily linked to the MUSLE's erosivity equation and topographic factor. A further issue that the current study has highlighted is the conceptual differences between the original USLE and the more recent MUSLE in terms of erosion and sediment delivery, which is clearly also related to spatial scale. The use of a runoff-derived erosivity factor was originally designed to allow the MUSLE to be used as an event-specific estimation of erosion, whereas the USLE was designed to generate long-term average erosion. However, it appears that some publications (e.g. Arekhi et al., 2012) consider this distinction also to mean that a sediment delivery ratio is no longer required. Although sediment routing is part of the SWAT model implementation of the MUSLE (Neitsch et al., 2005), it appears that the routing approach simply attenuates the sediment generated on any day. However, the long-term total mass of sediment delivery will approximately equal the sediment yield calculated by the MUSLE. Therefore, sediment routing

cannot be assumed to have any compensating effects on spatial scale dependencies associated with the MUSLE erosion estimates. Sediment routing may be necessary for estimating the likely range of suspended sediment concentrations in downstream river channels. However, if the long-term conservation of mass principle is not adhered to, sediment storages within the catchment will either progressively increase or decrease.

The overall conclusion is that potential scale dependency issues associated with the use of the MUSLE exist, and that these will be dependent upon the type of catchment discretization used in the modelling approach (lumped, semi-distributed or distributed), and whether all the model algorithms and recommended parameter estimation methods have been designed to be sensitive to the spatial scale dependencies. Perhaps the key issues are that any uncertainties in the estimates of the hydrological data used to force the MUSLE erosivity equation, or in the approaches used to estimate the *LS* factor, could be exacerbated by the spatial scale dependency problems that have been highlighted in the current study, and that these issues should be considered as part of a broader model sensitivity and uncertainty assessment. This is particularly relevant in data-scarce regions where there is often little information available to calibrate an environmental model and constrain the model outputs. The current investigation contributes to sediment yield modelling that uses MUSLE (and possibly other USLE variations) because it is one of the first to report the spatial scale effects of the MUSLE explicitly. The present study results should act as an essential guide to applying WQSED or other models incorporating the MUSLE. Other models related to the MUSLE, such as the USLE and RUSLE, could also be affected by such spatial scale effects. Given the popularity of the USLE, RUSLE and MUSLE worldwide, the present study's findings may ultimately change the way most sediment yield models are applied worldwide.

Concerning temporal scale effects in the MUSLE, the influence on sediment yield estimation in the MUSLE of changes over time to land cover, was investigated. The current study found that: 1) intra-year (seasonal) variability in vegetation cover exceeded that between years; 2) considering temporal changes in vegetation cover led to some improvement in sediment yield estimation; and 3) a seasonal *C* factor is vital in areas with seasonally-variable rainfall/runoff regimes which receive significant rainfall in winter when vegetation coverage is low.

Remotely-sensed NDVI data were used to provide a time series of land cover data instead of static land cover from land-use maps. Several NDVI to *C* factor conversion methods were evaluated, and despite limitations and uncertainties associated with these conversion methods,

the method of van der Knijff et al. (1999) was found to be generally appropriate for application to the selected study area. Therefore, it was crucial to test and validate the conversion methods through field observations before application to areas outside of the region for which they were developed. This result should be an important guide to future studies when adopting and applying existing *C* factor conversion methods.

The outcome of the current investigation highlights the potential importance of considering temporal scale effects in applying the MUSLE. However, the analysis was conducted on catchments with similar climatic and vegetation regimes over a few years; therefore, these conclusions are preliminary. Further analyses involving multiple catchments and more extended periods should be considered before more concrete conclusions can be made. Pre-processed NDVI data products are now commonly accessible on sites such as Google Earth Engine. The ready availability of NDVI products balances out the potential additional parameterisation burden associated with considering temporal aspects of vegetation cover. However, accounting for temporal changes in vegetation cover using the NDVI method remains constrained by the vegetation cover attributes that the index can represent (Schmidt et al., 2018) and satellite images' availability for historical applications. While the WQSED structure does not currently have an option for applying (possibly using a seasonal distribution) dynamic *C* factors, this could be considered as part of future model developments after a more robust assessment of *C* factor variations has been performed.

9.3 Application and evaluation of the WQSED model (Objectives C and D)

The application and evaluation of the WQSED model was a vital component of the current study, as the model had never been calibrated and validated against observed daily data after its initial development. In addition, the model had previously only been applied to three small catchments in South Africa that fell within the same region (Eastern Cape, South Africa). Therefore, additional testing was vital before the model could be incorporated for use within the water resources modelling framework in South Africa.

Good performance statistics were recorded in the catchments modelled in the present study. This was a positive development, particularly since the WQSED simulates sediment at a daily time scale and previous studies (Borah and Bera, 2004; Moriasi et al., 2007) have shown that sediment yield simulations rarely produce satisfactory results at a daily time step. The model calibration and validation exercise yielded the following outcomes: 1) results from the model

calibration and validation indicate that the model is stable and applicable; 2) the results provide considerable information on the rates and dynamics of sediment yield, which is essential for catchments management; and 3) sparse monthly observed data that were used to calibrate the model in some study areas could be infilled using a continuous simulated daily record of sediment yield, although the validity of the calibration was relatively uncertain. The model also demonstrated that it could perform relatively well when compared to other established models. Applying the model in 'ungauged' catchments yielded poor results, mainly because the model simulations (sheet and rill processes) were compared with sediment yield rates estimated from reservoir surveys measuring accumulated sediment from all sources that include gully and bank erosion, that are not represented by the WQSED. However, the model managed to replicate some of the regional sediment yield patterns primarily driven by erosivity, slope and vegetation coverage.

One of the key remaining questions in sediment transport studies is related to the role of gullies, not only as conduits of sediment but also as primary source areas of sediment. From a modelling perspective, this question relates to whether there is a need to simulate gully erosion in a sediment model explicitly. Unfortunately, there is insufficient real data available to answer these questions. Another possible reason for the model's failure to estimate some peaks could be due to significant mismatches between observed flow and observed sediment concentration data (also associated with hysteresis effects) that were explicitly noted for the Tsitsa catchment. However, significant uncertainties also encompass the observed sediment data. Measures of instantaneous suspended sediment concentration (SSC) collected using grab or automated sampling methods and converted to daily loads will not always be accurate representations of the daily sediment discharge, as they represent the sediment discharge collected at a single time and extrapolated to represent the entire day. Uncertainties in input data, calibration data and model structure make sediment yield modelling complex and uncertain.

The application and evaluation of the WQSED model in the current study indicated that the model is generally difficult to apply in ungauged catchments. This mainly applies to the calibration parameters associated with the storage model and storm duration. Adopting the simpler storage option could significantly reduce model complexity while maintaining effectiveness. Regardless of the storage option adopted, the application of the WQSED to areas lacking observed data could remain challenging. However, a parameter transfer assessment in Chapter 7 showed that there could be potential for regionalising the model's calibration

parameters. Although more assessments of the WQSED model are necessary, lengthy observed daily sediment data are scarce in South Africa.

Providing reliable sedimentation information is crucial for catchment management. Simulation models are vital tools that can be used to obtain this information. However, the calibration and validation of these models to provide reliable simulations is difficult, due to the scarcity of daily observed sediment yield data. This problem particularly affected the current research, and it is recommended that more funding be dedicated to data collection of daily sediment data. It is acknowledged that the problem of data scarcity has continuously compounded model application in Africa. There is perhaps a need to assess the minimum observed data requirements that can be used to constrain model outputs. One approach could be collecting spot sediment observations during high, moderate and low flow periods to develop realistic regional sediment discharges for constraining model outputs in ungauged basins. Another method would be developing a sediment rating curve, although this method may require daily observed sediment data, of which there is a short supply in African catchments. Although the above suggestions could be valuable in a data-scarce context, they may fail to capture or account for the complexity of sediment processes that result in the variability of sediment discharge.

The WQSED model was calibrated and validated using limited observed sediment data for a few catchments. Based on its performance, the model is recommended for simulating catchment sediment yield, particularly for catchments in which at least some calibration data are available. Further robust model application and testing are recommended to evaluate the model more broadly. Users of the WQSED model should be aware that no explicit gully function has yet been implemented, and this could affect model performance in areas where gullying is a significant source of sediment. Therefore, the addition of an explicit gully function represents an opportunity for further development of the model while ensuring these developments do not culminate in a complex model that is inappropriate for practical application in the intended catchments. Finally, there is a need to consider the current trends in research with regards to data sources. Earth observation is making data at a range of spatial and temporal resolutions increasingly available, and it is vital to carefully consider what these data mean and the associated limitations and uncertainties. Accordingly, there is a need to shape our existing approaches to seamlessly adopt valuable data anticipated to increase with advancements in Earth observation.

9.4 Limitations of the study

- The study was conducted mainly as a desktop study. Limitations associated with funding precluded the establishment of sediment monitoring stations and conducting field surveys and soil sampling to supplement existing data. In addition, the study areas of the current study range across Southern Africa and beyond, thereby making field assessment infeasible.
- The model does not simulate gully and channel erosion, which could be significant sediment sources in some South African catchments.
- The effect of stoniness (rock fragment factor) was not considered; therefore, estimates of the *K* factor could be slightly higher in some catchments.
- The unavailability of observed daily sediment data prevented rigorous testing of the model in South Africa, which is the primary area of application. Additionally, the lack of data for validating baseflow separation makes the estimated surface flows highly uncertain.

9.5 Conclusion

An erosion and transport model, the WQSED, has been evaluated and tested for specific application to catchments of South Africa and the sub-Saharan Africa region. Initial testing conducted within the present study demonstrated that the model could produce acceptable results. However, the model could not be thoroughly tested and validated because of a lack of observed daily sediment data in the region. Some uncertainties associated with the model have not been resolved within the current study. Some of these limitations and uncertainties relate to parameter estimation based on spatial data, model structure and the role of erosion originating from gully development (rather than their role as temporary sediment stores), the temporal changes in vegetation cover, the parameters used for baseflow separation and the determination of surface runoff. Most of these uncertainties may be resolved by the availability of high quality observed information and calibration data. However, attempts to minimise uncertainties and account for a greater number of erosion processes should avoid developing an overly complicated model with data requirements that cannot be met in most catchments in southern Africa. The WQSED model was developed to address the need for a sediment model

that can be integrated within the WQSAM model to simulate water quality within the broader water resources modelling framework in South Africa. While the WQSED model is generally considered fit-for-purpose from a practical application perspective, the unavailability of calibration data in most cases will mean that the model outputs will remain highly uncertain. While the provision of this model does not immediately solve the water resources challenges facing sustainable management of southern African catchments, the model is a valuable tool for generating scarce sediment yield information. It is only through knowledge and information that we can sustainably manage our natural ecosystems and realise water-safe and -secure African catchments.

References

Abrams, M.M., Jarrell, W.M., 1995. Soil-phosphorus as a potential non-point source for elevated stream phosphorus levels. Journal of Environmental Quality, 24, 132-138

Adimassu, Z., Tamene, L., Degefie, D.T., 2020. The influence of grazing and cultivation on runoff, soil erosion, and soil nutrient export in the central highlands of Ethiopia. Ecol. Process. 9. https://doi.org/10.1186/s13717-020-00230-z

Akamagwuna, F.C., Mensah, P.K., Nnadozie, C.F., Odume, O.N., 2019. Trait-based responses of Ephemeroptera, Plecoptera, and Trichoptera to sediment stress in the Tsitsa River and its tributaries, Eastern Cape, South Africa. River Res. Appl. 35, 999–1012. https://doi.org/10.1002/rra.3458

Alewell, C., Borrelli, P., Meusburger, K., Panagos, P., 2019. Using the USLE: Chances, challenges and limitations of soil erosion modelling. Int. Soil Water Conserv. Res. https://doi.org/10.1016/j.iswcr.2019.05.004

Alexandridis, T.K., Sotiropoulou, A.M., Bilas, G., Karapetsas, N., Silleos, N.G., 2015. The Effects of Seasonality in Estimating the C-Factor of Soil Erosion Studies. L. Degrad. Dev. 26, 596–603. https://doi.org/10.1002/ldr.2223

Almagro, A., Thomé, T.C., Colman, C.B., Pereira, R.B., Marcato Junior, J., Rodrigues, D.B.B., Oliveira, P.T.S., 2019. Improving cover and management factor (C-factor) estimation using remote sensing approaches for tropical regions. Int. Soil Water Conserv. Res. 7, 325–334. https://doi.org/10.1016/j.iswcr.2019.08.005

Amore, E., Modica, C., Nearing, M.A., Santoro, V.C., 2004. Scale effect in USLE and WEPP application for soil erosion computation from three Sicilian basins. J. Hydrol. 293, 100–114. https://doi.org/10.1016/j.jhydrol.2004.01.018

Arekhi, S., Shabani, A., Rostamizad, G., 2012. Application of the modified universal soil loss equation (MUSLE) in prediction of sediment yield (Case study: Kengir Watershed, Iran). Arab. J. Geosci. 5, 1259–1267. https://doi.org/10.1007/s12517-010-0271-6

Arnold, J.G., Srinivasan, R., Murruah, R.S., Williams, J.R., 1998. Large area hydrologic modelling and assessment part I: Model development. J. Am. Water Resour. Assoc. 34(1),73–89

Ayalew, G., 2015. A Geographic Information System Based Soil Loss and Sediment Estimation in Zingin Watershed for Conservation Planning, Highlands of Ethiopia. International Journal of Science, Technology and Society, 3(1), 28. http://doi.org/10.11648/j.ijsts.20150301.14

Azimi Sardari, M.R., Bazrafshan, O., Panagopoulos, T., Sardooi, E.R., 2019. Modeling the Impact of Climate Change and Land Use Change Scenarios on Soil Erosion at the Minab Dam Watershed. Sustainability 11, 3353. https://doi.org/10.3390/su11123353

Banda, T.D., Kumarasamy, M., 2020. Development of a universal water quality index (UWQI) for South African river catchments. Water (Switzerland) 12. https://doi.org/10.3390/W12061534

Blignaut, J., Mander, M., Schulze, R.E., Horan, M., Dickens, C., Pringle, C., 2010. Restoring and managing natural capital towards fostering economic development: Evidence from the Drakensberg, South Africa. Ecological Economics, 69 (6): 1313-1323.

Balaz, M., Danacova, M., and Szolgay, J., 2010. On the use of the Muskingum method for the simulation of flood wave movements. Slovak Journal of Civil Engineering, 18(3), 14–20.

Bannatyne, L.J., Rowntree, K.M., Waal, B.W. Van Der, Nyamela, N., 2017. Design and implementation of a citizen technician-based suspended sediment monitoring network: Lessons from the Tsitsa River catchment, South Africa. WaterSA 43, 365–377.

Bauer, S.W., Midgley, D.C., 1974. A simple procedure for synthesizing direct runoff hydrographs. Report No. 1/74, Hydrological Research Unit, University of the Witwatersrand, Johannesburg, South Africa.

Basson, M.S., Allen, R.B., Pegram, G.G.S., van Rooyen, J.A., 1994. Probabilistic Management of Water Resource and Hydropower Systems. Water Resources Publ., Colorado, USA, 424pp.

Benavidez, R., Jackson, B., Maxwell, D., Norton, K., 2018. A review of the (Revised) Universal Soil Loss Equation (R/USLE): with a view to increasing its global applicability and improving soil loss estimates. Hydrol. Earth Syst. Sci. Discuss. 22, 1–34. https://doi.org/10.5194/hess-2018-68

Beven, K., 1989. Changing ideas in hydrology—the case of physically-based models. J. Hydrol. 105, 157–172.

Bhat, S.A., Hamid, I., Rasool, D., Srinagar, N., Kashmir, J., Bashir, I., Pandit, A., Khan, S., Shakeel, C., Bhat, A., Din Dar, M.U., 2017. Soil erosion modeling using RUSLE & GIS on micro watershed of J&K. J. Pharmacogn. Phytochem. JPP 6, 838–842.

Bilotta, G.S., Brazier, R.E., 2008. Understanding the influence of suspended solids on water quality and aquatic biota. Water Res. https://doi.org/10.1016/j.watres.2008.03.018

Blake, W.H., Walsh, R.P.D., Barnsley, M.J., Palmer, G., Dyrynda, P., James, J.G., 2003. Heavy metal concentrations during storm events in a rehabilitated industrialised catchment. Hydrological Processes, 17, 1923-1939.

Boardman, J., 2013. The hydrological role of “sunken lanes” with respect to sediment mobilization and delivery to watercourses with particular reference to West Sussex, southern England. J Soils Sediments 13, 1636–1644. doi:10.1007/s11368-013-0754-7

Boardman, J and Foster, I., 2008. Badland and gully erosion in the Karoo, South Africa. J. Soil Water Conserv. 63, 121A-125A. https://doi.org/10.2489/63.4.121a

Borah, D.K., Bera, M., 2004. Watershed-scale hydrologic and nonpoint-source pollution models: review of applications. Transactions of the American Society of Agricultural Engineers. USA.

Borrelli, P., Robinson, D.A., Fleischer, L.R., Lugato, E., Ballabio, C., Alewell, C., Meusburger, K., Modugno, S., Schütt, B., Ferro, V., Bagarello, V., Oost, K. Van, Montanarella, L., Panagos, P., 2017. An assessment of the global impact of 21st century land use change on soil erosion. Nat. Commun. 8. https://doi.org/10.1038/s41467-017-02142-7

Bracken, L.J., Croke, J., 2007. The concept of hydrological connectivity and its contribution to understanding runoff-dominated geomorphic systems. Hydrological Processes 21, 1749–1763. doi:10.1002/hyp.6313

Briak, H., Moussadek, R., Aboumaria, K., Mrabet, R., 2016. Assessing sediment yield in Kalaya gauged watershed (Northern Morocco) using GIS and SWAT model. Int. Soil Water Conserv. Res. 4, 177–185. https://doi.org/10.1016/j.iswcr.2016.08.002

Brierley, G., Fryirs, K., Jain, V., 2006. Landscape connectivity: the geographic basis of geomorphic applications. Area 38, 165–174. doi:10.1111/j.1475-4762.2006. 00671.x

Bryson, L., 2015. An erosion and sediment delivery model for semi-arid catchments. Master's Thesis:http://vital.seals.ac.za:8080/vital/access/manager/Repository/vital:6056?site_name=GlobalView&exact=sm_creator%3A%22Bryson%2C+Louise+Kay%22&sort=sort_ss_title%2F.Grahamstown: Rhodes University.

Cadaret, E.M., Nouwakpo, S.K., McGwire, K.C., Weltz, M.A., Blank, R.R., 2016. Experimental investigation of the effect of vegetation on soil, sediment erosion, and salt transport processes in the Upper Colorado River Basin Mancos Shale formation, Price, Utah, USA. Catena 147, 650–662. https://doi.org/10.1016/j.catena.2016.08.024

Cai, C.F., Ding, S.W., Shi, Z.H., Huang, L., Zhang, G.Y., 2000. Study of applying USLE and geographical information system IDRISI to predict soil erosion in small watershed. J. Soil Water Conserv. 14, 19–24.

Cârdei, P., 2010. The dimensional analysis of the USLE-MUSLE soil erosion model. Proceedings of the Romanian Academy, Series B, No. 3: 249–253.

Chandramohan, T., Venkatesh, B., Balchand, A.N., 2015. Evaluation of Three Soil Erosion Models for Small Watersheds. Aquat. Procedia 4, 1227–1234. https://doi.org/10.1016/j.aqpro.2015.02.156

Chaplot, V., 2014. Impact of spatial input data resolution on hydrological and erosion modelling: recommendations from a global assessment. Physics and Chemistry of the Earth, 67–69, 23–35. doi:10.1016/j.pce.2013.09.020

Chen, E., Mackay, D.S., 2004. Effects of distribution-based parameter aggregation on a spatially distributed agricultural nonpoint source pollution model. J. Hydrol. 295, 211–224. https://doi.org/10.1016/j.jhydrol.2004.03.029

Chislock, M.F., Doster, E., Zitomer, R. A., Wilson, A.E., 2013. Eutrophication: Causes, Consequences, and Controls in Aquatic Ecosystems. Nat. Educ. Knowl. 1–8.

Climatology Staff., 2012. ARC-ISCW agro meteorology weather station network data for South Africa, Unpublished. In ARC-Institute for Soil, Climate and Water: Pretoria. South Africa.

Colman, C.B., Oliveira, P.T.S., Almagro, A., Soares-Filho, B.S., Rodrigues, D.B.B., 2019. Effects of Climate and Land-Cover Changes on Soil Erosion in Brazilian Pantanal. Sustain. 11. https://doi.org/10.3390/su11247053

Compton, J.S., Herbert, C.T., Hoffman, M.T., Schneider, R.R., Stuut, J.B., 2010. A tenfold increase in the Orange River mean Holocene mud flux: implications for soil erosion in South Africa. Th Holocene 20, 115–122. https://doi.org/10.1177/0959683609348860

Cowie, A. L., Orr, B. J., Castillo Sanchez, V. M., Chasek, P., Crossman, N. D., Erlewein, A., Louwagie, G., Maron, M., Metternicht, G. I., Minelli, S., Tengberg, A. E., Walter, S., & Welton, S., 2018. Land in balance: The scientific conceptual framework for land degradation neutrality. Environmental Science & Policy, 79, 25–35. https://doi.org/10.1016/j.envsci.2017.10.011

Czeglédi, N., 2013. Integrated assessment of human impacts on wetland services in the Upper Kromme River Catchment, South Africa. MSc Thesis, Wageningen University.

de Asis, A.M., Omasa, K., 2007. Estimation of vegetation parameter for modeling soil erosion using linear Spectral Mixture Analysis of Landsat ETM data. ISPRS J. Photogramm. Remote Sens. 62, 309–324. https://doi.org/10.1016/j.isprsjprs.2007.05.013

De Jong, S. M., 1994. Derivation of vegetative variables from a Landsat TM image for modelling soil erosion. Earth Surface Processes and Landforms, 19(2), 165– 178.

de Vente, J., Poesen, J., 2005. Predicting soil erosion and sediment yield at the basin scale: Scale issues and semi-quantitative models. Earth-Science Rev. 71, 95–125. https://doi.org/10.1016/j.earscirev.2005.02.002

de Vente, J., Poesen, J., Verstraeten, G., Govers, G., Vanmaercke, M., Van Rompaey, A., Arabkhedri, M., Boix-Fayos, C., 2013. Predicting soil erosion and sediment yield at regional scales: Where do we stand? Earth-Science Rev. 127, 16–29. https://doi.org/10.1016/j.earscirev.2013.08.014

Deksissa, T., Meirlaen, J., Ashton, P.J., Vanrolleghem, P.A., 2004. Simplifying dynamic river water quality modelling: A case study of inorganic nitrogen dynamics in the Crocodile River (South Africa). Water. Air. Soil Pollut. 155, 303–320. https://doi.org/10.1023/B:WATE.0000026548.20608.a0

Desta, L., Adugna, B., 2012. A field guide on gully prevention and control. Eastern Nile Subsidiary Action Program (ENSAP). Nile basin initiative.Addis Ababa, Ethiopia.

Devatha, C.P., Deshpande, V., Renukaprasad, M.S., 2015. Estimation of Soil loss Using USLE Model for Kulhan Watershed, Chattisgarh - A Case Study. Aquat. Procedia 4, 1429–1436. https://doi.org/10.1016/j.aqpro.2015.02.185

Ding, Z., Zhang, Z., Li, Y., Zhang, L., Zhang, K., 2020. Characteristics of magnetic susceptibility on cropland and pastureland slopes in an area influenced by both wind and water erosion and implications for soil redistribution patterns. Soil Tillage Res. 199, 104568. https://doi.org/10.1016/j.still.2019.104568

Dunkerley, D. L., 2008. Intra-storm evaporation as a component of canopy interception loss in dryland shrubs: Observations from Fowlers Gap, Australia. Hydrological Processes, 22, 1985–1995.

Durigon, V.L., Carvalho, D.F., Antunes, M.A.H., Oliveira, P.T.S., Fernandes, M.M., 2014. International Journal of Remote Sensing NDVI time series for monitoring RUSLE cover management factor in a tropical watershed, https://doi.org/10.1080/01431161.2013.871081

Dutton, C.L., Subalusky, A.L., Anisfeld, S.C., Njoroge, L., Rosi, E.J., Post, D.M., 2018. The influence of a semi-arid sub-catchment on suspended sediments in the Mara River, Kenya. PLoS One 13, e0192828. https://doi.org/10.1371/journal.pone.0192828

DWAF., 2009. State-of-rivers report White-Kei River system. Rivers Report for the Eastern Cape: https://www.dwa.gov.za/default.aspx

DWAF., 2004. State-of-rivers report buffalo river system. Rivers Report for the Eastern Cape: https://www.dwa.gov.za/default.aspx

Eekhout, J.P.C., De Vente, J., 2020. How soil erosion model conceptualization affects soil loss projections under climate change. Prog. Phys. Geogr. 44, 212–232. https://doi.org/10.1177/0309133319871937

Elwell, H.A., 1978. Modelling soil losses in Southern Africa. J. Agric. Eng. Res. 23, 117–127. https://doi.org/10.1016/0021-8634(78)90043-4

Elwell, H.A., Stocking, M.A., 1976. Vegetal cover to estimate soil erosion hazard in Rhodesia. Geoderma 15:61–70.

Evans, R., 1980. Mechanics of water erosion and their spatial and temporal controls: an empirical viewpoint. In: Kirkby, M.J., Morgan, R.P.C. (Eds.), Soil erosion. Wiley, Chichester., 109–128.

Ezzaouini, M.A., Mahé, G., Kacimi, I., Zerouali, A., 2020. Comparison of the MUSLE Model and Two Years of Solid Transport Measurement, in the Bouregreg Basin, and Impact on the Sedimentation in the Sidi Mohamed Ben Abdellah Reservoir, Morocco. Water. https://doi.org/10.3390/w12071882

Fan, L., Gao, Y., Brück, H., Bernhofer, C., 2009. Investigating the relationship between NDVI and LAI in semi-arid grassland in Inner Mongolia using in-situ measurements. Theor. Appl. Climatol. 95, 151–156. https://doi.org/10.1007/s00704-007-0369-2

Firth, C.R., 1991. Patterns of Gullying in Zimbabwe, GeoJournal.

Foster, I. D., Rowntree, K. M., 2012. Sediment yield changes in the semi-arid Karoo: a palaeo environmental reconstruction of sediments accumulating in Cranemere Reservoir, Eastern Cape, South Africa. Zeitschrift für Geomorphologie, Supplementary Issues, 56(3): 131-146.

Fryirs, K., 2002. Antecedent landscape controls on river character, behaviour and evolution at the base of the escarpment in Bega catchment, South Coast, New South Wales, Australia. Zeitschrift für Geomorphologie, NF 475–504.

Fryirs, K.A., Brierley, G.J., Preston, N.J., Kasai, M., 2007. Buffers, barriers and blankets: The (dis)connectivity of catchment-scale sediment cascades. Catena 70, 49–67. https://doi.org/10.1016/j.catena.2006.07.007

Gandhi, G.M., Parthiban, S., Thummalu, N., Christy, A., 2015. Ndvi: Vegetation Change Detection Using Remote Sensing and Gis - A Case Study of Vellore District. Procedia Comput. Sci. 57, 1199–1210. https://doi.org/10.1016/j.procs.2015.07.415

Gao, P., 2008. Understanding watershed suspended sediment transport. Prog. Phys. Geogr. 32, 243–263. https://doi.org/10.1177/0309133308094849

Gellis, A.C., Webb, R.M.T., McIntyre, S.C., Wolfe, W.J., 2006. Land-use effects on erosion, sediment yields, and reservoir sedimentation: A case study in the Lago Loíza Basin, Puerto Rico. Phys. Geogr. 27, 39–69. https://doi.org/10.2747/0272-3646.27.1.39

Glenn, E.P., Huete, A.R., Nagler, P.L., Nelson, S.G., 2008. Relationship between remotely-sensed vegetation indices and plant physiological processes: what vegetation indices can and cannot tell us about the landscape. Sensors 8, 2136. https://doi.org/10.3390/s8042136

Gourfi, A., Daoudi, L., Shi, Z., 2018. The assessment of soil erosion risk, sediment yield and their controlling factors on a large scale: Example of Morocco. J. African Earth Sci. 147, 281–299. https://doi.org/10.1016/J.JAFREARSCI.2018.06.028

Grenfell, S.E., Ellery, W.N., 2009. Hydrology, sediment transport dynamics and geomorphology of a variable flow river: The Mfolozi River, South Africa.

Grenfell, S. E., Grenfell, M. C., Rowntree, K. M., Ellery, W. N., 2014. Fluvial connectivity and climate: A comparison of channel pattern and process in two climatically contrasting fluvial sedimentary systems in South Africa. Geomorphology, 205: 142-154.

Griensven, A., Popescu, I., Abdelhamid, M.R., Ndomba, P.M., Beevers, L., Betrie, G.D., 2013. Comparison of sediment transport computations using hydrodynamic versus hydrologic models in the Simiyu River in Tanzania. Phys. Chem. Earth, Parts A/B/C 61–62, 12–21. https://doi.org/10.1016/J.PCE.2013.02.003

Gwapedza, D., Hughes, D.A., Slaughter, A.R., 2018b. Spatial scale dependency issues in the application of the Modified Universal Soil Loss Equation (MUSLE). https://doi.org/10.1080/02626667.2018.1546388

Gwapedza, D., Nyamela, N., Hughes, D.A., Slaughter, A.R., Mantel, S.K., van der Waal, B., 2020. Prediction of sediment yield of the Inxu River catchment (South Africa) using the MUSLE. Int. Soil Water Conserv. Res. https://doi.org/10.1016/j.iswcr.2020.10.003

Gwapedza, D., Slaughter, A., Hughes, D., Mantel, S., 2018a. Regionalising MUSLE factors for application to a data-scarce catchment. Proc. Int. Assoc. Hydrol. *Sci*. 377, 19–24. https://doi.org/10.5194/piahs-377-19-2018.

Harvey, A.M., 2001. Coupling between hillslopes and channels in upland fluvial systems: implications for landscape sensitivity, illustrated from the Howgill Fells, northwest England. Catena 42, 225– 250. doi:10.1016/S0341-8162(00)00139-9

Helden, U., 1987. An assessment of woody biomass, community forests, land use and soil erosion in Ethiopia. Lund: Lund University Press.

Hudson, N.W., 1981. Soil conservation, 2nd edn. Batsford, London.

Hudson, N.W., Jackson, D.C., 1959. Results achieved in the measurement of erosion and runoff in Southern Rhodesia. Proceedings of the Third Inter-African Soils Conference. Dalaba: 575–83.

Hughes, D., 2004. Three decades of hydrological modelling research in South Africa. S. Afr. J. Sci. 638–642.

Hughes, D.A., 2019. Facing a future water resources management crisis in sub-Saharan Africa. J. Hydrol. Reg. Stud. 23, 100600. https://doi.org/10.1016/J.EJRH.2019.100600

Hughes, D.A., 2013. A review of 40 years of hydrological science and practice in Southern Africa using the Pitman rainfall-runoff model. J. Hydrol. 501, 111–124. https://doi.org/10.1016/j.jhydrol.2013.07.043

Hughes, D.A., Forsyth, D.A., 2006. A Generic Database and Spatial Interface for the Application of Hydrological and Water Resource Models. Computers & Geosciences, 32, 1389-1402.http://dx.doi.org/10.1016/j.cageo.2005.12.013

Hughes, D.A., Hannart, P., Watkins, D., 2003. Con baseflow separation from time series of daily and monthly streamflow data. Water SA. 29(1), 43–48.

Hughes, D.A., Mazibuko, S., 2018. Simulating saturation-excess surface run-off in a semi-distributed hydrological model. Hydrol. Process. 32, 2685–2694. https://doi.org/10.1002/hyp.13182

Hughes, D.A., Slaughter, A., 2015. Daily disaggregation of simulated monthly flows using different rainfall datasets in southern Africa. J. Hydrol. Reg. Stud. 4, 153–171. https://doi.org/10.1016/j.ejrh.2015.05.011

IPCC (Intergovernmental Panel on Climate Change)., 2012. Managing the risks of extreme events and disasters to advance climate change adaptation. A special report of working groups I and II of the Intergovernmental Panel on Climate Change [C.B. Field, V. Barros, T.F. Stocker,

D. Qin, D.J. Dokken, K.L.Ebi (eds)]. Cambridge, UK and New York: Cambridge University Press.

IPCC., 2013. Climate Change 2013: the physical science basis. Contribution of Working Group I to the Fifth Assessment Report of the Intergovernmental Panel on Climate Change. Cambridge University Press, Cambridge, New York.

IPCC., 2007. Climate Change 2007: the physical science basis. Contribution of Working Group I to the Fourth Assessment Report of the Intergovernmental Panel on Climate Change, Cambridge, UK and New York, USA.

Islam, M.R., Jaafar, W.Z.W., Hin, L.S., Osman, N., Karim, M.R., 2020. Development of an erosion model for Langat River Basin, Malaysia, adapting GIS and RS in RUSLE. Appl. Water Sci. 10, 165. https://doi.org/10.1007/s13201-020-01185-4

Issaka, S., Ashraf, M.A., 2017. Impact of soil erosion and degradation on water quality: a review. Geol. Ecol. Landscapes 1, 1–11. https://doi.org/10.1080/24749508.2017.1301053

Jain, S.K., Tyagi, J., Singh, V., 2010. Simulation of runoff and sediment yield for a Himalayan watershed using SWAT model. J Water Resource Protection. 2:267–281.

Jang, C., Shin, Y., Kum, D., Kim, R., Yang, J.E., Kim, S.C., Hwang, S. Il, Lim, K.J., Yoon, J.K., Park, Y.S., Jung, Y., 2015. Assessment of soil loss in South Korea based on land-cover type. Stoch. Environ. Res. Risk Assess. 29, 2127–2141. https://doi.org/10.1007/s00477-015-1027-3

Jha, M., Gassman, P.W., Secchi. S., Gu, R., Arnold, J., 2004. Effect of watershed subdivision on swat flow, sediment, and nutrient predictions. Journal of the American Water Resources Association. 40(3): 811-825.

Kabuya, P.M., Hughes, D.A., Tshimanga, R.M., Trigg, M.A., Bates, P., 2020. Establishing uncertainty ranges of hydrologic indices across climate and physiographic regions of the Congo River Basin. J. Hydrol. Reg. Stud. 30, 100710. https://doi.org/10.1016/j.ejrh.2020.100710

Kapangaziwiri, E., Hughes, D., 2008. Towards revised physically based parameter estimation methods for the Pitman monthly rainfall- runoff model. Water SA. 34(2), 183–192.

Kapangaziwiri, E., Hughes, D.A., Tanner, J., Slaughter, S., 2011. Resolving uncertainties in the source of low flows in South African rivers using conceptual and modelling studies. Conceptual and Modelling Studies of Integrated Groundwater, Surface Water and Ecological Systems. Proceedings of Symposium H01, IUGG Conference held in Melbourne, Australia, July 2011, IAHS Publ. 345, pp. 127–132.

Karlsson, M., Rahmberg, M., 1999. Assessment of Suspended Sediment Variability in Odzi River, Zimbabwe. Uppsala University.

Karydas, C.G., Panagos, P., Gitas, I.Z., 2014. A classification of water erosion models according to their geospatial characteristics. https://doi.org/10.1080/17538947.2012.671380

Kavian, A., Mohammadi, M. A., 2012. Effect of rainfall type on runoff and sediment yield in plot scale. Journal of Range and Watershed Management, 65(1), 117–130.

Kemerink-Seyoum, J., Chinguno, N., Seyoum, S., Ahlers, R., Bolding, J., van der Zaag, P., 2017. Jumping the water queue: changing waterscapes under water reform processes in rural Zimbabwe. Water SA 43. https://doi.org/10.4314/wsa.v43i3.07

Kinnell, P.I.A., 2000. AGNPS–UM: applying the USLE–M within the agricultural nonpoint source pollution model. Environmental Modelling and Software. 15, 331– 341.

Kinnell, P. I., 2005. Why the universal soil loss equation and the revised version of it do not predict event erosion well. Hydrological Processes. 19: 851–854.

Kondolf, G.M. (1997). Hungry water: effects of dams and gravel mining on river channels. Environmental Management, 21, 533-551.

Korman, L.B., Goldsmith, S.T., Wagner, E.J., Rodrigues, L.J., 2020. Spatially distributed simulations of dry and wet season sediment yields: A case study in the lower Rio Loco watershed, Puerto Rico. J. South Am. Earth Sci. 103, 102717. https://doi.org/10.1016/j.jsames.2020.102717

Kundu, P.M., Chemelil, M.C., Onyando, J.O., 2015. The Use of GIS and Remote Sensing Techniques to Evaluate the Impact of Land use and Land Cover Change on the Hydrology of Luvuvhu River Catchment in Limpopo Province. Water Research Commission (WRC_SA) report no. 2246/1/15 http://www.wrc.org.za/wp-content/uploads/mdocs/2246-1-15.pdf

Langbein, W. B., Schumm, S. A.1958. Yield of sediment in relation to mean annual precipitation. Transactions American Geophysical Union, 39: 1076– 1084.

Larsen, M.C., Webb, R.M.T., 2009. Potential Effects of Runoff, Fluvial Sediment, and Nutrient Discharges on the Coral Reefs of Puerto Rico. J. Coast. Res. 251, 189–208. https://doi.org/10.2112/07-0920.1

Legates, D.R., McCabe Jr., G.J., 1999. Evaluating the use of "good-ness-of-fit" measures in hydrologic and hydro-climatic model validation. Water Resources Research. 35 (1), 233–241.

Le Roux, J., Waal, B. Van Der, 2020. Gully erosion susceptibility modelling to support avoided degradation planning. South African Geogr. J. 00, 1–15. https://doi.org/10.1080/03736245.2020.1786444

Le Roux, J.J., 2018. Sediment Yield Potential in South Africa's Only Large River Network without a Dam: Implications for Water Resource Management. L. Degrad. Dev. 29, 765–775. https://doi.org/10.1002/ldr.2753

Le Roux, J. J., Barker, C.H., Weepener, H. L., Berg, V. D., 2015. Sediment yield modelling in the Umzimvubu River Catchment. Water Research Commission Report, WRC project K5/2243/1December 2014.

Le Roux, J.J., Morgenthal, T., Malherbe, J., 2008. Water erosion prediction at a national scale for South Africa. Water SA 34, 305–314.

Le Roux, J. J., Newby, T. S., Sumner, P. D., 2007. Monitoring soil erosion in South Africa at a regional scale, review and recommendations. South African Journal of Science. 103: 329-335.

Le Roux, J.J., Sumner, P.D., 2013. Water erosion risk assessment in South Africa: A proposed methodological framework. Geogr. Ann. Ser. A Phys. Geogr. 95, 323–336. https://doi.org/10.1111/geoa.12018

Le Roux, J. J., Sumner, P. D., Lorentz, S. A., & Germishuyse, T., 2012. Connectivity aspects in sediment migration modelling using the Soil and Water Assessment Tool. Geosciences. 3(1):1–12.

Li, Z., Fang, H., 2016. Impacts of climate change on water erosion: A review. Earth-Science Rev. 163, 94–117. https://doi.org/10.1016/J.EARSCIREV.2016.10.004

Lidén, R., Harlin, J., Karlsson, M., Rahmberg, M., 2001. Hydrological modelling of fine sediments in the Odzi river, Zimbabwe. Water SA 27, 303–314. https://doi.org/10.4314/wsa.v27i3.4973

Lim, K.J., Sagong, M., Engel, B.A., Tang, Z., Choi, J., Kim, K.S., 2005. GIS-based sediment assessment tool. Catena. 64(1) 61–80.

Lobb, D.A., 2008. Soil Movement by Tillage and Other Agricultural Activities, in: Encyclopedia of Ecology, Five-Volume Set. Elsevier Inc., pp. 3295–3303. https://doi.org/10.1016/B978-008045405-4.00832-6

Loch, R.J., Silburn, D.M., 1996. Constraints to sustainability soil erosion. In: Clarke, L., Wylie, P.B. (Eds.), Sustainable Crop Production in the Sub-tropics: An Australian Perspective. QDPI.

Lötter, D., 2017. Risk and vulnerability in the South African farming sector: Implications for sustainable agriculture and food security. In: Understanding the Social & Environmental Implications of Global Change. https://www.csir.co.za/documents/csir-global-change-ebookpdf (Accessed 17 July 2010)

Luo, Y., Yang, S., Liu, X., Liu, C., Zhang, Y., Zhou, Q., Zhou, X., Dong, G., 2016. Suitability of revision to MUSLE for estimating sediment yield in the Loess Plateau of China. Stoch. Environ. Res. Risk Assess. 30, 379–394. https://doi.org/10.1007/s00477-015-1131-4

Maeda, E.E., Pellikka, P.K.E., Siljander, M., Clark, B.J.F., 2010. Potential impacts of agricultural expansion and climate change on soil erosion in the Eastern Arc Mountains of Kenya. Geomorphology 123 (3-4), 279–289.

Makungu, E., 2020. A combined modelling approach for simulating channel wetland exchanges in large African river basins. Rhodes University. PhD Thesis. Available at: http://hdl.handle.net/10962/123288

Mallory, S.J.L., Odendaal, P., Desai, A., 2011. The Water Resources Modelling Platform User's Guide v3.3. Unpublished document available from: stephen@ waterresources.co.za.

Mararakanye, N., Le Roux, J.J., 2012. Gully location mapping at a national scale for South Africa. South African Geogr. J. 94, 208–218. https://doi.org/10.1080/03736245.2012.742786

Mararakanye, N., Sumner, P.D., 2017. Gully erosion: A comparison of contributing factors in two catchments in South Africa. Geomorphology. 288, 99–110. https://doi.org/10.1016/j.geomorph.2017.03.029

Martin, S., Conklin, M., Bales, R., 2014. Seasonal Accumulation and Depletion of Local Sediment Stores of Four Headwater Catchments. Water. 6, 2144–2163. https://doi.org/10.3390/w6072144

Martinez, G., Weltz, M., Pierson, F.B., Spaeth, K.E., Pachepsky, Y., 2017. Scale effects on runoff and soil erosion in rangelands: Observations and estimations with predictors of different availability. Catena. 151, 161–173. https://doi.org/10.1016/j.catena.2016.12.011

Masipa, T.S., 2017. The impact of climate change on food security in South Africa: Current realities and challenges ahead. Jamba J. Disaster Risk Stud. 9, 1–7. https://doi.org/10.4102/jamba.v9i1.411

Merritt, W.S., Letcher, R.A., Jakeman, A.J., 2003. A review of erosion and sediment transport models. Environ. Model. Softw. 18, 761–799. https://doi.org/10.1016/S1364-8152(03)00078-1

Middleton, B.J. Bailey, A.K., 2008. Water Resources of South Africa, 2005 Study (WR2005). WRC Report No's. TT380 to 382/08 submitted by SRK Consulting, SSI Engineers and Environmental Consultants (Pty) Ltd., Knight Piesold, Arcus Gibb (Pty) Ltd., Ninham Shand Consulting Services, P D Naidoo & Associates, Umfula Wempilo Consulting on behalf of Water Research Commission, Gezina, South Africa.

Midgley, D. C., Pitman, W. V., Middleton, B. J., 1994. Surface Water Resources of South Africa 1990. Pretoria: Water Research Commission.

Milliman, J.D., Farnsworth, K.L., 2011. River Discharge to the Coastal Ocean – A Global Synthesis. Cambridge University Press.

MINADER., 2015. The State of Biodiversity for Food and Agriculture in the Republic of Cameroon. www.minader.gov.cm. Accessed: 19/04/19.

Mirzabaev, A., Nkonya, E.M., Goedecke, J., Johnson, T., Anderson, W., 2016. Global drivers of land degradation and improvement. In Nkonya, E., Mirzabaev, A., von Braun, J. (eds.), Economics of land degradation and improvement- A global assessment for sustainable development. Bonn: Springer Open, 167 - 195.

Mishra, S.K., Tyagi, J.V., Singh, V.P, Singh, R., 2006. SCS-CN-based modelling of sediment yield. J Hydrol. 324:301–322.

Mohamadi, M.A., Kavian, A., 2015. Effects of rainfall patterns on runoff and soil erosion in field plots. Int. Soil Water Conserv. Res. 3, 273–281. https://doi.org/10.1016/J.ISWCR.2015.10.001

Monroe, W.H., 1980. Some tropical landforms of Puerto Rico. US Geol. Surv. Prof. Pap. 1159.

Moore, I.D., Wilson, J.P., 1992. Length-slope factors for the revised universal soil loss equation: simplified method of estimation. J. Soil Water Conserv. 47 (5), 423–428.

Moore, R. J. (1984). A dynamic model of basin sediment yield. Water Resources Research, 20(1): 89-103.

Morgan, R. P.C., 2005. Soil Erosion and Conservation, Third edition. Oxford: Blackwell Science Ltd.

Morgan, R.P.C., Quinton, J.N., Smith, R.E., Govers, G., Poesen, J.W.A., Auerswald, K., Chisci, G., Torri, D., Styczen, M.E., 1998. The European soil erosion model (EUROSEM): a process-based approach for predicting soil loss from fields and small catchments. Earth Surf. Process. 23, 527–544.

Moriasi, D. N., Arnold J. G., Van Liew M. W., Bingner R. L., Harmel R. D., Veith T. L., 2007. Model Evaluation Guidelines for Systematic Quantification of Accuracy in Watershed Simulations. Trans. ASABE 50, 885–900. https://doi.org/10.13031/2013.23153

Msadala, V.C., Basson, G.R., 2017. Revised regional sediment yield prediction methodology for ungauged catchments in South Africa. J. South African Inst. Civ. Eng. 59, 28–36. https://doi.org/10.17159/2309-8775/2017/v59n2a4

Msadala, V., Gibson, L., Le Roux, J., Rooseboom, A., Basson, G., 2010. Revised sediment yield maps for South Africa. The new sediment yield map for southern Africa, WRC Project K5/765. http://wrcwebsite.azurewebsites.net/wp-content/uploads/mdocs/1765-1-101.pdf

Mucina, L., Rutherford, M. C., 2010. (CD set). The vegetation of South Africa, Lesotho and Swaziland. South African National Biodiversity Institute, Pretoria.

Mucina, L., Rutherford, M. C., 2006. The vegetation of South Africa, Lesotho and Swaziland, Strelitzia 19. South African National Biodiversity Institute, Pretoria, South Africa.

Mugambiwa, S.S., Tirivangasi, H.M., 2017. Climate change: A threat towards achieving 'Sustainable Development Goal number two' (end hunger, achieve food security and improved nutrition and promote sustainable agriculture) in South Africa. Jàmbá J. Disaster Risk Stud. 9, 1–6. https://doi.org/10.4102/jamba.v9i1.350

Murata, C., Mantel, S., De Wet, C., Palmer, A.R., 2019. Lay Knowledge of Ecosystem Services in Rural Eastern Cape Province, South Africa: Implications for Intervention Program Planning. Water Econ. Policy 5, 1–29. https://doi.org/10.1142/S2382624X19400010

Nash, J. E., Sutcliffe, J. V., 1970. River flow forecasting through conceptual models. Part I – a discussion of principles. J. Hydrol. 10, 282–290.

National Land Cover (NLC)., 2014. 2014 South African National Land-Cover. Retrieved from Biodiversity GIS: http://bgis.sanbi.org/DEA_Landcover

Ndomba, P.M., Mtalo, F., Killingtveit, A., 2009. Estimating gully erosion contribution to large catchment sediment yield rate in Tanzania. Phys. Chem. Earth. 34, 741–748. https://doi.org/10.1016/j.pce.2009.06.009

Nearing, M.A., 2013. Soil Erosion and Conservation, Environmental Modelling: Finding Simplicity in Complexity: Second Edition. https://doi.org/10.1002/9781118351475.ch22

Nearing, M.A., Jetten, V., Baffaut, C., Cerdan, O., Couturier, A., Hernandez, M., Le Bissonnais, Y., Nichols, M.H., Nunes, J.P., Renschler, C.S., Souchère, V., Van Oost, K., 2005. Modeling response of soil erosion and runoff to changes in precipitation and cover. Catena 61, 131–154. https://doi.org/10.1016/j.catena.2005.03.007

Nearing, M.A., Xie, Y., Liu, B., Ye, Y., 2017. Natural and anthropogenic rates of soil erosion. Int. Soil Water Conserv. Res. 5, 77–84. https://doi.org/10.1016/j.iswcr.2017.04.001

Neitsch, S.L., Arnold, J.G., Kiniry, J.R., Williams, JR., 2005. Soil and Water Assessment Tool Theoretical Documentation. Agricultural Research Service. Temple, Texas, USA.

Ni, S., Zhang, D., Wen, H., Cai, C., Wilson, G. V., Wang, J., 2020. Erosion processes and features for a coarse-textured soil with different horizons: a laboratory simulation. J. Soils Sediments. 20, 2997–3012. https://doi.org/10.1007/s11368-020-02665-5

Noor, H., Mirnia, S.K., Fazli, S., Raisi, M.B., Vafakhah, M., 2010. Application of MUSLE for the prediction of phosphorus losses. Water Sci. Technol. 62, 809–815. https://doi.org/10.2166/wst.2010.092

Nouwakpo, S.K., Williams, C.J., Al-Hamdan, O.Z., Weltz, M.A., Pierson, F., Nearing, M., 2016. A review of concentrated flow erosion processes on rangelands: Fundamental understanding and knowledge gaps. Int. Soil Water Conserv. Res. 4, 75–86. https://doi.org/10.1016/J.ISWCR.2016.05.003

Ochoa, P.A., Fries, A., Mejía, D., Burneo, J.I., Ruíz-Sinoga, J.D., Cerdà, A., 2016. Effects of climate, land cover and topography on soil erosion risk in a semiarid basin of the Andes. Catena. 140, 31–42. https://doi.org/10.1016/j.catena.2016.01.011

Oliveira, J.A., Dominguez, J.M.L., Nearing, M.A., Oliveira, P.T.S., 2015. A GIS-Based procedure for automatically calculating soil loss from the universal soil loss Equation: GISus-M. Appl. Eng. Agric. 31, 907–917. https://doi.org/10.13031/aea.31.11093

O'Neal, M.R., Nearing, M.A., Vining, R.C., Southworth, J., Pfeifer, R.A., 2005. Climate change impacts on soil erosion in Midwest United States with changes in crop management. Catena 61 (2-3), 165–184.

Otim, D., Smithers, J., Senzanje, A., van Antwerpen, R., 2020. Verification of runoff volume, peak discharge and sediment yield simulated using the ACRU model for bare fallow and sugarcane fields. Water SA 46, 182–196. https://doi.org/10.17159/wsa/2020.v46.i2.8233

Owens, M. K., Lyons, R. K., Alejandro, C. L., 2006. Rainfall partitioning within semiarid juniper communities: effects of event size and canopy cover. Hydrological Processes, 20,3179–3189.

Owens, P.N., Batalla, R.J., Collins, A.J. Gomez, B., Hicks, D.M., Horowitz, A.J., Kondolf, G.M., Marden, M., Page, M.J. Peacock, D.H., Petticrew, E.L., Salomonsk, W., Trustrum, N.A., 2005. Fine-grained sediment in river systems: environmental significance and management issues. River Research andApplications, 21, 693-717.

Palmer, A.R., Finca, A., Mantel, S.K., Gwate, O., Münch, Z., Gibson, L.A., 2017. Determining fPAR and leaf area index of several land cover classes in the Pot River and Tsitsa River catchments of the Eastern Cape, South Africa. African J. Range Forage Sci. 34, 33–37. https://doi.org/10.2989/10220119.2017.1306582

Pan, J., Wen, Y., 2014. Estimation of soil erosion using RUSLE in Caijiamiao watershed, China. Nat. Hazards 71, 2187–2205. https://doi.org/10.1007/s11069-013-1006-2

Panagos, P., Borrelli, P., Poesen, J., Ballabio, C., Lugato, E., Meusburger, K., Montanarella, L., Alewell, C., 2015. The new assessment of soil loss by water erosion in Europe. Environ. Sci. Policy. 54, 438–447. https://doi.org/10.1016/j.envsci.2015.08.012

Panagos, P., Karydas, C., Borrelli, P., Ballabio, C., Meusburger, K., 2014. Advances in soil erosion modelling through remote sensing data availability at European scale. Second Int. Conf. Remote Sens. Geoinf. Environ. 9229, 92290I. https://doi.org/10.1117/12.2066383

Pandey, A., Himanshu, S.K., Mishra, S.K.K., Singh, V.P., 2016. Physically based soil erosion and sediment yield models revisited. Catena. 147, 595–620. https://doi.org/10.1016/j.catena.2016.08.002

Parsons, A.J., Wainwright, J., Brazier, R.E., Powell, D.M., 2006. Is sediment delivery a fallacy? Earth Surf. Process. Landforms 31, 1325–1328. doi:10.1002/esp.1395

Phinzi, K., Ngetar, N.S., Ebhuoma, O., 2020. Soil erosion risk assessment in the Umzintlava catchment (T32E), Eastern Cape, South Africa, using RUSLE and random forest algorithm. South African Geogr. J. 00, 1–24. https://doi.org/10.1080/03736245.2020.1716838

Picouet, C., Hingray, B., Olivry, J.C., 2001. Empirical and conceptual modelling of the suspended sediment dynamics in a large tropical African river: The Upper Niger river basin. J. Hydrol. 250, 19–39. https://doi.org/10.1016/S0022-1694(01)00407-3

Pierson, F. B., & Williams, C. J., 2016. Ecohydrologic impacts of rangeland fire on runoff and erosion: a literature synthesis (p. 200) Fort Collins, CO: U.S. Department of Agriculture, Forest Service, Rocky Mountain Research Station.

Pierson, F. B., Moffet, C. A., Williams, C. J., Hardegree, S. P., Clark, P. E., 2009. Prescribed-fire effects on rill and interrill runoff and erosion in a mountainous sagebrush landscape. Earth Surface Processes and Landforms, 34,193–203.

Pierson, F. B., Williams, C. J., Hardegree, S. P., Clark, P. E., Kormos, P. R., Al-Hamdan, O.Z., 2013. Hydrologic and erosion responses of sagebrush steppe following juniper encroachment, wildfire, and tree-cutting. Rangeland Ecology and Management, 66,274–289.

Pierson, F. B., Williams, C. J., Kormos, P. R., Al-Hamdan, O. Z., 2014. Short-term effects of tree removal on infiltration, runoff, and erosion in woodland-encroached sagebrush steppe. Rangeland Ecology and Management, 67, 522–538.

Pignotti, G., Rathjens, H., Cibin, R., Chaubey, I., Crawford, M., 2017. Comparative analysis of HRU and grid-based SWAT models. Water (Switzerland). 9, 272. https://doi.org/10.3390/w9040272

Pike, A., Schulze, R.1995. AUTOSOILS: A program to convert ISCW soils attributes to variables usable in hydrological models. University of KwaZulu-Natal, School of Bioresources Engineering and Environmental Hydrology: Pietermaritzburg.

Pimentel, D., Burgess, M., 2013. Soil Erosion Threatens Food Production. Agriculture. 3, 443–463. https://doi.org/10.3390/agriculture3030443

Pimentel, D., Harvey, C., Resosudarmo, P., Sinclair, K., Kurz, D., McNair, M., Crist, S., Sphpritz, L., Fitton, L., Saffouri, R., 1995. Environmental and economic costs of soil erosion and conservation benefits. Science, 267,1117–1123.

Pitman, W.V., 1973. A Mathematical Model for Generating River Flows from Meteorological Data in South Africa. Report No. 2/73, Hydrological Research Unit. University of the Witwatersrand, Johannesburg, South Africa.

Pruski, F., Nearing, M., 2002. Climate-induced changes in erosion during the 21st century for eight US locations. Water Resour. Res. 38 (12).

Ranzi, R., Le, T. H., Rulli, M. C., 2012. A RUSLE approach to model suspended sediment load in the Lo river (Vietnam): Effects of reservoirs and land use changes. Journal of Hydrology. 422–423(February), 17–29. http://doi.org/10.1016/j.jhydrol.2011.12.009

Renard, K., Foster, G., Weesies, G., McCool, D., Yoder, D., 1997. Predicting soil erosion by water: a guide to conservation planning with the Revised Universal Soil Loss Equation (RUSLE). Agricultural Handbook No. 703. http://doi.org/DC0-16-048938-5 65–100

Richter, G., Negendank, J.F.W., 1977. Soil erosion processes and their measurement in the German area of the Moselle river. Earth Surface Processes. 2: 261–78.

Rooseboom, A., 1992. Sediment transport in rivers and reservoirs - a southern African perspective. Water Research Commission. WRC Report No. 297/1/92.

Rooseboom, A., Lotriet, N.H., 1992. The new sediment yield map for southern Africa. Eros. Sediment Transp. Monit. Program. River Basins (Proceedings Oslo Symp. https://doi.org/WRC Report No 297/2/92

Rose, C.W., 1993. Erosion and sedimentation. In: Bonell, M., Hufschmidt, M.M., Gladwell, J.S. (Eds.), Hydrology and Water Management in the Humid Tropics: Hydrological Research Issues and Strategies for Water Management. Cambridge University Press. 301–343.

Rosen, T., Xu, Y.J., 2011. Riverine sediment inflow to Louisiana Chenier Plain in the Northern Gulf of Mexico. Estuar. Coast. Shelf Sci. 95, 279–288. https://doi.org/10.1016/j.ecss.2011.09.013

Rowntree, K.M., van der Waal, B.W., Pulley, S. 2016. Magnetic susceptibility as a simple tracer for fluvial sediment source ascription during storm events. J. Environ. Manage. https://doi.org/10.1016/j.jenvman.2016.11.022

Sabine River Basin (SRB)., 2009. Basin characterization report for the Sabine River Basin. Louisiana State Reservoir Priority and Development Program.USA.

Sadeghi, S.H.R., Bashari Seghaleh, M., Rangavarm, A.S., 2014. Plot sizes dependency of runoff and sediment yield estimates from a small watershed. Catena. 102, 55–61. doi:10.1016/j.catena.2011.01.003

Sadeghi, S.H.R., Gholami, L., Khaledi Darvishan, A., Saeidi, P., 2013. A review of the application of the MUSLE model worldwide. Hydrol. Sci. J. 00, 1–11. https://doi.org/10.1080/02626667.2013.866239

Sadeghi, S.H.R., Mizuyama, T., 2007. Applicability of the modified universal soil loss equation for prediction of sediment yield in khanmirza watershed, Iran. Hydrol. Sci. Journal-Journal Des Sci. Hydrol. 52, 1068–1075. https://doi.org/10.1623/hysj.52.5.1068

Schmidt, J., Elliott, S., McKergow, L., 2008. Land-use impacts on catchment erosion for the Waitetuna catchment, New Zealand. In: Schmidt J, Cochrane T, Phillips C, Elliott S, Davies T, Basher L (Eds), Sediment dynamics in changing environments, IAHS Publication. 325: 453-457.

Schmidt, S., Alewell, C., Meusburger, K., 2018. Mapping spatio-temporal dynamics of the cover and management factor (C-factor) for grasslands in Switzerland. Remote Sens. Environ. 211, 89–104. https://doi.org/10.1016/j.rse.2018.04.008

Schmitt, R.J.P., Bizzi, S., Castelletti, A., 2016. Water Resources Research. J. Am. Water Resour. Assoc. 5, 2–2. https://doi.org/10.1111/j.1752-1688.1969.tb04897.x

Schulze, R., 1989. ACRU: background, concepts and theory. Report 35. Pietermaritzburg: Agricultural Research Unit, Department of Agricultural Engineering, University of Natal.

Schulze, R.E. 2007. South African Atlas of Climatology and Agrohydrology. Water Research Commission, Pretoria, RSA, WRC Report 1489/1/06.

Schulze, RE., 1995. Hydrology and Agrohydrology: A Text to Accompany the ACRU 3.00 Agrohydrological Modelling System. Water Research Commission, Pretoria, RSA, Report TT 69/9/95, 552.

Schulze, R.E., Horan, M.J.C., 2007. Soils: Hydrological Attributes. In: Schulze, R.E. (Ed), 2007. South African Atlas of Climatology and Agrohydrology. Water Research Commission, Pretoria, RSA, WRC Report 1489/1/06, Section 4.2.

Schulze, R.E., Lorentz, S.A.,1995. Chapter 16 of Hydrology and Agrohydrology, Department of Agricultural Engineering, University of Natal, Pietermaritzburg.

Schulze, R.E., Lorentz, S.A., Horan, M.J.C., Maharaj, M., 1995. Sediment yield. In: Schulze, R.E. (Ed), 2007. South African Atlas of Climatology and Agrohydrology. Water Research Commission, Pretoria, RSA, WRC Report 1489/1/06.

Schumm, S.A., 1977. The fluvial system. John Wiley, New York.

Scott, D.F., Versfeld, D.B., Lesch, W., 1998. Erosion and Sediment Yield in Relation To Afforestation and Fire in the Mountains of the Western Cape Province, South Africa. South African Geogr. J. 80, 52–59. https://doi.org/10.1080/03736245.1998.9713644

Scott-Shaw, B.C., Hill, T.R., Gillham, J.S., 2020. Calibration of a modelling approach for sediment yield in a wattle plantation, KwaZulu-Natal, South Africa. Water SA. 46, 171–181. https://doi.org/10.17159/wsa/2020.v46.i2.8232

Seeger, M., Errea, M.P., Beguería, S., Arnáez, J., Martí, C., García-Ruiz, J.M., 2004. Catchment soil moisture and rainfall characteristics as determinant factors for discharge/suspended sediment hysteretic loops in a small headwater catchment in the Spanish pyrenees. J. Hydrol. 288, 299–311. https://doi.org/10.1016/j.jhydrol.2003.10.012

Sepuru, T.K., Dube, T., 2018. An appraisal on the progress of remote sensing applications in soil erosion mapping and monitoring. Remote Sens. Appl. Soc. Environ. https://doi.org/10.1016/j.rsase.2017.10.005

Shinde, V., Sharma, A., Tiwari, K. N., Singh, M., 2011. Quantitative Determination of Soil Erosion and Prioritization of Micro-Watersheds Using Remote Sensing and GIS. Journal of the Indian Society of Remote Sensing. 39(2), 181–192. http://doi.org/10.1007/s12524-011-0064-8

Sidorchuk, A., Smith, A. and Nikora, V., 2004. Probability distribution function approach to stochastic modelling of soil erosion. In: Proceeding of Sediment Transfer through the Fluvial System symposium (IAHS Publ. 288, Moscow, Russia).

Slaughter, A.R., 2011. Modelling the relationship between flow and water quality in South African rivers. PhD thesis, Rhodes University. South Africa. http://vital.seals.ac.za:8080/vital/access/manager/Repository/vital:6039?site_name=GlobalView&exact=sm_creator%3A%22Slaughter%2C+Andrew+Robert%22&sort=sort_ss_title%2F

Slaughter, A.R., Hughes, D.A., Retief, D.C.H., Mantel, S.K., 2017. Environmental Modelling & Software A management-oriented water quality model for data scarce catchments. Environ. Model. Softw. 97, 93–111. https://doi.org/10.1016/j.envsoft.2017.07.015

Slaughter, A.R., Mantel, S.K., 2018. Water quality modelling of an impacted semi-arid catchment using flow data from the WEAP model. Proc. Int. Assoc. Hydrol. Sci. 377, 25–33. https://doi.org/10.5194/piahs-377-25-2018

Slaughter, A.R., Retief, D.C.H. and Hughes, D.A., 2015. A method to disaggregate monthly flows to daily using daily rainfall observations: model design and testing. Journal of Hydrology: Regional Studies. 4(B): 153–171.

Smetanová, A., Müller, A., Zargar, M., Suleiman, M.A., Gholami, F.R., Mousavi, M., 2020. Mesoscale mapping of sediment source hotspots for dam sediment management in data-sparse semi-arid catchments. Water (Switzerland). 12, 1–27. https://doi.org/10.3390/w12020396

Smith, H.J., 1999. Application of Empirical Soil Loss Models in southern Africa: a review, South African Journal of Plant and Soil, 16:3, 158-163, DOI: 10.1080/02571862.1999.10635003

Smith, S., Williams, J.R., Menzel, R.G., Coleman, G. a, 1984. Prediction of Sediment Yield from Southern Plains Grasslands with the Modified Universal Soil Loss Equation. J. Range Manag. 37, 295–297.

Soler, M., Latron, J., Gallart, F., 2008. Relationships between suspended sediment concentrations and discharge in two small research basins in a mountainous Mediterranean area (Vallcebre, Eastern Pyrenees). Geomorphology 98, 143–152. https://doi.org/10.1016/j.geomorph.2007.02.032

Sorooshian, S., 1991. Parameter Estimation, Model Identification, and Model Validation: Conceptual-Type Models. Recent Advances in the Modelling of Hydrologic Systems. Springer, Netherlands, pp. 443–467.

Sulistyo, B., 2016. The effect of choosing three different C factor formulae derived from NDVI on a fully raster-based erosion modelling. IOP Conf. Ser. Earth Environ. Sci. 47. https://doi.org/10.1088/1755-1315/47/1/012030

Sun, W., Shao, Q., Liu, J., Zhai, J., 2014. Assessing the effects of land use and topography on soil erosion on the Loess Plateau in China. Catena. 121, 151–163. https://doi.org/10.1016/j.catena.2014.05.009

Suriyaprasit, M., Shrestha, D.P., 2008. Deriving land use and canopy cover factor from remote sensing and field data in inaccessible mountainous terrain for use in soil erosion modelling Technical Session TS-34:SS-7 Global Monitoring For Environment and Security (GMES). Int. Arch. Photogramm. Remote Sens. Spat. Inf. Sci. Vol. XXXVI.

Syvitski, J.P.M., 2003. Supply and flux of sediment along hydrological pathways: Research for the 21st century. Glob. Planet. Change. 39, 1–11. https://doi.org/10.1016/S0921-8181(03)00008-0

Tan, Z., Leung, L.R., Li, H.Y., Tesfa, T., 2018. Modeling Sediment Yield in Land Surface and Earth System Models: Model Comparison, Development, and Evaluation. J. Adv. Model. Earth Syst. 10, 2192–2213. https://doi.org/10.1029/2017MS001270

Taucer, P. I., Munster, C. L., Wilcox, B. P., Owens, M. K., Mohanty, B. P., 2008. Large-scale rainfall simulation experiments of juniper rangelands. Transactions of the American Society of Agricultural and Biological Engineers, 51, 1951–1961.

Thompson, H.E., Berrang-Ford, L., Ford, J.D., 2010. Climate change and food security in Sub-Saharan Africa: A systematic literature review. Sustainability. https://doi.org/10.3390/su2082719

Tian, J., Zhu, X., Wu, J., Shen, M., Chen, J., 2020. Coarse-Resolution Satellite Images Overestimate Urbanization Effects on Vegetation Spring Phenology. Remote Sens. 12, 117. https://doi.org/10.3390/rs12010117

Tundu, C., James Tumbare, M., Kileshye Onema, J.-M., 2018. Sedimentation and Its Impacts/Effects on River System and Reservoir Water Quality: Case Study of Mazowe Catchment, Zimbabwe. Proc. IAHS 377, 57–66. https://doi.org/10.5194/piahs-377-57-2018

Turner, B.L., Fuhrer, J., Wuellner, M., Menendez, H.M., Dunn, B.H., Gates, R., 2018. Scientific case studies in land-use driven soil erosion in the central United States - Why soil potential and risk concepts should be included in the principles of soil health. Int. Soil Water Conserv. Res. 6, 63–78. https://doi.org/10.1016/j.iswcr.2017.12.004

Tya, T.S.K., Oluwaseye, A.E., 2015. Evaluation of soil erodibility on the agricultural soil of the central zone of Adamawa state, Nigeria. Swift Journal of Research in Environmental Studies. 1(3), 014-017 October, 2015. http://www.swiftjournals.org/sjres

Ustaoğlu, F., Tepe, Y., 2019. Water quality and sediment contamination assessment of Pazarsuyu Stream, Turkey using multivariate statistical methods and pollution indicators. Int. Soil Water Conserv. Res. 7, 47–56. https://doi.org/10.1016/j.iswcr.2018.09.001

Valentin, C., Poesen, J., Li, Y., 2005. Gully erosion: Impacts, factors and control. CATENA, 63 (2), 132–153. https://doi.org/10.1016/j.catena.2005.06.001

Van der Knijff, J. M., Jones, R. J. A., Montanarella, L., 1999. Soil Erosion Risk Assessment in Italy. Ispra: European Commission Directorate General JRC, Joint Research Centre Space Applications Institute European Soil Bureau.

Van Rijn, L.C., 2012. Principles of sediment transport in rivers, estuaries and coastal seas. Aqua Publications, Amsterdam, The Netherlands (www.aquapublications.nl).

van Rijn, L.C., 1984. Sediment Transport, Part II: Suspended Load Transport. J. Hydraul. Eng. 110, 1613–1641. https://doi.org/10.1061/(ASCE)0733-9429(1984)110:11(1613)

van Tol, J., Akpan, W., Kanuka, G., Ngesi, S., Lange, D., 2016. Soil erosion and dam dividends: Science facts and rural fiction around the Ntabelanga dam, Eastern Cape, South Africa. South African Geogr. J. 98, 169–181. https://doi.org/10.1080/03736245.2014.977814

Van Zyl, A.J., 2007. A knowledge gap analysis on multi-scale predictive ability for agriculturally derived sediments under South African conditions. Water Science and Technology 55(3): 107-114.

Vanmaercke, M., Poesen, J., Broeckx, J., Nyssen, J., 2014. Sediment yield in Africa. Earth-Science Rev. 136, 350–368. https://doi.org/10.1016/j.earscirev.2014.06.004

Vanmaercke, M., Poesen, J., Van Mele, B., Demuzere, M., Bruynseels, A., Golosov, V., Bezerra, J.F.R., Bolysov, S., Dvinskih, A., Frankl, A., Fuseina, Y., Guerra, A.J.T., Haregeweyn, N., Ionita, I., Makanzu Imwangana, F., Moeyersons, J., Moshe, I., Nazari Samani, A., Niacsu, L., Nyssen, J., Otsuki, Y., Radoane, M., Rysin, I., Ryzhov, Y. V., Yermolaev, O., 2016. How fast do gully headcuts retreat? Earth-Science Rev. 154, 336–355. https://doi.org/10.1016/j.earscirev.2016.01.009

Vigiak, O., Malagó, A., Bouraoui, F., Vanmaercke, M., Poesen, J., 2015. Adapting SWAT hillslope erosion model to predict sediment concentrations and yields in large Basins. Sci. Total Environ. 538, 855–875. https://doi.org/10.1016/j.scitotenv.2015.08.095

Volpe, V., Silvestri, S., Marani, M., 2011. Remote sensing retrieval of suspended sediment concentration in shallow waters. Remote Sens. Environ. 115, 44–54. https://doi.org/10.1016/j.rse.2010.07.013

Vrieling, A., de Jong, S.M., Sterk, G., Rodrigues, S.C., 2008. Timing of erosion and satellite data: A multi-resolution approach to soil erosion risk mapping. Int. J. Appl. Earth Obs. Geoinf. 10, 267–281. https://doi.org/10.1016/j.jag.2007.10.009

Walker, C., Lucke., 2019. Chapter 13 - Urban Lakes as a WSUD System, Editor(s): Ashok K. Sharma, Ted Gardner, Don Begbie, Approaches to Water Sensitive Urban Design, Woodhead Publishing, Pages 269-285 ISBN 9780128128435, https://doi.org/10.1016/B978-0-12-812843-5.00013-7

Walling, D.E., 1983. The sediment delivery problem. Journal of Hydrology 65, 209–237. doi:10.1016/0022-1694(83)90217-2

Wang, Y., Dong, Y., Su, Z., Mudd, S., Zheng, Q., Hu, G., Yan, D., 2020. Spatial distribution of water and wind erosion and their influence on the soil quality at the agropastoral ecotone of North China. Int. Soil Water Conserv. Res. https://doi.org/10.1016/j.iswcr.2020.05.001

Wang, B., Zheng, F., Guan, Y., 2016. Improved USLE-K factor prediction: A case study on water erosion areas in China. Int. Soil Water Conserv.Res. 4, 168–176. https://doi.org/10.1016/j.iswcr.2016.08.003

Wang, G.,Wente, S., Gertner, G.Z., Anderson, A., 2002. Improvement in mapping vegetation cover factor for the universal soil loss equation by geostatistical methods with Landsat Thematic Mapper images. International Journal of Remote Sensing 23 (18), 3649–3667.

Ward, P.R.B., 1980. Sediment transport and a reservoir siltation formula for Zimbabwe-Rhodesia. Die Siviele Ingenieur in Suid-Afrika.

Wei W, Chen L, Fu B, Huang Z, Wu D, Gui L., 2007. The effect of land uses and rainfall regimes on runoff and soil erosion in the semi-arid loess hilly area, China. J Hydrol. 335: 247–258.

Weier, J., Herring, D., 2000. Measuring Vegetation (NDVI & EVI). NASA Earth Observatory, Washington DC.

Wheater, H.S., Jakeman, A.J., Beven, K.J., 1993. Progress and directions in rainfall–runoff modelling. In: Jakeman, A.J., Beck, M.B., McAleer, M.J. (Eds.), Modelling Change in Environmental Systems. John Wiley and Sons. Chichester, 101–132.

Williams, C. J., Pierson, F. B., Robichaud, P. R., Al-Hamdan, O. Z., Boll, J., Strand, E. K., 2016. Structural and functional connectivity as a driver of hillslope erosion following disturbance. International Journal of Wildland Fire, 25, 306–321. http://dx. doi.org/10.1071/WF14114

Williams, C. J., Pierson, F. B., Robichaud, P. R., Boll, J., 2014. Hydrologic and erosion responses to wildfire along the rangeland-xeric forest continuum in the western US: a review and model of hydrologic vulnerability. International Journal of Wildland Fire, 23,155–172.

Williams, J. R., 1995. The EPIC model. In: Computer Models of Watershed Hydrology, 909-1000. V. P. Singh, ed. Highlands Ranch, Colo.: Water Resources Publications.

Williams, J. R., 1975. Sediment yield prediction with universal equation using runoff energy factor. In: Present and Prospective Technology for Predicting Sediment Yield and Sources. 40: 244-254. Washington DC: USDA-ARS.

Williams, J. R., Berndt, H. D., 1977. Sediment yield based on watershed hydrology. Transactions of the Society of Agricultural Engineers. 20: 1100-1104.

Wischmeier, W. H., 1962. Storms and soil conservation. J. Soil and water conserve. 17: 55-59.

Wischmeier, W.H., Smith, D.D., 1962. A universal soil-loss equation to guide conservation farm planning. Trans. Int. Congr. Soil Sci. 7: 418–425.

Wischmeier, W. H., Smith, D. D., 1978. Predicting rainfall erosion losses. Agriculture Handbook No. 537, (537), 285–291. http://doi.org/10.1029/TR039i002p00285

Wong, D.W., 2009. Modifiable Areal Unit Problem. Editor(s): Rob Kitchin, Nigel Thrift, International Encyclopaedia of Human Geography, Elsevier, Pages 169-174, ISBN 9780080449104, https://doi.org/10.1016/B978-008044910-4.00475-2.

Xu, E., Zhang, H., 2020. Change pathway and intersection of rainfall, soil, and land use influencing water-related soil erosion. Ecol. Indic. 113, 106281. https://doi.org/10.1016/j.ecolind.2020.106281

Xu, Y.J., Rosen, T., 2012. Are riverine sediment discharges sufficient to offset the sinking coast of Louisiana? IAHS-AISH Publ. 356, 104–113.

Yamazaki, D., Ikeshima, D., Tawatari, R., Yamaguchi, T., O'Loughlin, F., Neal, J.C., Sampson, C.C., Kanae, S., Bates, P.D., 2017. A high-accuracy map of global terrain elevations. Geophys. Res. Lett. 44, 5844–5853. https://doi.org/10.1002/2017GL072874

Yang, X., Lu, X.X., 2014. Estimate of cumulative sediment trapping by multiple reservoirs in large river basins: An example of the Yangtze River basin. Geomorphology. 227, 49–59. https://doi.org/10.1016/j.geomorph.2014.01.014

Yesuf, H.M., Assen, M., Alamirew, T., Melesse, A.M., 2015. Modeling of sediment yield in Maybar gauged watershed using SWAT, northeast Ethiopia. Catena. 127, 191–205. https://doi.org/10.1016/j.catena.2014.12.032

Yuan, Y., Hu, W., Li, G., 2016. Evaluation of Soil Erosion and Sediment Yield from Ridge Watersheds Leading to Guánica Bay, Puerto Rico, Using the Soil and Water Assessment Tool Model. Soil Sci. 181, 315–325. https://doi.org/10.1097/SS.0000000000000166

Yuan, Y., Jiang, Y., Taguas, E. V., Mbonimpa, E.G., Hu, W., 2015. Sediment loss and its cause in Puerto Rico watersheds. Soil. 1, 595–602. https://doi.org/10.5194/soil-1-595-2015

Yue, L., Juying, J., Bingzhe, T., Binting, C., Hang, L., 2020. Response of runoff and soil erosion to erosive rainstorm events and vegetation restoration on abandoned slope farmland in the Loess Plateau region, China. J. Hydrol. 584, 124694. https://doi.org/10.1016/j.jhydrol.2020.124694

Zhang, X.C., 2007. A comparison of explicit and implicit spatial downscaling of GCM out- put for soil erosion and crop production assessments. Clim. Chang. 84 (3), 337–363.

Zhang, H., Yang, Q., Li, R., Liu, Q., Moore, D., He, P., Ritsema, C.J., Geissen, V., 2013. Extension of a GIS procedure for calculating the RUSLE equation LS factor. Comput. Geosci. 52. https://doi.org/10.1016/j.cageo.2012.09.027

Zhang, X.C., Nearing, M.A., 2005. Impact of climate change on soil erosion, runoff, and wheat productivity in central Oklahoma. Catena 61 (2-3), 185–195.

Zhao, N., Yu, F., Li, C., Wang, H., Liu, J., Mu, W., 2014. Investigation of rainfall-runoff processes and soil moisture dynamics in grassland plots under simulated rainfall conditions. Water (Switzerland). 6, 2671–2689. https://doi.org/10.3390/w6092671

Zhu, Y., Weindorf, D.C., Zhang, W., 2011. Characterizing soils using a portable X-ray fluorescence spectrometer: 1. Soil texture. Geoderma. 167–168, 167–177. https://doi.org/10.1016/j.geoderma.2011.08.010

ZINWA. 2019. Gwayi Catchment. Zimbabwe National Water Authority. http://www.zinwa.co.zw/catchments/gwayi-catchment/ accessed: 19/04/19

Appendix A

App A.1 South African catchments

*****_Images of all dams were all accessed from Department of Water and Sanitation website; http://www.dwa.gov.za/Hydrology/Weekly/Province.aspx. Other images were taken during field visits by the author._

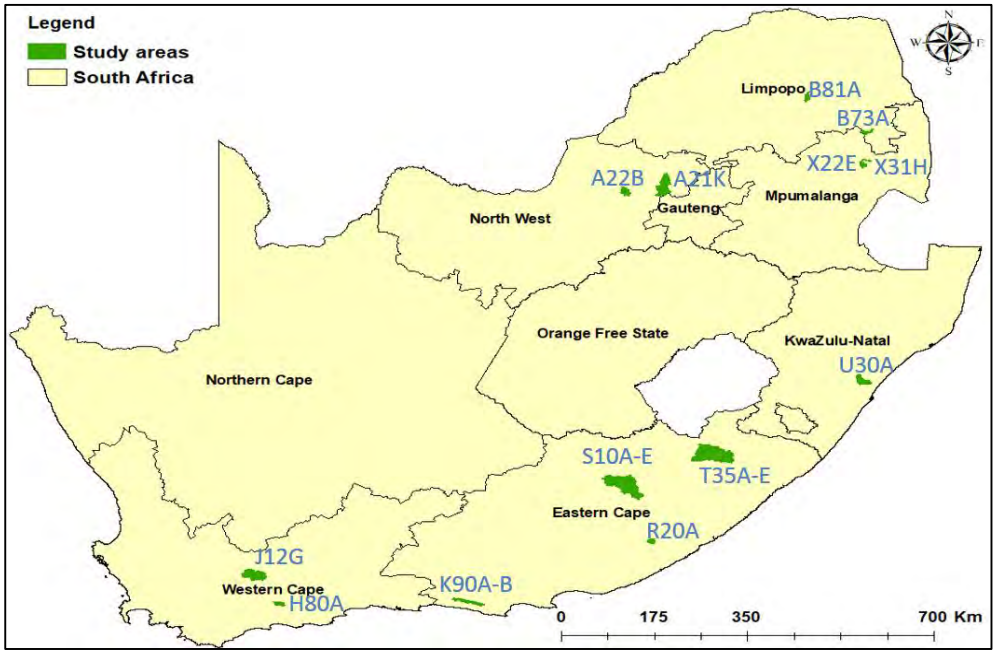

Figure A3.3: Map showing the location of the study areas in South Africa.

1. Tsitsa River catchment (T35A-E)

Figure A3.4: Steep gullied slopes in quaternary T35E.

Figure A3.5: Gulley erosion and sediment transport in quaternary T35E.

2. Duiwenhoks Dam catchment (H80A)

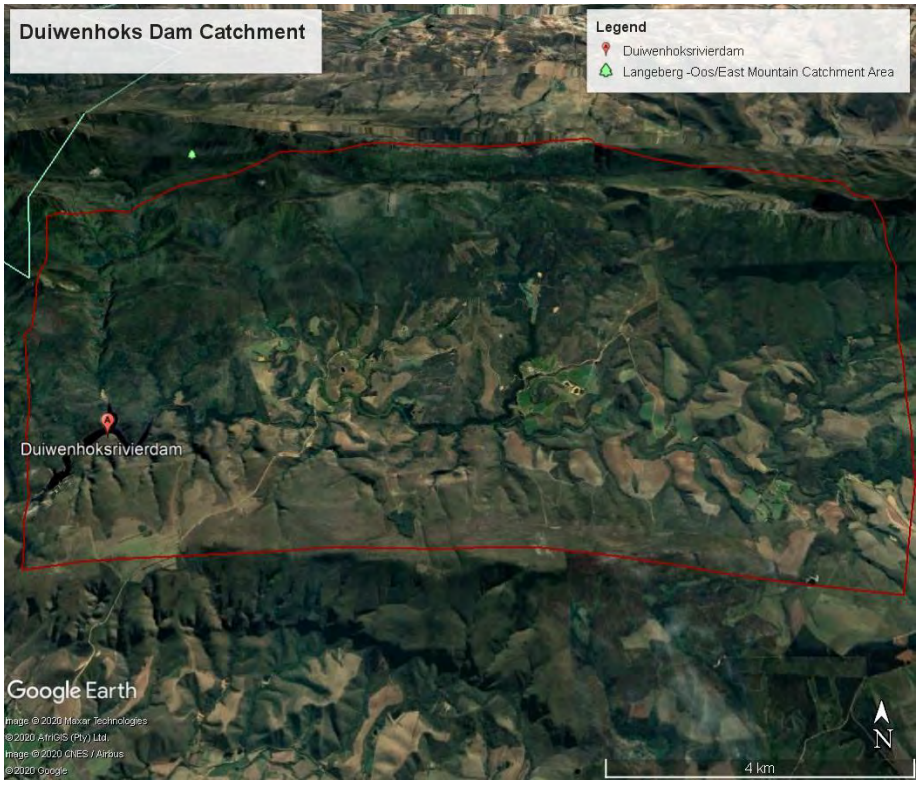

Figure A3.6: Imagery showing the topography and vegetation of the study area.

Figure A3.7: The Duiwenhoks Dam and topography and vegetation of part of the catchment.

3. Prinsrivier Dam catchment (J12G)

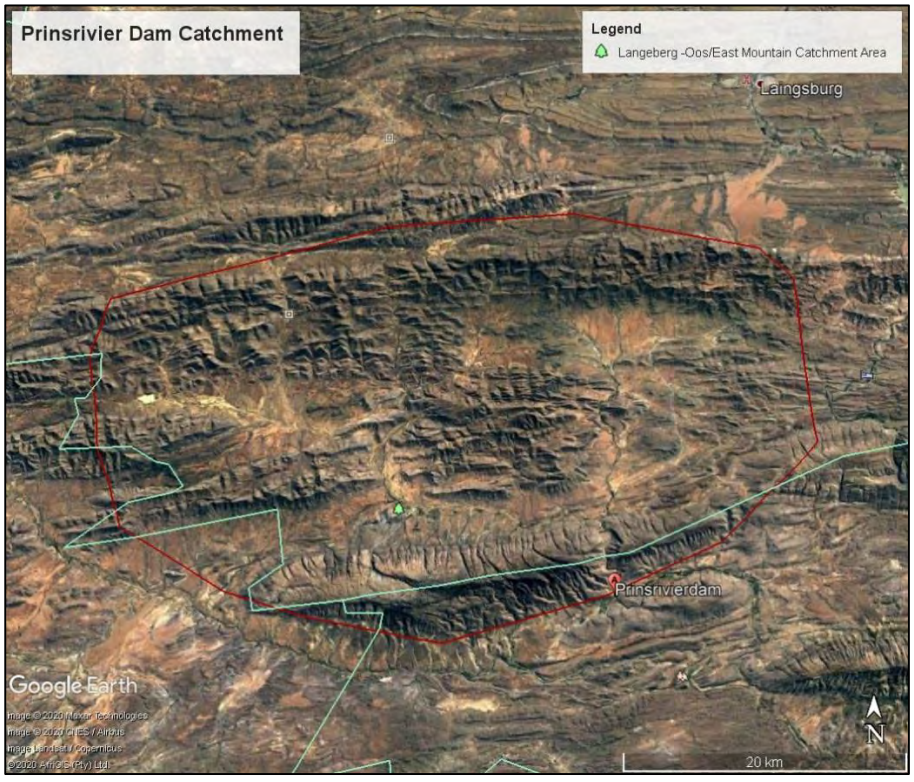

Figure A3.8: Imagery showing the topography of the study area.

Figure A3.9: The Prinsriver Dam, illustrating the topography and vegetation of the lower part of the catchment.

4. Churchill Dam catchment (K90A-B)

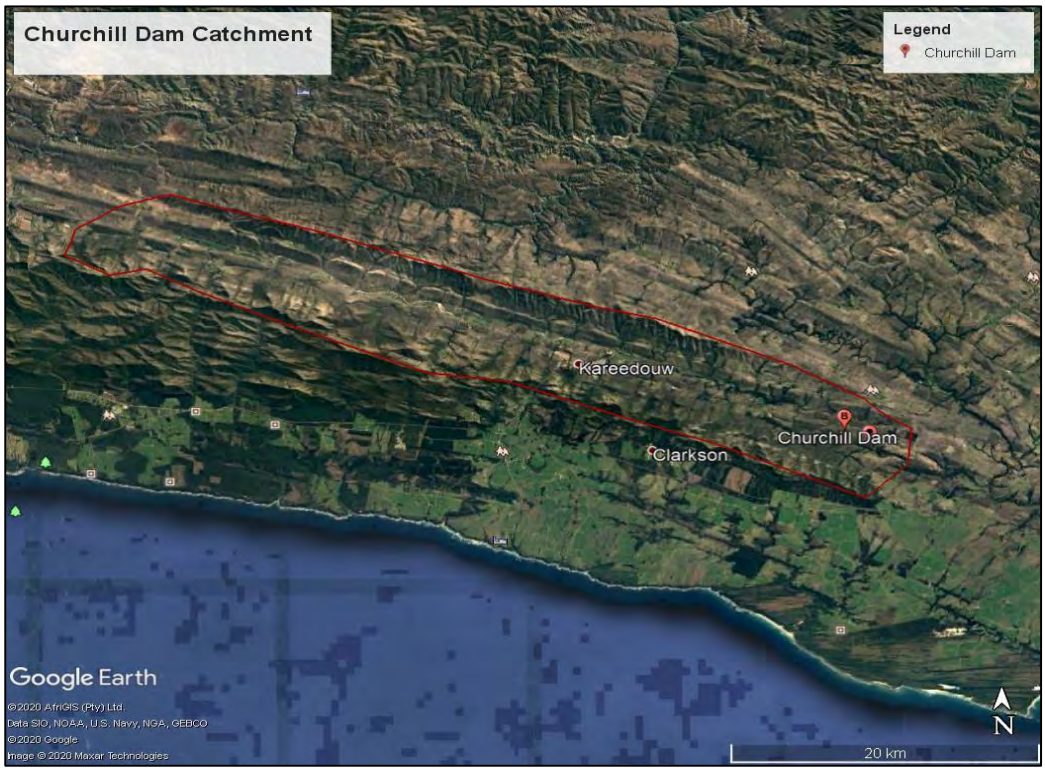

Figure A3.10: Imagery showing the location and topography of the study area.

Figure A3.9: Imagery showing the Churchill Dam and surrounding area.

5. Maden Dam catchment (R20A)

Figure A3.11: Imagery showing the topography and vegetation of the study site.

6. Klaserie Dam catchment (B73A)

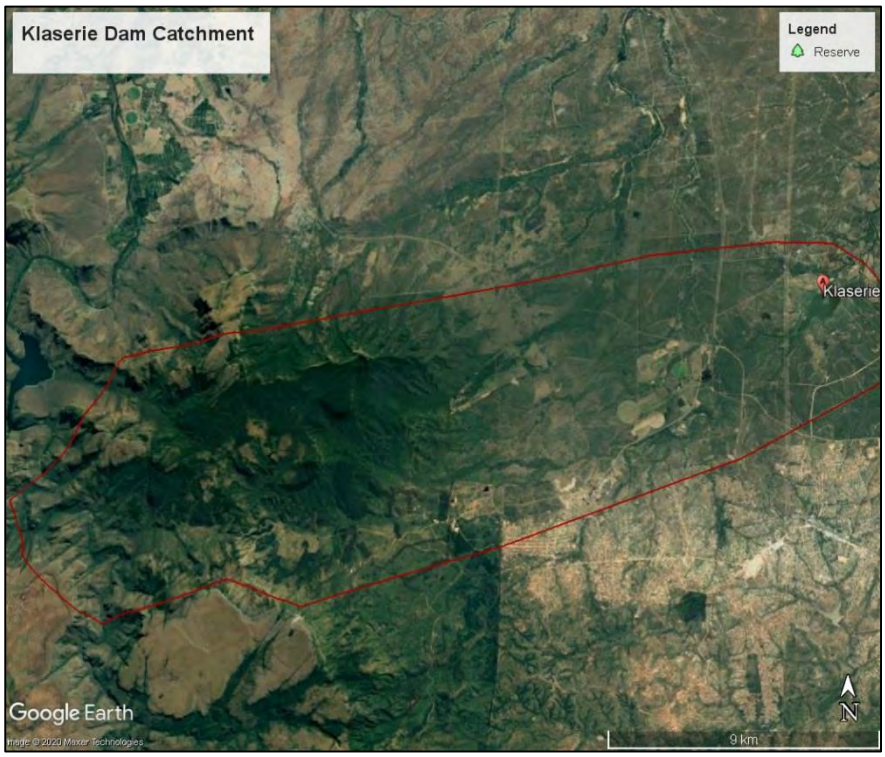

Figure A3.12: Imagery showing the topography and vegetation of the study site.

Figure A3.12: Image showing the Klaserie Dam.

7. Xonxa Dam Catchment (S10A-E)

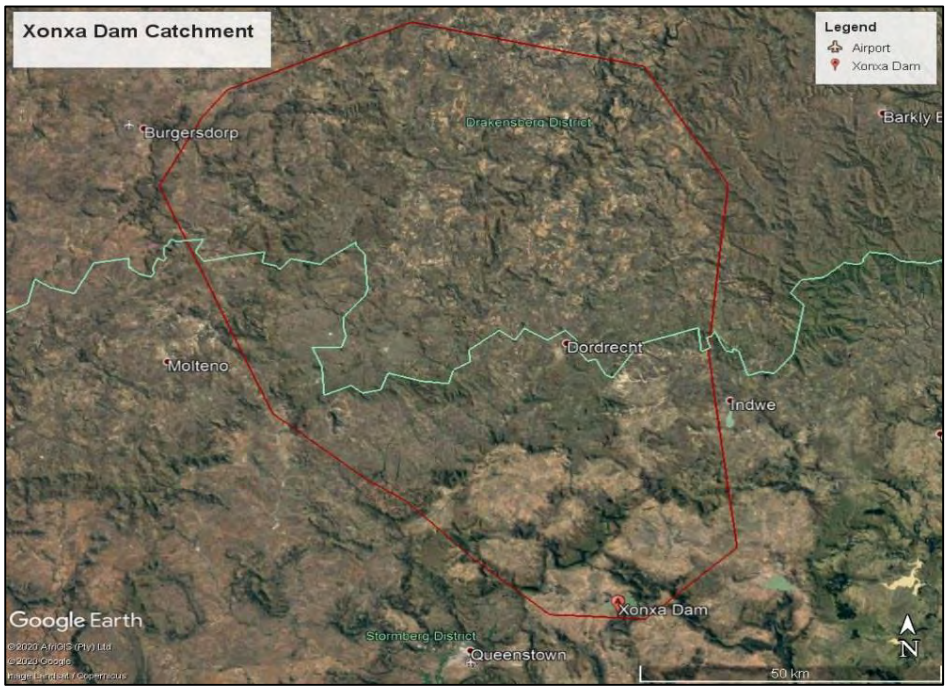

Figure A3.13: Imagery showing the topography the study site

Figure A3.14: Imager showing the Xonxa Dam and surrounding vegetation and topography.

8. Koster Dam catchment (A22B)

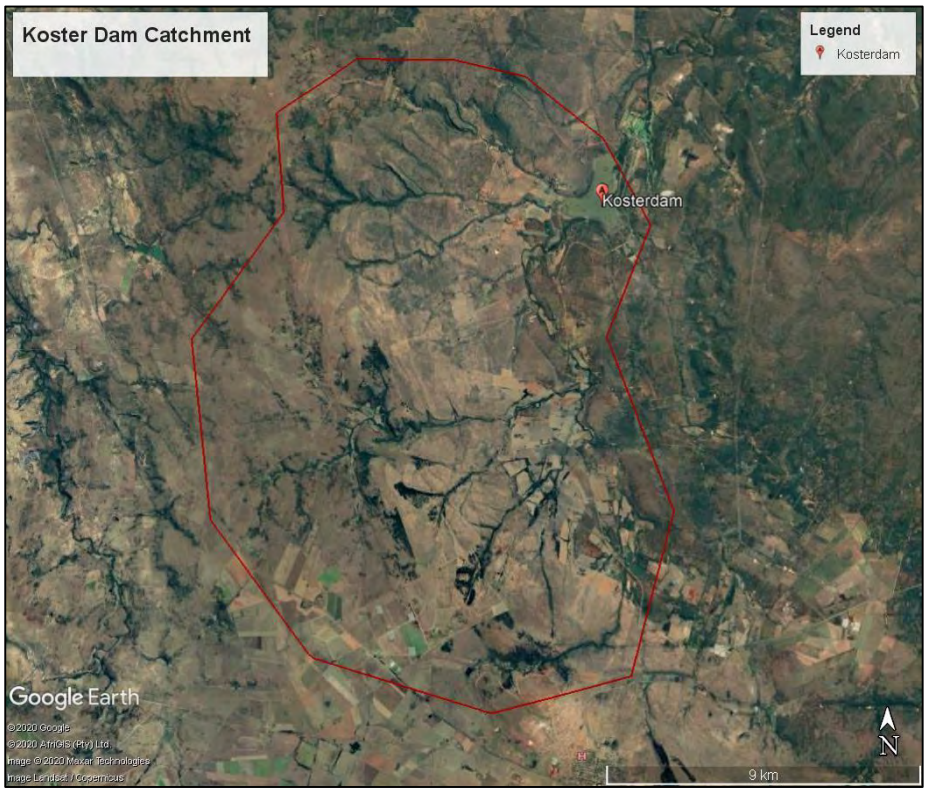

Figure A3.15: Imagery showing the Koster Dam catchment.

Figure A3.16: Image showing the Koster Dam.

9.Buffelspoort Dam catchment (A21K)

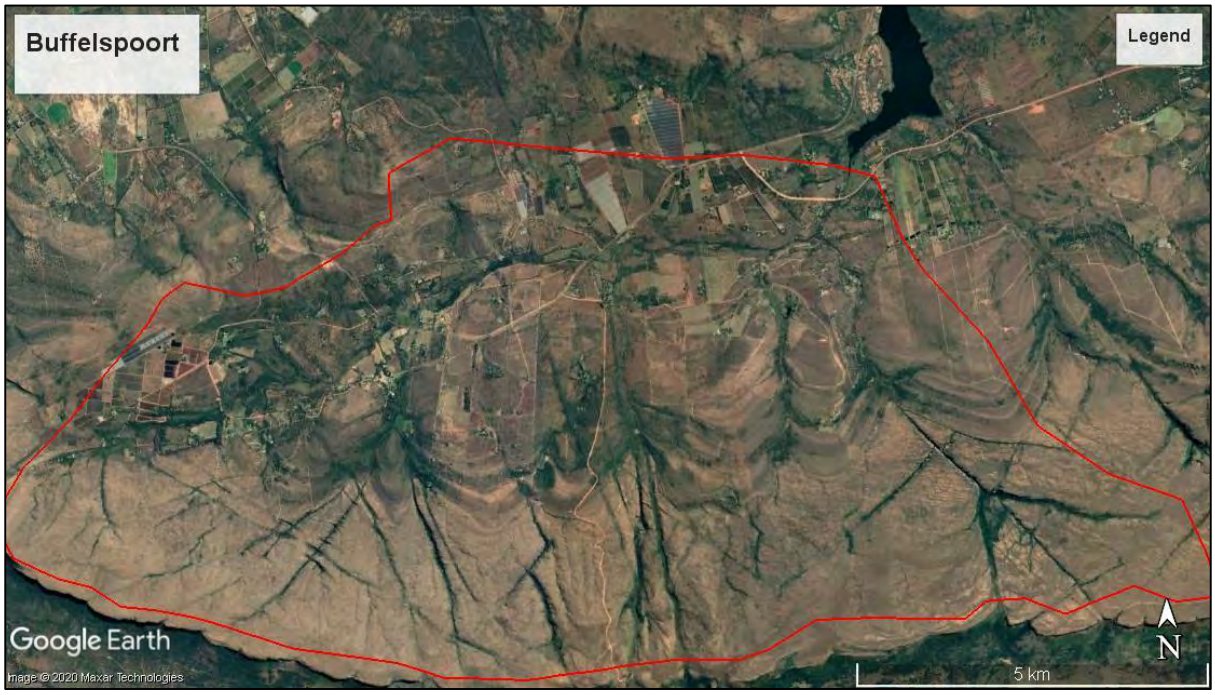

Figure A3.17: Imagery showing the Buffelspoort Dam catchment.

Figure A3.18: Image showing the Buffelspoort Dam.

10. Da Gama Dam catchment (X31H)

Figure A3.17: Imagery showing the Da Gama Dam catchment.

11. Ebenezer Dam catchment (B81A)

Figure A3.18: Imagery showing the Ebenezer Dam catchment.

Figure A3.19: Image showing the Ebenezer Dam and surrounding catchment.

12. Hazelmere Dam catchment (U30A)

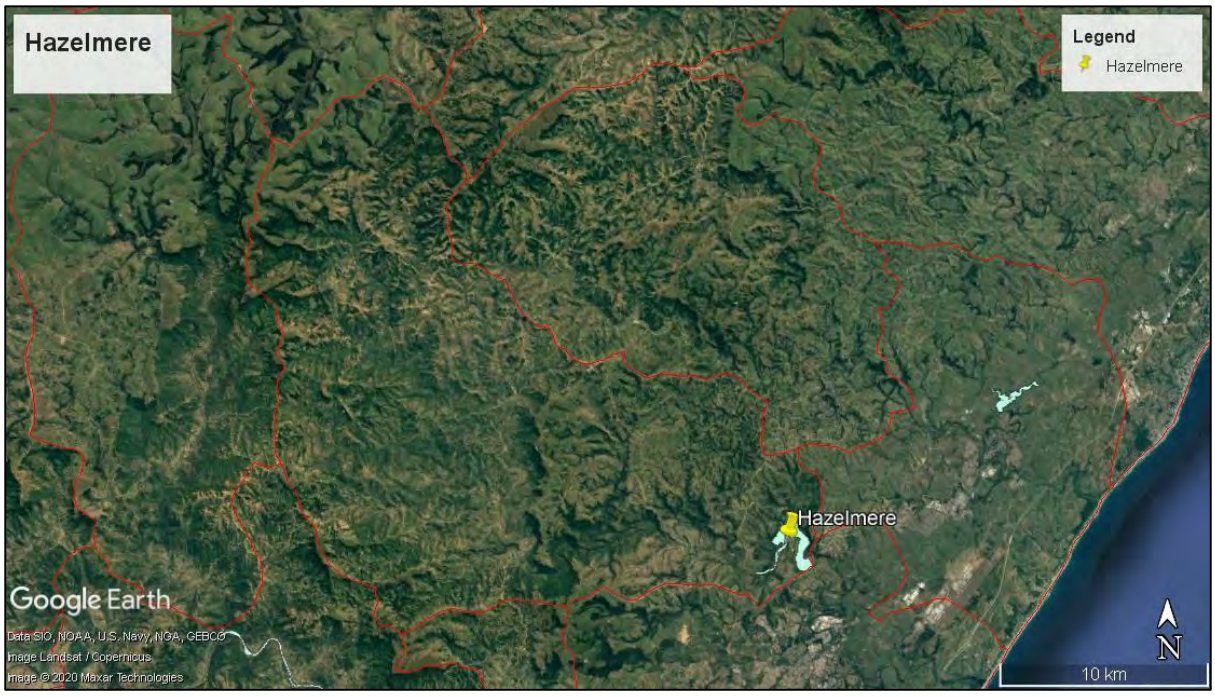

Figure A3.20: Imagery showing the Hazelmere Dam catchment.

Figure A3.21: Image showing the Hazelmere Dam and surrounding densely populated catchment.

13. Witklip Dam catchment (X22E)

Figure A3.22: Imagery showing the Witklip Dam catchment.

Figure A3.23: Image showing the Witklip Dam and surrounding forested catchment.

App A.2 USA catchments

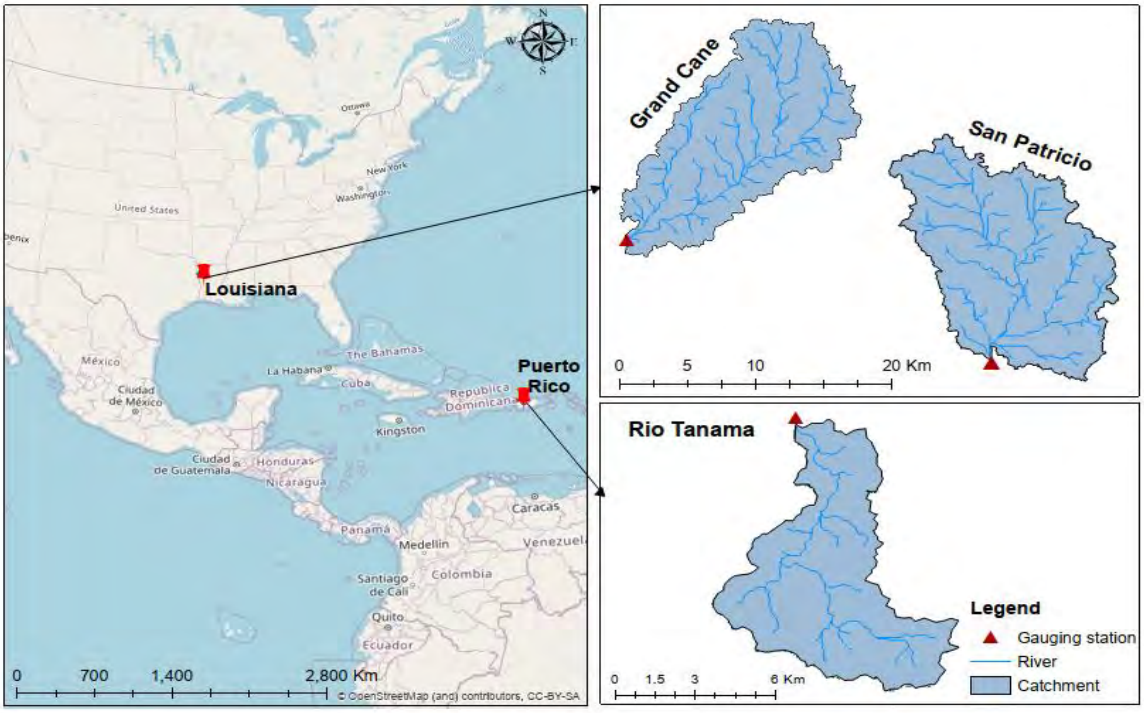

Figure A3.24: Image showing the location of selected catchments in the USA and Puerto Rico.

Figure A3.25: Topography, vegetation and land use in the Rio Tanama catchment.

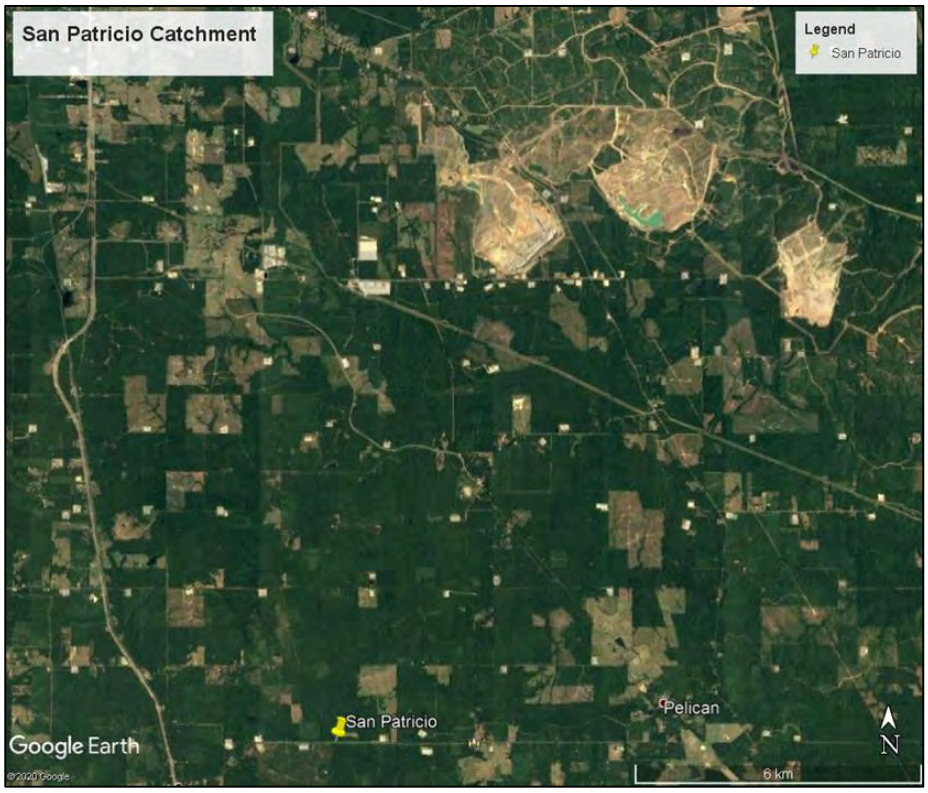

Figure A3.26: Topography, vegetation and land use in the San Patricio catchment.

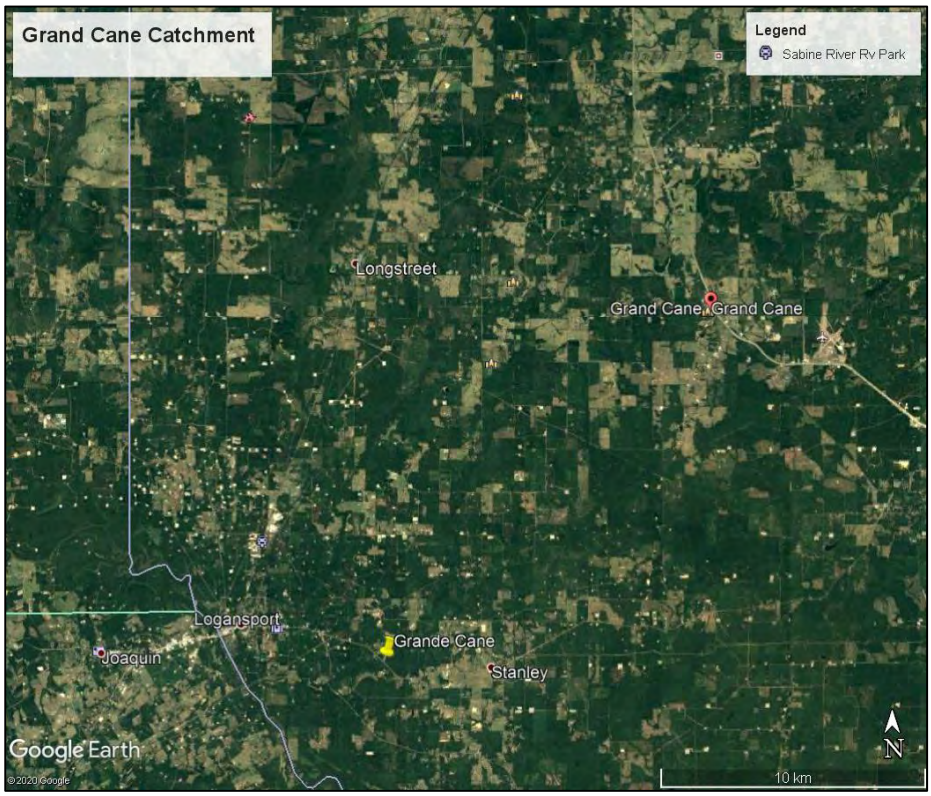

Figure A3.27: Topography, vegetation and land use in the Grande Cane catchment.

App A.3 Zimbabwean Catchments

1. Odzi River catchment

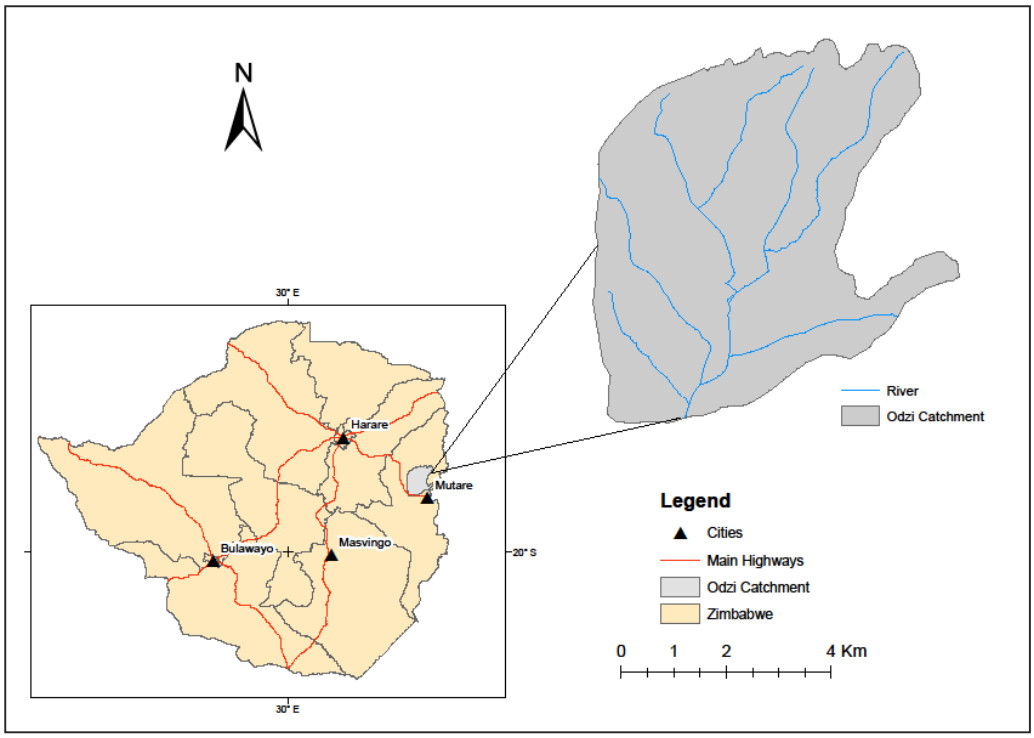

Figure A3.28: Map showing the location of the Odzi study area.

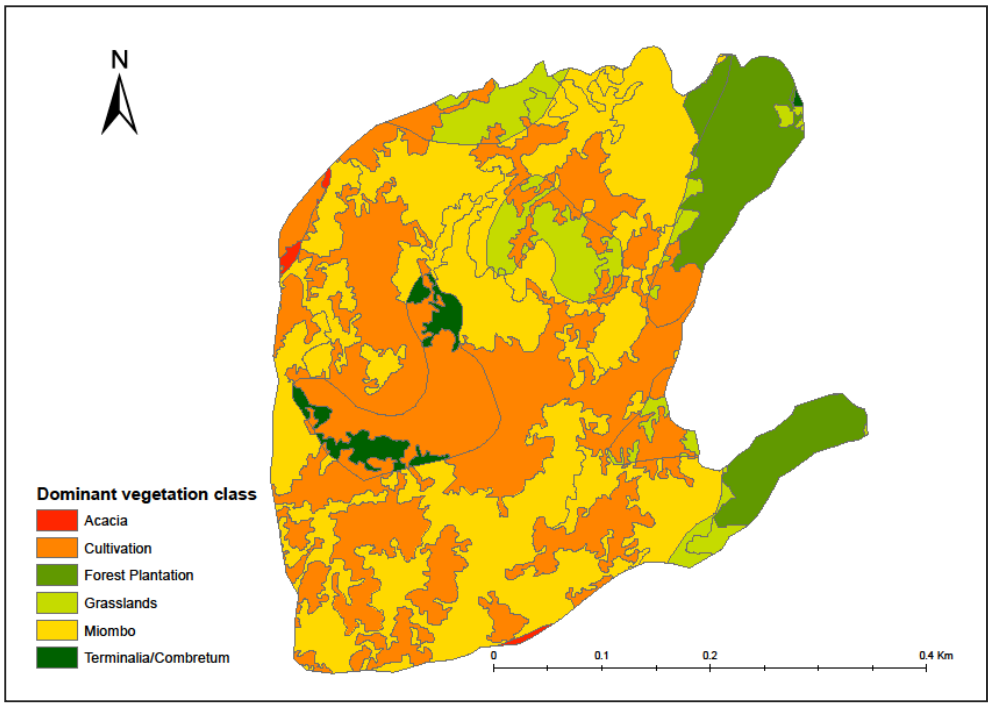

Figure A3.29: Map showing vegetation coverage of the Odzi catchment area.

Figure A3.30: Topography, vegetation and land use in the Odzi catchment.

2. Gwai River catchment

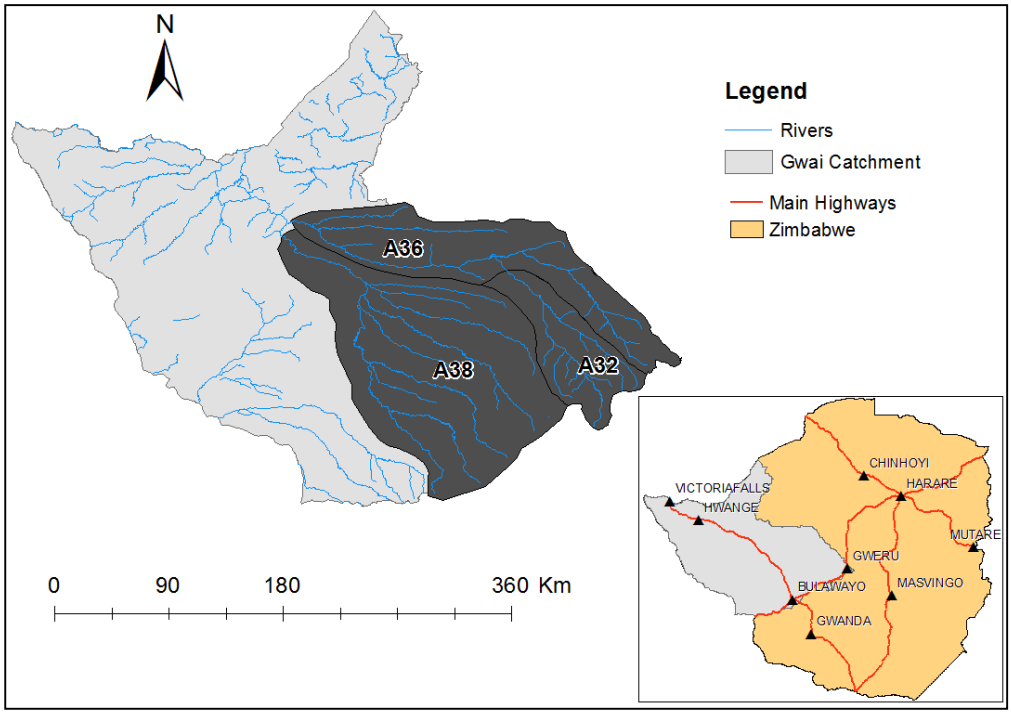

Figure A3.31: Map showing the location of the Gwai catchment in Zimbabwe.

Figure A3.32: Imagery part of the Gwai River catchment.

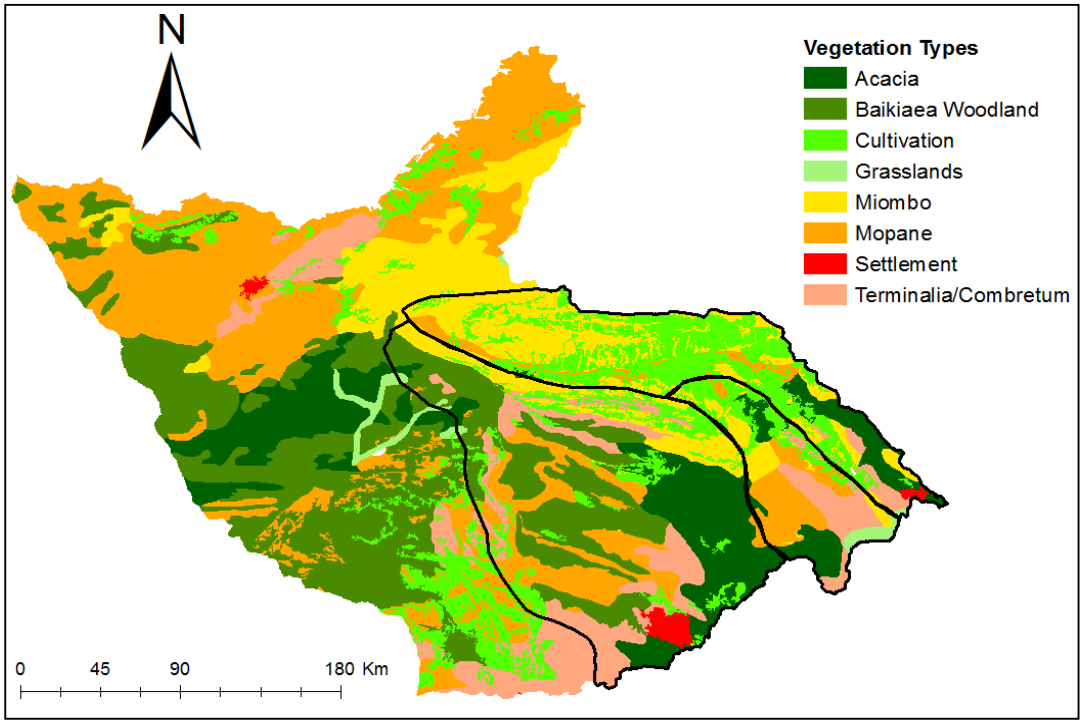

Figure A3.34: Map showing vegetation coverage of the Gwai River catchment.

Appendix B

App B.1 NDVI to *C* factor assessments.

A) Validating NDVI *C* with control points collected in the field.

Land cover	NDVI	NDVI_C	Fixed_C
grasslands	0.48	0.16	0.12
bare/degraded	0.23	0.56	1
grasslands	0.54	0.09	0.12
bare/degraded	0.44	0.21	1
grasslands	0.54	0.10	0.12
grasslands	0.46	0.19	0.12
bare/degraded	0.37	0.32	1
low shrub	0.49	0.14	0.013
bare/degraded	0.22	0.57	1
wetlands	0.57	0.07	0.038
grasslands	0.52	0.12	0.12
open bush	0.59	0.06	0.012
bare/degraded	0.21	0.58	1
plantation	0.65	0.03	0.012
bare/degraded	0.30	0.43	1
bare/degraded	0.18	0.64	1
bare/degraded	0.23	0.55	1
grasslands	0.49	0.14	0.12
low shrub	0.59	0.06	0.013
grasslands	0.55	0.08	0.12
settlements	0.52	0.12	0.1
settlements	0.54	0.10	0.1
settlements	0.62	0.04	0.1
wetlands	0.66	0.02	0.038
wetlands	0.67	0.02	0.038
grasslands	0.48	0.16	0.12
forest/thicket	0.74	0.00	0.009
grasslands	0.58	0.06	0.12
wetlands	0.61	0.05	0.038
grasslands	0.45	0.19	0.12
grasslands	0.54	0.10	0.12
grasslands	0.40	0.26	0.12
bare/degraded	0.34	0.35	1
low shrub	0.56	0.08	0.012
grasslands	0.52	0.12	0.12
low shrub	0.47	0.17	0.012
grasslands	0.63	0.04	0.012
low shrub	0.49	0.15	0.013
bare/degraded	0.37	0.31	1
grasslands	0.54	0.09	0.12
open bush	0.51	0.13	0.012
forest/thicket	0.71	0.01	0.009
cultivated land	0.40	0.26	0.37
settlements	0.38	0.29	0.1
Average	**0.49**	**0.19**	**0.29**

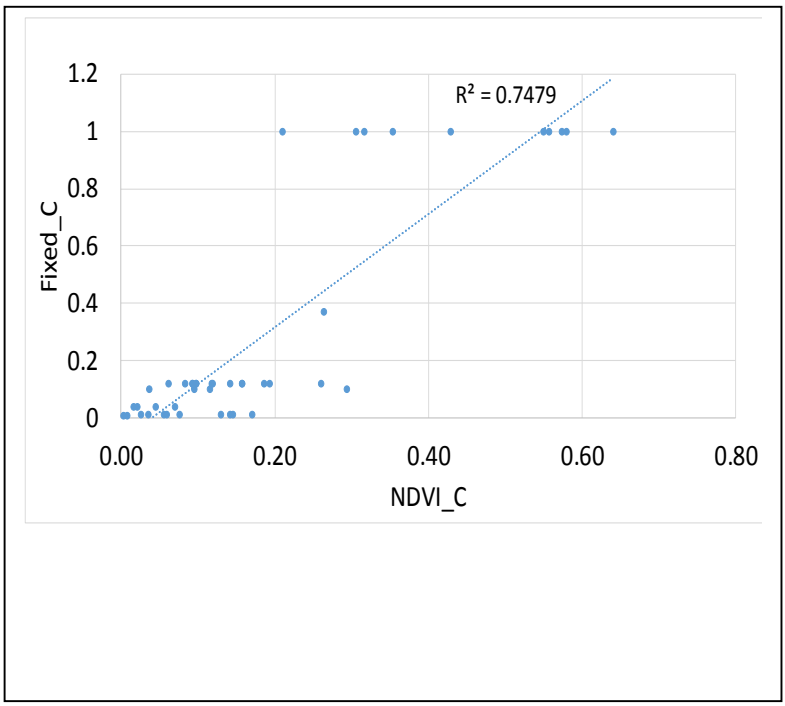

B) Assessing the performance of some of the NDVI to *C* conversion methods for use within the study area.

Vegetation class	NDVI	Map (fixed) *C*	Van der Knijff	Colman	Durigon	Sulistiyo[1]	Sulistiyo[2]	Suriyaprasit	De Jong
Low shrub	0.59	0.013	0.06	-0.009	-0.086	0.149	0.214	0.003	-0.041
Grasslands	0.55	0.12	0.08	-0.005	-0.054	0.173	0.256	0.004	-0.015
Settlements	0.52	0.1	0.12	-0.002	-0.019	0.200	0.312	0.005	0.013
Wetlands	0.66	0.038	0.02	-0.016	-0.158	0.093	0.143	0.002	-0.099
Forest/thicket	0.74	0.009	0.003	-0.024	-0.240	0.030	0.090	0.001	-0.165
Average	**0.61**	**0.056**	**0.06**	**-0.011**	**-0.111**	**0.129**	**0.203**	**0.003**	**-0.061**

App B.2 Average MUSLE factors (including fixed *C*) calculated for the catchments

T35C

Factor	Value
LS	6.6
C	0.098
K	0.35
P	0.94

Tsitsa catchment

Factor	Value
LS	6.22
C	0.12
K	0.33
P	0.96

Inxu catchment

Factor	Value
LS	6.95
C	0.13
K	0.35
P	0.8

Appendix C

App C.1. Discharge and sediment load time series graphs for all the selected catchments.

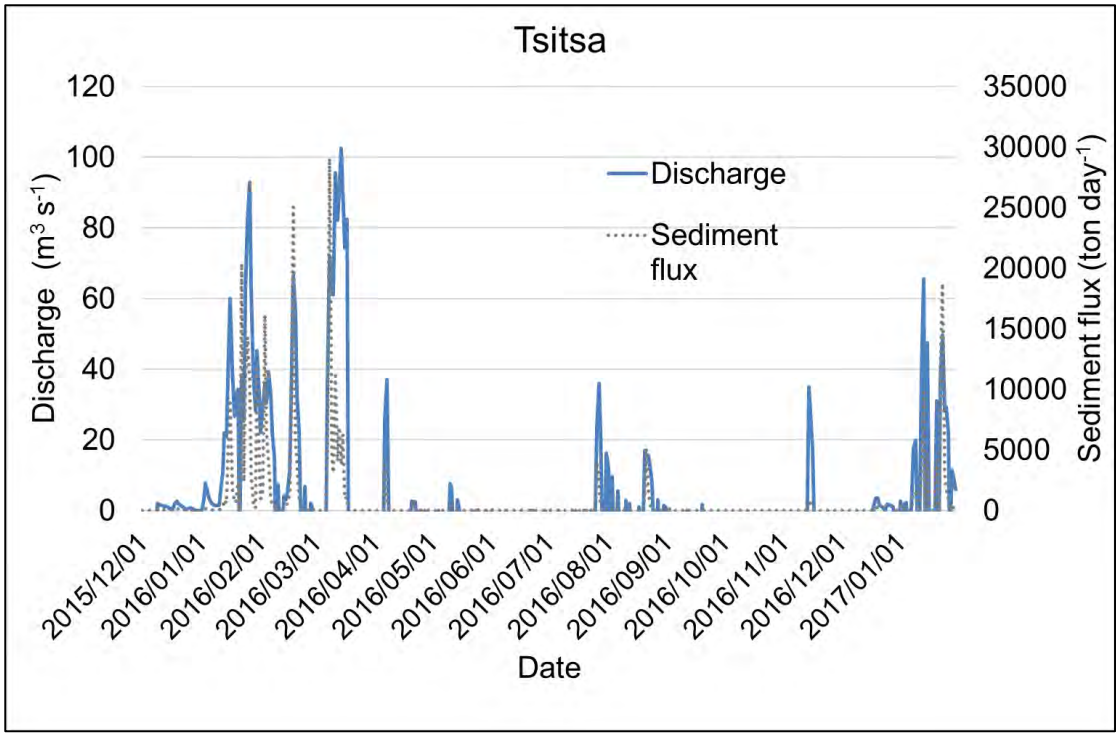

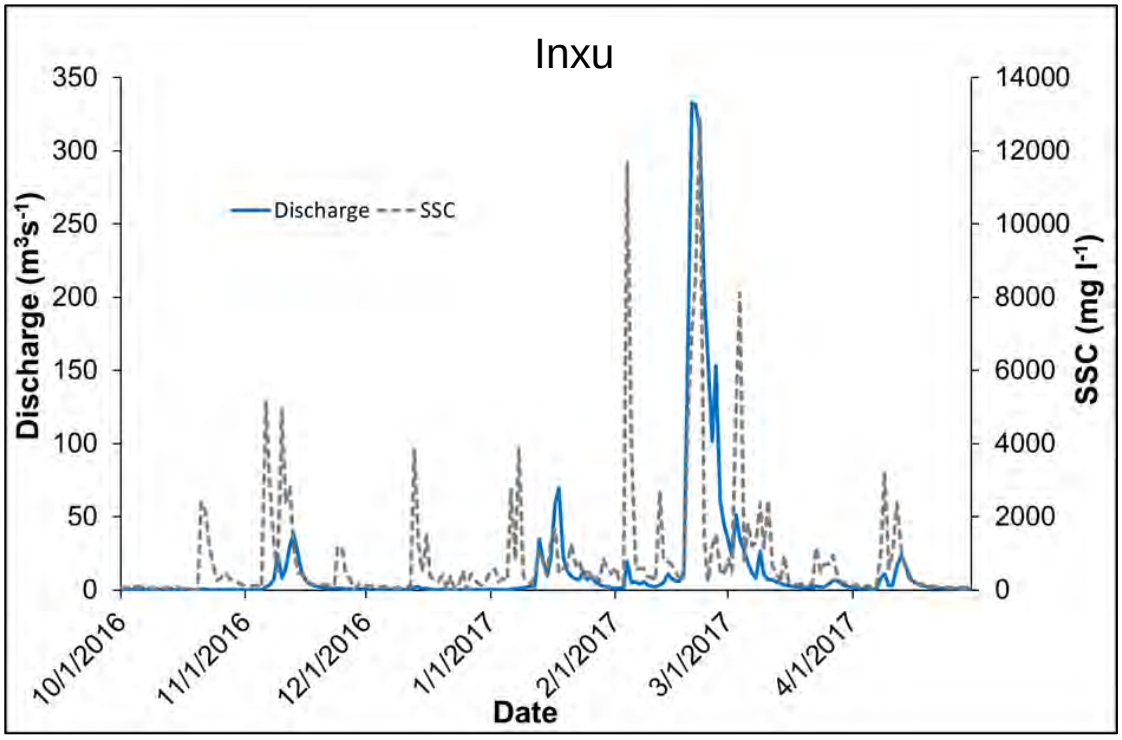

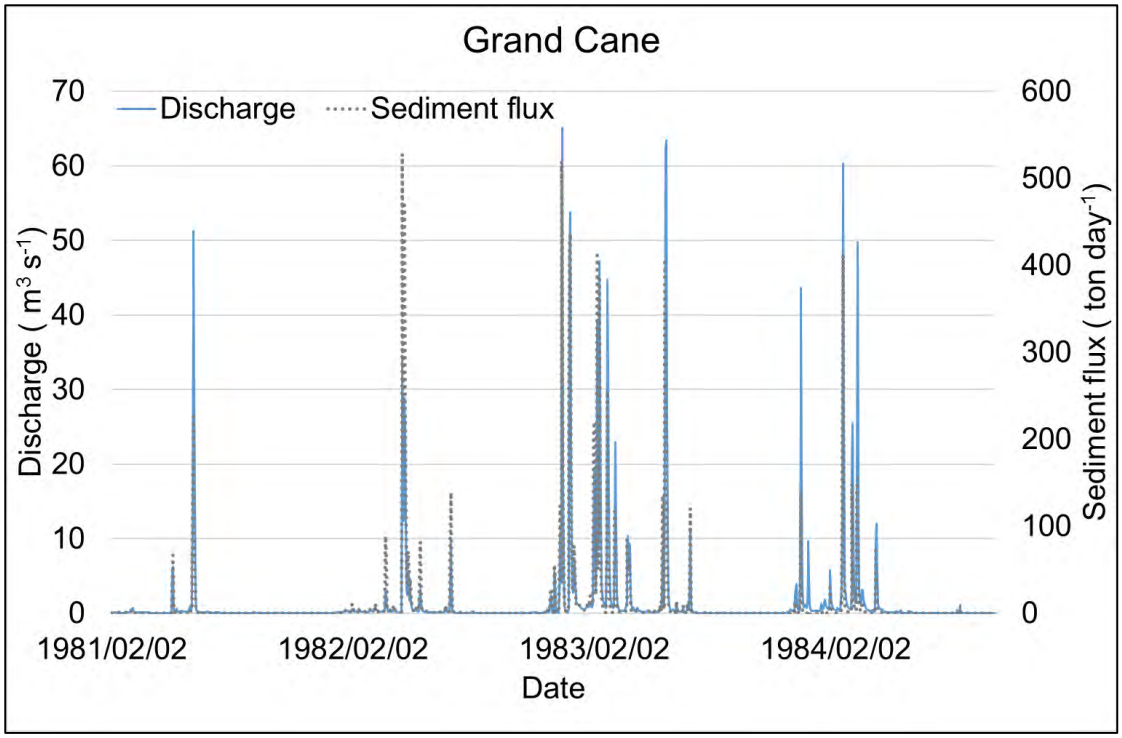
Grand Cane
Discharge
Sediment flux
Discharge (m3 s-1)
Sediment flux (ton day-1)
70
60
50
40
30
20
10
0
600
500
400
300
200
100
0
1981/02/02
1982/02/02
1983/02/02
1984/02/02
Date

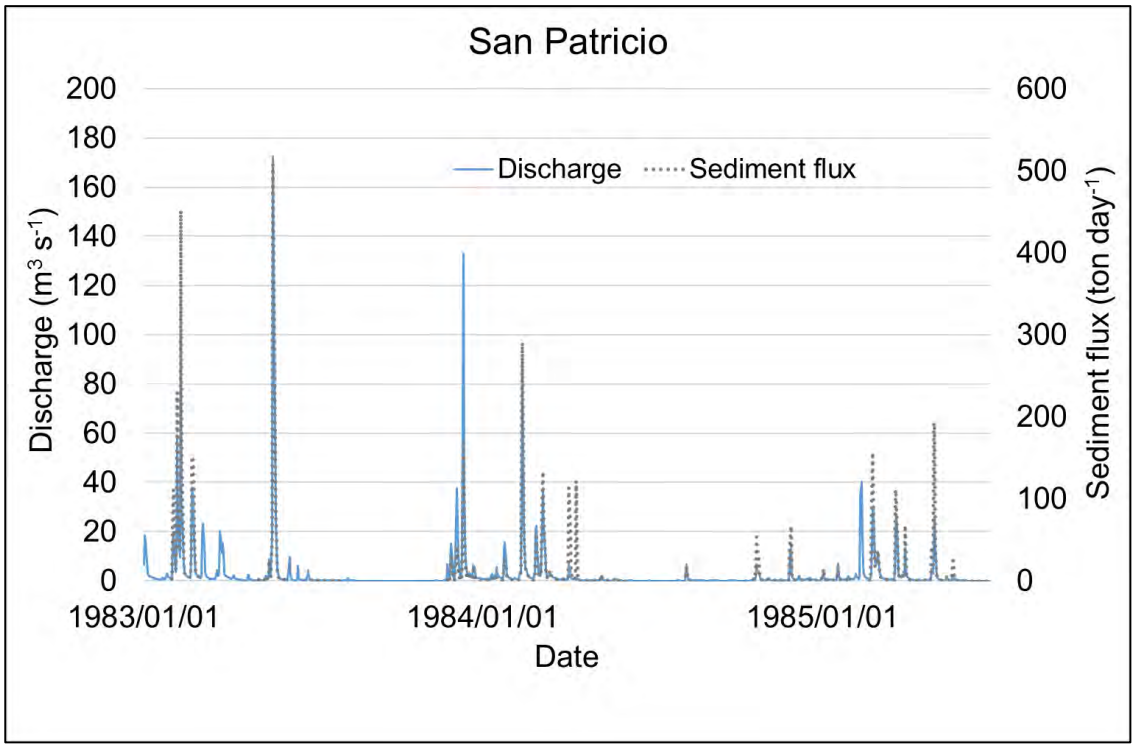
San Patricio
Discharge
Sediment flux
Discharge (m3 s-1)
Sediment flux (ton day-1)
200
180
160
140
120
100
80
60
40
20
0
600
500
400
300
200
100
0
1983/01/01
1984/01/01
1985/01/01
Date

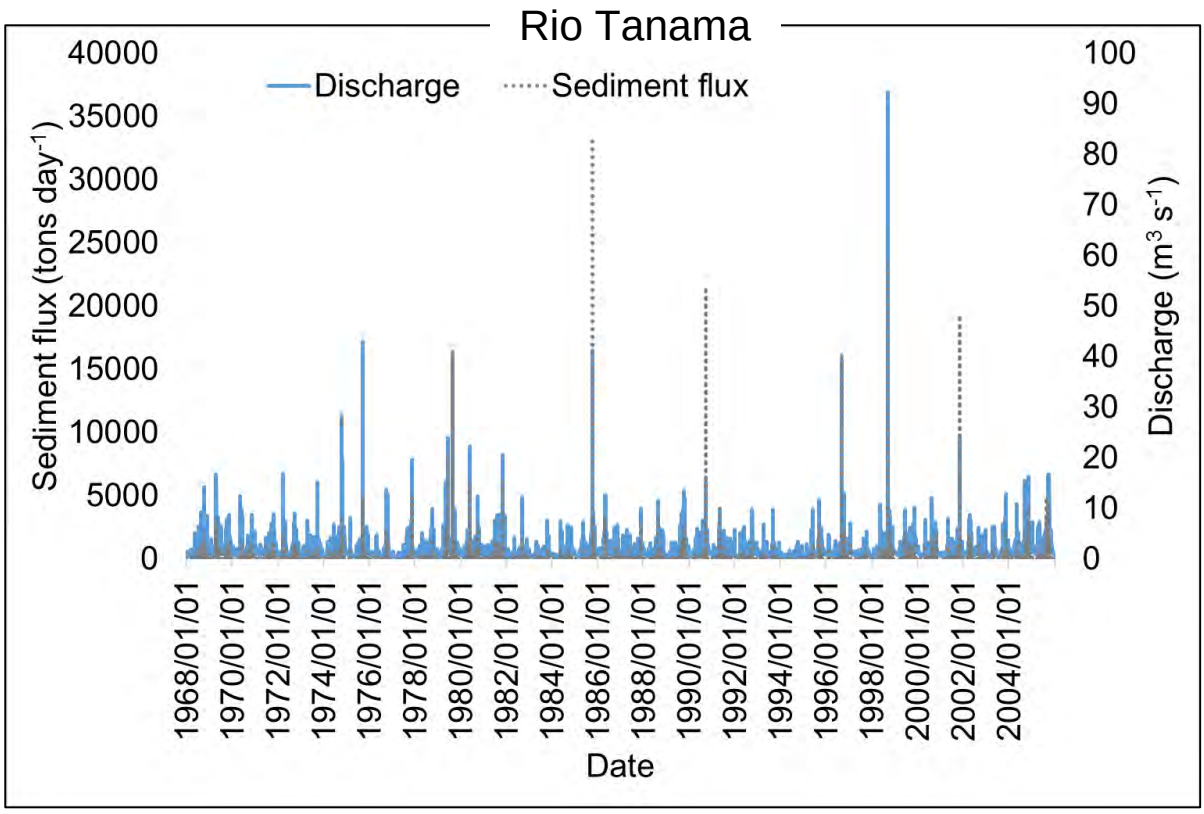
Rio Tanama
Discharge
Sediment flux
Sediment flux (tons day-1)
Discharge (m3 s-1)
40000
35000
30000
25000
20000
15000
10000
5000
0
100
90
80
70
60
50
40
30
20
10
0
1968/01/01
1970/01/01
1972/01/01
1974/01/01
1976/01/01
1978/01/01
1980/01/01
1982/01/01
1984/01/01
1986/01/01
1988/01/01
1990/01/01
1992/01/01
1994/01/01
1996/01/01
1998/01/01
2000/01/01
2002/01/01
2004/01/01
Date

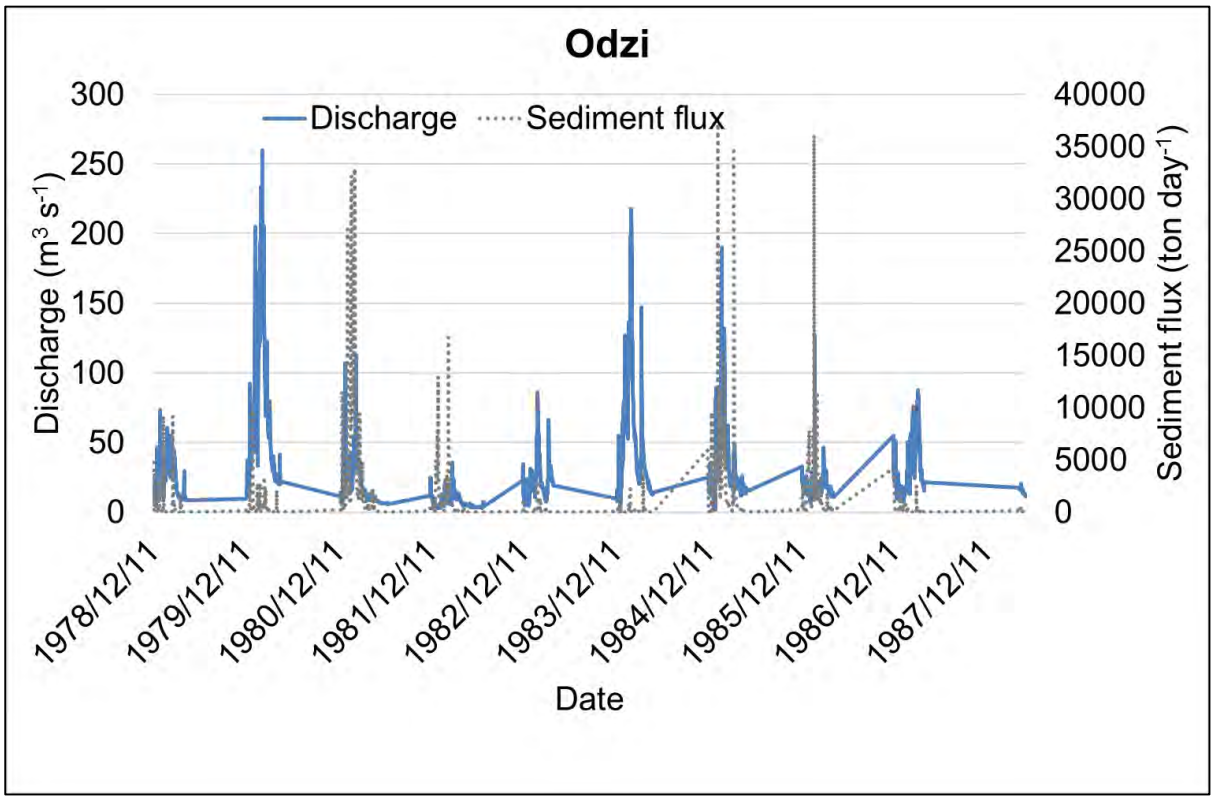
Odzi
Discharge
Sediment flux
Discharge (m3 s-1)
Sediment flux (ton day-1)
300
250
200
150
100
50
0
40000
35000
30000
25000
20000
15000
10000
5000
0
1978/12/11
1979/12/11
1980/12/11
1981/12/11
1982/12/11
1983/12/11
1984/12/11
1985/12/11
1986/12/11
1987/12/11
Date

App C.2 Final model parameters for the selected catchments.

Parameter			Catchment name				
Number	Name		OdziD	Tsitsa	A38	A36	A32
1	*Q* depth power		0.8	0.8	0.8	0.8	0.8
2	*Q* depth constant		12	12	3	3.5	4
3	Drainage density		1.2	1.5	1.3	1.5	1.5
4	Initial storage fraction		0.8	0.1	0.2	0.2	0.2
5	Sediment storage ratio		0.8	0.2	0.8	0.8	0.8
6	Threshold flow (mm/hr)		0.01	0.1	0.1	0.1	0.1
7	Peak scaling		1	1	1	1	1
8	Channel width (m)		10	25	80	60	60
9	Channel slope (degrees)		0.05	0.05	0.005	0.050	0.005
10	Channel length (Km)		450	250	350	150	300
11	Catchment area (Km^2)		2 436	3944	21 200	17 200	5 900
12	Catchment area proportion in each slope zone	**H**	0.1	0.12	0.01	0.01	0.01
		M	0.48	0.38	0.02	0.02	0.02
		L	0.42	0.5	0.97	0.97	0.97
13	Soil erodibility (*K*)	**H**	0.26	0.35	0.38	0.54	0.44
		M	0.21	0.33	0.42	0.42	0.33
		L	0.24	0.32	0.53	0.36	0.3

App C.2 (cont.) Final model parameters for the selected catchments.

14	Catchment slope (*LS*)	**H**	14.00	17	14	17.2	18.3
		M	5.16	5.7	6.3	6.1	5.4
		L	0.35	0.97	0.87	1	1.4
15	Cover (*C*)	**H**	0.001	0.009	0.15	0.22	0.18
		M	0.01	0.1	0.18	0.24	0.22
		L	0.01	0.15	0.22	0.35	0.27
16	Practice (*P*)	**H**	1	1	1	1	1
		M	1	0.99	0.9	0.9	0.9
		L	0.9	0.9	0.9	0.9	0.9
17	Maximum storage (Kilotons)	**H**	100	61	159	129	44
		M	400	500	500	500	200
		L	500	600	1 200	1 000	800
18	Gully store proportion	**H**	0.5	0.3	0.1	0.1	0.1
		M	0.5	0.6	0.2	0.1	0.1
		L	0.5	0.8	0.3	0.3	0.3

App C.2 (cont.) Final model parameters for the selected catchments.

Parameter			Catchment name			
Number	Name		Inxu	Grand Cane	San Patricio	Rio Tanama
1	*Q* depth power		0.8	1.3	0.8	0.8
2	*Q* depth constant		12	10	10	10
3	Drainage density		1.5	1.2	1.2	1.2
4	Initial storage fraction		0.2	0.090	0.090	0.4
5	Sediment storage ratio		0.8	1.2	0.8	0.8
6	Threshold flow (mm/hr)		0.1	0.1	0.5	0.3
7	Peak scaling		1	1	1.2	1.2
8	Channel width (m)		20	4	4	4
9	Channel slope (degrees)		0.05	0.05	0.05	0.05
10	Channel length (Km)		150	151	157	40
11	Catchment area (Km^2)		2 062	183	202	49
12	Catchment area proportion in each slope zone	**H**	0.12	0.05	0.01	0.2
		M	0.43	0.25	0.14	0.6
		L	0.45	0.70	0.85	0.2
13	Soil erodibility (*K*)	**H**	0.2	0.30	0.39	0.24
		M	0.35	0.39	0.39	0.24
		L	0.4	0.39	0.38	0.24

App C.2 (cont.) Final model parameters for the selected catchments.

14	Catchment slope (*LS*)	**H**	15.00	3	3.55	15
		M	5.00	1	1.44	7
		L	0.86	0.32	0.28	1.6
15	Cover (*C*)	**H**	0.01	0.006	0.001	0.001
		M	0.05	0.006	0.01	0.009
		L	0.18	0.005	0.009	0.009
16	Practice (*P*)	**H**	1	0.6	0.6	0.8
		M	0.8	0.6	0.6	0.8
		L	0.6	0.5	0.6	0.8
17	Maximum storage (Kilotons)	**H**	100	40	8	100
		M	300	100	45	400
		L	400	300	485	80
18	Gully store proportion	**H**	0.2	0.3	0.1	0.3
		M	0.3	0.3	0.1	0.1
		L	0.5	0.3	0.2	0.5

App C.3 A list of parameters for the simple storage option of the erosion and sediment transport (WQSED) model

Number	Parameter	Odzi	Tsitsa	Inxu	Grand Cane	San Patricio	Rio Tanama
1	Maximum catchment storage (SS_{max})(Kilotons)	1 200	1000	1000	500	500	500
2	Initial storage (TS_i) (Kilotons)	100	100	100	50	60	20
3	Sediment storage power ($QPOW$)	0.1	1.8	1.5	0.9	1.8	0.8
4	Threshold flow for sediment delivery ($m^3\ s^{-1}$)	0.1	0.5	0.1	0.5	0.5	0.9
5	Peak flow scaling	2	2	2	2	2	2
6	Maximum daily total flow (Q_{max}) ($m^3\ s^{-1}$)	298	125	399	78	229	50